AN ABSTRACT OF THE THESIS OF

Gudni Axelsson for the degree of Doctor of Philosophy in Geophysics presented on June 6, 1985

Title: HYDROLOGY AND THERMOMECHANICS OF LIQUID-DOMINATED HYDROTHERMAL SYSTEMS IN ICELAND

Abstract approved: Gunnar Bodvarsson

Low-temperature hydrothermal activity in Iceland is apparently mostly controlled by dikes and fractures. Conventional methods of production data analysis are not readily applicable in cases of heterogeneous/anisotropic fracture dominated hydrothermal systems. Moreover, the dikes and fractures may control the heat uptake mechanism of low-temperature activity.

The free-surface response functions of analytical reservoir models are presented and methods for analyzing production data on the basis of such models are developed. Based on a homogeneous and isotropic half-space model apparent permeability estimates of 0.7 millidarcy are obtained for two low-temperature systems in Tertiary strata in N-Iceland whereas estimates of 5-20 millidarcy are obtained for two systems in Quaternary

strata in SW-Iceland. A vertical two-dimensional flow model is, however, more consistent with the apparent linear dike/fracture control of many hydrothermal systems and results in higher permeability estimates.

Methods of simulating long term production data by simple lumped capacitor/conductor ladders based on only production/drawdown data are developed and the responses of analytical as well as real systems are shown to be easily simulated by such simple systems. The parameters of simulation ladders also provide information on global hydrological characteristics of hydrothermal systems.

A possible dike/fault controlled source mechanism of low-temperature activity in Iceland is considered. This process involves the downward migration of open sections of unwelded quasi-vertical fractures resulting from cooling and contraction of the adjacent rock, in conjunction with vertical heat transfer in the fracture. The rate of downward migration is estimated and found to depend very strongly on the magnitude of the horizontal regional stress. Stress conditions may therefore determine whether a low-temperature system can evolve at a given location as well as determine the intensity of hydrothermal activity.

HYDROLOGY AND THERMOMECHANICS OF LIQUID-DOMINATED HYDROTHERMAL SYSTEMS IN ICELAND

by

Gudni Axelsson

A THESIS

submitted to

Oregon State University

in partial fulfillment of
the requirements for the
degree of

Doctor of Philosophy

Completed June 6, 1985

Commencement June 1986

APPROVED:

Redacted for Privacy

Professor of Geophysics and Mathematics in charge of major

Redacted for Privacy

Dean of College of Oceanography

Redacted for Privacy

Dean of Graduate School

Date thesis is presented June 6, 1985

Typed by C. K. Correia, Admin. HQ for Gudni Axelsson

TABLE OF CONTENTS

LIST OF FIGURES

LIST OF TABLES

HYDROLOGY AND THERMOMECHANICS OF LIQUID-DOMINATED HYDROTHERMAL SYSTEMS IN ICELAND

I. INTRODUCTION

The evolution of the Earth is dominated by thermal processes, that at the surface are manifested by plate motions, volcanism, hydrothermal and tectonic activity. These phenomena are mostly concentrated at or near the plate boundaries of the Earth's crust. The hydrothermal activity accounts for a small fraction of the Earth's heat loss, while most of the loss of internal heat is by thermal conduction. Until recently, most known examples of hydrothermal activity were at or near the destructive plate margins, with some known activity at the very few subaerial segments of the oceanic rift system, the constructive plate boundaries. About half of the global heat loss is through the oceanic rift system (< 50 Myrs) and a significant fraction of this heat flow is now believed to be by advection of hot water in hydrothermal systems.

Geothermal energy has been of growing economic importance during the last few decades. Low temperature (< 150°C) geothermal resources are for the most part utilized directly, mainly for space and district heating, while higher temperature resources are in most cases

utilized for electrical power production. However, the high expectations of the mid-1970's for the rapid development of geothermal energy have been lowered because of a few unsuccessful ventures of high temperature geothermal energy exploitation (Kerr, 1982).

The successful development of hydrothermal energy resources is possible only on the basis of a sound understanding of the main geological and physical characteristics of the hydrothermal systems. Although the intensified research has resulted in greatly enhanced understanding, there still remain several unresolved problems concerning the nature of hydrothermal activity.

The purpose of the present work is to address a few of these problems, in particular; (1) develop methods for estimating the hydrological properties of liquid-dominated hydrothermal systems, (2) simulate the long-term behavior of the systems under production and (3) investigate the heat uptake mechanism of hydrothermal activity.

Iceland is a conspicuous part of the North Atlantic Ridge where geothermal energy has been utilized for decades. More accumulated data and knowledge on hydrothermal activity are available for Iceland than any other part of the oceanic rift system. The second chapter of this work is devoted to a brief review of the characteristics of hydrothermal activity in Iceland, with

particular emphasis on the aspects relevant to our study. Hydrothermal activity in Iceland appears to be mostly controlled by linear fluid conductors, such as dikes and fratures. However, conventional interpretation methods for well test data are not readily applicable in such situations. Furthermore, the specific role of the dikes and fractures in the heat uptake mechanism of thermal activity has not received much attention.

Some of the most important information on hydrothermal systems is obtained during production over long periods of time, that is periods of the order of years. The third chapter of this work is devoted to the long term evolution of liquid dominated hydrothermal systems under production. The response of unconfined hydrothermal reservoirs will be investigated on the basis of a free-surface model (Bodvarsson, 1977; 1984) that is of particular interest in the case of complex fracture dominated reservoirs. In particular, new models that are more consistent with the apparent linear dike/fracture control of the hydrothermal flow will be developed. Methods of production data analysis, aimed at estimating global hydrological reservoir parameters, such as permeability and porosity, will be developed on the basis of these models. Our free-surface analysis considers the effects of the large liquid-surface drawdown observed in many hydrothermal systems in Iceland.

As will be shown in the third chapter of this work simple lumped capacitor/conductor ladders can be very efficient simulators of the long term evolution of liquid dominated hydrothermal systems. Methods aimed at estimating parameters of simulation ladders, for actual production data, will be developed. In contrast to numerical modeling by complex distributed parameter models, which is a highly underdetermined and complex problem, lumped parameter simulation requires only production/drawdown data.

Part of the third chapter is devoted to applications of the theoretical results to long term data from several hydrothermal systems in Iceland. The results will provide some information on the hydrological characteristics of these systems, as well as providing effective, simple, lumped simulators.

The fourth chapter of this work is devoted to thermoelastic phenomena in hydrothermal systems, with particular emphasis on the role of the dike/fracture flow channels in the heat uptake mechanism of hydrothermal activity. The significance of thermoelastic stresses in low-temperature hydrothermal systems will be investigated. Thermoelastic stresses are likely to seriously influence hydrological parameters within a hydrothermal system, but have received little attention in the geothermal literature.

A major part of the fourth chapter is devoted to a possible heat source mechanism of dike/fault controlled hydrothermal activity, where thermoelastic stress plays an important role. This mechanism involves a downward migration of open fracture spaces, such as along the walls of dikes, by convective heat transfer in the fracture and associated cooling and contraction of rock adjacent to the fracture (Bodvarsson, 1982b). This process will be considered as a possible source-mechanism for low-temperature activity in Iceland. Crustal temperature and stress conditions, favorable to this mechanism, will be estimated along with rates of the downward migration and rock/water transfer.

II. SOME CHARACTERISTICS OF HYDROTHERMAL ACTIVITY IN ICELAND

1. The Geology of Iceland

Iceland forms a 500km broad landmass located at the crest of the Mid-Atlantic Ridge. The island is composed almost entirely of subaerial basalts, except for some 10% silicic and intermediate rocks. The presently active zone of rifting and volcanism, referred to as the Neovolcanic zone, crosses the country in a complex pattern from the SW to the NE (Figure 1). This zone is believed to be the surface expression of the constructive plate boundary between the N-American and European plates. The presently available K/Ar age determinations indicate a trend of increasing age with distance from the active zone of rifting and volcanism, the oldest rocks dated at 16 Myrs (Palmason and Saemundsson, 1974). Three stratigraphic units are identified:

- Tertiary rocks formed up to 3.1 Myrs ago, composed mainly of subaerial basalts.
- Plio-Pleistocene rocks, formed between 3.1 and 0.7 Myrs ago, containing a substantial amount of subglacially erupted pillow lavas and hyaloclastites.

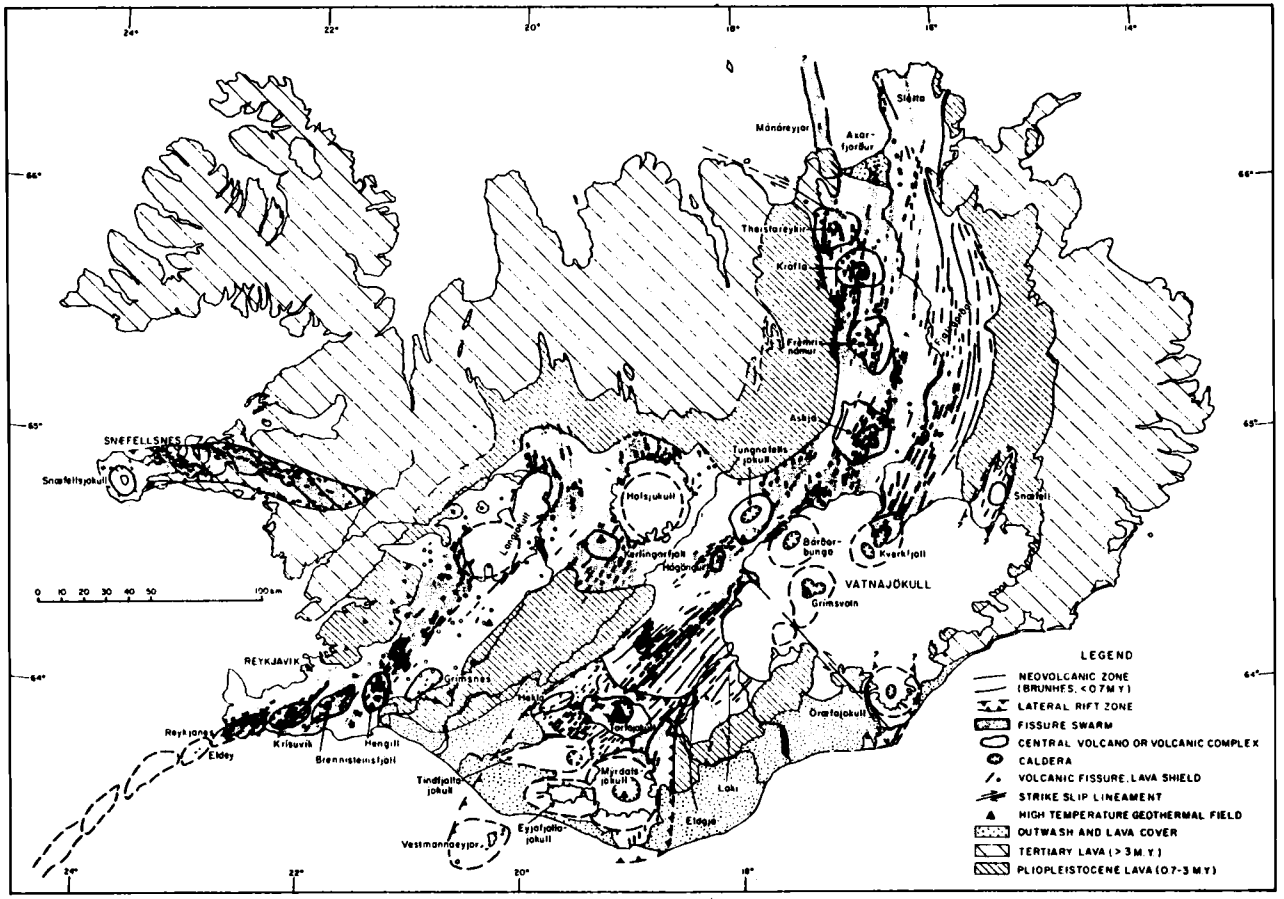

Figure 1. Geological map of Iceland. Compiled by K. Saemundsson (from Stefansson,1984).

- Late Quaternary rocks of the Neovolcanic zone formed during the Brunhes epoch, that is the last 0.7 Myrs.

The Neovolcanic zone is characterized by several fault and fissure swarms, most passing through central volcanoes, as well as eruptive fissures. A central volcano is commonly a site of repeated eruptions in a relatively small area. Most of the silicic rocks in Iceland are associated with central volcanoes. The interaction between central volcanoes and the associated fissure swarms, as well as their role in rifting and fissure eruptions, has been clearly demonstrated during a rifting episode in NE-Iceland (Bjornsson et al., 1979). Swarms of dikes passing through extinct central volcanoes are found in the Tertiary lava pile (Walker, 1960).

The crustal structure of Iceland has been studied by relatively detailed seismic refraction measurements (Bath, 1960; Palmason, 1971). Palmason (1971) concludes that the Icelandic crust consists of up to four seismic layers (termed layers 0, 1, 2 & 3) underlain by mantle with compressional wave velocity of only 7.2 km/s. Flovens (1980), however, concludes that since it does not satisfy observed amplitude variations or second arrivals, the layered model is an unacceptable interpretation. Flovens (1980) has reinterpreted the seismic data and concludes the Icelandic crust can be divided into two parts.

- Upper crust characterized by velocity continuously increasing with depth from about 2.0 km/s to 6.5 km/s.
- Lower crust (layer 3 of Palmason (1971)) characterized by a nearly constant 6.5 km/s p-wave velocity.

Flovens (1980) finds that where the crust is not heavily eroded the depth to layer 3 is about 5 km, which is slightly greater than the average depth obtained on basis of the layered model (Palmason, 1971). The upper crust is believed to be composed mostly of basaltic lavas with minor amounts of intrusions. The lower crust can probably be equated with layer 3 in the oceanic crust (Palmason and Saemundsson, 1974). The estimated thickness of the Icelandic crust 8-15 km (Palmason, 1971), is considerably greater than for average oceanic crust (7 km). It has been proposed that layer 3 is largely composed of intrusives (Palmason and Saemundsson, 1974) or that the layer 2- layer 3 boundary might be a metamorphic boundary (Palmason, 1971). Considerable additional evidence on the structure of the upper crust of Iceland has been provided by about 150 drillholes deeper than 1000m, the deepest hole reaching 3085m (Palmason *et al.*, 1979).

Present knowledge on the thermal state of the lithosphere below Iceland is reviewed by Palmason (1981). Three independent methods, temperature gradient measurements (Palmason and Saemundsson, 1979), magneto-

telluric (MT) measurements (Beblo and Bjornsson, 1980) and modelling of the accreation process (Palmason, 1981) all indicate that the depth to the 1000°C isotherm is on the average less than 10km below the Neovolcanic zone. The depth increases with distance from the rift zone. The MT work (Beblo and Bjornsson, 1980; Thayer et al., 1981) indicates the presence of a high conductivity layer at the base of the crust beneath the Neovolcanic zone. This layer is a few km thick and may be partially molten.

The low seismic velocities below the base of the crust also indicate an anomalous mantle below Iceland. Teleseismic p-wave delays and a Bouger gravity low over central Iceland (Palmason and Saemundsson, 1974) indicate a mantle with anomalously low density and p-wave velocity, possibly down to a depth of 200 km.

2. Terrestrial Heat Flow

The major part of the heat now escaping from the solid Earth is regarded as coming from the decay of long-lived radioactive isotopes. A small but significant fraction may result from a slight cooling of the interior of the Earth, resulting from mantle convection (Bott, 1982). Heat reaches the Earth's surface by two main processes, thermal conduction and advection (e.g. through the discharge of thermal water or lava). An estimate of

the global loss of heat from the Earth's surface is presented in Table I (Sclater et al., 1980). The conductive part of the heat flow has been estimated from numerous local heat flow measurements. The advective part of the oceanic heat flow is estimated as the difference between heat flow computed by theoretical models, based on the theory of plate tectonics, and the observed conductive heat flow. These models have been very successful in predicting the mean depth of the oceans as a function of age as well as heat flow in areas with thick sediment cover where we do not expect any advection to the surface. This estimate of the advective loss is therefore considered reliable. The relation between the heat flow and crustal age used is (Sclater et al., 1980):

$$(1) \qquad q(t) = 0.473t^{-1/2} \quad , \quad t < 120 \text{ Myrs}$$

where q is in W/m^2 and t in Myrs.

In the oceans the estimated advective energy current is quite substantial, or about 1/3 of the total estimated energy current. At the present we are, however, unable to estimate the relative importance of thermal water and lava in the advective transport. But we can mention that 10^{13}W corresponds to a current of 10^7 kg/s of 250°C hot water or about 200 kg/s per km along the oceanic rift system.

Table I Global Heat Flow (Sclater et al., 1980)

	Average heat flow (mW/m^2)	Rate of heat loss ($TW = 10^{12}W$)
Continents and shields	57	11.6
Oceans		
conduction	66	20.3
advection	33	10.1
total	99	30.3
Earth total	82	42

3. Heat Flow in Iceland

In this chapter we review some of the present day knowledge on hydrothermal activity in Iceland. It is therefore of interest to compare the estimated energy currents in Iceland with the results of Sclater et al. (1980). Bodvarsson (1982b) has improved previous estimates of Bodvarsson (1954), Palmason (1974) and Palmason and Saemundsson (1979) and has obtained, on the basis of considerable amounts of geological and geophysical data, the estimates in Table II. The average integrated flow through the surface of 300 mW/m^2 is about 5 times the average global conduction flow.

Based on the results of Sclater et al. (1980) and Bodvarsson (1982b) we can then make the comparison for Iceland, the oceanic rift system and the Earth presented in Table III below. When making this comparison we have to keep in mind that most of the heat flow through the oceanic rift system originates at the fast spreading ridges of the Pacific where 0-20 Myr old crust corresponds to a much wider region, and hence higher energy current per unit length of rift axis than at the slowly (2cm/yr whole rate) spreading Mid-Atlantic Ridge. On the basis of equation (1) and the fact that the oldest rocks on the east and west coasts of Iceland are about 16 Myrs old we estimate the following:

Table II Heat Flow in Iceland[1] (Bodvarsson, 1982b)

	Rate of heat loss (GW = 10^9W)	Average heat flow (mW/m^2)
Conduction	15	150
Advection by lava	7	70
Advection by thermal waters	8.5	85
Total	30.5	305

1) Area of Iceland $10^5 km^2$

Table III Heat Flow Comparison (Bodvarsson, 1982b; Sclater et al., 1980).

	Per km of axis (MW/km)[1]	Average heat flow (mW/m^2)
Iceland (0-16 Myrs)		
conduction	50	150
advection	52	155
total	102	305
Oceans (0-20 Myrs)		
conduction	90	
advection	202	
total	292	
Earth		
conduction		64
total		82

1) length of rift axes
Iceland: 300 km
Oceans: 50000 km

- The average heat flow through 0-16 Myr old oceanic crust should be about 235 mW/m^2.
- The total energy current through an area the size of Iceland ($10^5 km^2$), on both sides of an ocean ridge with a spreading rate of 2 cm/yr, should be about 24 GW.

We therefore conclude that the total heat flow through Iceland of 31 GW is about 30% higher than the expected heat flow at oceanic rift axes with the same spreading rate. The difference of about 7 GW could be explained by a supply of magma (enthalpy 1.6 x 10^6 J/kg) greater than normal, for the North Atlantic Ridge, by 1.5 m^3/s. This happens to be the same as the estimated average rate of extrusion of lava in Iceland of 0.045 km^3/yr = 1.4 m^3/s (Palmason and Saemundsson, 1979).

4. Classification of Hydrothermal Systems

In Iceland hydrothermal systems are commonly classified with regard to the base temperature of the systems (Bodvarsson, 1964). Systems with base temperature < 150°C are classified as low temperature (LT) systems whereas high temperature (HT) systems have base temperature in excess of 200°C. Systems with base temperature in the range 150 to 200°C can be called intermediate temperature systems. The HT systems in Iceland are associated with the presently active rift

zone and quite commonly situated in central volcanoes. The LT activity is distributed over the Tertiary and early Quaternary flood basalt areas. Bodvarsson (1982b) estimates the heat dissipated by the HT and LT activity to be about 8 GW and 0.6 GW, respectively.

Hydrothermal systems are also classified on the basis of the physical state of the system fluid. Thus reservoirs are conveniently classified as either liquid-dominated or vapor-dominated. In each case the name refers to the dominant mobile phase in the reservoir in its undisturbed state (Donaldson and Grant, 1981). The pressure gradient is then close to the static pressure gradient of the dominant mobile phase. Liquid-dominated systems may contain a steam-water mixture. There are also systems of intermediate and more complex nature, the so-called two-phase systems. Most LT and intermediate temperature systems are liquid-dominated but HT systems can be liquid-dominated, vapor-dominated or two-phase.

5. Earlier vs. Current Views on Hydrothermal Activity

The origin of hydrothermal fluids was a subject of dispute for more than a century. Two general views prevailed since the latter half of the last century. One favoring volcanic or juvenile origin of the thermal waters, the other favoring meteoric origin (Stefansson

and Bjornsson, 1982). It has now been established that meteoric water is the dominant source of fluid in most active nonoceanic hydrothermal systems. As an example the very comprehensive study of Arnason (1976) of stable oxygen and hydrogen isotopes in hydrothermal waters in Iceland indicates quite clearly the meteoric origin of the waters. Further evidence for the meteoric origin of the thermal waters was obtained by Ellis and Mahon (1964, 1977) and Arnorsson (1974), for example, who showed that the chemical composition of most hydrothermal waters could be attained by leaching from the rock surfaces in contact with the circulating water (Bodvarsson, 1983a).

But not all hydrothermal fluids are of meteoric origin. It is now well established that hydrothermal systems are important on ocean ridges where ocean water is the dominant fluid source. Ocean water is also a major part of the hydrothermal fluid in a few terrestrial geothermal systems (Bjornsson et al., 1972; Kjaran et al., 1979).

The source of energy for the hydrothermal systems has also been a subject of dispute. The close association of major geothermal HT-activity with volcanic activity was noticed early (Thoroddsen, 1925). It was therefore taken to be only reasonable to extend the theory of a volcanic origin to the LT-activity in Iceland also. This view was challenged by Einarsson (1942) who

concluded, on the basis of his work in N-Iceland, that the LT-systems there are entirely of non-volcanic nature. Einarsson (1966) later extended his theory to all LT systems in Iceland. He envisioned a general circulation of meteoric water from the central highlands out to the coastal areas and assumes that the circulation base is deep enough for the water to be heated by the terrestrial conduction current to the temperatures observed in the LT-areas. The heat transfer process is thus taken to be essentially of a steady state nature. This theory received some support when data on the deuterium content of thermal waters in Iceland (Arnasson, 1976) indicated quite clearly that the recharge of LT-systems is to a considerable extent derived from the central highlands. Bodvarsson (1950, 1964) agreed with the non-volcanic nature of the LT-activity, but concluded that the conduction process must be of a transient nature (see section 7 below). The HT-activity is, however, obviously generated by magmatic processes, that is, contact of meteoric water with shallow magma intrusions.

6. The Nature of HT-hydrothermal Systems in Iceland

All known HT geothermal systems in Iceland are located in the Neovolcanic zone (Figure 1). The HT areas seem to act as chimneys for the heat dissipated in the

rift zone (Fridleifsson, 1979). The HT activity is concentrated in a few specific locations, with a spacing of 12-15 km, a distance which is about equal to the estimated thickness of the crust of Iceland. This HT activity is associated with volcano-tectonic features such as volcanic fissure swarms and, more commonly, central volcanoes (CV), fault swarms and calderas. To emphasize the close correlation between HT activity and CVs, it can be pointed out that all CVs in the Neovolcanic zone of Iceland have HT systems. Extinct HT systems have been found in the deeply dissected roots of Icelandic Tertiary CVs (Walker, 1960; Fridleifsson, 1983). The host rock is highly altered and the altered rock aids in delineating the extinct HT systems. At CVs there is a great abundance of dikes, sheets and other minor intrusions at a shallow depth in the crust. The roots of extinct CVs are characterized by a high density (50-100%) of such intrusions. These intrusions are considered the main heat source for the HT systems (Fridleifsson, 1979) indicating convective hot-spots at and around the magmatic intrusions (Bodvarsson, 1982b). The surface manifestations of the HT systems are steamholes, boiling mudpools and highly altered ground. From these surface manifestations the sizes of the HT systems have been estimated. Most HT areas cover from 1 to 20 km^2, but a few up to 100 km^2. The most powerful HT

system, the Grimsvotn subglacial area (Bjornsson et al., 1982), dissipates about 5 GW or over 60% of the total estimated HT heat dissipation of 8 GW.

Wells have been drilled into 8 HT-systems and of these 5 are under some form of exploitation. In their natural state most of these systems appear to be liquid dominated. Three systems have been found to include two-phase sections.

Isotope studies (Arnason, 1976; Fridleifsson, 1979) indicate that the recharge of the HT-systems is more localized than in the case of the LT-systems. Local meteoric water may seep through fractures inside the CV and/or in the active fault swarm outside the CV. In 3 HT-systems the hydrothermal fluid is known to be partially seawater.

Quantitative investigations into the source mechanism of HT activity (Bodvarsson, 1951; White, 1968) indicate that it is difficult to account for the rapid rate of heat dissipation unless the water actually penetrates into the intrusions that are in the process of cooling. Evidence in support of water penetration into hot rock boundaries of solidifying magma is reported by Bjornsson et al. (1982). Water cooling of a recent lava flow in Heimaey, Iceland, demonstrated a heat extraction efficiency of 40 kW/m^2 and a rate of penetration of the order 1 m/day. Bjornsson et al. (1982) conclude that a

process of this nature is required to explain the intense heat output of the subglacial Grimsvotn HT-area which according to calorimetric observations of ice melting in the area dissipates 5 GW of heat.

The possible mechanism of this process has been described by Bodvarsson (1979, 1982b), which refers to it as convective downward migration (CDM). The process has also been discussed by Lister (1976). The underlying ideas are closely related to the theories for the penetration of sea water into the ocean floor by Palmason (1967), Bodvarsson and Lowell (1972) and Lister (1972, 1974, 1982). CDM operates on the principle that convective fluid motion in open vertical fractures is associated with the withdrawal of heat from the formation at the lower boundary resulting in thermoelastic contraction of the adjacent rock that tends to increase the local fracture aperture, cause further cracking of the rock and opening of additional fracture space at the bottom. Fractures harboring such convecting fluid motion can therefore migrate downward by the process.

Foulger and Long (1984) report anomalous focal mechanisms (predominantly compressional first arrivals) for many small magnitude earthquakes in the Hengill HT-system in SW-Iceland. They interpret these events to be due to tensile crack formation within a cooling intrusive body above a depth of 7 km. This observation supports

the notion that CDM may be the source mechanism of HT-activity.

7. The Nature of LT-hydrothermal Systems in Iceland

Hydrothermal activity in Iceland is not confined to the Neovolcanic zone. LT systems are quite common in the Plio-Pleistocene and Tertiary flood basalt areas, as shown in Figure 2. The physical characteristics of this LT-activity are the fundamental subjects of the present work. The largest and most powerful LT areas are located in SW and S-Iceland on the flanks of the active rift zone. The surface manifestations of LT systems are less pronounced than those of HT systems, hot or boiling springs and minor ground alteration. Spring flow rates range from almost zero to a maximum of 180 kg/s from a single spring. The total integrated natural mass output of LT systems in Iceland is now estimated at 1800 kg/s (Saemundsson and Fridleifsson, 1980), dissipating about 600 MW (Bodvarsson, 1982b). This estimate is quite small compared to the energy dissipated by the HT-activity. The figure does not, however, include dissipation due to subsurface flow losses or possible LT flow to the oceans. By drilling and pumping, the natural flow has in some areas been increased by roughly an order of magnitude.

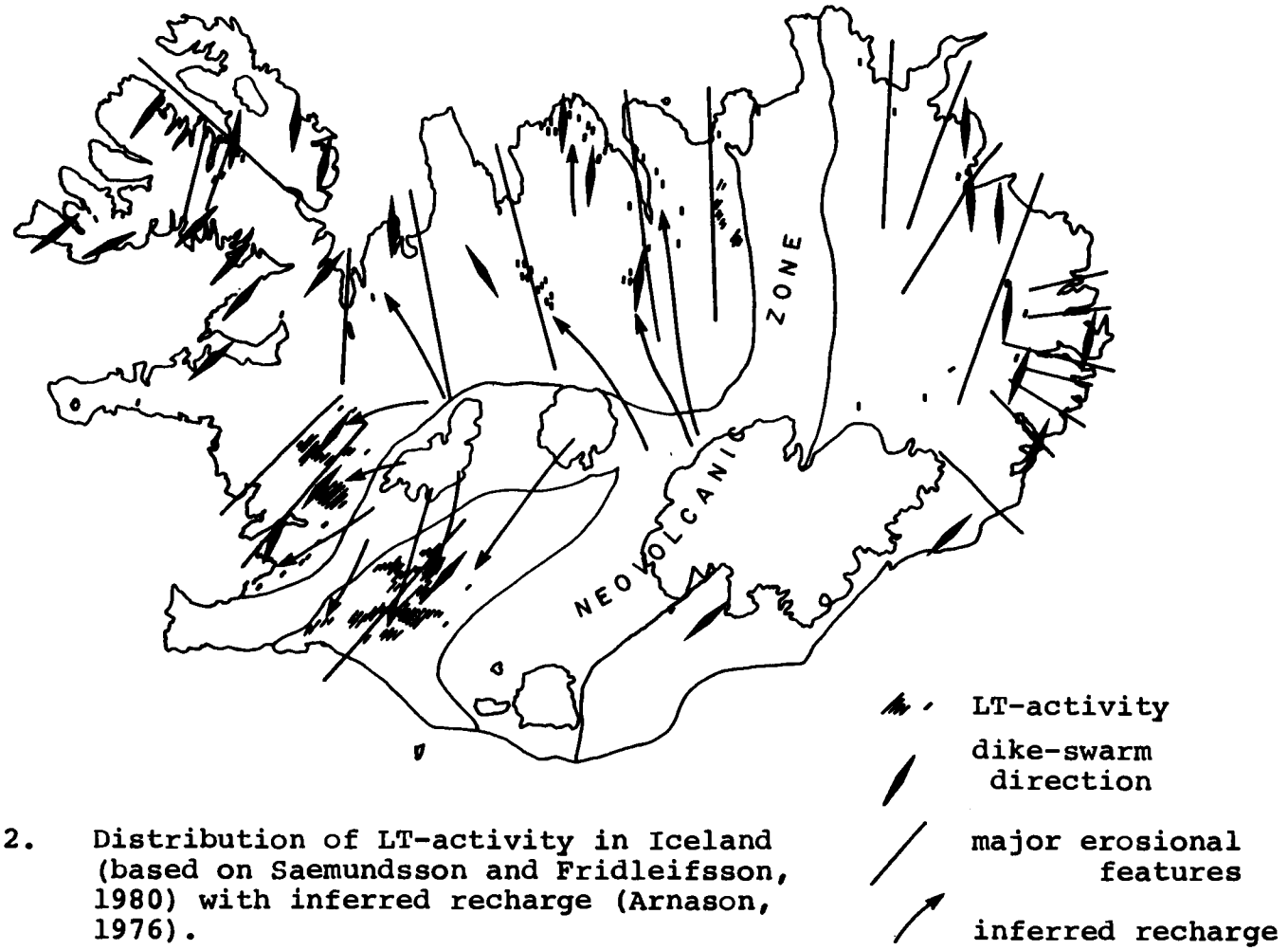

Figure 2. Distribution of LT-activity in Iceland (based on Saemundsson and Fridleifsson, 1980) with inferred recharge (Arnason, 1976).

As mentioned earlier, the isotope work of Arnason (1976) indicates quite clearly the meteoric origin of the water in the LT systems. By comparing the deuterium content of the thermal waters of LT systems and the spatial variations in deuterium content of precipitation falling in Iceland Arnason (1976) shows that the recharge of the LT systems is to a considerable extent derived from the central highlands of Iceland (see Figure 2). There are, however, a few localities where the deuterium content is not comparable to the deuterium content of meteoric water falling anywhere in Iceland today (Arnason, 1976; Kristmannsdottir and Johnsen, 1982). The implications of this phenomenon are not well understood.

Low temperature fields in Iceland are predominantly located in valleys and other topographic lows (Stefansson, 1984). This may result partially from the fact that since the recharge of the LT systems is most likely in the highlands, larger pressure differences are available for driving the recharge of LT systems at lower elevations. Stefansson (1984) points out that on the ocean floor this situation is reversed, such that the pressure situation favors discharge at topographic highs. The locations of LT systems may also reflect anomalous subsurface temperature fields below deep erosional features such as valleys.

The aquifers of many LT-systems have been identified on the basis of geological and structural studies. The structural control is most commonly provided by dikes (Fridleifsson, 1979) although the situation appears to vary from the Tertiary to the Plio-Pleistocene provinces.

In the subaerially erupted Tertiary volcanics the flow channels appear to be mainly dikes and faults. Thin high porosity stratiform horizons are much less important. The bulk of most lavabeds has apparently very low permeability. In the Tertiary areas, such as at Laugaland in N-Iceland (Bjornsson, 1980), surface hot springs as well as aquifers at depth in boreholes are mostly associated with dikes. Yet only a fraction of the visible dikes are hydrothermally active.

In the Plio-Pleistocene strata, which are characterized by successions of subaerial lavas interlaced with thick piles of subglacially erupted pillow lavas and hyaloclastities, potential flow channels are much more abundant. There the most effective large scale reservoirs and flow channels are thought to be the pillow lava cores of hyaloclastic ridges and high porosity stratiform horizons, which are likewise cut by dikes and faults. At depth, such as in the intensely drilled Reykir thermal area in SW-Iceland (Thorsteinsson, 1976), most large aquifers seem to occur at contacts between lava flows and hyaloclastic or pillow lava beds.

These more local observations appear to apply on a larger scale to the recharge flow of the LT-systems. Fridleifsson (1979) points out that the LT-areas of the country are predominantly located where dike-swarm directions (mostly parallel to the geological strike) are approximately parallel to the direction of major erosional features, such as glacial valleys (Figure 2), whereas regions where the erosional features are nearly perpendicular to dike swarm directions are almost devoid of hot springs. Since the recharge of the LT-systems is driven by hydrostatic head, controlled by topography, the recharge flow is parallel to major erosional features. These observations indicate that the recharge flow of LT-systems is mostly parallel to dike swarm directions and the geological strike, such as along walls of dikes or along vertical fractures, but not along horizontal permeable horizons.

No reliable data are available on the depth of the hydrothermal circulation in Iceland. However in the Reykjavik and Laugaland areas boreholes have produced thermal water from depths up to 3 km (Palmason et al., 1979). Temperature profiles from these two areas (Figure 3), as well as other LT areas in Iceland, indicate a disturbance of the thermal state of the crust well below 3 km (Palmason et al., 1979). The convex profiles in Figure 3 show that the temperature at depth in the

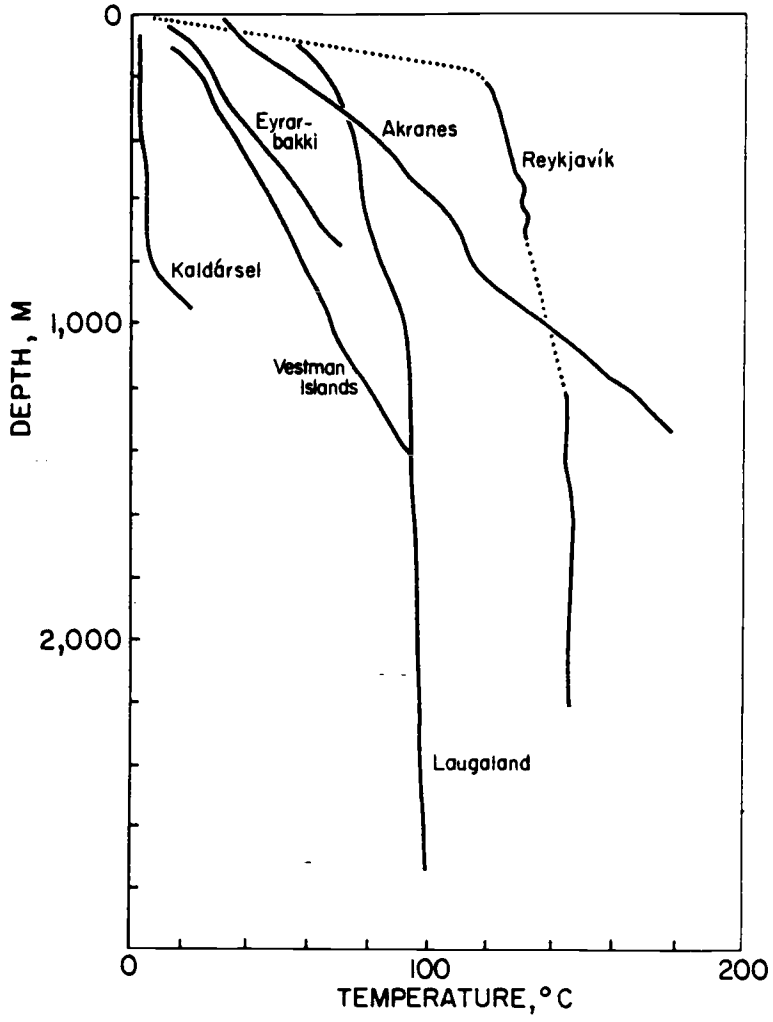

Figure 3. Examples of temperature profiles from deep boreholes in Iceland (from Bodvarsson, 1983b). Reykjavik and Laugaland are LT-areas whereas Akranes, Eyrarbakki and Vestman Islands are areas of relatively undisturbed thermal state of the crust. The Kaldarsel profile indicates local cooling by downward flow of cold water.

systems in question is abnormally low and indicate hydrothermal convection is active at great depths. It is clear that the upper crust (Palmason, 1971; Flovens, 1980) is permeable to water. Microearthquake studies (Ward and Bjornsson, 1971) indicate that water may penetrate into the upper parts of layer 3.

The overall model for the flow pattern and heat uptake of the LT-activity in Iceland, generally accepted by most geothermologists today, is the model proposed by Einarsson (1942; 1966), as discussed in section 5 above. Bodvarsson (1983b), however, proposes a rather different model that can also fit the presently available data on the LT-activity.

The characteristics of the two different models are summarized by Bodvarsson (1983b) as follows. The first model, sketched in Figure 4, is essentially the generally accepted steady state model of Einarsson (1942). Precipitation falling on the highlands percolates deep into the bedrock in the highland areas. Here the water takes up its entire sensible enthalpy by flowing laterally at depths of 2 to 4 km en route from the highlands towards dikes that provide channels for the ascent to the surface. The heat supply is provided by the general regional conductive heat flow (Fridleifsson, 1979). The heat conduction process is taken to be

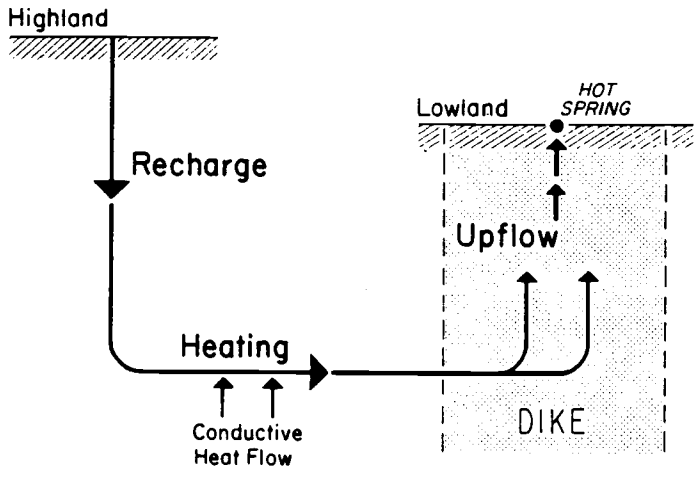

Figure 4. Pattern of flow on the deep recharge forced flow heating model of Einarsson (1942). From Bodvarsson (1983b).

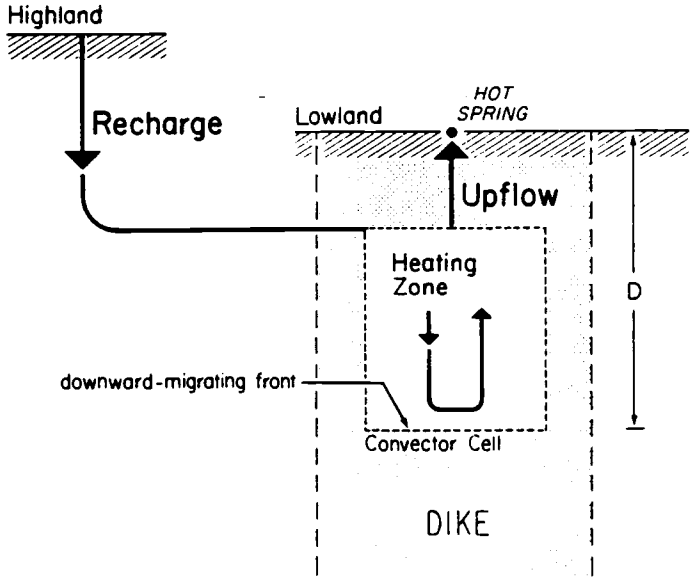

Figure 5. Pattern of flow on the dike-convector model (Bodvarsson,1983b).

essentially of a steady state nature (Bjornsson, 1980; Georgsson et al., 1984).

On this model the flow along the rock/water heat transfer surfaces is driven predominantly by the hydrostatic head, and the cooling of the deep formations, as observed in some LT systems in Iceland (Figure 3), will have to be of an upward type, having proceeded from below. Cooling from below would be the result of the upward movement of relatively cold water from depths in excess of 3 km. The principal problem with this model relates to the depth of the recharge flow. The question arises whether the water can flow at such depths over distances of tens of km in the flood basalt plateau of Iceland. This model can be classified as a hydrostatic or forced flow mode of heating where thermobuoyancy plays a minor role.

Bodvarsson (1982a) concludes that a steady state conduction process can hardly be invoked as a basis for the energy supply. He points out that it is rather likely that the deglaciation of Iceland, only 10^4 yrs ago, may have activated many of the LT-systems. During the period of glaciation recharge must have been quite limited and the deglaciation must have seriously affected the subsurface crustal stress-field, enhancing subsurface permeability. Transient models (Bodvarsson, 1982a) lead to plausible estimates of rock/water contact areas

required to maintain the energy dissipation of LT-systems, whereas steady-state models lead to contact area estimates that are an order of magnitude larger and hence hardly acceptable.

The second model, proposed by Bodvarsson (1983b), is sketched in Figure 5. This model involves downhill recharge flow along relatively shallow paths such that little heat is added until the water reaches a hydrothermally active dike where it is deflected and sinks by convective downward migration (CDM) through cracks or fractures along the walls of the dike. Reaching depths of the order of a few km, the water takes up heat from the hot adjacent rock and ascends subsequently along the dike. Cooling of the formations proceeds from above. This is a free thermobuoyant mode of heating.

As reviewed above, the CDM-process is presently considered a possible source mechanism for HT-activity. Bodvarsson (1982b) estimates that quite small temperature differentials should be sufficient for CDM, hence CDM may also be an important source mechanism for LT-activity. This process will be more thoroughly studied in the fourth chapter of this work. We will estimate the crustal temperature and stress conditions where the CDM-process may be possible.

Bodvarsson (1983b) sites some evidence consistent with a CDM source mechanism (Figure 5):

- The temperature profiles presented in Figure 3 are probably the result of local hydrothermal convection, that may be of the CDM type.
- Temperature/flow statistics of LT-activity in Central N-Iceland show a strong positive correlation between the temperature and mass flow of individual systems (Figure 6). It is to be expected that the spring temperature should increase with increasing flow depth and since the evolution of the second model involves a simultaneous increase in flow depth and rock/water contact area, Bodvarsson (1983b) concludes that this alternative model is more likely to show a positive temperature/flow correlation. Since the flow permeability is likely to decrease with depth decreasing flow with increasing temperature would appear more consistent with the forced flow model.
- The fact that most identified flow channels of LT-systems are dikes and quasi-vertical fractures is consistent with a CDM source mechanism.

It should be remarked that the two models possibly represent somewhat extreme situations and that real systems may be a combination of both models with additional modifications.

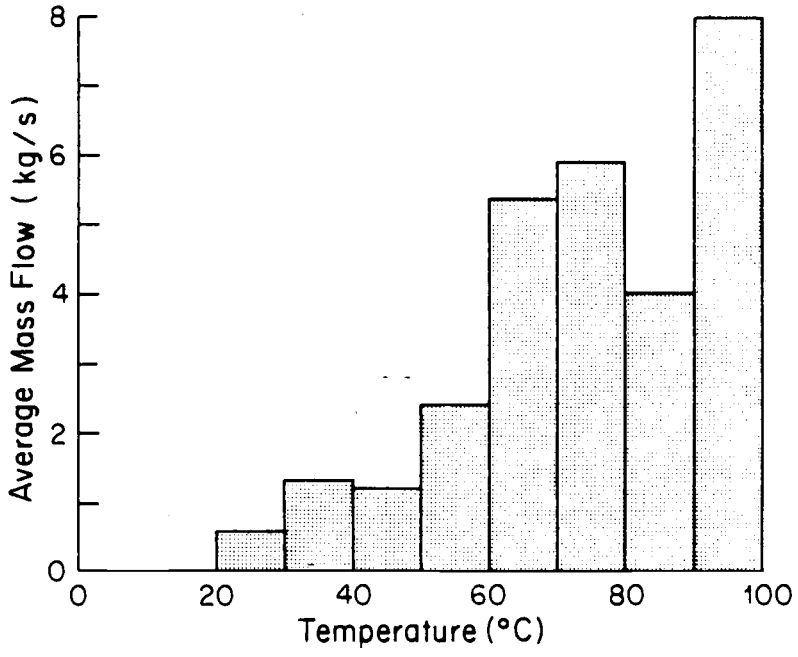

Figure 6. Temperature/flow statistics for LT-systems in central N-Iceland (from Bodvarsson,1983b).

8. Utilization of Geothermal Energy in Iceland

The economic importance of geothermal energy in Iceland has made the gathering of the considerable amount of information on hydrothermal activity reviewed above possible. For the last 1100 yrs hot springs have been widely used for washing and bathing. Commercial exploitation of geothermal resoures dates back to the 1920's with large scale utilization of geothermal energy, for space heating, starting in the 1940's. Relative to other primary energy sources geothermal energy has steadily grown in importance during the last four decades. In 1983 geothermal energy accounted for about 30% of the total energy consumption in Iceland (Palmason et al., 1983). Space heating is the most important use of geothermal energy, about 80% of the total space heating requirements are met with geothermal energy, while agricultural and industrial utilization is also of importance. Electricity is produced from geothermal steam at the Krafla field in NE-Iceland, presently at a rate of about 30 MW.

Most of the geothermal energy is extracted from liquid dominated systems and the thermal water used for space heating is mostly derived from LT-systems.

9. Reservoir Engineering Studies of Hydrothermal Systems in Iceland

While geological and structural studies have provided information on the structural control of hydrothermal reservoirs, such studies provide limited quantitative information on the reservoir parameters. However, when wells have been drilled into a hydrothermal system a possibility opens for reservoir testing that enables the estimating of physical reservoir properties such as the permeability distribution. The following reservoir testing methods are commonly in use (Grant et al., 1982).

- Short term single well tests, lasting a few hours.

(1) Injection/drawdown tests: response of reservoir to variable or constant injection/withdrawal of fluid into/from a well, observed as water level or pressure changes in the same well.

- Intermediate term well tests, lasting up to a few days or weeks.

(2) Interference tests: response of reservoir to injection/withdrawal into/from one well observed as water level or pressure in a different well at some distance.

(3) Buildup tests: recovery of water level or pressure, observed in one or more wells, when production from reservoir is discontinued for some time.

- Long term production tests, lasting several months or years.

(4) Water level or pressure drawdown resulting from long term production observed in one or more wells.

Permeability estimates for a few Icelandic systems that are based on short to intermediate term tests are presented in Table IV below. These results presume confined compressible aquifer models with horizontal Darcy-type flow (see for example equation (25) below). Note the lower permeability estimated for the Tertiary LT-systems. This is to be expected in view of the differences between the Tertiary and Plio-Pleistocene strata both in age and nature. The difference between the two HT-systems is also noticeable. However, Svartsengi is located inside an active fissure swarm, whereas the drilled part of the Krafla field is outside the active Krafla fissure swarm.

It has also been observed that shorter term tests result in much higher values than long term tests (Palmason et al., 1983) and that there appears to be an inverse relation between the time scale of the experiment and the permeability estimated (Bodvarsson and Zais, 1978). As an example we can take the Laugarnes area (Table IV) where the short term tests indicate a permeability of 150 millidarcy (md). Based on two different longer term data sets and two considerably

Table IV Permeability estimates for Icelandic hydrothermal systems[1)]

	Transmissivity[2)] (m^2/s)	Global Permeability[3)] (millidarcy)
LT-systems		
Tertiary (N-Iceland)		
Laugaland	2.6×10^{-3}	80
Botn	5.1×10^{-5}	2.0
Plio-Pleistocene (SW-Iceland)		
Reykir	2.5×10^{-2}	850
Laugarnes	6.0×10^{-3}	150
HT-systems		
Svartsengi (SW-Iceland)	1.2×10^{-2}	200
Krafla (NE-Iceland)	1.2×10^{-4}	2.0

1) Fridleifsson (1979), Palmason et al. (1983), Thorsteinsson (1976), Kjaran et al. (1979) and Bodvarsson et al. (1984a).

2) $T = \beta h/(\nu/g)$, β: permeability, h: reservoir thickness, ν: kinematic viscosity

3) Estimated by assuming the same reservoir thickness of 1000 m.

different models Bodvarsson and Zais (1978) and Palmason et al. (1983) both obtain estimates in the range 10-20 md. The apparent dependence of the permeability estimates on the time scale of the reservoir tests may result from

- Heterogeneity and fractured nature of the reservoir in question (Bodvarsson and Zais, 1978; Palmason et al., 1983).
- Limited size of the reservoir. In short term tests the boundaries are not felt whereas in longer tests they are. Using models without boundaries thus results in lower permeability estimates.

In addition to the conventional methods, geothermal systems can also be modeled as unconfined reservoirs with a free liquid surface, neglecting compressibility (Bodvarsson, 1977; 1984). The very large drawdown observed in some geothermal systems in Iceland (Palmason et al., 1983) indicates the importance of the free surface effect. This method will be considered to some length in the following chapter. Theoretical model-responses will be derived and applied to some actual field data.

The conventional models, referred to above, are hardly compatible with the known structural control of LT-systems (section 7). We will present a simple model of an unconfined vertical slab reservoir with two-

dimensional flow that should be more consistent with the nature of the identified flow channels.

Permeability estimates are important in the development of models aimed at simulating the behavior of geothermal reservoirs under exploitation, as well as for enabling comparison with estimates from other reservoirs. Simple models have been developed to simulate the behavior of the Laugarnes LT-field (Thorsteinsson and Eliasson, 1970) and the Svartsengi HT-field (Kjaran et al., 1979). A complex numerical model, with an inhomogeneous, anisotropic permeability distribution and two-phase flow, has been developed for the Krafla HT-system (Bodvarsson et al., 1984b). This kind of modeling is, of course, highly underdetermined and requires various assumptions on the parameter distribution within the reservoir in question.

The responses of complex liquid dominated geothermal systems are easily simulated by a much simpler lumped networks of capacitors and conductors (Bodvarsson and Axelsson, 1985). This topic will be discussed in chapter three below. In addition to being mathematically much simpler than standard numerical modelling this kind of simulation is based on long term production data and does not require any assumptions on parameters of the

reservoirs. Lumped simulators also provide important information on global hydrological characteristics of hydrothermal systems.

III. HYDROLOGY OF LIQUID-DOMINATED GEOTHERMAL SYSTEMS

1. Basic Pressure Equations in Liquid Dominated Aquifers

Consider a domain B occupied by a permeable porous medium of porosity ϕ that is saturated with a liquid of density ρ. If $\bar{q}$ is the mass flow of the liquid through the medium and f the mass source density, the equation for the conservation of mass can be written

$$\partial_t(\rho\phi) = - \nabla\cdot\bar{q} + f \tag{2}$$

We assume the flow of the liquid can be adequately described by Darcy's law

$$\bar{q} = - c(\nabla p_T - \rho\bar{g}) \tag{3}$$

where p_T is the total liquid pressure and c is the liquid conductivity, $c = \beta/\nu$ where β is the permeability of the medium and ν the kinematic viscosity of the liquid. In a general setting c is a tensor and only in homogeneous, isotropic and isothermal cases can c be taken to be a constant. The total liquid pressure is the sum of the flow pressure (p) and the hydrostatic pressure (p_h). For a homogeneous, slightly compressible liquid the term on the left of equation (2) can be rewritten

$$\partial_t(\rho\phi) = \rho S \partial_t p \tag{4}$$

where S is the capacivity or storage coefficient expressed by

$$S = \phi C_f + (1 - \phi) C_r \tag{5}$$

and C_f and C_r the compressibilities of the liquid and rock, respectively. By inserting (3) in (2) and using (4) we obtain the basic diffusion equation for the flow pressure

$$\rho S\, \partial_t p = \nabla \cdot (c\, \nabla\, p) + f. \tag{6}$$

In the homogeneous, isotropic and isothermal case

$$\rho S\, \partial_t p = c \nabla^2 p + f. \tag{7}$$

Now let us consider the presence of a free liquid surface in the medium that at equilibrium is represented by the horizontal plant Σ (see Figure 7). The nonequilibrium surface Ω is a boundary of constant pressure which can be assumed to be zero. The free surface condition is then expressed

$$Dp_T/Dt\,|_{P_T=o} = o \quad \text{on } \Omega \tag{8}$$

where D/Dt is the material derivative. Equation (6) with condition (8) and appropriate boundary/initial conditions now governs the flow of the liquid in the domain B.

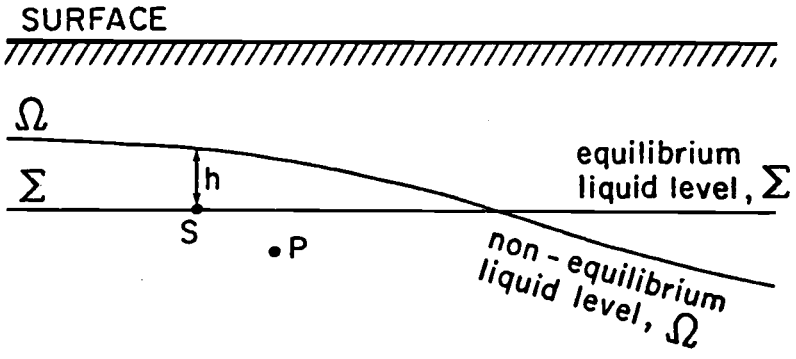

Figure 7. The free liquid surface (from Bodvarsson,1984).

2. Linearized Free Surface Condition

Condition (8) is nonlinear and the solution of equation (6) thus becomes a difficult task. However, Bodvarsson (1977; 1984) has shown that when Ω deviates only a little from Σ condition (8) can be linearized. We place a rectangular coordinate system with the z-axis vertically down such that the xy-plane coincides with Σ. We approximate

$$p = \rho g h \quad , \; z = o \tag{9}$$

where h is the deviation of Ω from Σ. Moreover, Bodvarsson (1984) approximates

$$q_z = - \rho \phi \, \partial_t h \quad , \quad z = o \tag{10}$$

and since (3) implies

$$q_z = - c \, \partial_z p \tag{11}$$

we can combine (10) and (11) in

$$\partial_t p - w \partial_z p = o \quad , \quad z = o \tag{12}$$

where $w = cg/\phi$ is a characteristic liquid velocity. This approximation is valid when $|h/L| << 1$ where L is the horizontal scale of undulation of Ω.

Condition (8) is now replaced by (12) and the basic mathematical problem consists in solving (6) with condition (12).

3. Separation of Compressibility and Free Surface Effects

Even though linearized, the problem above is still highly complex because of the two different capacitances involved, (1) the fluid/rock compressibility and (2) the free liquid surface mobility. But the relative importance of these two effects is different for different time scales. Considering equation (6) we see that compressibility effects are not important for

$$t \gg \frac{\rho S L^2}{c} \quad , \tag{13}$$

where L is a length scale characteristic of the reservoir in question, whereas free surface effects are not important (equation (12)) for

$$t \ll \frac{\phi L}{cg} \quad . \tag{14}$$

Considering a specific example, typical for many geothermal reservoirs, with $\phi = 0.01$, $S = 2 \times 10^{-11}$ Pa^{-1}, $c = 3 \times 10^{-7}$s and L = 1000 m, we obtain

$$\begin{aligned} \rho S L^2/c &= 0.8 \text{ days} \\ \phi L/cg &= 35 \text{ days} \end{aligned} \tag{15}$$

We see that at early times the reservoir response is dominated by compressibility and at later times by the free surface effect.

We will be able to separate these two different responses if

$$(16) \qquad \frac{\phi}{\rho g S L} \gg 1.$$

Considering the parameters above we obtain

$$\frac{\phi}{\rho g S L} = 50$$

Condition (16) is independent of the conductivity c and should hold for different reservoir conditions. Bodvarsson (1984) obtains the same condition and concludes that amplitude attenuation due to purely diffusive effects proceeds at a considerably faster rate than the decay resulting from gravity effects.

We therefore conclude that the long term evolution of unconfined liquid dominated reservoirs is likely to be dominated by free surface effects such that compressibility usually can be neglected.

It can also be shown (Zais and Bodvarsson, 1980) that field capacitivity or storativity due to the free surface effect is much larger than the capacitivity due to compressibility. If $(\Delta Q/\Delta P)_c$ is the amount of liquid mass released, per unit pressure decline, due to compressibility and $(\Delta Q/\Delta p)_f$ that released due to the

free surface effect, the ratio between the two can be shown to equal (Zais and Bodvarsson, 1980)

$$(17) \qquad \frac{(\Delta Q/\Delta p)_c}{(\Delta Q/\Delta p)_f} = \frac{\rho S H}{\phi/g}$$

where H is the reservoir thickness. Thus the ratio between the pressure declines equals

$$(18) \qquad \frac{(\Delta p)_f}{(\Delta p)_c} = \frac{\rho g S H}{\phi} \frac{\Delta Q_f}{\Delta Q_c}$$

At a constant flow rate q, $\Delta Q = qT$ and

$$(19) \qquad \frac{(\Delta p)_f}{(\Delta p)_c} = \frac{\rho g S H}{\phi} \frac{T_f}{T_c}$$

where T_f and T_c are the time scales of the free surface and compressibility effects, respectively. Using equations (13) and (14) we obtain

$$(20) \qquad \frac{(\Delta p)_f}{(\Delta p)_c} = \frac{H}{L}$$

and if H and L are of the same order of magnitude, the pressure decline due to the two different effects will be of the same order.

4. Short Term Compressibility Dominated Solutions

Before we turn to long term free surface dominated processes let us briefly consider the short term compressibility dominated case by stating a few important results for homogeneous, isotropic and isothermal Darcy-

type formations. The most fundamental solutions to problem (7) is the whole space Green's function or impulse response k(P,Q,t) at a field point P due to an impulsive unit mass source at a point Q at time $t = o^+$, or

$$(21) \qquad f = \delta(P-Q)\ \delta_+(t)$$

Thus (Carslaw and Jaeger, 1959)

$$(22)\quad k(P,Q,t) = \frac{1}{8\rho S}\ \frac{1}{(\pi a t)^{3/2}}\ \exp(-r_{PQ}^2/4at)\ U_+(t)$$

where r_{PQ} is the distance between P and Q and $a = c/\rho S$ is the hydraulic diffusivity. The pressure field due to a more general source rate f(t) at the point Q is then obtained by (Duff and Naylor, 1966)

$$(23)\quad p(P,t) = \int_o^t k(P,Q,t-\tau)f(\tau)d\tau$$

Of particular interest is the response to a constant source rate $f(t) = f_o$ or the step response

$$(24)\quad p(P,t) = \frac{f_o}{4\pi r_{PQ} c}\ \operatorname{erfc}\left[r_{PQ}/2(at)^{1/2}\right] = \frac{f_o}{8\rho S}\int_o^t \frac{1}{(\pi a\tau)^{3/2}}\ \exp(-r_{PQ}^2/4a\tau)d\tau$$

The corresponding solution in the case of two-dimensional flow, due to a line source of strength f_o, in a slab of thickness b is

$$(25)\qquad \begin{aligned} p(P,t) &= -\frac{f_o}{4\pi bc}\,\mathrm{Ei}[-r_{PQ}^2/4at] \\ &= \frac{f_o}{4\pi bc}\int_o^t \frac{1}{\tau}\,\exp(-r_{PQ}^2/4a\tau)d\tau. \end{aligned}$$

This expression is the so-called Theis-solution which is very commonly used as the basis for the interpretation of well test data.

5. General Half-Space Free Surface Solutions

Turning now to the long term free surface dominated case we are interested in general solutions to problem (6) when compressibility can be neglected, the domain B is the half-space and the conductivity c(P) is inhomogeneous and anisotropic, that is

$$(26)\qquad c(P) = \begin{bmatrix} c_x(P) & 0 & 0 \\ 0 & c_y(P) & 0 \\ 0 & 0 & c_z(P) \end{bmatrix}.$$

Two specific cases are of interest here. First the source free case with a given initial free surface

amplitude $h_o(S)$, where S is a point on Σ

$$
\begin{aligned}
&- \nabla\cdot(c\nabla p) = o \quad , \quad z > 0 \\
&\partial_t p - w\partial_z p = o \quad , \quad z = 0;\ w = w(S) \\
&p = \rho g h_o \quad , \quad t = o;\ z = o
\end{aligned}
\tag{27}
$$

Second the case with a source density f(P)

$$
\begin{aligned}
&- \nabla\cdot(c\nabla p) = f \quad , \quad z > 0 \\
&\partial_t p - w\partial_z p = 0 \quad , \quad z = 0;\ w = w(S) \\
&p = 0 \quad , \quad t = 0;\ z = 0
\end{aligned}
\tag{28}
$$

To solve (27) we first solve

$$
\begin{aligned}
&- \nabla\cdot(c\nabla p_1) = o \quad , \quad z > o \\
&p_1 = p_o \quad , \quad z = o
\end{aligned}
\tag{29}
$$

and use the fact that $p_1(Pt)$, where $Pt = (x,y,z + wt)$, then solves (27). To solve (29) we use the results in Appendix A

$$
p_1(P) = - \int_{\Sigma} c_z(Q) \ \frac{\partial G(P,Q)}{\partial n_Q} \ p_o(Q) dS_Q \tag{30}
$$

where G(P,Q) is the Dirichlet type Green's function for the half-space, or the solution to

$$
\begin{aligned}
&- \nabla\cdot(c\nabla G(P,Q)) = \delta(P-Q), \ z > o \\
&G(P,Q) = o \quad , \quad z = o
\end{aligned}
\tag{31}
$$

Thus we obtain the general solution to (27), the source

free case

$$(32)\quad p(P,t) = -\int_{\Sigma} c_z(Q)\ \frac{\partial G(Pt,Q)}{\partial n_Q}\ p_o(Q)\,dS_Q U_+(t)$$

where $p_o = \rho g h_o$.

To solve (28) we first solve

$$(33)\qquad \begin{aligned} -\nabla\cdot(c\nabla p_1) &= f \quad , \quad z > o \\ \partial_z p_1 &= o \quad , \quad z = o \end{aligned}$$

and then solve

$$(34)\qquad \begin{aligned} -\nabla\cdot(c\nabla p_2) &= o \quad , \quad z > o \\ p_2 &= -p_1 \quad , \quad z = o \end{aligned}$$

The solution of (28) is then given by

$$p(P,t) = p_1(P) + p_2(Pt)$$

where Pt is defined as above. Note that p(P,t) satisfies the free surface condition as well as the initial condition. To solve (33) we use again the results in Appendix A

$$(35)\qquad p_1(P) = \int_B N(P,Q) f(Q)\,dV_Q$$

where N(P,Q) is the Neumann type Green's function or Neumann function (Duff and Naylor, 1966) for the half-space, or the solution to

$$
\begin{aligned}
-\nabla\cdot(c\nabla N(P,Q)) &= \delta(P-Q) \quad , \quad z > o \\
\frac{\partial N(P,Q)}{\partial n_P} &= o \quad , \quad z = o
\end{aligned}
\tag{36}
$$

The solution to (34) is the same as the solution to (29). Thus we obtain the general solution to (28), the case with sources

$$
\begin{aligned}
p(P,t) &= \int_B N(P,Q)f(Q)dV_Q U_+(t) \\
&+ \int_\Sigma c_z(Q)\,\frac{\partial G(Pt,Q)}{\partial n_Q} \int_B N(Q,R)f(R)dV_R dS_Q U_+(t)
\end{aligned}
\tag{37}
$$

It should be noted here that implicit in the above are assumptions on the existence of the Green's functions. The question of existence is of course dependent on c(P). From the point of view of pure mathematics these results are thus incomplete unless we prove the existence of these functions. However, these proofs are beyond the scope of this work and we can be sure that in all physically realistic cases solutions exist.

We are also interested in the pressure response due to a general variable source density f(P,t), which is given by

$$(38) \qquad p(P,t) = \int_0^t \int_B f(Q,t)k(P,Q,t-\tau)dV_Q d\tau$$

where

$$k(P,Q,t) = N(P,Q)\delta_+(t)$$

$$(39) \qquad + \int_\Sigma c_z(R) \frac{\partial G(Pt,R)}{\partial n_R} N(R,Q)dS_R\delta_+(t)$$

$$+ \int_\Sigma c_z(R) \frac{\partial^2 G(Pt,R)}{\partial t \partial n_R} N(R,Q)dS_R U_+(t)$$

6. The Homogeneous and Isotropic Unconfined Half-Space

Turning to more specific cases, let us first consider the long term response of an unconfined half-space, which is homogeneous, isotropic and isothermal such that $c(P) = c$ is constant. The initial fluid surface coincides with the $z = o$ plane and a concentrated sink of strength f_o is located at the point $Q = (o,o,d)$ (Figure 8), starting to withdraw fluid at time $t = o^+$. The solution is given by equation (37) with

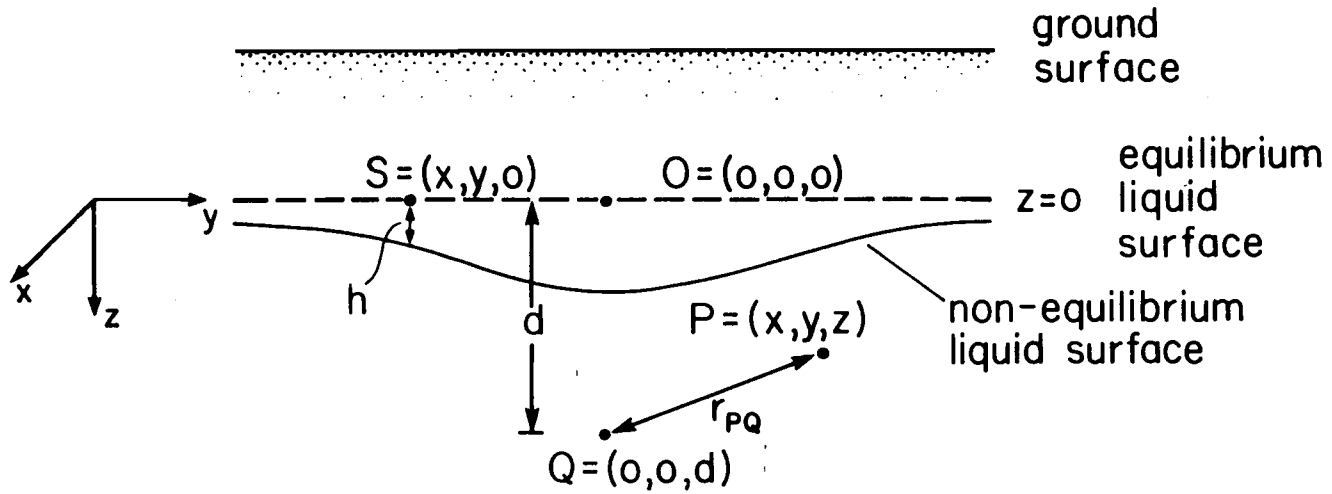

Figure 8. The unconfined half-space reservoir.

$$f(P) = - f_o \, \delta(P-Q) U_+(t)$$

$$(40) \qquad G(P,Q) = \frac{1}{4\pi c r_{PQ}} - \frac{1}{4\pi c r_{PQ'}}$$

$$N(P,Q) = \frac{1}{4\pi c r_{PQ}} + \frac{1}{4\pi c r_{PQ'}}$$

where

$$(41) \qquad r_{PQ} = (x^2+y^2+(z-d)^2)^{1/2}$$

$$r_{PQ'} = (x^2+y^2+(z+d)^2)^{1/2}$$

Using the following (see Appendix B)

$$(42) \qquad \int_\Sigma \frac{\partial G(P,R)}{\partial n_R} N(R,Q) dS_R = \frac{1}{2\pi c} \frac{z}{2\pi} \int_\Sigma \frac{1}{r_{PR}^3 \, r_{RQ}} dS_R = \frac{1}{2\pi c r_{PQ'}}$$

we obtain the pressure response of the half-space:

$$(43) \qquad p(P,t) = \frac{-f_o}{4\pi c} \left[\frac{1}{r_{PQ}} + \frac{1}{r_{PQ'}} - \frac{2}{r_{PQ't}} \right] U_+(t)$$

where

$$(44) \qquad r_{PQ't} = (x^2+y^2+(z+wt+d)^2)^{1/2}$$

This is the solution derived by Bodvarsson (1977).

The elevation of the free surface, due to the point sink, is then given by

$$h(S,t) =$$

$$(45) \qquad \frac{-f_o}{2\pi\rho g c d} \left[\frac{1}{((r/d)^2+1)^{1/2}} - \frac{1}{((r/d)^2+(1+wt/d)^2)^{1/2}} \right]$$

where S = (x,y,o) and $r = (x^2 + y^2)^{1/2}$ the radial coordinate. Directly above the sink

$$(46)\quad h(S,t) = \frac{-f_o}{2\pi\rho g c d}\left(\frac{wt/d}{1 + wt/d}\right).$$

The elevation of the fluid surface following a period T of constant withdrawal f_o is given by equation (32), or

$$h(S,t) =$$

$$(47)\quad \frac{-f_o}{2\pi\rho g c d}\left[\frac{1}{((r/d)^2+(1+w_\Delta t/d)^2)^{1/2}} - \frac{1}{((r/d)^2+(1+wt/d)^2)^{1/2}}\right]$$

where Δt is the time since the withdrawal stopped and $t = T + \Delta t$. For $\Delta t << T$ the recovery of the water level is given by

$$\Delta h(S,\Delta t) = h(S,T+\Delta t) - h(S,T) =$$

$$(48)\quad \frac{f_o}{2\pi\rho g c d}\left[\frac{1}{((r/d)^2+1)^{1/2}} - \frac{1}{((r/d)^2+(1+w_\Delta t/d)^2)^{1/2}}\right]$$

$$= - h(S,\Delta t)$$

The pressure response to a variable flow rate q(t) is given by

$$(49)\quad p(P,t) = \int_o^t q(\tau)k(P,t-\tau)d\tau$$

with

$$k(P,t) = \frac{-1}{4\pi c}\left[\frac{1}{r_{PQ}} - \frac{1}{r_{PQ'}}\right]\delta_+(t) - \frac{1}{2\pi c}\frac{w(z+wt+d)}{r^3_{PQ't}}U_+(t) \tag{50}$$

7. The Homogeneous and Isotropic Vertical, Unconfined Slab with 2-D Flow

Now let us consider the long term response of a vertical slab of thickness b with a free surface, which is homogeneous, isotropic and isothermal. A line sink of strength f_o/b (kg/sm) is located at depth d, such that the flow is two-dimensional, and the initial free surface is at a depth z = 0 (Figure 9). The solution is again given by (37) with

$$f(P) = -(f_o/b)\delta(y)\delta(z-d)U_+(t)$$

$$G(P,Q) = \frac{-1}{2\pi c}\left[\ln(r_{PQ})-\ln(r_{PQ'})\right] \tag{51}$$

$$N(P,Q) = \frac{-1}{2\pi c}\left[\ln(r_{PQ})+\ln(r_{PQ'})\right]$$

where

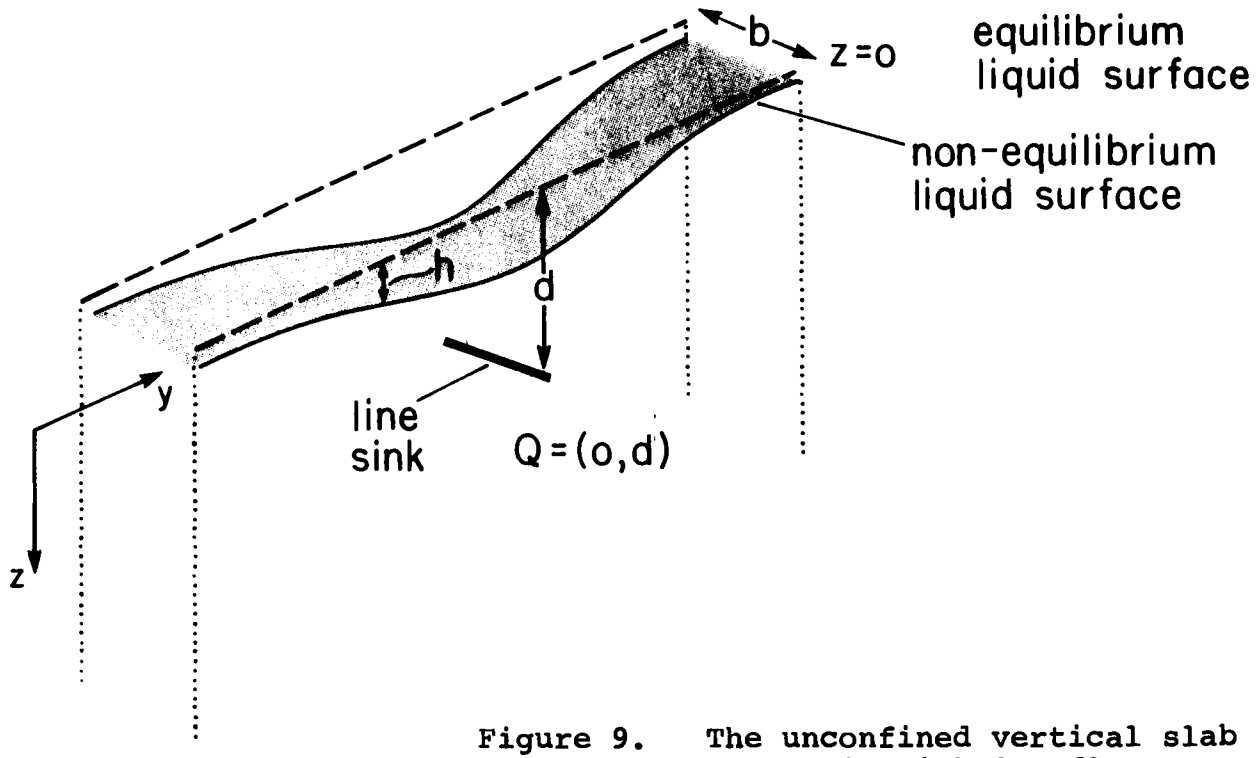

Figure 9. The unconfined vertical slab reservoir with 2-D flow.

$$(52) \qquad r_{PQ} = (y^2+(z-d)^2)^{1/2}$$
$$r_{PQ'} = (y^2+(z+d)^2)^{1/2}$$

Using the results of Appendix B

$$(53)\int_{-\infty}^{\infty} \frac{\partial G(P,R)}{\partial n_R} N(R,Q)dy_R = \frac{1}{\pi c}\frac{z}{2\pi}\int_{-\infty}^{\infty} \frac{\ln(r_{RQ}^2)}{r_{PR}^2} dy_R = \frac{1}{\pi c}\ln(r_{PQ'})$$

we obtain the pressure response of the 2-D slab:

$$(54)\ p(P,t) = \frac{f_o}{2\pi bc}\left[\ln(r_{PQ})+\ln(r_{PQ'})-2\ln(r_{PQ't})\right]U_+(t)$$

where $r_{PQ't}$ is defined as above.

The elevation of the free surface is given by

$$(55) \qquad h(S,t) = \frac{f_o}{2\pi\rho gbc} \ln\left[\frac{(y/d)^2+1}{(y/d)^2+(1+wt/d)^2}\right]$$

where S = (y,o). Directly above the sink

$$(56) \qquad h(O,t) = -\frac{f_o}{\pi\rho gbc}\ln(1+wt/d).$$

The elevation of the fluid surface following a period T of constant withdrawal f_o is

$$(57) \qquad h(S,t) = \frac{f_o}{2\pi\rho gbc}\ln\left[\frac{(y/d)^2+(1+w\Delta t/d)^2}{(y/d)^2+(1+wt/d)^2}\right]$$

where Δt and t are as defined earlier. For $\Delta t << T$ the recovery of the water level is

$$\Delta h(S,\Delta t) = h(S,T+\Delta t) - h(S,T)$$

$$(58) = \frac{f_o}{2\pi\rho gbc} \ln\left[\frac{(y/d)^2+(1+wt/d)^2}{(y/d)^2+1}\right] = - h(S,\Delta t)$$

To calculate the pressure response due to a variable flow rate q(t) we use

$$k(P,t) = \frac{1}{2\pi bc}\left[\ln(r_{PQ}) - \ln(r_{PQ'})\right] \delta_+(t)$$

$$(59) \qquad - \frac{1}{\pi bc} \frac{w(z+wt+d)}{r^2_{PQ't}} U_+(t)$$

and equation (49).

8. The Unconfined, Horizontal Slab Reservoir

We are also interested in the free surface response of more limited reservoirs with 3-D flow. Let us consider an unconfined aquifer of infinite areal extent but of finite thickness D. Let there be a sink of strength f_o at the point Q = (o,o,d) starting at time o^+ and let the initial fluid surface coincide with the z = o plane (Figure 10). We can solve this problem as outlined in section 5 above by using the method of images (Duff and Naylor, 1966) to find the Green's functions. It is,

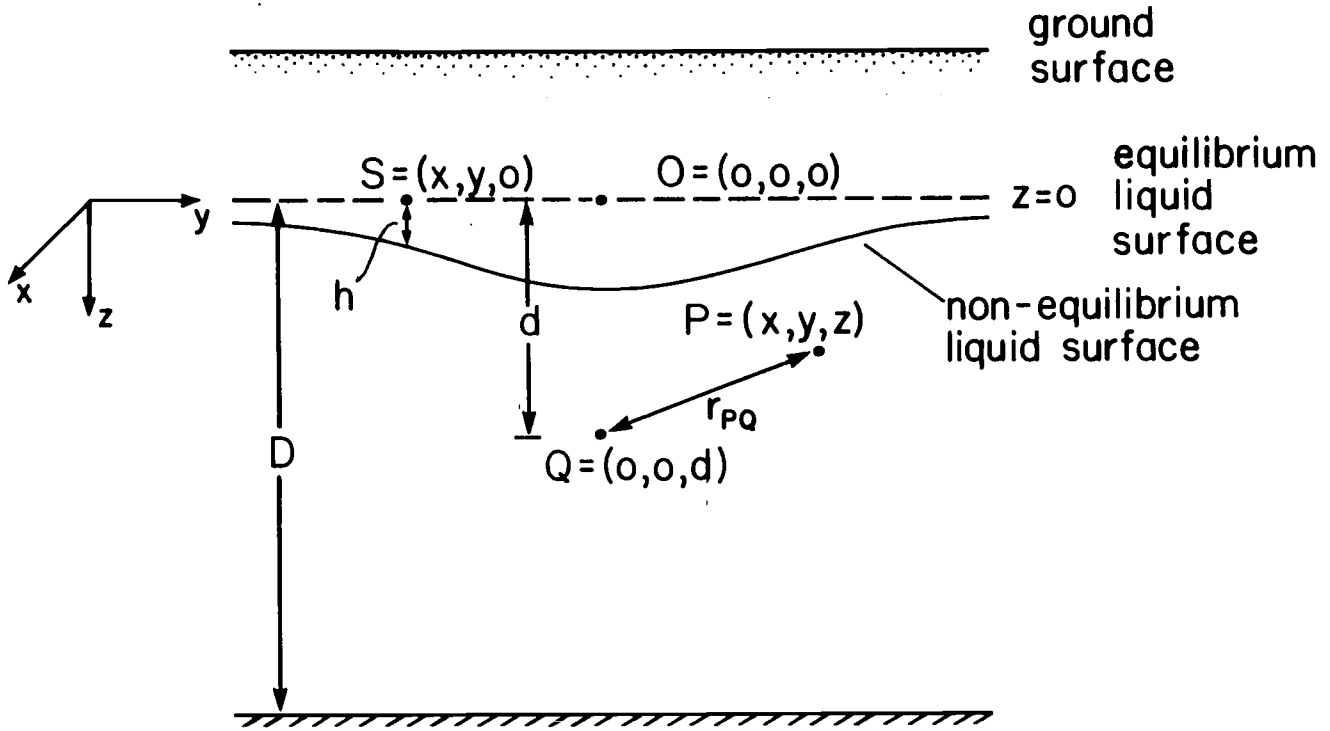

Figure 10. The unconfined horizontal slab reservoir.

however, of interest to solve this problem directly by a different method as outlined below.

Writing the Laplacian operator in cylindrical coordinates, we now need to solve

$$(60)\quad \frac{1}{r}\,\partial_r\,(r\,\partial_r p) + \partial_z^2 p = f_o\,\frac{\delta_+(r)}{2\pi c r}\,\delta(z-d)U_+(t)$$

where r is the radial coordinate. Our solution will have to satisfy the free surface condition (12) as well as a no flow condition at the bottom of the aquifer

$$(61)\qquad \partial_z p = o \qquad \text{at} \qquad z = D,$$

and the initial condition p = o when t = o. To solve we employ the Hankel transform (Duff and Naylor, 1966) and equation (60) is transformed into

$$(62)\quad \partial_z^2 \hat{p} - k^2 \hat{p} = \frac{f_o\,\delta(z-d)U_+(t)}{2\pi c}$$

where $\hat{p}$ is the transformed pressure and k the transform variable

$$(63)\qquad \hat{p}(k) = \int_o^\infty rp(r)J_o(kr)dr$$

$$p(r) = \int_o^\infty k\hat{p}(k)J_o(kr)dr$$

The general solution of (62) is

$$\begin{aligned} \hat{p}(k,z,t) &= A(k,t)e^{kz} + B(k,t)e^{-kz} \quad , \quad z < d \\ \hat{p}(k,z,t) &= C(k,t)e^{kz} + D(k,t)e^{-kz} \quad , \quad z > d \end{aligned} \tag{64}$$

This solution must satisfy the boundary conditions (12) and (61), be continuous at z = d and satisfy the source condition

$$\partial_z \hat{p}(k,d^+,t) - \partial_z \hat{p}(k,d^-,t) = \frac{f_o}{2\pi c} \tag{65}$$

After some algebra we arrive at the following solution:

$$\hat{p}(k,z,t) = F(e^{kz}+e^{-kz}) - \frac{2F}{(1+e^{-2kD})} e^{-wkRt} (e^{-k(2D-z)} + e^{-kz}) \tag{66}$$

$$F = - f_o \frac{e^{-kd}}{4\pi ck} \frac{(1+e^{-2k(D-d)})}{(1 - e^{-2kD})}$$

$$R = \frac{1 - e^{-2kD}}{1 + e^{-2kD}}$$

This solution can be inverted analytically, by expanding it in a series. Thus we obtain the same type of solution as by the method of images mentioned above. More conveniently the inverse Hankel transform can be calculated numerically.

Note that if we let $D \to \infty$ in (66) we obtain

$$\hat{p}(k,z,t) = \tag{67}$$

$$\frac{-f_o}{4\pi ck} \left[e^{-k(d-z)} + e^{-k(d+z)} - 2e^{-k(d+z+wt)}\right]$$

and inverting we obtain the same solution as in section 6 (equation (44)), as expected.

Finally, the Hankel transform of the water level is given by

$$\hat{h}(k,t) = \frac{f_o e^{-kd}}{2\pi c\rho g} (1 - e^{-wkRt}) \frac{(1 + e^{-2k(D-d)})}{(1 - e^{-2kD})} \tag{68}$$

By inverting this solution numerically we obtain the results in Figure 11, which present the free surface response of a finite thickness aquifer as well as that of a half-space aquifer for comparison.

9. The Unconfined Box-Type Reservoir

As the last specific case of the long term free surface response of a liquid reservoir let us consider the homogeneous, isotropic and isothermal box-type domain of Figure 12, with Σ the equilibrium free surface. We will derive the impulse response instead of the step response as in the last three sections, the step response

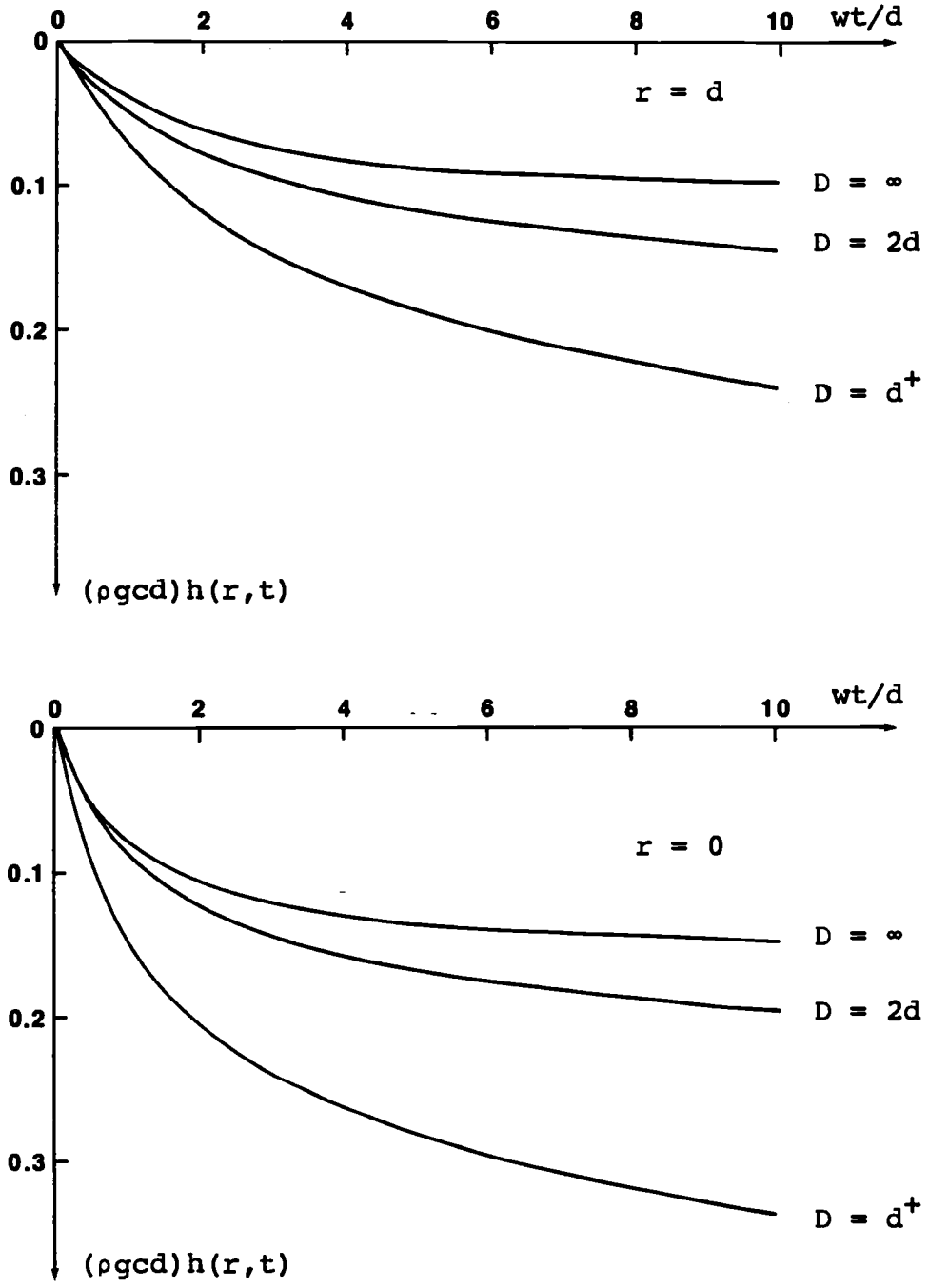

Figure 11. The free surface response of a horizontal slab reservoir of thickness D, at S = (r,0), due to an unit sink at Q = (0,d).

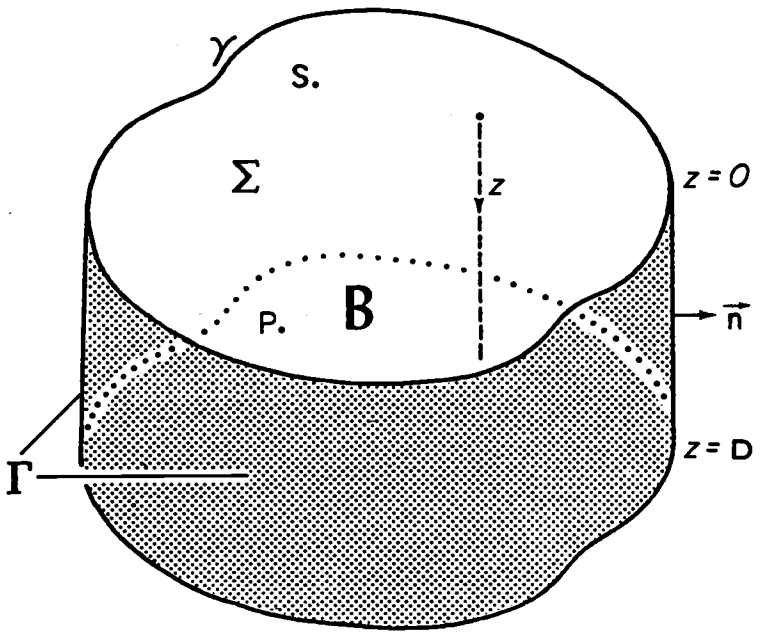

Figure 12. The unconfined box-type reservoir.

is then simply given by (49). The solution below has been presented by Bodvarsson (1984).

To obtain the pressure impulse response, k, due to an impulsive unit mass source at the point Q = (o,o,d), at time $t = o^+$, we need to solve

$$(69) \quad -\nabla^2 k = \delta(S-O)\delta(z-d)\delta_+(t)/c$$

where S = (x,y,o), a point in Σ. The pressure has to satisfy (12) in Σ and no-flow boundary conditions on the sides and bottom of the domain. We assume the pressure can be represented by a series in the eigenfunctions $\phi_j(S)$ of the Laplacian in Σ, that is (Bodvarsson, 1984)

$$(70) \quad k(P,t) = \sum_j a_j(t,z)\phi_j(S)$$

where

$$-\nabla_2^2 \phi_j = \lambda_j \phi_j \qquad j = 1,2,\ldots \quad , \quad S \text{ in } \Sigma$$

$$(71) \qquad \partial\phi_j/\partial n = o \qquad S \text{ on boundary of } \Sigma$$

$$\text{and} \qquad \nabla_2^2 = \partial_x^2 + \partial_y^2$$

The eigenfunctions are orthogonal and normalized

$$(72) \quad \int_\Sigma \phi_i(S)\phi_j^*(S)da_S = \delta_{ij}$$

and we can expand (Duff and Naylor, 1966)

$$(73) \quad \delta(S-O) = \sum_j \phi_j(S)\phi_j^*(O)$$

Inserting (70) in (69) and using (71) and (73) we obtain

$$\lambda_j a_j - \partial_z^2 a_j = \delta(z-d)\, \phi_j^*(0)\delta_+(t)/c \qquad (74)$$

Taking the Laplace transform of (74) and (12), with respect to time, where $\hat{a}_j(z,s)$ is the transform of $a_j(z,t)$

$$\lambda_j \hat{a}_j - d^2\hat{a}_j/dz^2 = \delta(z-d)\phi_j^*(0)/c \qquad (75)$$

$$s\hat{a}_j - w\, d\hat{a}_j/dz = o \quad , \quad z = o \qquad (76)$$

Equation (75) is satisfied by

$$\begin{aligned} \hat{a}_j(z,s) &= C_{j1}e^{\lambda_j^{1/2} z} + C_{j2}e^{-\lambda_j^{1/2} z} \quad , \quad z < d \\ \hat{a}_j(z,s) &= C_{j3}e^{\lambda_j^{1/2} z} + C_{j4}e^{-\lambda_j^{1/2} z} \quad , \quad z > d \end{aligned} \qquad (77)$$

This solution must satisfy the boundary conditions, be continuous at z = d and satisfy the source condition

$$(d\hat{a}_j/dz)_{z=d^+} - (d\hat{a}_j/dz)_{z=d^-} = \phi_j^*(0)/c \qquad (78)$$

Omitting some lengthy algebra, we obtain the following solution (Bodvarsson, 1984):

$$k(P,t) = \frac{1}{cA}\,[zU(d-z) + dU(z-d)]\;\delta_+(t)$$

$$(79)\quad + (1/c)\sum_{j=2}^{\infty} E_j\phi_j(S)\phi_j^*(0)\delta_+(t) + (g/\phi A)U_+(t)$$

$$+ (g/\phi)\sum_{j=2}^{\infty} F_j\phi_j(S)\phi_j^*(0)e^{-t/t_j}\,U_+(t)$$

where A is the area of the system in the Σ plane,

$$(80)\qquad t_j = \frac{1}{w\mu_j\,\lambda_j^{1/2}}\ ,$$

$$(81)\qquad \mu_j = \frac{1 - e^{-2\lambda_j^{1/2}D}}{1 + e^{-2\lambda_j^{1/2}D}}\ ,$$

$$E_j = (1/2\lambda_j^{1/2})\,[e^{-\lambda_j^{1/2}(d-z)} + e^{-\lambda_j^{1/2}(2D-d-z)}$$

$$(82)\qquad -e^{-\lambda_j^{1/2}(d+z)} - e^{-\lambda_j^{1/2}(2D\,d+z)}][1 + e^{-2\lambda_j^{1/2}D}]-1$$

and

$$F_j = [e^{-\lambda_j^{1/2}(d+z)} + e^{-\lambda_j^{1/2}(2D+d-z)} + e^{-\lambda_j^{1/2}(2D-d+z)}$$

$$(83)\qquad + e^{-\lambda_j^{1/2}(4D-d-z)}]\,[1 + e^{-2\lambda_j^{1/2}D}]-2$$

The response of the water level to a source of constant strength f_o starting at $t = o^+$, or the step response, is then simply

$$(84)\quad h(S,t) = \frac{f_o}{\phi\rho A}\, t + \frac{f_o}{\phi\rho} \sum_{j=2}^{\infty} F_j \phi_j(S) \phi_j^*(0) t_j (1-e^{-t/t_j})$$

where

$$(85)\quad \begin{aligned} F_j = {} & [e^{-\lambda_j^{1/2} d} + e^{-\lambda_j^{1/2}(2D+d)} + e^{-\lambda_j^{1/2}(2D-d)} \\ & + e^{-\lambda_j^{1/2}(4D-d)}][1 + e^{-2\lambda_j^{1/2} D}]^{-2} \end{aligned}$$

Turning now to a more specific reservoir model, of the box type, let us consider the simple example of a reservoir of circular form of radius R with a source located at depth d on the axis of the system. Then the eigenfunctions and eigenvalues are as follows

$$(86)\quad \begin{aligned} \phi_j(r) &= c_j J_o(\lambda_j^{1/2} r) \\ \lambda_j &= (a_j/R)^2 \end{aligned}$$

where $J_1(a_j) = o \qquad j = 1,2,3...$

and the c_js are normalization constants,

$$(87) \qquad 2\pi c_j^2 \int_o^R J_o^2(\lambda_j^{1/2} r) r dr = 1,$$

thus

$$(88) \qquad c_j = 1/(A^{1/2} |J_o(\lambda_j^{1/2} R)|)$$

The water level step response is then given by

$$(89) \quad \frac{h(S,t)}{R} = \frac{f_o}{cA\rho g}\left[t_D + \sum_{j=2}^{\infty} \frac{F_j}{\mu_j} \frac{J_o(a_j r/R)}{a_j J_o^2(a_j)} (1-e^{-\mu_j a_j t_D})\right]$$

where $t_D = wt/R$ is a dimensionless time. For $r << R$ the solution simplifies further to

$$(90) \quad \frac{h(S,t)}{R} = \frac{f_o}{cA\rho g}\left[t_D + \sum_{j=2}^{\infty} \frac{F_j}{\mu_j a_j J_o^2(a_j)} (1-e^{-\mu_j a_j t_D})\right]$$

Using the above we obtain the results in Figure 13 as examples of the free surface step response of a cylindrical reservoir.

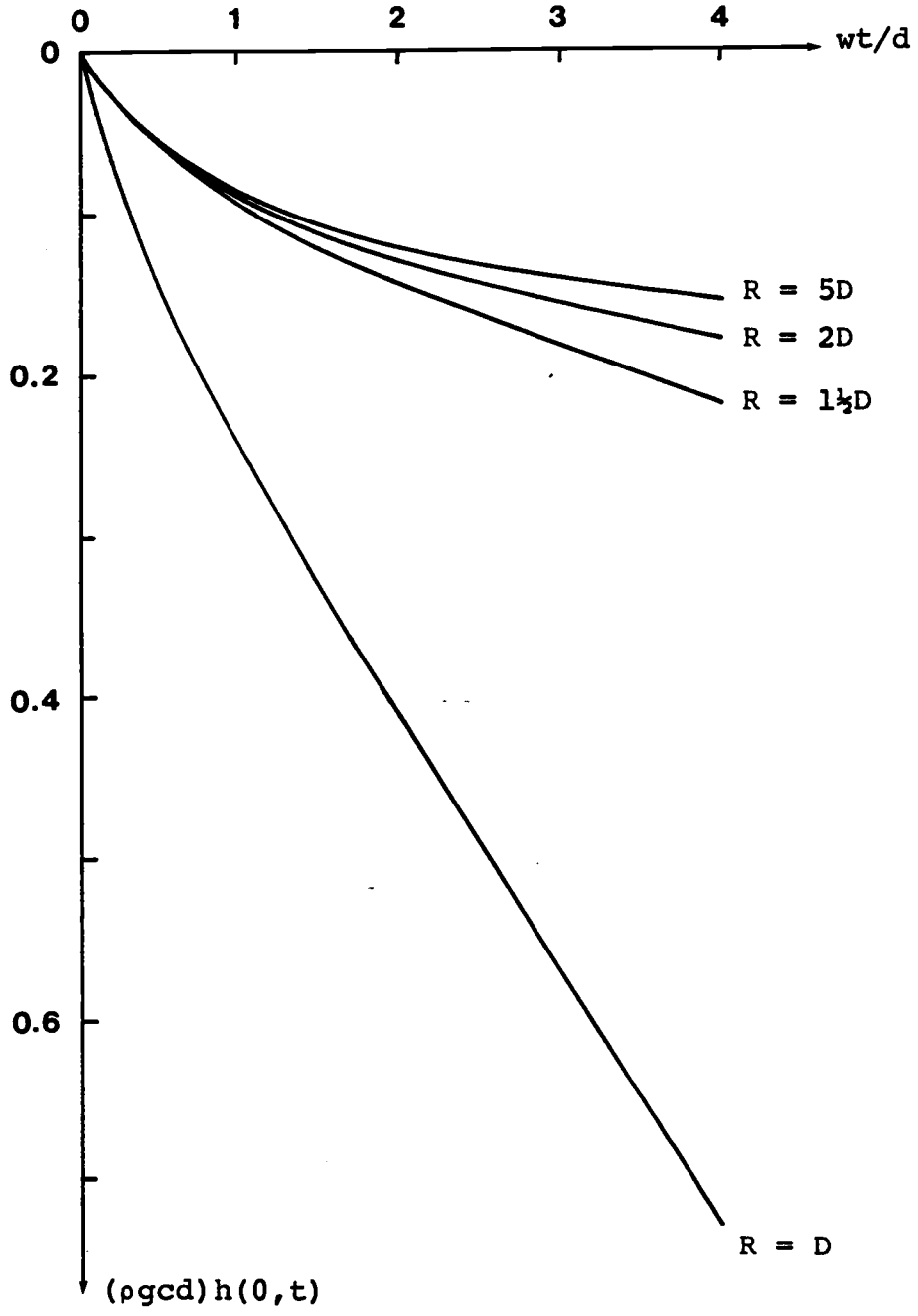

Figure 13. The free surface response of a cylindrical reservoir of radius R and thickness D, at O = (0,0), due to an unit sink at Q = (0,D/2).

10. Discussion of Free-Surface Results

The validity of the small-amplitude approximation (section 2) places some restrictions on the applicability of the above free surface results. The principal criterion is that the liquid level amplitude, directly above the source, be small compared to the source depth d, $h(0,t) \ll d$. This condition places a restriction on the magnitude of mass flows that can be considered. In the specific case of the free surface step response of the half-space (section 6), the linearization is valid for all times if

$$|f_o| \ll 2\pi\rho g c d \tag{91}$$

For the specific example, considered in section 4 above, this constraint implies $|f_o| \ll 6 \times 10^3$ kg/s, such that the linearization would be valid for very large flow rates indeed. The small amplitude condition places similar, yet somewhat greater, restrictions on the results for the other cases.

Considering the 3-D half-space and 2-D vertical slab model results we observe the following: The initial pressure response is instantaneous and at time $t = o^+$ (see equations (43) and (54))

$$(92) \quad p(P,o^+) = \frac{-f_o}{4\pi c}\left[\frac{1}{r_{PQ}} - \frac{1}{r_{PQ'}}\right], \text{ 3-D}$$

$$(93) \quad p(P,o^+) = \frac{f_o}{2\pi bc}\left[\ln(r_{PQ})-\ln(r_{PQ'})\right], \text{ 2-D}$$

This results from the fact that we have neglected compressibility. Only at the free surface, where $r_{PQ} = r_{PQ'}$, is the initial pressure field zero. These results indicate that the free-surface results are more readily applicable to data that represent the true free surface level rather than the pressure at greater depth.

In the 3-D case the water level reaches a stationary level at very large times

$$(94) \quad h_s(S) = \frac{-f_o}{2\pi\rho g c_{(r^2+d^2)^{1/2}}}$$

The free surface drawdown directly above the sink reaches 90% of its stationary value at $t = 9d/w$ and using the same numerical example as before we obtain t = 1 yr. However, in the 2-D case the water level never reaches a stationary value. Directly above the 2-D line sink

$$(95)\quad h(0,t) = \frac{-f_o}{\pi \rho g c b} \ln(wt/d) \quad \text{for} \quad t >> \frac{d}{w}$$

It is of interest to estimate the horizontal distance from the source/sink at which noticeable free surface response occurs. This distance is in the 3-D case given by

$$(96)\qquad \frac{r}{d} < \frac{(1-\chi^2)^{1/2}}{\chi}$$

where χ is the ratio between the free surface amplitudes at the distance r and directly above the source/sink. For $\chi = 1/10$, for example, we obtain $r < 10d$. Based on equation (55) in the 2-D case this distance (y) is given by

$$(97)\quad \left(\frac{y}{d}\right)^2 = \frac{(1+wt/d)^2 - (1+wt/d)^{2\chi}}{(1+wt/d)^{2\chi} - 1}$$

Numerical results are presented in Figure 14. In the 2-D case the drawdown extends much further than in the 3-D case.

Even though simple, the 2-D flow, vertical slab model is more consistent with the apparent linear dike/fracture control of the global hydrothermal flow in Iceland, reviewed in Chapter II above.

It is also of interest to note that in the case of a uniform-unidirectional flow, an open fracture of constant aperture H and a slab of thickness b and conductivity c

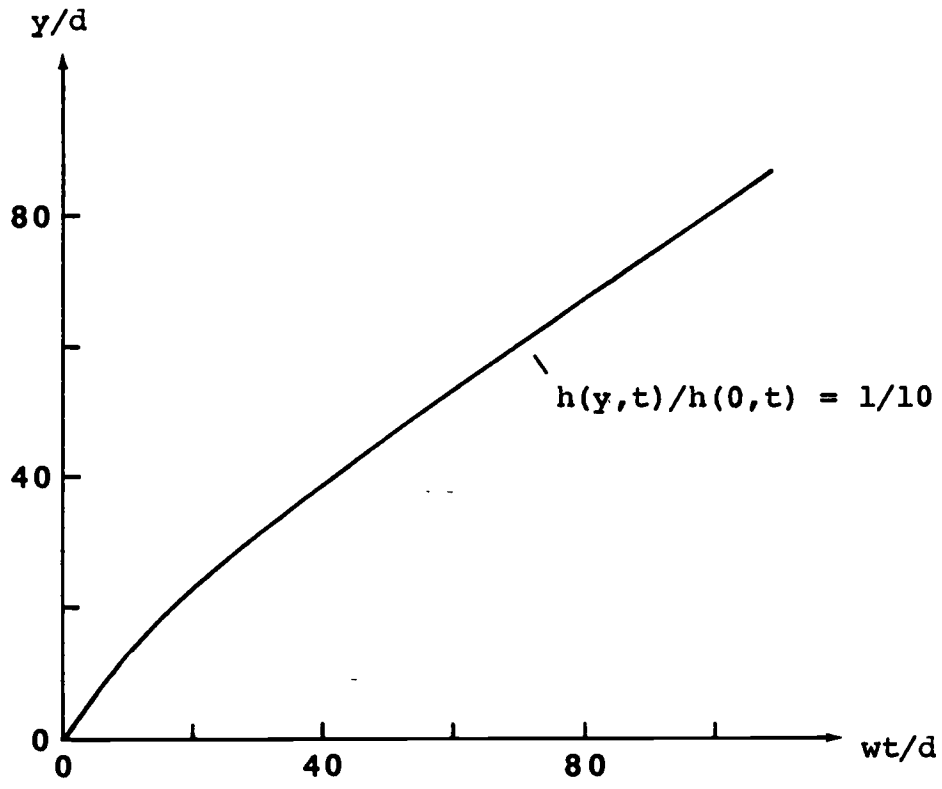

Figure 14. The distance (y) from a source/sink in a vertical slab reservoir with 2-D flow at which noticable free surface response occurs.

are equivalent when (Bodvarsson, 1981)

$$(98) \qquad cb = \frac{H^3}{12\nu}$$

Considering the responses of the other two models we observe the following. The free-surface response of the horizontal slab reservoir (section 8) appears to be unaffected by the limited thickness of the reservoir if the thickness is somewhat greater than twice the source-depth. Furthermore, the response of the box-type reservoir is unaffected by the lateral boundaries, for times of the order of a few w/d, if its radius is somewhat greater than twice the depth of the reservoir.

Based on the results of sections 6 and 7 we observe that following a period of constant withdrawal the functional form of the initial ($\Delta t << t$) water level recovery is antisymmetric (i.e. of same magnitude but opposite sign) to the initial water level drawdown (see equations (48) and (58)). The functional form of the initial water level recovery for the general box-type reservoir (section 9) can be obtained from equations (49) and (79). For $\Delta t << T$

$$\Delta h(S,\Delta t) = h(S,T+\Delta t) - h(S,T)$$

$$(99) \qquad = -\frac{f_o}{\phi\rho} \sum_{j=2}^{\infty} F_j \phi_j(S)\phi_j(0)t_j(1-e^{-\Delta t/t_j}).$$

The initial recovery is obviously not antisymmetric to the initial drawdown unless the surface area of the reservoir A is very large. Thus we can expect buildup and drawdown data to be antisymmetric only for open reservoirs.

We may be interested in using the theoretical results, of the sections above, to estimate some parameters of hydrothermal reservoirs in nature. Unfortunately, the equations for the response of these models are nonlinear in the parameters of interest, w and c, as well as time. However, based on the equations for the free surface response of the 3-D half-space, directly above a point sink, and the 2-D vertical slab, directly above a line sink we can make the following approximations

3-D:

$$h(0,t) = \frac{-f_o}{2\pi\rho g c d} \frac{wt}{d} \quad , \; t << \frac{d}{w}$$

$$h(0,t) = \frac{-f_o}{2\pi\rho g c d} \quad , \; t >> \frac{d}{w} \tag{100}$$

2-D:

$$h(0,t) = \frac{-f_o}{\pi \rho g c d} \quad \frac{wt}{d} \qquad , \; t << \frac{d}{w}$$

(101)

$$h(0,t) = \frac{-f_o}{\pi \rho g c d} \quad \left(\ln \left(\frac{w}{d}\right) + \ln (t)\right), \quad t >> \frac{d}{w}$$

In the 2-D case the water level response following a period of constant production can be approximated

(102) $$h(0,t) = \frac{-f_o}{\pi \rho g c d} \quad \ln\left(\frac{T + \Delta t}{\Delta t}\right) \; , \; \Delta t >> \frac{w}{d}$$

When these approximations apply they can be easily used to simulate field data and hence to estimate the parameters c and w. However, they are of limited validity and later in this chapter a much more general interpretation technique, based on free surface models, will be developed.

11. Lumped Element Networks

Above we have been mainly concerned with deriving the long term responses of some realistic distributed parameter models of hydrothermal systems. This was done to enable the simulation of the observed behavior of hydrothermal systems under production as well as to predict their future behavior. It is, however, often quite helpful to invoke simpler model systems to

approximate the observed response in order to simulate and predict. Because of simple mathematical and physical characteristics, lumped element models consisting of networks of liquid capacitors and conductors are very convenient simulators (Bodvarsson, 1966; Bodvarsson and Axelsson, 1985). In the next three sections we will discuss the theoretical aspects and derive response solutions of such lumped element networks. In later sections we will address the problem of determining the parameters of such simulators from observed response functions.

We will first consider a general network of the type sketched in Figure 15 consisting of a total of N capacitors with capacitances κ_j. The capacitors are linear and time-independent, that is, simple liquid containers with vertical walls of sufficient depth such that they will not be emptied during any admissable flow process. A capacitor has the mass capacitance κ when it responds to a load of liquid mass m with a pressure $p = m/\kappa$, where $\kappa = a/g$ and a is the area of the capacitor. The network capacitors are pairwise connected by up to $N(N-1)/2$ conductors of conductances σ_{ik} ($\sigma_{ii} = 0$). The mass conductance of a conductor is σ when it transfers $q = \sigma \Delta p$ units of liquid mass per unit time at the impressed pressure differential Δp. The particular element σ_{ik} connects the i'th and k'th capacitors and because of

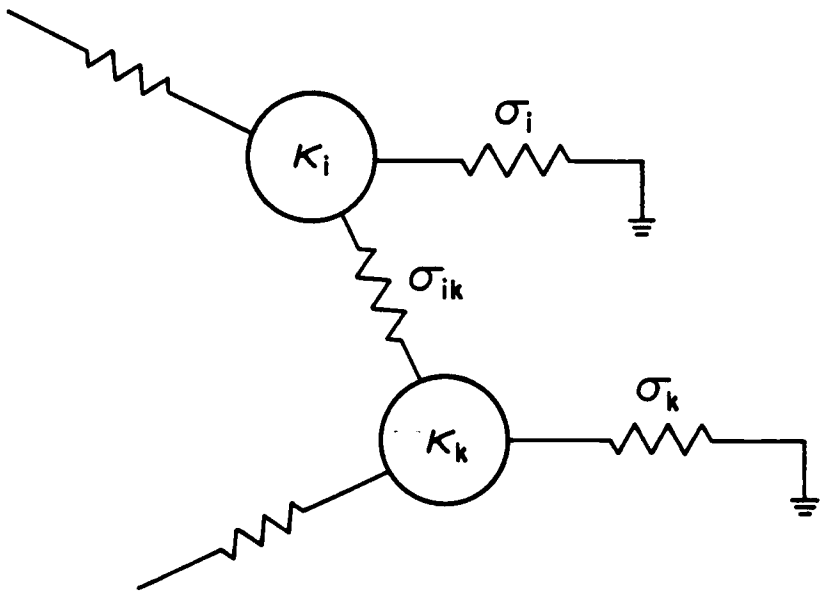

Figure 15. General lumped capacitor/conductor network.

linearity $\sigma_{ik} = \sigma_{ki}$. The network is open in the sense that the i'th capacitor is connected by a conductor of conductance σ_i to an external capacitor that maintains equilibrium pressure of magnitude zero. The network is closed when $\sigma_i = o$ for $i = 1,2...N$.

Let $p_i(t)$ be the pressure in the i'th capacitor and $q_{ik}(t)$ be the mass flow from the k'th to the i'th element. Then the basic equations are the mass flow equations

$$(103) \qquad q_{ik} = \sigma_{ik}(p_k - p_i)$$

and the conservation of liquid mass requires that

$$(104) \qquad \kappa_i \, dp_i/dt = \sum_{k=1}^{N} q_{ik} - \sigma_i p_i + f_i$$

where f_i represents an external source mass flow into the i'th capacitor. Inserting (103) in (104) we obtain the basic system equations

$$(105) \qquad \kappa_i \, dp_i/dt - \sum_{k=1}^{N} \sigma_{ik} p_k + p_i \left(\sum_{k=1}^{N} \sigma_{ik} + \sigma_i\right) = f_i \qquad i = 1,2... N$$

or in matrix form

$$(106) \qquad K \, d\bar{p}/dt + A\bar{p} = \bar{f}$$

where the vectors and matrices are defined as follows

$$
\begin{aligned}
&\bar{p} = (p_i) \\
&\bar{f} = (f_i) \\
&K = (\kappa_i \delta_{ik}) \\
&A = ((\sum_j \sigma_{ij} + \sigma_i)\delta_{ik} - \sigma_{ik})
\end{aligned}
\tag{107}
$$

Note that K is diagonal and A is symmetric.

12. General Solutions for Response of Lumped Networks

To obtain general solutions of the system of equations (106), we first derive the response of the network to an impulsive drive of the k'th capacitor given by $\bar{f}(t) = \bar{\Delta}_k \delta_+(t)$. Here $\bar{\Delta}_k$ is a vector having only one non-vanishing component equal to unity at the k'th entry. The response to this particular drive is $\bar{h}_k(t)$, the k'th impulse response vector of the network that is the solution of

$$K\, d\bar{h}_k/dt + A\bar{h}_k = \bar{\Delta}_k \delta_+(t) \tag{108}$$

If the network is driven by a general causal drive $\bar{f}(t)$, and can be taken to be in equilibrium at t = o, the response is obtained by

$$p(t) = \sum_{k=1}^{N} \int_0^t \bar{h}_k(t-\tau) f_k(\tau)\, d\tau\, U_+(t) \tag{109}$$

We will now restate equation (108) as follows

$$(110) \quad d\bar{h}_k/dt + R\bar{h}_k = K^{-1}\bar{\Delta}_k \delta_+(t)$$

where $R = K^{-1}A$ is the decay rate matrix defined by Bodvarsson and Axelsson (1985). Equation (110) can be solved by an operational approach and since R is independent of time we immediately obtain

$$(111) \quad \bar{h}_k(t) = e^{-tR}\, K^{-1}\bar{\Delta}_k U_+(t)$$

where the exponential operator is to be interpreted as follows

$$(112) \quad \bar{h}_k(t) = \left[\sum_{n=o}^{\infty} (-tR)^n/n!\right] K^{-1}\bar{\Delta}_k\, U_+(t)$$

Bodvarsson and Axelsson (1985) point out that (112) represents an iterative solution of (110). This type of solution is of particular importance for computations of $\bar{h}_k(t)$ for small values of time.

Equation (110) can also be solved by considering the associated eigenvector problem

$$(113) \quad A\bar{\tau} = \lambda K\bar{\tau} \quad \text{or} \quad R\bar{\tau} = \lambda\bar{\tau}$$

where $\bar{\tau}$ and λ are the eigenvectors and eigenvalues, respectively. Note that A is real symmetric, but singular in the case of a closed network. In the general case where A is a nonsingular N x N matrix we can

conclude that equation (113) has N distinct real eigenvectors $\bar{\tau}_j$, associated with up to N non-negative real eigenvalues λ_j. We form the eigenvector matrix T out of the column vectors $\bar{\tau}_j$. The eigenvectors can be normalized and are orthogonal in the following sense

$$(114) \qquad \langle \bar{\tau}_i | K\bar{\tau}_k \rangle = \delta_{ik}$$

where the brackets denote an inner product. Thus

$$(115) \qquad T'KT = I$$

where T' is the transpose of the matrix T. We can also show that

$$(116) \qquad TT'K = I$$

Then we can diagonalize the matrix A as follows

$$(117) \qquad T'AT = \Lambda \quad \text{or} \quad A = KT\Lambda T'K$$
$$\text{and} \quad R = T\Lambda T'K$$

where Λ is the diagonal eigenvalue matrix. Using these results we can rewrite solution (111) as

$$(118) \qquad \bar{h}_k(t) = e^{-tT\Lambda T'K} K^{-1}\bar{1}_{\Delta k} U_+(t)$$

and using the fact that if f is an analytic function

$$(119) \qquad f(R) = T\, f(\Lambda) T'K, \quad 1)$$

where $f(\Lambda) = (f(\lambda_i)\delta_{ik})$, and then

$$(120) \qquad \bar{h}_k(t) = T\, e^{-t\Lambda}\, T'\bar{\Delta}_k\, U_+(t)$$

From (120) we obtain the response of the i'th capacitor, in normal mode form (Bodvarsson and Axelsson, 1985)

$$(121) \qquad h_{ik}(t) = \sum_{j=1}^{N} \tau_{ij}\tau_{kj}\, e^{-\lambda_j t}\, U_+(t)$$

The same solution would have been obtained by taking the Laplace-transform of (108)

$$(122) \qquad [sK + A]\hat{\bar{h}}_k = \bar{\Delta}_k$$

and then solving this resulting system of equations to obtain

$$(123) \qquad \hat{h}_{ik}(s) = \sum_{j=1}^{N} \tau_{ij}\tau_{kj}/(s+\lambda_j)$$

---

1) To prove this expand f(R) in power series

$$f(R) = f(o) + f'(o)R + f''(o)\, R^2/2 + \ldots.$$

and use $R^2 = T\Lambda T'KT\Lambda T'K = T\Lambda^2 T'K$

and $R^n = T\Lambda^n T'K.$

The solutions (112), (120) and (121) are equivalent solutions of the basic problem, however, the expressions given by (120) and (121) are convenient for computing long term responses.

In practical situations a step response is often more convenient than the impulse response. The response of the i'th capacitor to a mass flow input $q_k\ U_+(t)$ into the k'th capacitor is obtained by applying the integral (109)

$$(124)\quad p_{ik}(t) = q_k \sum_{j=1}^{N} (\tau_{ij}\tau_{kj}/\lambda_j)(1-e^{-\lambda_j t})U_+(t)$$

It should be mentioned here that closed networks have a singular matrix A such that the lowest eigenvalue $\lambda_1 = 0$. The corresponding eigenvector has the components $\tau_{i1} = V^{-1/2}$ where $V = \sum \kappa_i$. The solution (121) remains valid, but care has to be exercised in the case of the step response where the first term of the sum becomes t/V.

Finally we should point out that when dealing with very simple networks it may be simpler to solve the system of equations (122) directly and then invert, rather than use solution (121).

13. Response of a Simple Lumped Capacitor, Conductor Ladder

For later reference we will now present the response solutions for a simple two capacitor ladder as shown in Figure 16. We will consider the network to be closed (i.e. $\sigma_2 = 0$) as well as open and present the response of the first capacitor to different source situations. We concentrate here on the two capacitor ladder, because of its simple mathematical characteristics yet great simulation power. As a supplement we present the response of a closed three capacitor ladder in Appendix C.

In the case of Figure 8 we have

$$(125) \quad A = \begin{bmatrix} \sigma_1 & -\sigma_1 \\ -\sigma_1 & \sigma_1+\sigma_2 \end{bmatrix}, \quad K = \begin{bmatrix} \kappa_1 & 0 \\ 0 & \kappa_2 \end{bmatrix}$$

and we will consider

$$(126) \quad \bar{f}(t) = \begin{bmatrix} -q_1 \\ q_2 \end{bmatrix}, 0<t\leq T \; ; \; \bar{f}(t) = \begin{bmatrix} 0 \\ q_2 \end{bmatrix}, t>T$$

That is, production from the first capacitor for a period T and a constant flow into the second capacitor. Thus we can consider three different source situations, (i) $q_1 \neq 0$, $q_2 = 0$, (ii) $q_1 = 0$, $q_2 \neq 0$ and (iii) $q_1 \neq 0$, $q_2 \neq 0$.

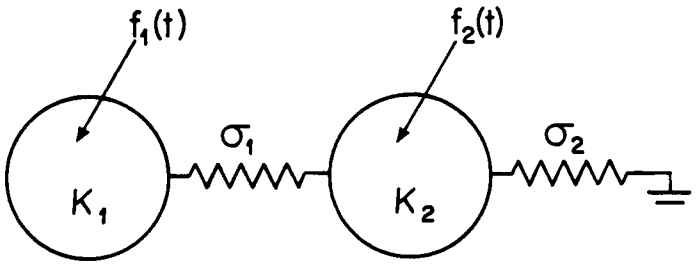

Figure 16. Open two capacitor ladder.

The responses in the different situations are then as follows:

- Open ladder with $q_2 = 0$

$0 < t \leq T$, drawdown:

$$(127)\quad p_1(t) = \frac{-q_1\tau_{11}^2}{\lambda_1}(1-e^{-\lambda_1 t}) - \frac{q_1\tau_{12}^2}{\lambda_2}(1-e^{-\lambda_2 t})$$

$t > T$, buildup:

$$(128)\quad p_1(t) - p_1(T) = \frac{q_1\tau_{11}^2}{\lambda_1}(1-e^{-\lambda_1 T})(1-e^{-\lambda_1 \Delta t}) + \frac{q_1\tau_{12}^2}{\lambda_2}(1-e^{-\lambda_2 T})(1-e^{-\lambda_2 \Delta t})$$

where $\Delta t = t-T$ and

$$\lambda_1 = \frac{1}{2}\left[\frac{\sigma_1+\sigma_2}{\kappa_2} + \frac{\sigma_1}{\kappa_1} - \left(\left(\frac{\sigma_1+\sigma_2}{\kappa_2}\right)^2 + 2\frac{\sigma_1}{\kappa_1}\left(\frac{\sigma_1-\sigma_2}{\kappa_2}\right) + \left(\frac{\sigma_1}{\kappa_1}\right)^2\right)^{1/2}\right]$$

$$\lambda_2 = \frac{1}{2}\left[\frac{\sigma_1+\sigma_2}{\kappa_2} + \frac{\sigma_1}{\kappa_1} + \left(\left(\frac{\sigma_1+\sigma_2}{\kappa_2}\right)^2 + 2\frac{\sigma_1}{\kappa_1}\left(\frac{\sigma_1-\sigma_2}{\kappa_2}\right) + \left(\frac{\sigma_1}{\kappa_1}\right)^2\right)^{1/2}\right]$$

$$(129)\quad \tau_{11}^2 = \frac{\sigma_1^2}{\kappa_1^2\kappa_2} \frac{1}{\left(\frac{\sigma_1}{\kappa_1\kappa_2} + \left(\frac{\sigma_1}{\kappa_1} - \lambda_1\right)^2\right)^2}$$

$$\tau_{12}^2 = \frac{\sigma_1^2}{\kappa_1^2\kappa_2} \frac{1}{\left(\frac{\sigma_1}{\kappa_1\kappa_2} + \left(\frac{\sigma_1}{\kappa_1} - \lambda_2\right)^2\right)^2}$$

- Closed ladder with $q_2 = 0$

$0 < t \leq T$, drawdown:

$$(130)\quad p_1(t) = -\frac{q_1}{A}t - q_1 \frac{\kappa_2}{\kappa_1 A\lambda}\ (1-e^{-\lambda t})$$

$t > T$, buildup:

$$(131)\quad p_1(t)-p_1(T) = q_1 \frac{\kappa_2}{\kappa_1 A\lambda}\ (1-e^{-\lambda T})(1-e^{-\lambda \Delta t})$$

where

$$(132)\qquad \lambda = \sigma_1 \frac{\kappa_1+\kappa_2}{\kappa_1\kappa_2}$$
$$A = (\kappa_1 + \kappa_2)$$

- Closed ladder with $q_1 = 0$

$t > 0$

$$(133)\quad p_1(t) = \frac{q_2}{A}\ t\ - \frac{q_2}{A\lambda}\ (1-e^{-\lambda t})$$

where A and λ are again given by (132).

- Closed ladder with $q_1,\ q_2 \neq 0$

$0 < t \leq T$, drawdown:

$$(134)\quad p_1(t) = \frac{(q_2-q_1)}{A}t - \frac{(\kappa_2 q_1+\kappa_1 q_2)}{\kappa_1 A\lambda}\ (1-e^{-\lambda t})$$

$t > T$, buildup:

$$(135)\quad p_1(t) - p_1(T) = \frac{q_2}{A}\Delta t + \frac{(\kappa_2 q_1(1-e^{-\lambda T}) - \kappa_1 q_2 e^{-\lambda T})}{\kappa_1 A\lambda}(1-e^{-\lambda\Delta t})$$

when $\lambda T >> 1$ and $\Delta t \ll T$ (135) can be written

$$(136)\quad p_1(t)-p_1(T) = \frac{q_2}{A}\Delta t + \frac{q_1\kappa_2}{\kappa_1 A\lambda}(1-e^{-\lambda\Delta t})$$

The response of the still simpler one capacitor open ladder is also of some interest:

$0 < t \leq T$, drawdown:

$$(137)\quad p_1(t) = \frac{-q_1}{\sigma_1}(1-e^{-\sigma_1 t/\kappa_1})$$

$t > T$, buildup:

$$(138)\quad p_1(t)-p_1(T) = \frac{q_1}{\sigma_1}(1-e^{-\sigma_1 T/\kappa_1})(1-e^{-\sigma_1\Delta t/\kappa_1})$$

Based on the above results we make the following observations on the response of the first capacitor:

- The initial buildup and the drawdown for open ladders are antisymmetric, i.e. of the same magnitude but opposite sign.
- The buildup and drawdown of a closed ladder are not antisymmetric, the drawdown is more rapid than the buildup.

- The buildup of a closed two capacitor ladder and the buildup of an open one capacitor ladder have the same functional form.
- We therefore conclude that if the response of a real hydrothermal system can be approximated by the response of a capacitor/conductor ladder we are not able to determine from buildup data whether a system is open or closed. Hence some drawdown data is needed to complement all buildup data (see also section 10 above).

14. Short Term Simulation of Analytical Reservoir Models

Later in this chapter we will consider methods of deriving parameters of simulation ladders for actual production data. At this point, however, we can simulate the responses of analytical reservoir models to demonstrate the efficacy of our methods.

We will here consider short term simulations such that the Taylor series solution given by equation (112) is appropriate. The response of the first capacitor of a simulation ladder to an impulse source in the same capacitor (front end driving point impulse response) is then

$$h_{11}(t) = \left[\frac{1}{\kappa_1} - \frac{\sigma_1}{\kappa_1^2}\,t + \left(\frac{\sigma_1^2}{\kappa_1^3} + \frac{\sigma_1^2}{2\kappa_1\kappa_2}\right)\frac{t^2}{2!}\right.$$

(139)

$$\left. - \left(\frac{\sigma_1^3}{\kappa_1^4} + 2\frac{\sigma_1^3}{\kappa_1^3\kappa_2} + \frac{\sigma_1^2(\sigma_1+\sigma_2)}{2\kappa_1^2\kappa_2}\right)\frac{t^3}{3!} + \ldots\ldots\right] U_+(t)$$

Note that as we proceed up the series each term takes up one, and only one, additional ladder parameter. In other words, the zero'th order term depends on κ_1, the first order term on κ_1 and σ_1, the second order term on κ_1, σ_1 and κ_2, etc. From the derivatives, at t = 0, of the response function we want to simulate, we can thus derive the parameters of the simulation ladder relatively simply. The initial value and the first three derivatives of the ladder impulse response are given by

$$h_{11}(o) = \frac{1}{\kappa_1}$$

$$\dot{h}_{11}(o) = \frac{-\sigma_1}{\kappa_1^2}$$

(140)

$$\ddot{h}_{11}(o) = \frac{\sigma_1^2(\kappa_1+\kappa_2)}{\kappa_1^3\kappa_2}$$

$$h'''_{11}(o) = -\left(\frac{\sigma_1^3}{\kappa_1^4} + 2\frac{\sigma_1^3}{\kappa_1^3\kappa_2} + \frac{\sigma_1^2(\sigma_1+\sigma_2)}{\kappa_1^2\kappa_2^2}\right)$$

As an example of this procedure we will carry out the simulation of the unconfined half-space model by a two capacitor open ladder. The impulse response of the half-space is given by equation (50), and hence

$$k(P,O) = \frac{g}{2\pi\phi d^2}\,\frac{(1+\frac{z}{d})}{((\frac{r}{d})^2+(1+\frac{z}{d})^2)^{3/2}}$$

$$k_t(P,O) = \frac{g}{2\pi\phi d^2}\,\frac{w}{d}\,\frac{((\frac{r}{d})^2-2(1+\frac{z}{d})^2)}{((\frac{r}{d})^2+(1+\frac{z}{d})^2)^{5/2}}$$

(141)

$$k_{tt}(P,O) = \frac{3g(1+\frac{z}{d})}{2\pi\phi d^2}\,(\frac{w}{d})^2\,\frac{(-3(\frac{r}{d})^2+2(1+\frac{z}{d})^2)}{((\frac{r}{d})^2+(1+\frac{z}{d})^2)^{7/2}}$$

$$k_{ttt}(P,O) = \frac{3g(\frac{w}{d})^3}{2\pi\phi d^2}\,\frac{(-3(\frac{r}{d})^4+24(\frac{r}{d})^2(1+\frac{z}{d})^2-8(1+\frac{z}{d})^4)}{((\frac{r}{d})^2+(1+\frac{z}{d})^2)^{9/2}}$$

By equating these results with the results given by equation (140) we obtain ($a = \kappa g$)

$$(142) \qquad a_1 = 2\pi\phi d^2 \frac{((\frac{r}{d})^2+(1+\frac{z}{d})^2)^{3/2}}{(1+\frac{z}{d})}$$

$$(143) \qquad \sigma_1 = 2\pi cd \frac{[2(1+\frac{z}{d})^2-(\frac{r}{d})^2][(\frac{r}{d})^2+(1+\frac{z}{d})^2]^{1/2}}{(1+\frac{z}{d})^2}$$

$$(144) \qquad \frac{a_1}{a_2} = 3(1+\frac{z}{d})^2 \frac{[2(1+\frac{z}{d})^2-3(\frac{r}{d})^2]}{[2(1+\frac{z}{d})^2-(\frac{r}{d})^2]}$$

and finally

$$(145) \qquad \sigma_2 = -\left[\frac{a_1 a_2}{g^2 \sigma_1}\right]^2 k_{ttt}(P,0) - \sigma_1(\frac{a_1+a_2}{a_1})^2$$

Using these results together with equations (127) and (129) we then obtain the response of the simulation ladder in each specific case. Figures 17 through 20 give a few examples of the short term simulation of the pressure unit step response of the unconfined half-space (Figure 8 above) at different field points P = (r,z)

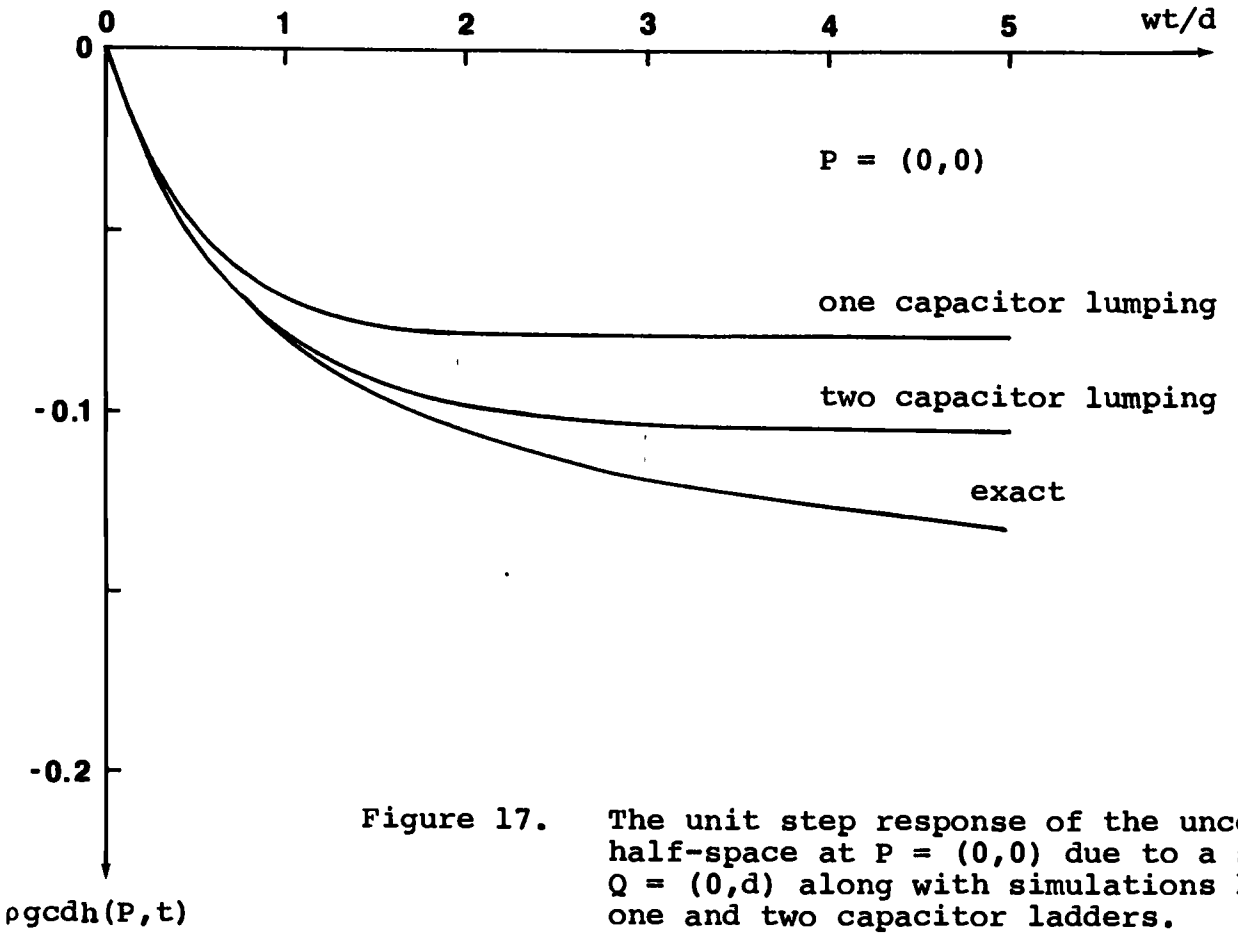

Figure 17. The unit step response of the unconfined half-space at P = (0,0) due to a sink at Q = (0,d) along with simulations by open one and two capacitor ladders.

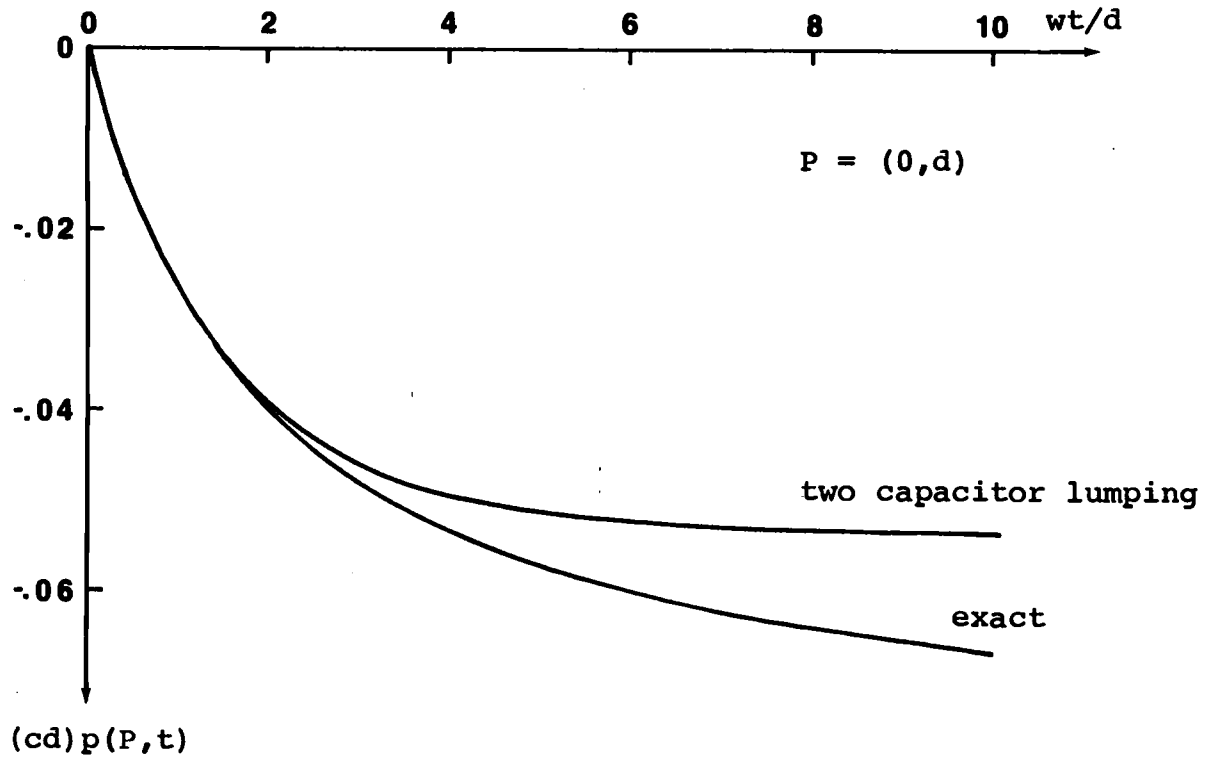

Figure 18. The unit step response of the unconfined half-space at P = (0,d) due to a sink at Q = (0,d) along with a simulation by an open two capacitor ladder.

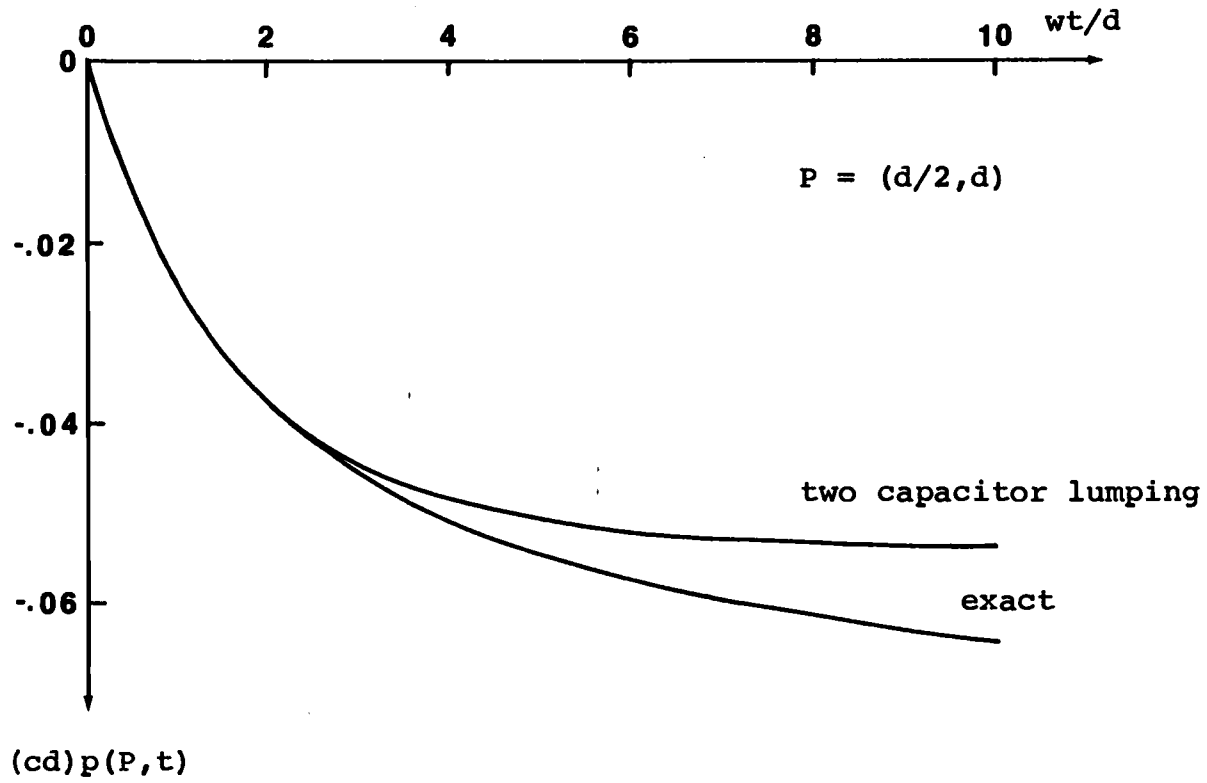

Figure 19. The unit step response of the unconfined half-space at P = (d/2,d) due to a sink at Q = (0,d) along with a simulation by an open two capacitor ladder.

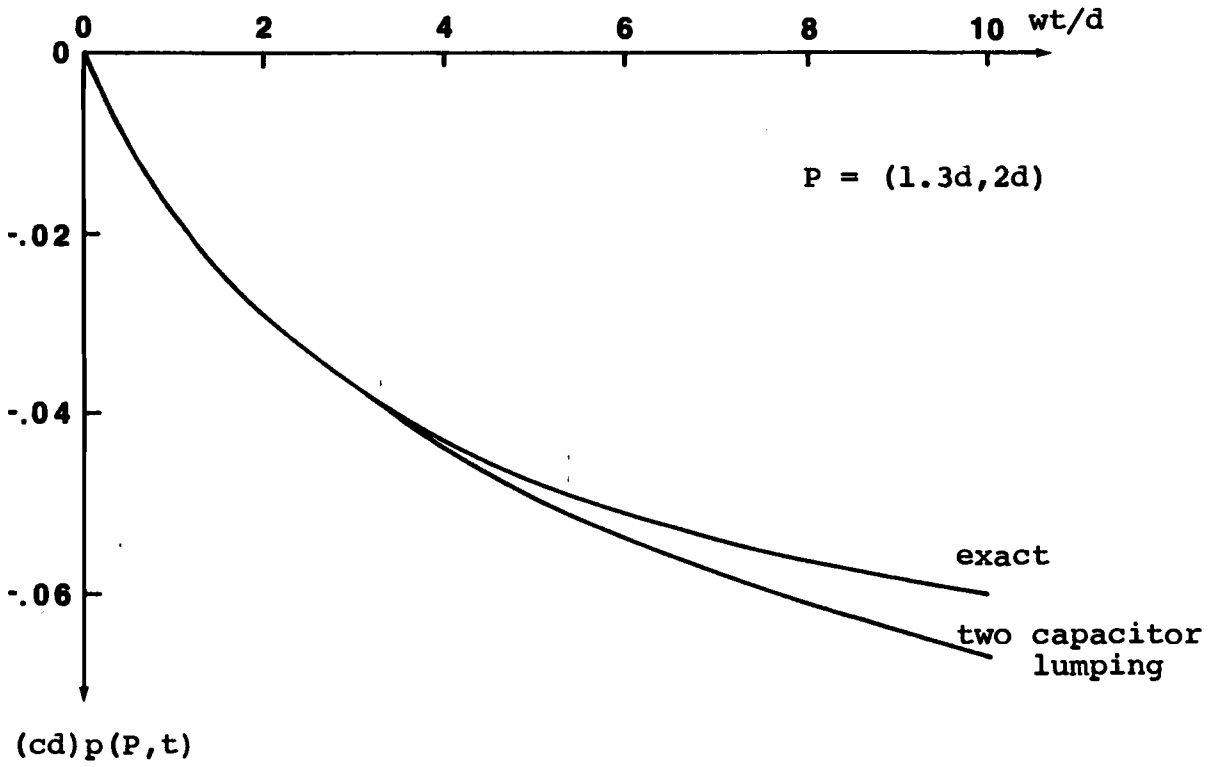

Figure 20. The unit step response of the unconfined half-space at P = (1.3d,2d) due to a sink at Q = (0,d) along with a simulation by an open two capacitor ladder.

caused by a sink at Q = (o,d). The results for the response of the free surface, that is $h(S,t) = p(S,t)/\rho g$, directly above the sink are presented in Figure 17. In this case the parameters of the simulation ladder are simply

$$(146)\qquad \begin{aligned} a_1 &= 2\pi\phi d^2 \\ a_2 &= 4\pi\phi d^2 \qquad \text{for } z = o \\ &\qquad\qquad\qquad\qquad \& \; r << d \\ \sigma_1 &= 4\pi cd \\ \sigma_2 &= 12\pi cd \end{aligned}$$

and the equation for the two capacitor simulation is

$$(147)\qquad p_1(t) = \frac{1}{cd}\left(0.099(1-e^{-1.27t_D}) + 0.0071(1-e^{-4.73t_D})\right)$$

where $t_D = wt/d$. In Figure 17 we also present, for comparison, open one capacitor simulation given by

$$(148)\qquad p_1(t) = \frac{1}{4\pi cd}\left(1-e^{-2t_D}\right)$$

It is evident from the results in Figures 17 through 20 that the short term lumped approximations hold quite well for times up to a few d/w.

It should be pointed out here that the response of the half-space can only be simulated by the ladder front-end driving point response (equation (127)) when the field point P is sufficiently close to the source point

Q. Greater distances between the points would result in negative ladder capacitances or conductances and hence unacceptable results. In the case of the two capacitor simulator the following criterion should hold

$$(149)\quad k_{tttt}(P,0) > \sigma_1^3 \left(\frac{a_1+a_2}{a_2}\right)^2 \left(\frac{g}{a_1}\right)^4$$

which for P = (r,o) implies r < 0.43d.

As further examples of the short term simulation of analytical reservoir models we consider the unconfined box type reservoir (section 9). Here we obtain the derivatives of the response functions numerically and from these we derive the ladder parameters as above. The results for two reservoir geometries, one with R = D and the other with R = 5D, are presented in Figures 21 and 22 and the ladder parameters are listed in Table V. We see that an open second order ladder is a very efficient simulator for the deep reservoir. The simulation of the shallow reservoir is less efficient. Satisfactory simulation is however obtained for t < 1.6d/w.

Methods for long term lumped network simulations of actual reservoir response data are discussed later in this chapter. Using such methods, and closed two capacitor ladders to simulate the response of the box type reservoir we obtain the parameters presented in Table VI. The results can be summarized as follows:

- For the deep reservoir (R/D = 1) the simulation is

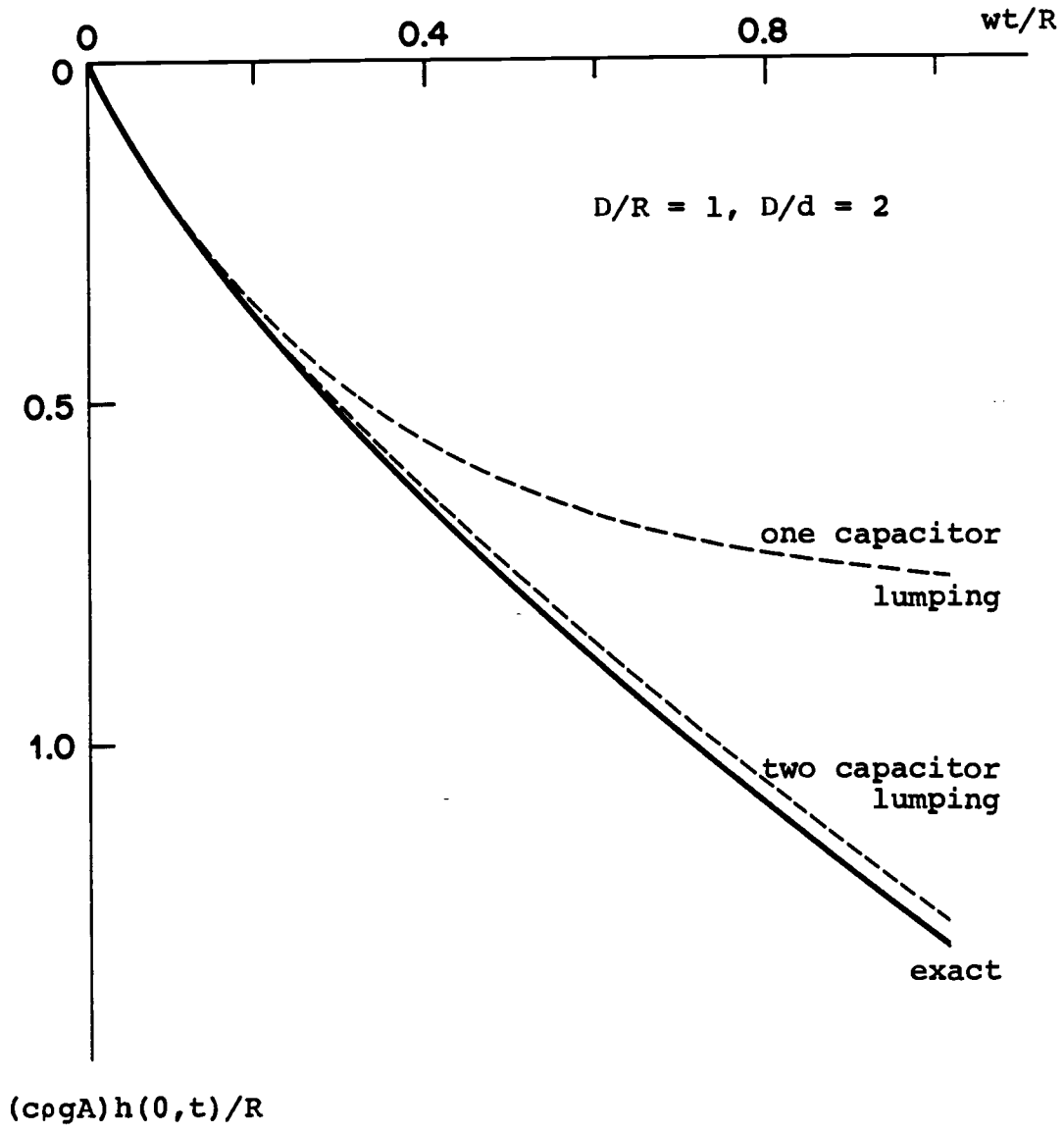

Figure 21. The unit step response of the unconfined cylindrical reservoir with D/R = 1 at P = (0,0) along with short term simulations.

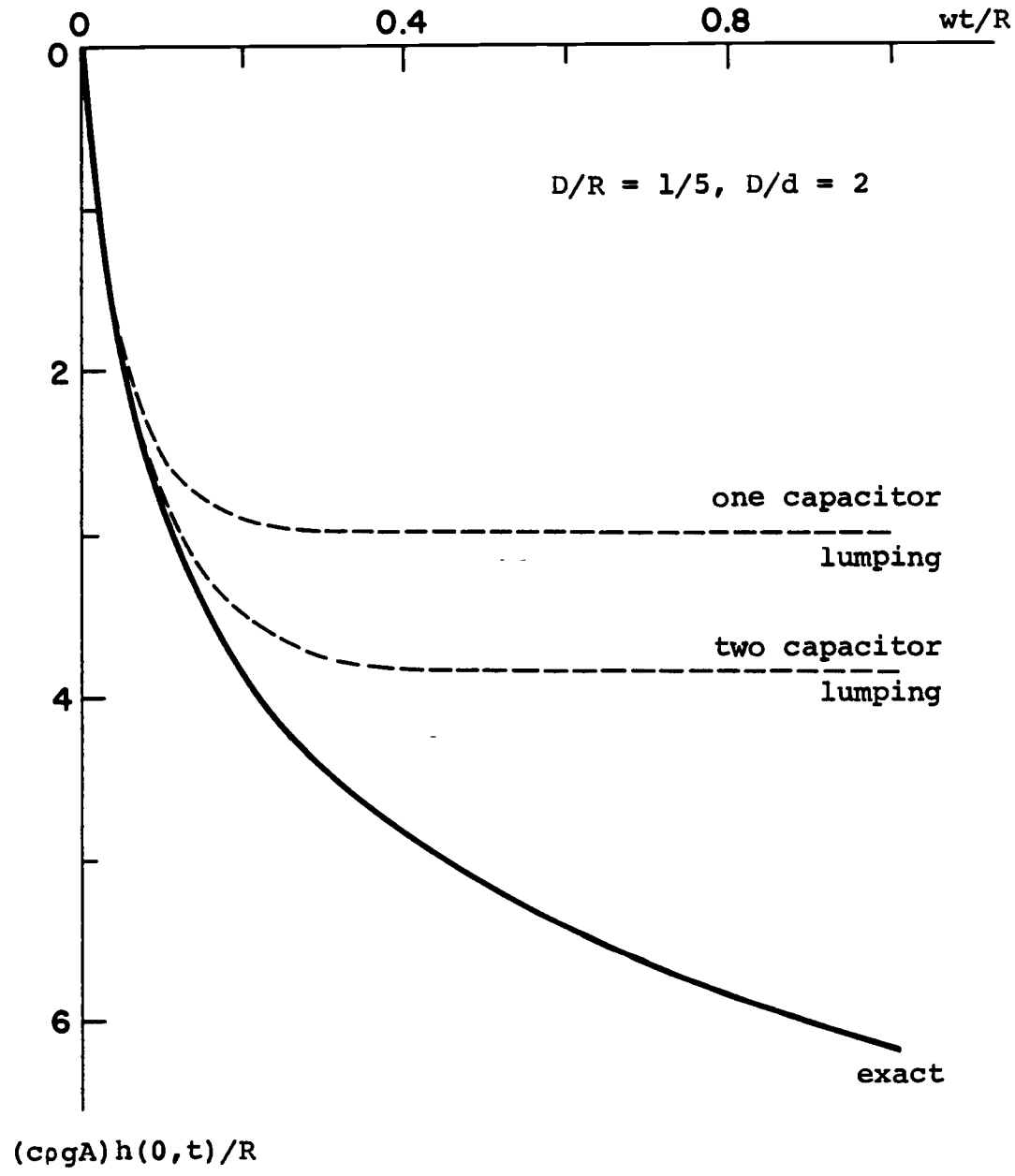

Figure 22. The unit step response of the unconfined cylindrical reservoir with D/R = 1/5 at P = (0,0) along with short term simulations.

Table V Short-term simulation ladder parameters for the response of the unconfined cylindrical reservoir

	R/D = 1	R/D = 5
a_1	0.42 A_ϕ	0.019 A_ϕ
a_2	0.58 A_ϕ	0.033 A_ϕ
σ_1	4.0 Rc	1.1 Rc
σ_2	$\simeq$ 0	2.9 Rc

Table VI Long-term simulation ladder parameters for the response of the unconfined cylindrical reservoir

	R/D = 1	R/D = 5
a_1	0.43 A_ϕ	0.06 A_ϕ
a_2	0.57 A_ϕ	0.94 A_ϕ
σ_1	3.3 Rc	0.5 Rc

highly efficient, so much that for wt/d > 0.1 the deviation is less than 1%, decreasing with increasing time. We see that the ladder parameters are not very different from the parameters used for the short term simulation.

- The results for the long term simulation of the shallow reservoir (R/D = 5) are presented in Figure 23. Here the simulation is only satisfactory for times greater than t = 10d/w. This is reflected in the very different parameters obtained for the short and long term simulations. A third order simulator would, however, be more efficient (Bodvarsson and Axelsson, 1985).

From the above we conclude that the efficacy of simulation by simple ladders (two capacitors) is dependent on the global geometry of the reservoir being simulated. For certain geometries, such as the deep box-type reservoir, this simulation can be excellent. The ratio D/R being close to unity is not atypical for geothermal reservoirs.

15. Unit Step Response from Actual Production Data

Above we have obtained theoretical results on the long term behavior of unconfined aquifers as well as the simulation power of simple lumped element ladders. We are now interested in utilizing these results in

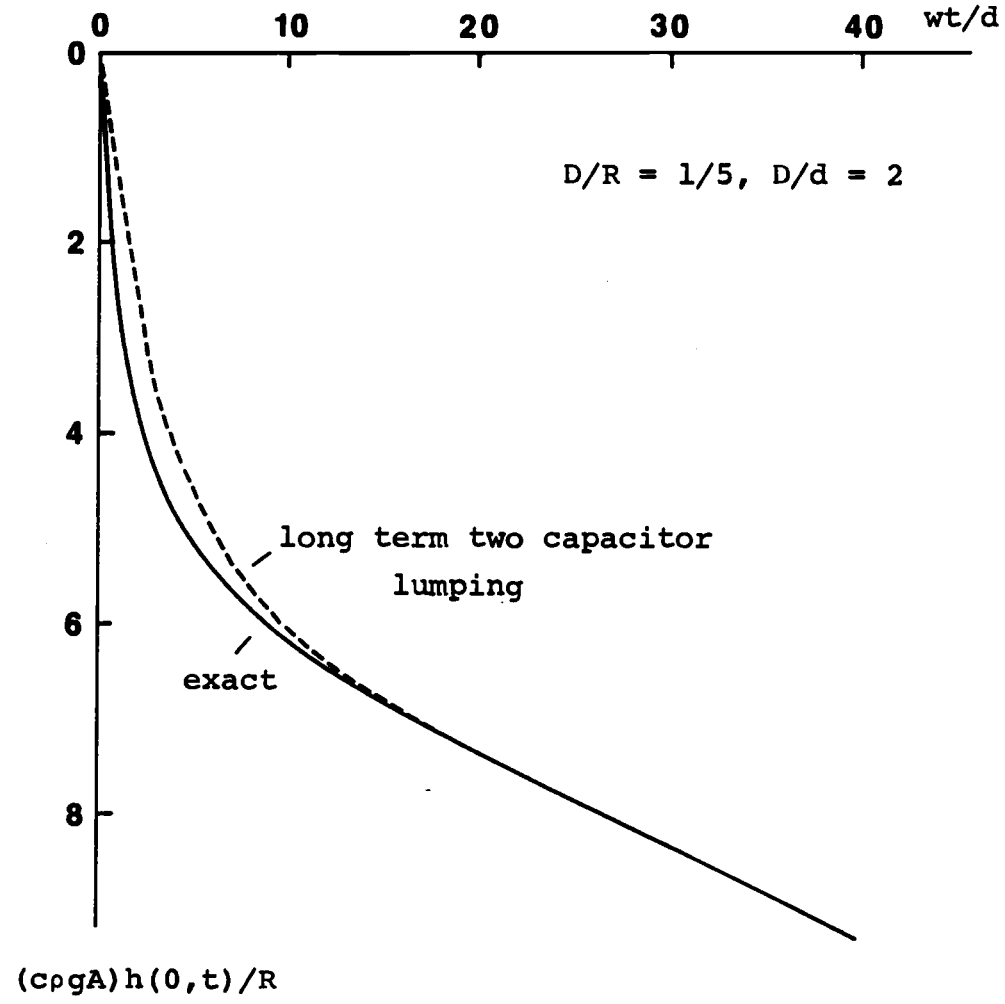

Figure 23. The unit step response of the unconfined cylindrical reservoir with D/R = 1/5 at P = (0,0) along with a long term simulation.

analyzing data on the evolution of actual hydrothermal reservoirs. At this juncture we make the following observation. When comparing the response of an actual reservoir with the response of a theoretical model, the unit step response (or impulse response) of the reservoir is of main interest. In practice geothermal reservoirs are rarely produced at a constant rate over long periods of time. However, knowing the response to a variable production rate, as well as the varying flow rate, one can in principle estimate the step response as follows:

The pressure (or water level) at variable flow rate is given by (see also equations (49) and (109))

$$(150) \quad p(t) = \int_0^t q(t-\tau)G(\tau)d\tau$$

where G(t) is the impulse response and q(t) the flow rate. Then the unit step response equals

$$(151) \quad u(t) = \int_0^t G(\tau)d\tau$$

Here we need to solve the integral equation (150) to obtain G(t). We discretize this problem by approximating

$$(152) \quad q(t) \approx q_i \quad , \quad t_{i-1} \leq t < t_i \quad i = 1,2...N$$

where $t_i = i\Delta t$. Equation (150) can be written

$$(153) \qquad p(t_k) = \sum_{i=i}^{d} \int_{t_{i-1}}^{t_i} q(t_k-\tau)G(\tau)d\tau$$

and $q(t_k-\tau) = q_{(k-i+1)}$ if $t_{i-1} \leq t < t_i$. We define

$$(154) \qquad G_i = \int_{t_{i-1}}^{t_i} G(\tau)d\tau$$

and (153) can be rewritten

$$(155) \qquad p_k = p(t_k) = \sum_{i=1}^{k} q_{(k-i+1)}G_i$$

This equation is easily solved

$$(156) \qquad G_i = \frac{1}{q_i}\left(p_i - \sum_{j=1}^{i-1} q_{(i-j+1)}G_j\right) , \quad i = 1,2...N$$

and we thus obtain the unit step response

$$(157) \qquad u(t_k) = \sum_{i=1}^{k} G_i \quad , \quad k = 1,2,...N$$

Equation (155) can also be set up as a matrix problem

$$(158) \qquad G\bar{m} = \bar{d}$$

where

$$G = \begin{bmatrix} q_1 & 0 & 0 & \cdots & 0 \\ q_2 & q_1 & 0 & \cdots & 0 \\ q_3 & q_2 & q_1 & \cdots & 0 \\ & & & q_1 & \\ q_n & q_{n-1} & q_{n-2} & & q_1 \end{bmatrix} \tag{159}$$

$$\bar{m} = \begin{bmatrix} -G_1 \\ -G_2 \\ \vdots \\ -G_N \end{bmatrix} \quad \text{and} \quad \bar{d} = \begin{bmatrix} -p_1 \\ -p_2 \\ \vdots \\ -p_N \end{bmatrix}$$

Even though the above method produces a solution that exactly fits the data, it is very sensitive to noise in the data (pressure and/or flow rate) and it may easily result in a unit step response that is physically meaningless. It can be shown both on physical grounds and theoretically that the unit step response is a completely monotonous function that must satisfy (Coats et al., 1964):

$$u(t) < o$$

$$\frac{du(t)}{dt} \leq o \tag{160}$$

$$\text{and} \quad \frac{d^2u(t)}{dt} \geq o$$

Coats et al. (1964) suggest using linear programming techniques to find the unit step response that best fits the data as well as satisfying the above constraints. We then need to solve the following problem:

$$\text{Minimize} \quad \sum_i |d_i - (Gm)_i| \tag{161}$$

$$\text{with constraints} \quad m_i > 0 \quad i = 1,2...N$$

$$m_{i-1} - m_i \geq 0 \quad i = 2,....N$$

The above is set up as a linear programming problem in Appendix D.

We are now able to analyze variable flow rate production data for the characteristic unit step response and then compare this with step responses of analytical reservoir models.

16. Non-linear Free Surface Analysis

We are now interested in fitting some theoretical models, specificly models of unconfined reservoirs when compressibility can be neglected, to actual field data and estimate the parameters describing the best fitting models. As mentioned earlier the responses of free surface reservoirs do not depend linearly on the parameters of interest. Below we will develop a non-linear iterative technique for estimating the parameters

describing the model chosen, applicable to variable flow rate data.

We assume the observed pressure is given by equation (49), or

$$(162) \quad p(P,t) = \int_0^t q(\tau)k(P,t-\tau)d\tau$$

where k is the impulse response for the specific free surface model chosen (sections 6 through 9). This model response can be written as

$$(163) \quad k(P,t) = AK(P,\alpha t)$$

where A and α are constants depending on the unknown parameters of interest c and w, and on the specific models. By the method developed below we estimate A and α, and from these parameters we obtain c and w.

The observed pressure and flow rate data are

$$p_i = p(t_i) \quad ; \quad t_i = i\Delta t, \; i = 1,2...N$$

(164)

$$\text{and} \quad q(t) = q_i \quad \text{for} \quad (i-1)\Delta t \leq t < i\Delta t$$

Equation (162) can then be written as

$$(165) \quad \bar{g}(\bar{m}) = \bar{d}$$

where

$$(166)\qquad \bar{m} = \begin{bmatrix} m_1 \\ m_2 \end{bmatrix} = \begin{bmatrix} A \\ \alpha \end{bmatrix}$$

$$\bar{d} = \begin{bmatrix} d_1 \\ d_2 \\ \cdot \\ \cdot \\ \cdot \\ d_N \end{bmatrix} = \begin{bmatrix} p_1 \\ p_2 \\ \cdot \\ \cdot \\ \cdot \\ p_N \end{bmatrix}$$

and $\bar{g}$ is a vector-valued function defined as

$$(167)\qquad \bar{g} = (g_i) \quad ; \quad g_i(\bar{m}) = p(t_i)$$

Expanding equation (165) into a Taylor series we can set up the following iterative scheme (Menke, 1984)

$$(168)\qquad \begin{aligned} G_n \Delta\bar{m}_{n+1} &= \bar{d} - \bar{g}(\bar{m}_n^{est}) \\ \bar{m}_{n+1}^{est} &= \bar{m}_n^{est} + \Delta\bar{m}_{n+1} \end{aligned}$$

where $\bar{m}_o^{est}$ is an initial guess and

$$(169)\qquad (G_n)_{ij} = \frac{\partial \bar{g}_i}{\partial m_j}\Big|_{\bar{m} = \bar{m}_n^{est}} \quad , \quad j = 1,2$$

or

$$(170)\qquad \begin{aligned} (G_n)_{i1} &= \int_o^{t_i} q(\tau)K(P, m_2(t-\tau))d\tau \\ (G_n)_{i2} &= m_1 \int_o^{t_i} q(\tau)(t-\tau)K'(P, m_2(t-\tau))d\tau \end{aligned}$$

where $\bar{m} = \bar{m}_n^{est}$ and $K'(P,t) = \partial_t K(P,t)$.

The least squares solution of (168) is given by (Menke, 1984)

$$(171) \qquad \Delta\bar{m}_{n+1} = (G_n^T G_n)^{-1} G_n^T \{d - \bar{g}(\bar{m}_n^{est})\} \qquad n = 0,1,2,....$$

where G_n^T is the transpose of G_n. We make an initial guess and then use iterations and equations (168) through (171) to estimate the parameters that best fit the data and the specific functional form of the impulse response assumed. We use the following criterion to terminate the iterations

$$(172) \qquad \sum_{i=1}^{2} \left(\frac{(\Delta m_{n+1})_i}{(m_{n+1}^{est})_i}\right)^2 << 1$$

The matrix $G_n^T G_n$ is a simple 2 x 2 matrix which we can invert analytically

$$(173) \qquad G_n^T G_n = \begin{bmatrix} \sum_i (G_n)_{i1}^2 & \sum_i (G_n)_{i1}(G_n)_{i2} \\ \sum_i (G_n)_{i2}(G_n)_{i1} & \sum_i (G_n)_{i2}^2 \end{bmatrix}$$

Thus

$$(G_n{}^T G_n)^{-1} =$$

(174)

$$\frac{1}{\sum_i (G_n)_{i1}^2 \sum_i (G_n)_{i2}^2 - (\sum_i (G_n)_{i1}(G_n)_{i2})^2} \begin{bmatrix} \sum_i (G_n)_{i2}^2 & -\sum_i (G_n)_{i1}(G_n)_{i2} \\ -\sum_i (G_n)_{i1}(G_n)_{i2} & \sum_i (G_n)_{i1}^2 \end{bmatrix}$$

More detailed equations for $(G_n)_{ij}$, in two specific cases, are given in Appendix E.

To compare the three different methods for analyzing variable flow rate data developed above (direct method, linear programming method and non-linear iterative method), we have applied the procedures to a few different synthetic data sets. We have computed the long term water level response of the 2-D unconfined vertical slab aquifer (section 7) directly above a line sink of variable flow rate, and added some random noise. Using the rms-difference between the exact and the estimated unit step responses as the criterion for the efficacy of the different methods, we came to the following conclusions:

- The linear programming method is better than the direct solution method, giving on the average an rms-difference smaller by a factor of two. In the presence

of noise the direct inversion technique gives poor results.

- The iterative non-linear solution technique is better than the linear programming method, giving on the average an rms-difference smaller by a factor of two. Thus in cases when we want to fit specific models to data, the non-linear least-squares iterative technique gives the best results.

17. Estimating Ladder Parameters for Simulation of Actual Field Data

Being able to estimate unit step responses from field data (section 15) we are now interested in simulating these by simple open/closed two capacitor ladders (section 13). As will be discussed below there are several possible ways of estimating the parameters of the ladders as well as ways of performing the simulation directly on variable flow rate data.

First, we can fit a polynomial to the early time behavior of the unit step response, i.e.

$$(175) \quad u(t) = \sum_{k=1}^{n} A_k \frac{t^k}{k!} \quad , \quad t < T \ , \ n \geq 4$$

and by equating the estimated parameters, A_k, k = 1,2,3 & 4, with the derivatives of the front end driving point unit step response (equation (140) with $u^{(n)}(t)$ =

$h^{(n-1)}(t)$) we obtain the parameters for a short term simulation ladder. This method is, however, not without problems, other than being only a short term simulation method:

- Inevitable noise in data causes serious difficulties.
- The period T has to be so short that a polynomial of type (175) is appropriate, however, long enough such that enough data can be incorporated.

We are more interested in fitting all the data available and in long term simulations. This can in many cases be successfully achieved by a trial and error visual/manual fitting. Consider, for example, simulation by a closed two capacitor system (equation (130)). Provided enough data is available, the unit step response should be asymptotically linear such that we can estimate $A = (\kappa_1 + \kappa_2)$ from its slope. Subtracting the linear part t/A from the observed unit step response we are left with fitting

$$(176) \qquad \frac{\kappa_2}{\kappa_1 A \lambda} (1-e^{-\lambda t})$$

to the remainder. Having a sufficiently long data set such that $e^{-\lambda t}$ is negligible at later times, we can easily estimate $\kappa_2/\kappa_1 A\lambda$ and finally λ from the early time behavior.

This manual method is of course useful albeit time consuming. We are therefore interested in more automatic methods that can be implemented on modern day computers.

One method of long term fitting, which we mention in passing, may be of some use. We want to fit a function of the form (equation (127))

$$(177) \qquad u(t) = \sum_{j=1}^{2} \frac{\tau_{ij}^2}{\lambda_j} (1-e^{-\lambda_j t})$$

to the data. Transforming the data set to $g(t) = u(t)/t$ and then taking the inverse Laplace transform of $g(t)$, with s the transform variable results in

$$(178) \qquad \hat{g}(s) = \left(\frac{\tau_{11}^2}{\lambda_1} + \frac{\tau_{12}^2}{\lambda_2}\right) - \sum_{j=1}^{2} \frac{\tau_{1j}^2}{\lambda_j} U(s-\lambda_j)$$

where U is the unit step function. This method should in principle enable good estimates of τ_{1j}^2 and λ_j for $j = 1,2$, however, in the case of noisy data its accuracy is doubtful.

We will now present a method which in conjunction with the above methods should enable us to obtain good estimates of simulation ladder parameters. This is a non-linear iterative least-squares technique, applicable to variable flow rate data. As before, we assume the pressure to be given by

$$(179) \qquad p(t) = \int_o^t q(\tau)h(t-\tau)d\tau = \int_o^t q(t-\tau)h(\tau)d\tau$$

where h(t) is the simulation ladder impulse response (section 13). We are interested in two kinds of responses

$$h(t) = Ae^{-\lambda 1 t} + Be^{-\lambda 2 t}$$

(180) and

$$h(t) = Ae^{-\lambda 1 t} + B$$

The first equation applies to the general responses of two capacitor ladders (equations (127) and (128)), whereas the second can be used for the responses of closed two capacitor ladders, (equations (130) and (131)) or the responses of one capacitor systems. From A, B, λ_1 and λ_2 we can then obtain the ladder parameters. This problem is set up as the non-linear problem of section 16:

$$(181) \qquad \bar{g}(\bar{m}) = \bar{a}$$

where $\bar{m} = (m_i)$ and $m_1 = A$, $m_2 = B$, $m_3 = \lambda_1$ (and $m_4 = \lambda_2$), $\bar{a}$ is defined by equation (166) and $\bar{g}$ by (167). The iterative scheme is given by equation (168) and the matrix G_n defined by (169). In the two cases being considered here (equation (180)) we have

$$(182) \qquad (G_n)_{ij} = \int_o^{t_i} q(t-\tau)e^{-m_j+2\tau}d\tau \quad , \quad j = 1,2$$

where in the second case of equation (198) $m_4 = 0$, and

$$(183) \qquad (G_n)_{ij} = -m_{j-2} \int_o^{t_i} q(t-\tau)\tau e^{-m_j\tau} d\tau \ , \ j = 3,(4)$$

In the above $\bar{m} = \bar{m}_n^{est}$. More specific formulas for $(G_n)_{ij}$, when we approximate q(t) as in equation (164), are presented in Appendix F. The solution of the iterative scheme is again given by equation (171) where we now invert $G_n{}^T G_n$ numerically since it is either a 3 x 3 or 4 x 4 matrix. By trying this non-linear method on synthetic data sets we arrive at the following conclusions:

- The method is very efficient for the second case of equation (180), i.e. when we only need to fit one exponential.
- The successful use of this method for the first case of equation (180) depends critically on the first guess. When we need to fit two exponentials the first guess may not be farther off the best fitting solution than 10-20%.

We now have some tools that in many cases will enable us to successfully estimate parameters for simulating reservoir responses. The three first mentioned methods of this section may be used to obtain first rough estimates and these, in turn, may then be used as first guesses in the non-linear iterative technique.

18. Analysis of Actual Field Data, Prelude

At this juncture we are interested in applying the methods developed above, as well as the analytical results, to some actual field data. As examples of the long term pressure evolution of liquid dominated reservoirs we will present some data from hydothermal systems in Iceland. We estimate unit step responses from variable flow rate data, perform free surface analysis and simulate the behavior of systems by simple lumped capacitor/conductor ladders. It should be emphasized that the analysis below is not intended as a comprehensive study of each of these geothermal systems, but rather as examples of the practical use of the theory and methods developed above.

Surface exploration of geothermal systems provides practically no information on fluid conductivity or production characteristics. Such information will generally have to be obtained by tests performed within the reservoir, primarily by production tests as discussed earlier (section 9, chapter II). Reservoir testing involves the interpretation of reservoir response to the withdrawal or injection of fluids. Pressure data are of particular importance and provide the main basis for the estimating of physical reservoir properties such as permeability and porosity. Well-pressure buildup/

drawdown test methods, employed in petroleum engineering since the 1930's, are now highly developed (Earlougher, 1977; Ramey, 1982).

In addition to conventional procedures the free surface analysis method, as applied to long term data, provides supplementary results (Bodvarsson and Zais, 1978). In section 19 we present several field examples of the application of this method. Bodvarsson and Zais (1978) have presented results of such an analysis of data from the Laugarnes field in SW-Iceland, their results are plausible yet quite different from results obtained by conventional well testing methods and short term data.

We will also simulate the response data by simple lumped parameter ladders. Due to their very simple mathematical characteristics such simulators can be very efficient, even in the case of very complex systems. Distributed parameter models have been used as simulators, but they require considerable information on the distribution of the physical parameters of the system in question which is seldom available and thus resulting in complex highly underdetermined problems. Furthermore, even though very different from real systems, lumped parameter simulators provide important information on global characteristics (see section 19). We should mention that lumped parameter models have been used with success in simulating the behavior of the Wairakei

geothermal reservoir in New Zealand (Fradkin et al., 1981).

We will present these examples as follows. In section 19 we present the results of free surface analysis and lumping of data from several hydrothermal systems. The emphasis is on data analysis methods and results rather than on detailed studies of each individual system. In section 20 we will, however, carry out a more comprehensive study of the Laugarnes system in SW-Iceland.

19. Brief Analysis of Data from Several Hydrothermal Systems

As examples for the demonstration of the application of our methods we present data from the geothermal systems listed in Table VII (see Figure 24). The data used is mostly from Palmason et al. (1983) as well as from Thorsteinsson (1976) and Kjaran et al. (1979). The material that has been collected by scientists at the National Energy Authority of Iceland is presented in Figures 25 through 30.

The data in Figures 25, 26 and 27 are the responses to variable rates of production. Other data are for approximately constant rates of production or pressure buildup situations. The data from Ytritjarnir and

Table VII Data-base for free-surface analysis and lumping

Geothermal field	Location & classification	Nature of data	Dates collected & length of data set
Reykir	SW Iceland LT-field	Production water level decline	1972-1982 4000 days
Svartsengi	SW Iceland HT/liquid dominated	-"-	1976-1978, 800 days 1980-1982, 900 days
Laugarnes	SW Iceland LT-field	Water level buildup following a break in production	1982, 83 days
Laugaland	N Central Iceland LT-field	Production water level decline	1978-1982, 1500 days
Ytritjarnir	N Central Iceland LT-field	-"-	1980, 500 days

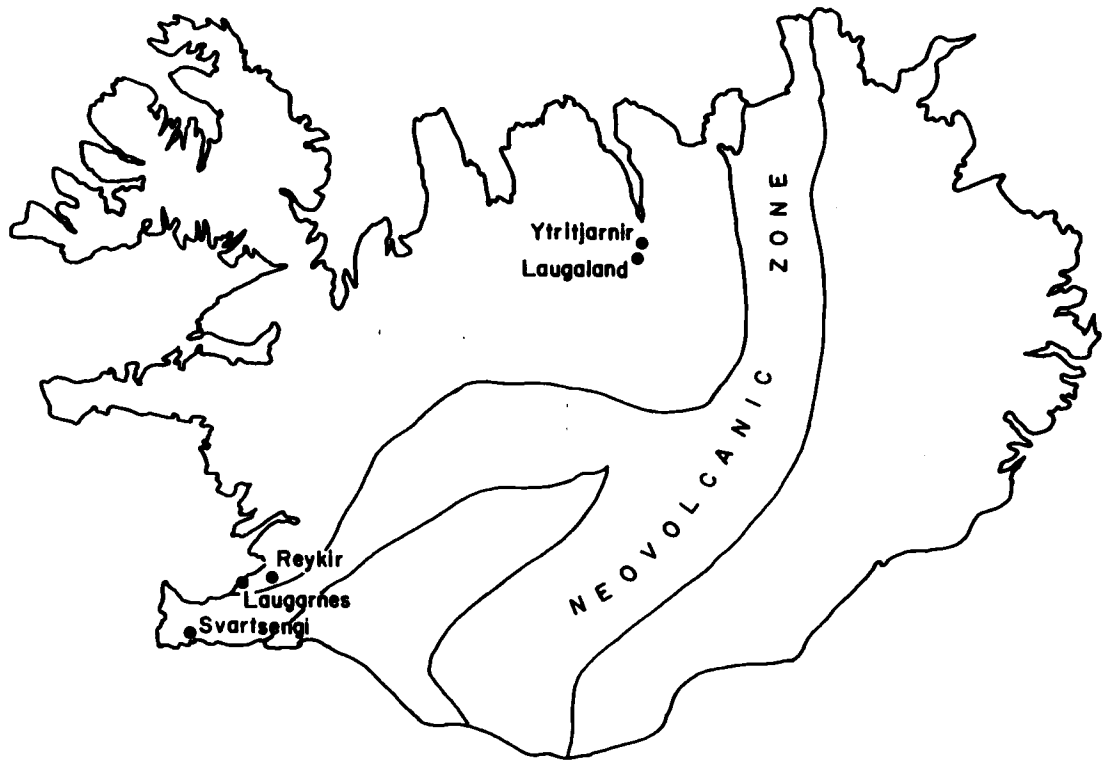

Figure 24. Location of liquid-dominated hydrothermal systems included in the present study

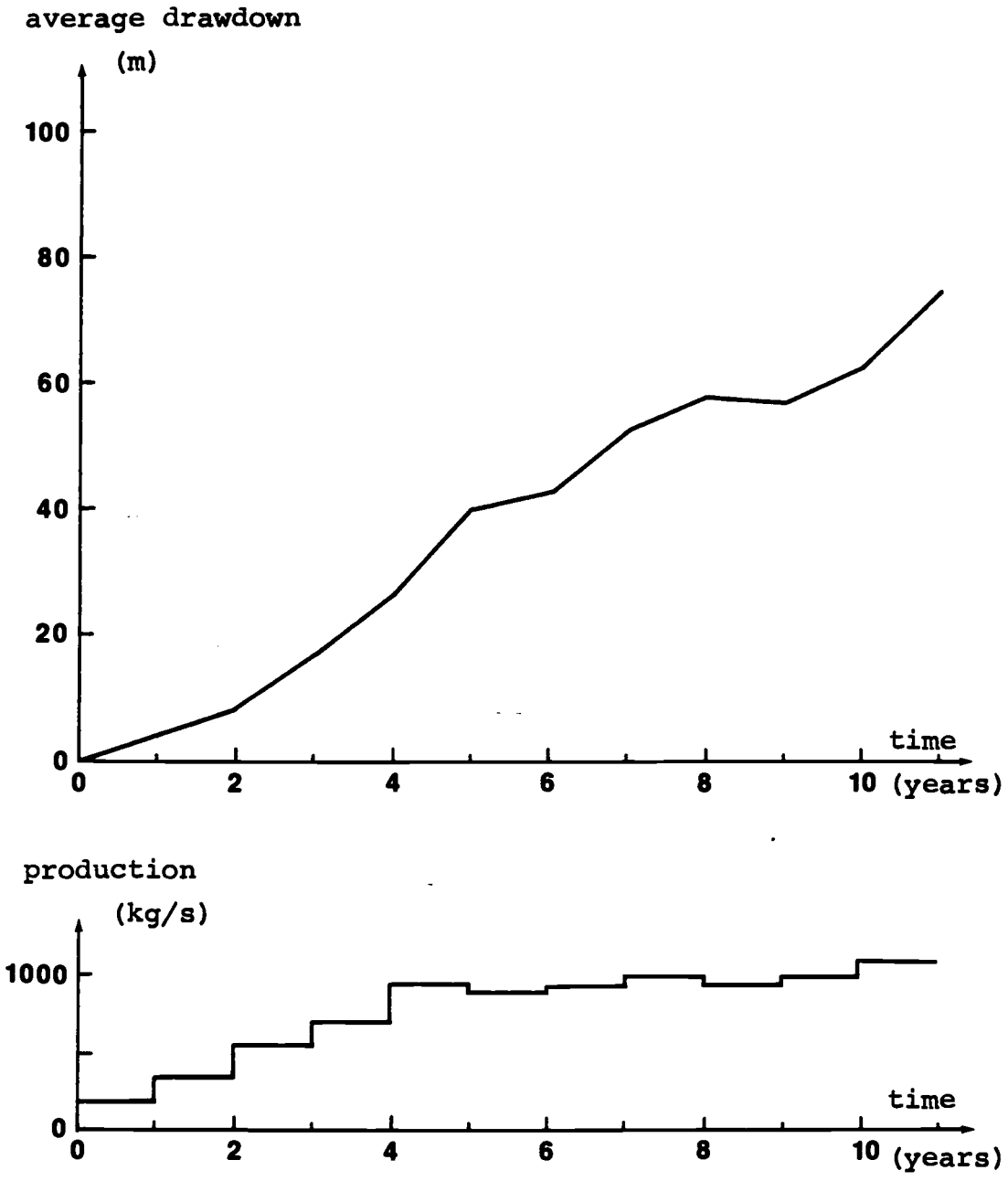

Figure 25. Average yearly drawdown (well SR-38) and production in the Reykir field sinc 1972.

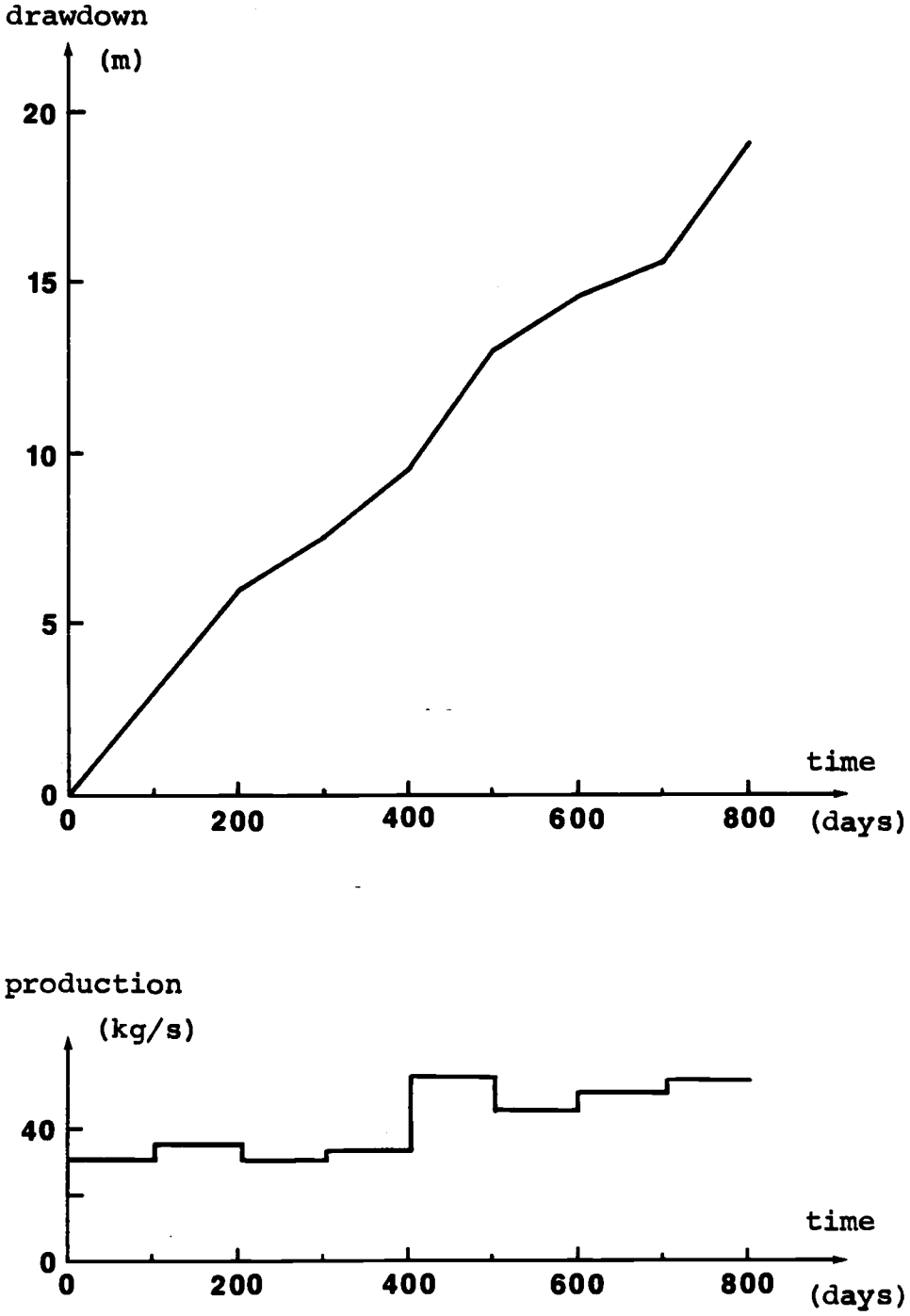

Figure 26. Drawdown (well SG-5) and production in the Svartsengi field since late 1976.

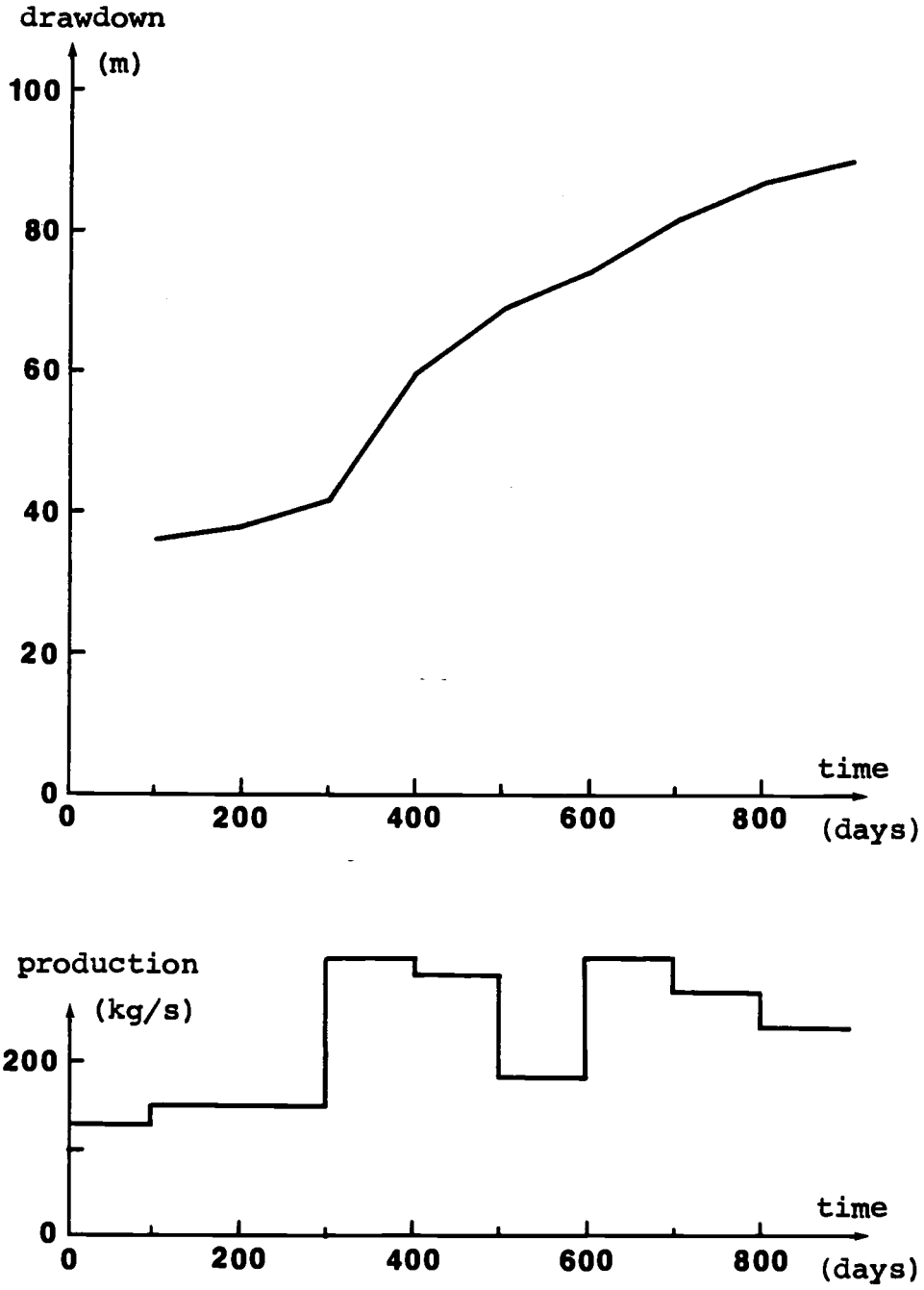

Figure 27. Drawdown (well SG-4) and production in the Svartsengi field since middle of 1980.

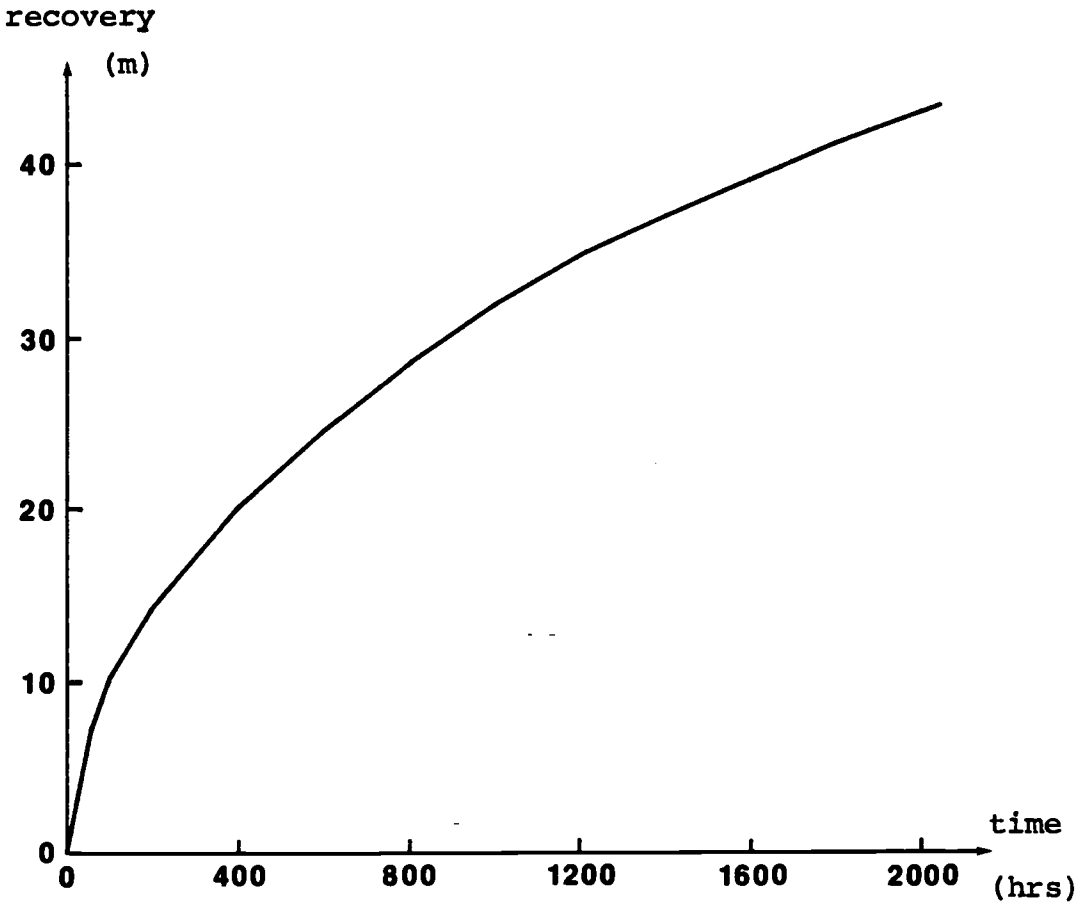

Figure 28. Water level recovery in the Laugarnes field (well RG-21) following a break in production from June 1, 1982.

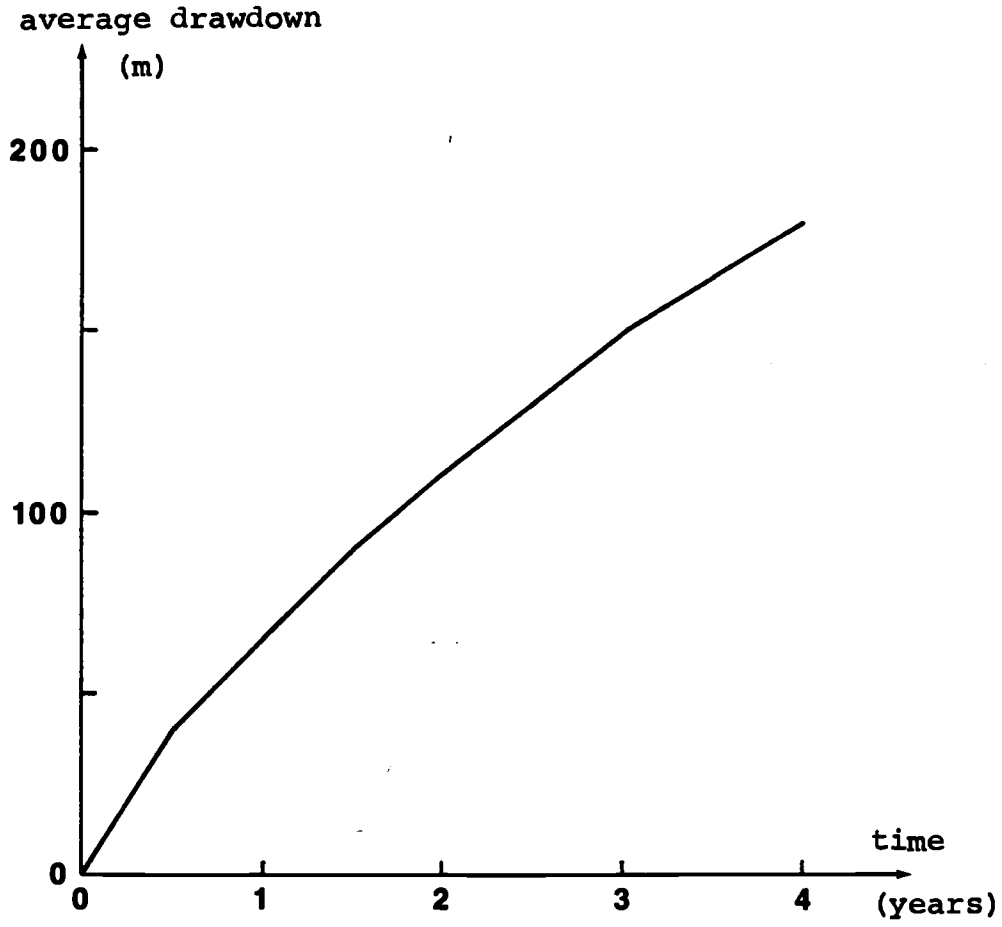

Figure 29. Average drawdown in the Laugaland field since early 1978 due to an average production of 75 kg/s.

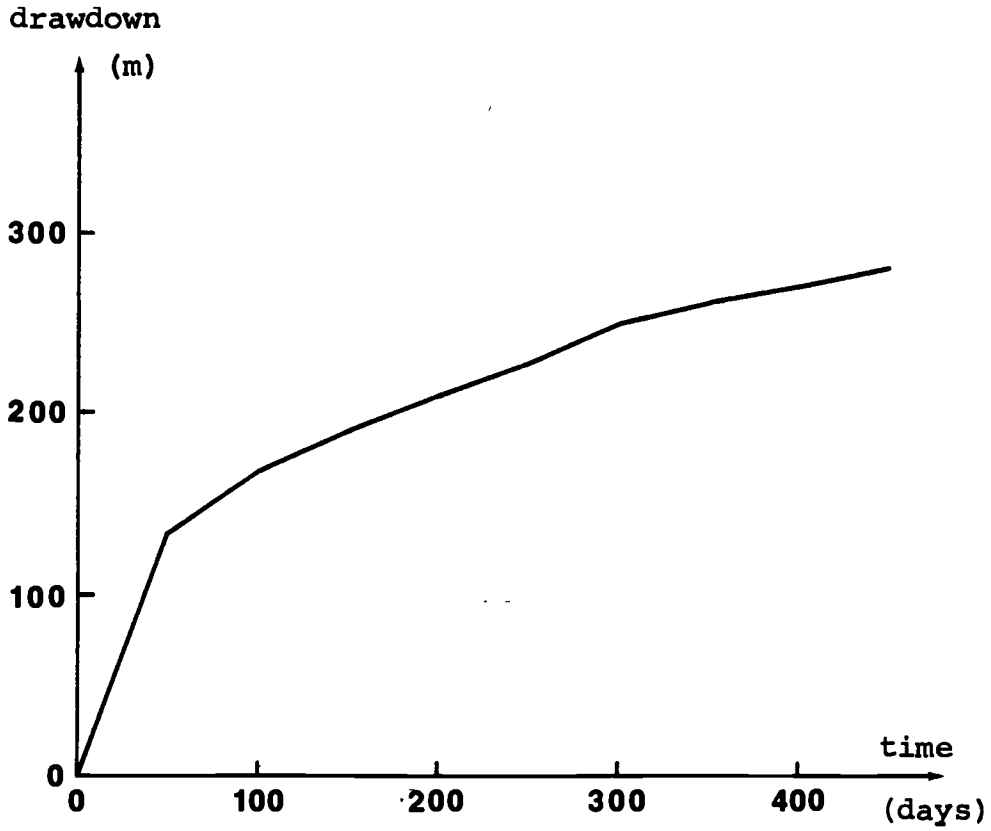

Figure 30. Average drawdown in the Ytritjarnir field (well TN-1) from July 1, 1980 due to an average production of 46 kg/s.

Laugaland can be considered to be approximate step responses. To estimate the unit step responses of the Reykir and Svartsengi fields, we use the linear programming method developed earlier. The direct inversion technique does not give satisfactory results in either case. The results are presented in Figures 31 and 32.

We will now analyze the data in Figures 26 through 30 on the basis of two ultra-simple free surface models, neglect compressibility and assume that the borehole data approximately represent the position of the true free liquid surface. First the small amplitude free surface response of a 3-D half-space (section 6) and, second, the free surface response of a vertical slab of thickness b with 2-D flow (section 7). We will assume we can approximate the production from the reservoir by point sinks at depth d and that the observation point is close to being directly above the sink (compared to the depth of the sink). By using the non-linear iterative least squares solution technique developed above we obtain the results in Figures 33 through 36 and in Table VIII. When analyzing the recovery data from Laugarnes we can assume that $\Delta t \ll T$ ($\Delta t < 80$ days, $T > 20$ yrs) and base the analysis on equations (48) and (58).

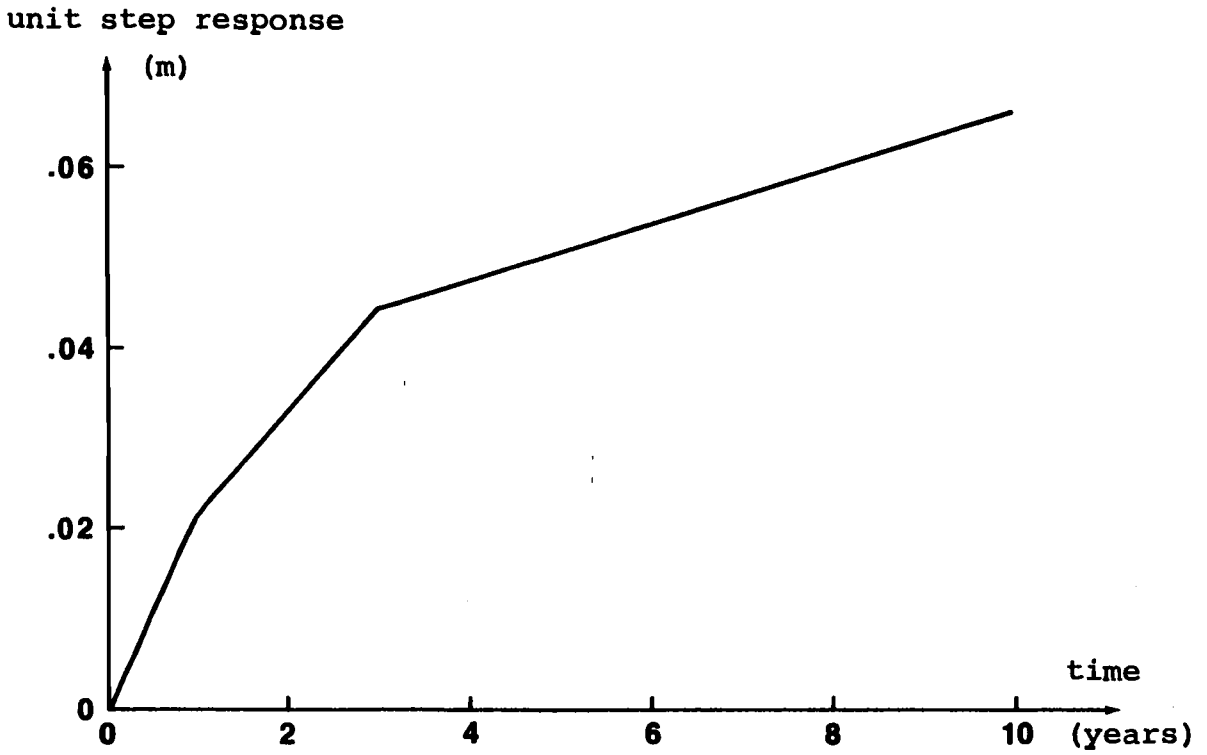

Figure 31. Estimated unit step response of the Reykir field. Based on data in Figure 25.

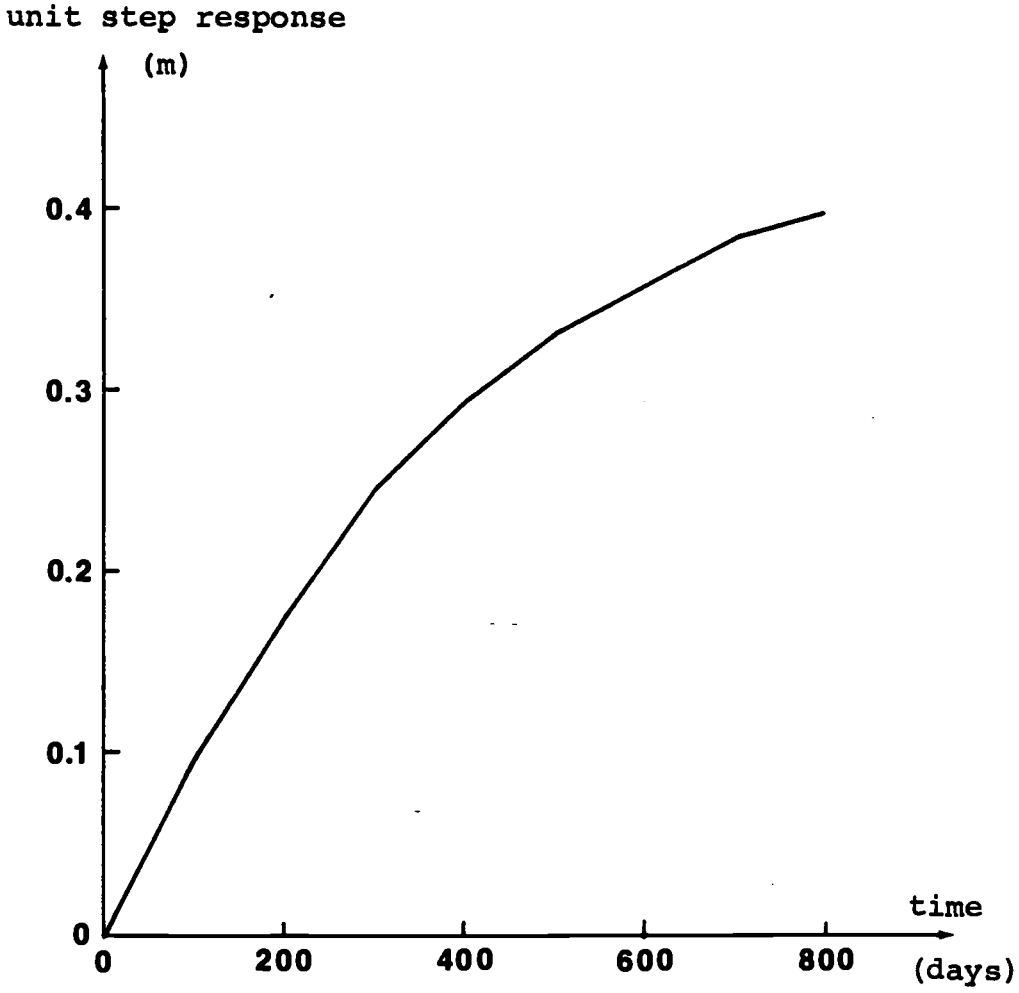

Figure 32. Average unit step response of the Svartsengi field. Based on two 800 hr. datasets (Figures 26 and 27).

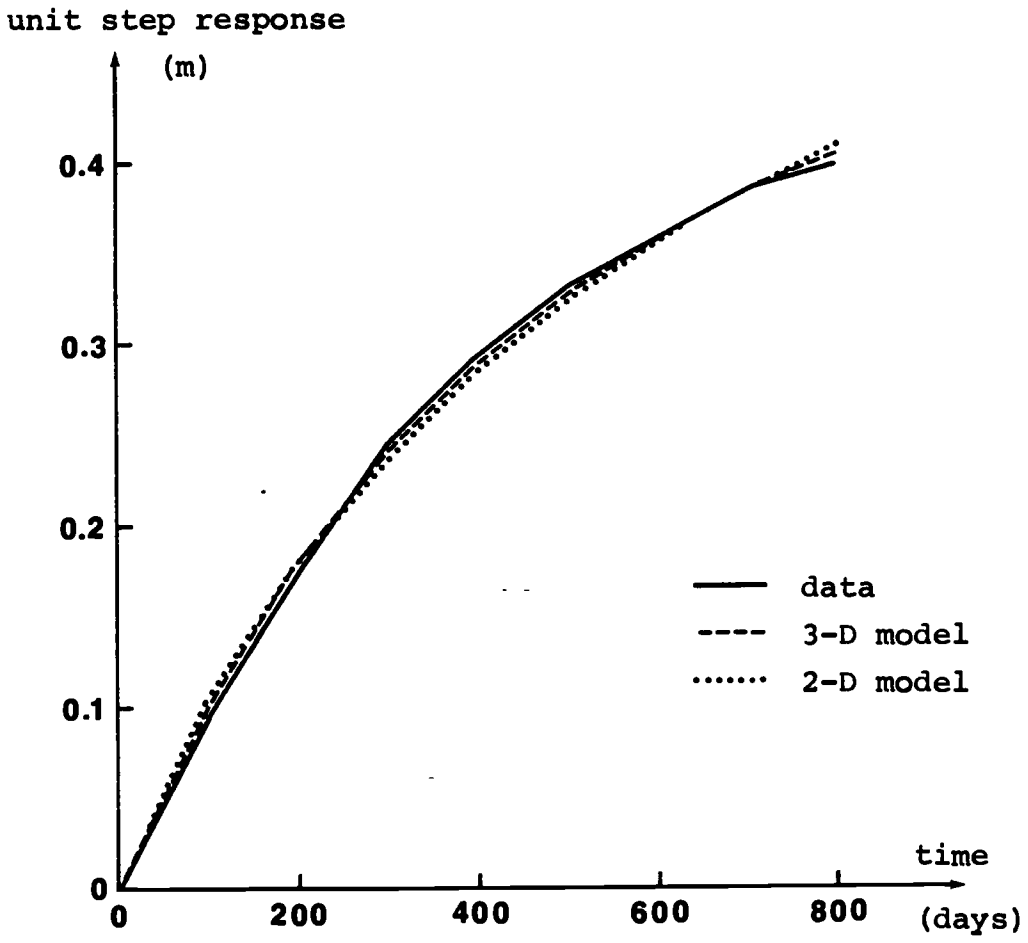

Figure 33. Unit step response of the Svartsengi field along with responses of best fitting simple free surface models. Rms-difference between data and model response equals (i) 0.006m for the 3-D case and (ii) 0.0085m for the 2-D case.

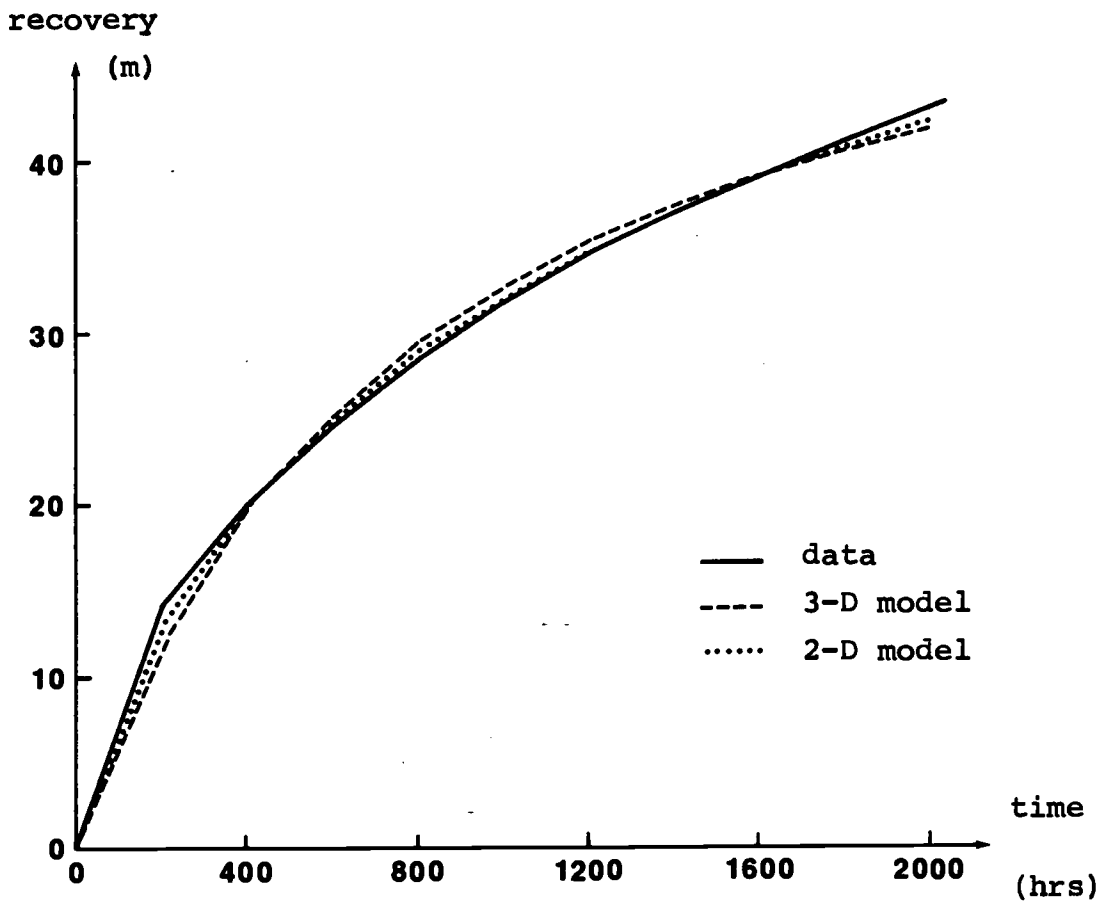

Figure 34. Water level recovery in the Laugarnes field along with responses of best fitting simple free surface models. Rms-difference between data and model response equals (i) 1.0m for the 3-D case and (ii) 0.6m for the 2-D case.

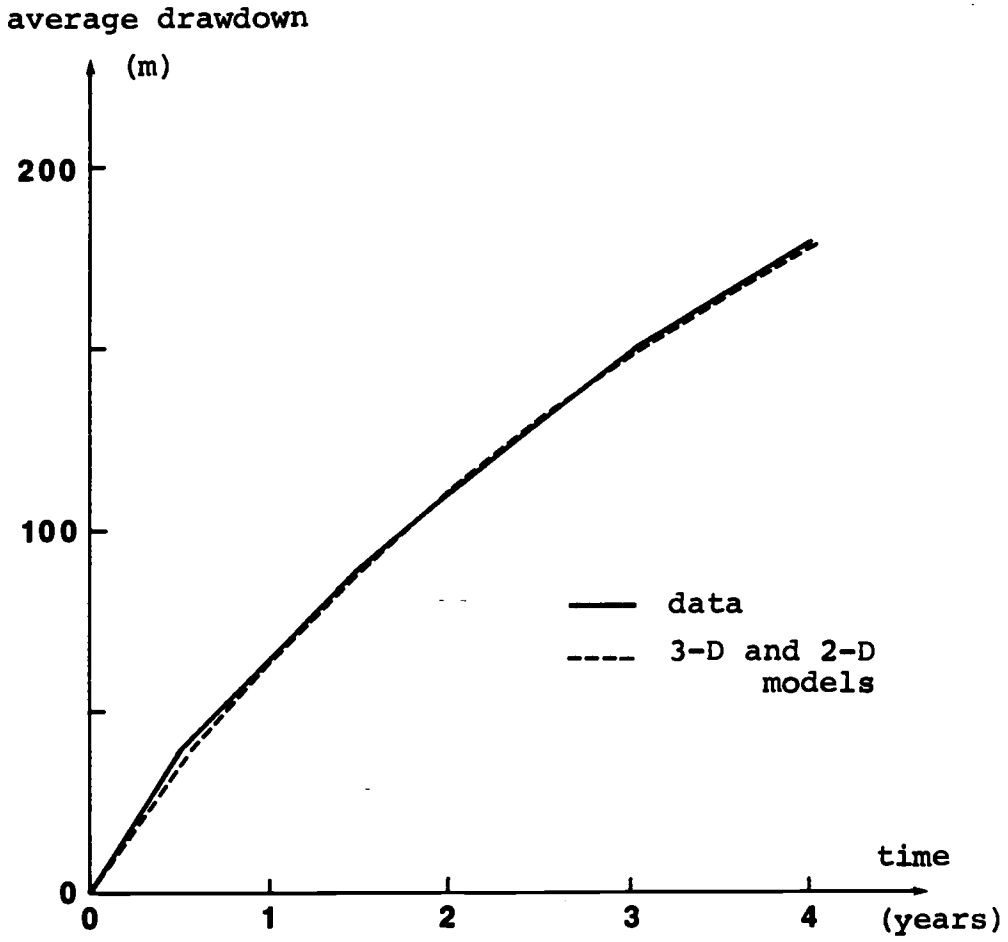

Figure 35. Average drawdown in the Laugaland field along with responses of best fitting simple free surface models. Rms-difference between data and model responses equals (i) 2.1m for the 3-D case and (ii) 1.7m for the 2-D case.

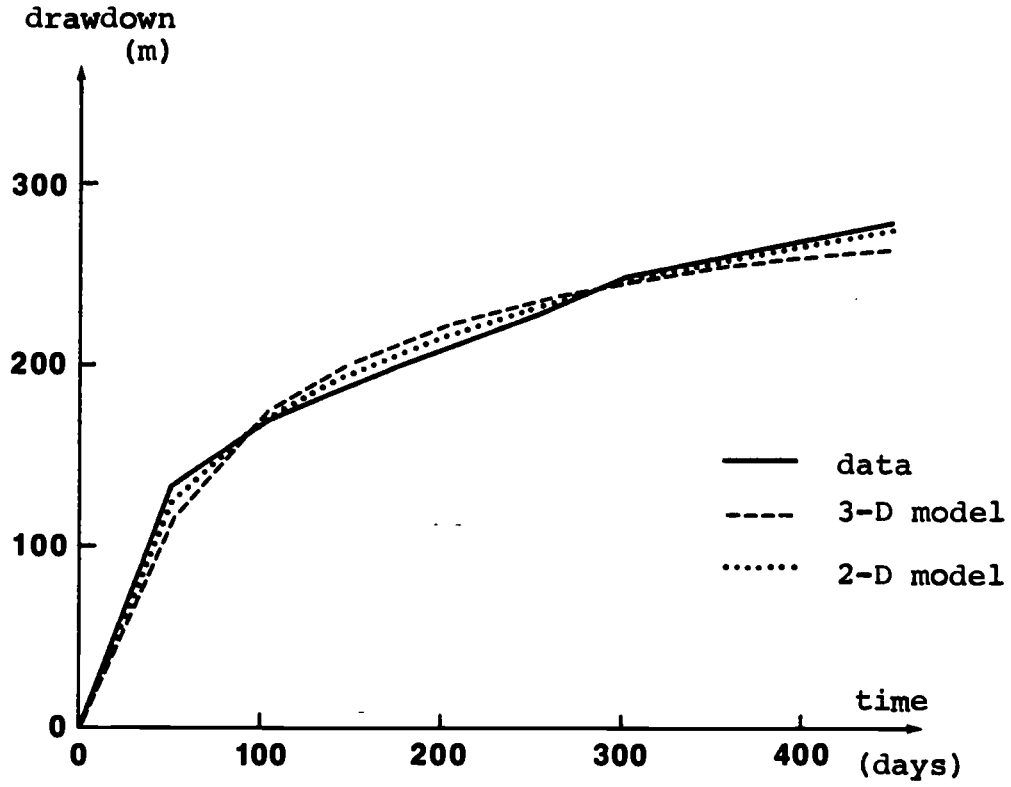

Figure 36. Average drawdown in the Ytritjarnir field along with responses of best fitting simple free surface models. Rms-difference between data and model response equals (i) 10m for the 3-D case and (ii) 5.6m for the 2-D case.

Table VIII Parameters of best fitting, simple free surface models.

Geothermal field	3-D cd(ms)	3-D w/d(s^{-1})	2-D cb(ms)	2-D w/d(s^{-1})
Laugarnes[1)]	4.37×10^{-5}	3.51×10^{-7}	3.07×10^{-4}	1.61×10^{-6}
Laugaland	2.95×10^{-6}	5.52×10^{-9}	1.51×10^{-5}	1.48×10^{-8}
Ytritjarnir	2.48×10^{-6}	1.36×10^{-7}	2.12×10^{-5}	1.04×10^{-6}
Svartsengi	2.76×10^{-5}	2.06×10^{-8}	1.60×10^{-4}	6.63×10^{-8}

1) assuming $\langle f_o \rangle$ = 150 kg/s

The figures present how these model results fit the data. Table VIII gives our estimates of the parameters defining the best fitting free surface models. These models are very simple, but they suffice as initial models, resulting in good order of magnitude estimates, and for illustrating the use of the methods employed. We have tried more complex models, such as with a sink corresponding to each production well, obtaining not very different results. As we see from the figures the 2-D model seems to fit slightly better. This is not surprising and supports the belief that the flow channels of hydrothermal systems in Iceland are mostly along walls of dikes and within fracture zones.

From the results in Table VIII we can obtain estimates of the parameters of main interest, the average system permeability and porosity, as presented in Table IXa and IXc. Only in the cases of Laugarnes and Svartsengi do we have reliable estimates of the dimension b. In Table IXb we present permeability-thickness, $b\beta$, and porosity-thickness, $b\phi$, estimated on the basis of the 2-D model. These estimates are considerably lower than previous estimates obtained by conventional methods (see Table IV, chapter II), in particular, the extremely low estimates of permeability for the systems in Tertiary strata, that is, Laugaland and Ytritjarnir. The porosity estimates, which are of the same order for both 3-D and

Table IXa Estimates of permeability and porosity, 3-D case.

	d[1]	c	permeability β[2]	porosity φ
Laugarnes	800m	5.5×10^{-8}s	17md	1.9×10^{-3}
Laugaland	1500m	2.0×10^{-9}s	0.6md	2.4×10^{-3}
Ytritjarnir	1000m	2.5×10^{-9}s	0.7md	1.8×10^{-4}
Svartsengi	1000m	2.8×10^{-8}s	5.5md	1.3×10^{-2}

1) from borehole data

2) $\nu = 2 \times 10^{-7} m^2/s$ for Svartsengi
$\nu = 3 \times 10^{-7} m^2/s$ for other fields

Table IXb Estimates of permeability-thickness, $b\beta$, and porosity-thickness, $b\phi$, 2-D case.

	$b\beta$ [1]	$b\phi$
Laugarnes	92 darcy m	2.3 m
Laugaland	4.5 dm	6.6 m
Ytritjarnir	6.4 dm	0.2 m
Svartsengi	32 dm	24 m

1) ν the same as in Table IXa.

Table IXc Estimates of permeability and porosity, 2-D case.

	b [1]	c	permeability β [2]	porosity ϕ
Laugarnes	1000 m	3.1×10^{-7} s	92 md	2.3×10^{-3}
Svartsengi	500 m	3.2×10^{-7} s	64 md	4.7×10^{-3}

1) estimated from known surface area of system.

2-D models, are very low yet plausible considering the fractured nature of the flood basalts and the fact that the porosity estimates reflect conditions in the uppermost sections of the reservoirs. Furthermore the porosity estimates are estimates of the interconnected porosity rather than the total porosity. Our results for the Laugarnes field are comparable to the results of Bodvarsson and Zais (1978) and confirm the apparent dependence of results on the time scale of the tests. At this juncture we refer the reader to the possible explanations offered earlier (section 9, chapter II). We will discuss the results for the Laugarnes field in more detail in section 20.

The fact that the 2-D permeability estimates are somewhat closer to the estimates obtained on basis of shorter term well tests (Table IV above), than the 3-D estimates, again supports our contention that the 2-D model more accurately reflects the hydrological characteristics of Icelandic hydrothermal systems.

Next we will attempt to simulate the observed responses presented above by the responses of simple open or closed capacitor/conductor ladders. Without going into details we employ the methods developed in section 17 above and obtain the results presented in Tables Xa and Xb. We will refrain from a pictorial representation

Table Xa Eigenvector components and eigenvalues of simulation ladders.

Geothermal Field	Ladder Type	τ_{11}^2 ($m^{-1}s^{-2}$)	τ_{12}^2 ($m^{-1}s^{-2}$)	λ_1 (s^{-1})	λ_2 (s^{-1})	Sol. method
Reykir	2-cap. closed	8.6×10^{-7}	7.4×10^{-6}	0	2.3×10^{-8}	manual
Svartsengi	1-cap. open	1.25×10^{-4}	0	2.93×10^{-8}	-	manual
Laugarnes	2-cap. open	5.33×10^{-4}	1.84×10^{-3}	1.93×10^{-7}	3.14×10^{-6}	nonlinear iterative
Laugaland	2-cap. closed	1.26×10^{-4}	2.17×10^{-4}	0	3.24×10^{-8}	-"-
	2-cap. open	2.54×10^{-4}	3.67×10^{-5}	7.90×10^{-9}	3.05×10^{-8}	-"-
Ytritjarnir	2-cap. open	1.49×10^{-3}	1.47×10^{-2}	2.85×10^{-8}	6.48×10^{-7}	-"-

Table Xb Simulation ladder parameters and rms-difference between data and simulation.

Field	Ladder Type	a_1 (m^2)	a_2 (m^2)	σ_1 (sm)	σ_2 (sm)	rms-diff (m)
Reykir	2-cap. closed	1.2×10^6	1.0×10^7	2.5×10^{-3}	0	0.0014[1]
Svartsengi	1-cap. open	7.84×10^4	∞	2.34×10^{-4}	-	0.0037[2]
Laugarnes	2-cap. open	4.13×10^3	2.58×10^4	1.05×10^{-3}	6.21×10^{-4}	0.13m
Laugaland	2-cap. closed	2.86×10^4	4.92×10^4	5.98×10^{-4}	0	1.5m
	2-cap. open	3.37×10^4	6.95×10^4	3.70×10^{-5}	1.59×10^{-4}	2.6m
Ytritjarnir	2-cap. open	6.05×10^2	6.70×10^3	3.65×10^{-5}	2.18×10^{-5}	1.9m

1) based on unit step response Figure 27

2) based on unit step response Figure 28

of these results, since the fit is in general better than the fit of the free-surface models above.

Before discussing these results we can use the simulators, developed above, to make some simple predictions on the future behavior of each of the systems. To briefly study the predicting power of the simulators let us consider the data from the Svartsengi-field (Figure 26 and 27). The simulator for the Svartsengi-field is based on two 800 day data sets, whereas we know the drawdown in the field after 2100 days of production (Figure 27). Based on the simulator and the known production (Palmason et al., 1982) we can then predict the drawdown after 2100 days (in July 1982) by

$$h(t_k) = 0.46e^{-\lambda t_k} \sum_{i=1}^{k} q_i(e^{\lambda t_i} - e^{\lambda t_{i-1}}) \qquad (184)$$

$$\lambda = 0.00253 \text{ days}^{-1}$$

with the production approximated by (see equation (150))

i	t_i (days)	q_i (kg/s)
1	800	40
2	1500	135
3	1700	310
4	1800	180
5	2000	300
6	2100	240

On the basis of the above we predict a drawdown of 87.7m. The observed drawdown is 88m.

This excellent result confirms our confidence in the predicting power of simple capacitor/conductor ladders. We can then make the following simple predictions on the future evolution of the systems we have been considering (Table XI). We will leave out the Laugarnes system since its simulator is based on buildup data. The Laugarnes-field will be considered to a greater length below. Consider now the simulator parameters presented in Table Xb. We are interested in obtaining some information on global characteristics of the systems in question on the basis of these parameters. We can attempt to obtain the following information:

- Knowing the surface area of a hydrothermal system we can estimate an average porosity on the basis of the total capacitance of a simulation ladder, or vice versa, based on known average porosity we can estimate the total areal extent of the system.
- Based on the conductance of a lumped element conductor we can attempt to estimate average permeability.

Below we compare the known surface areas of the systems being considered and the total surface areas of the simulator capacitors and attempt some porosity estimates (Table XII).

Table XI Future Predictions

	Production (kg/s)	10yrs	20yrs	50yrs	100yrs
Svartsengi	200	90m	-	-	-
	500	230m	-	-	-
Reykir	1000	65m	95m	180m	330m
Laugaland open	75	250m	270m	-	-
Laugaland closed	75	375m	695m	(1650m)	
Ytritjarnir	50	350m	-	-	-

Table XII Porosity estimates based on simulation ladder parameters.

Field	Estimated Surface Area (km^2)	$(a_1 + a_2)$ (km^2)	porosity ϕ
Reykir[1)]	20	1.2	0.06
Svartsengi	2	0.078	0.04
Laugarnes	3	0.030	0.01
Laugaland	10	0.090	0.01
Ytritjarnir	-	0.0073	-

1) a_1 only

We make the following observations:

- The apparent capacitance of the Reyleir system is very great ($a_1 + a_2 = 11$ km^2) and actually much greater than appears from the known surface area. This indicates that the second simulation capacitor (a_2) may correspond to a recharge reservoir of the system.
- The parameters for the Laugarnes-system are based on buildup-data only, which may not be sufficient as discussed at the end of section 13 above.
- The local Ytritjarnir-system is obviously very small, probably with a surface area somewhat less than 1 km^2.

To obtain crude estimates of the average system conductivity we will consider the two simple conductor models of Figure 37. Based on these models, the conductances of simulator conductors (Table Xb) and some assumptions on corresponding dimensions of the real systems, we obtain the estimates in Table XIII. These results are comparable to the permeability estimates obtained on the basis of the 2-D free surface model (Table Xc above).

20. The Long Term Production Response of the Laugarnes-field

The Laugarnes LT hydrothermal field is located within the city of Reykjavik in SW-Iceland (see Figure 1). Thermal water from the Laugarnes field has been used

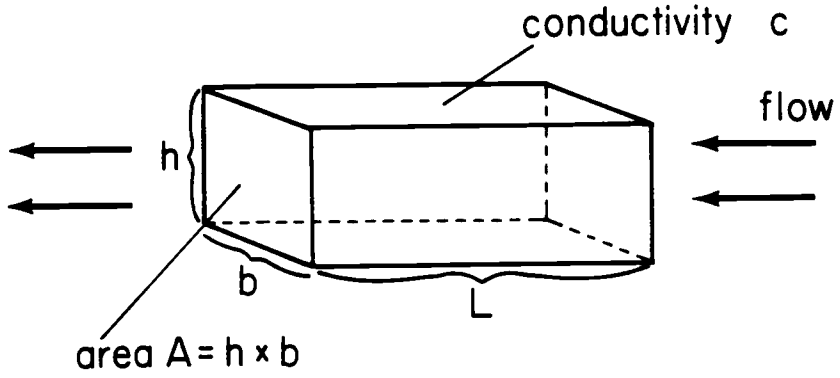

lumped conductance $\sigma = cA/L$

Figure 37a. Box-type conductor.

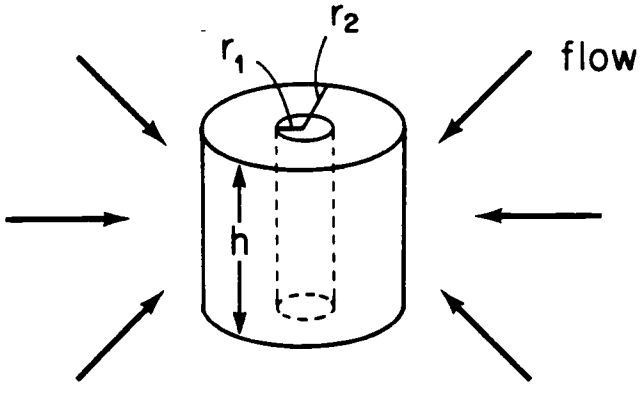

lumped conductance $\sigma = 2\pi ch/\ln(r_2/r_1)$

Figure 37b. Cylindrical conductor.

Table XIII Permeability estimates based on simulation ladder parameters.

Field	Model	Dimensions	σ_1(ms)	Estimated β(md)
Reykir	Fig.36a	$A = 4km^2$ $L = 1km$	$2.5x10^{-3}$	210
	37b	$r_2/r_1 = 10$ $h = 2km$	$2.5x10^{-3}$	130
Svartsengi	37a	$A = 2km^2$ $L = 2km$	$2.3x10^{-4}$	70
Laugarnes	37a	$A = 2km^2$ $L = 0.5km$	$1.1x10^{-3}$	80
Laugaland closed	37b	$r_2/r_1 = 10$ $h = 3km$	$6.0x10^{-4}$	20
open	37a	$A = 6km^2$ $L = 1.5km$	$3.7x10^{-5}$	3

for space heating since 1930 and several tens of deep (>1km) production wells have been drilled in the area since about 1960. Thorsteinsson and Eliasson (1970) have described the field in some detail and they have also discussed and interpreted the early production experience. Bodvarsson and Zais (1978) have performed free surface analysis of the early production response.

The Laugarnes reservoir is embedded in Plio-Pleistocene strata and located about 10 km N of the Neovolcanic zone in SW-Iceland. The reservoir strata is characterized by alternating basalt flows, pyroclastic layers and minor amounts of pillow lava. Fluid conductivity is believed to be mainly along layer contacts and up through dikes and fracture zones, as discussed for LT-activity in general in section II.7 above. The main production is obtained from an aquifer extending from 700 to 1250m depth with a temperature of 135°C. Some production has been obtained from depths up to 3km where the temperature is 155°C (Palmason et al., 1982). The results of Arnason (1976) on the deuterium content of the thermal water of the Laugarnes system indicate that the recharge of this system may be derived from the central highlands about 50km NE of Reykjavik.

Above we performed a brief analysis of the pressure response of the Laugarnes reservoir based on a relatively short (80 days) pressure buildup event. As mentioned

above, this analysis may be somewhat incomplete. However, a considerable amount of water-level data has been collected in the field during the last two decades (Thorsteinsson and Eliasson, 1970; Stefansson and Thorsteinsson, personal communication, 1984). In Figure 38 we present the water level in the area, on a day in November 1967, whereas Figure 39 illustrates a 12 year record of the water level response of the Laugarnes-reservoir to the seasonally varying production rate, as observed in the centrally located well designated G-7. This is an extremely long and detailed data-set, which should enable us to obtain important information on the hydrological characteristics of the reservoir. Below we will extend our free surface analysis, of section 19 above, and attempt to develop a simple lumped capacitor/conductor simulator for the Laugarnes-system, based on the data in Figure 39.

We start out by making the following observation based on a simple mass balance argument. Estimating the average drawdown in 1977 over an area of $3km^2$ to be about 40m we estimate the drawdown volume of the reservoir to be about $1.2x10^8m^3$. However, the volume of water produced at an average rate of 150 kg/s, for 13 yrs, equals $6.5x10^7m^2$. Since this is about 50% of the drawdown volume, while the porosity of the Laugarnes-strata is certainly no more than of the order of a few

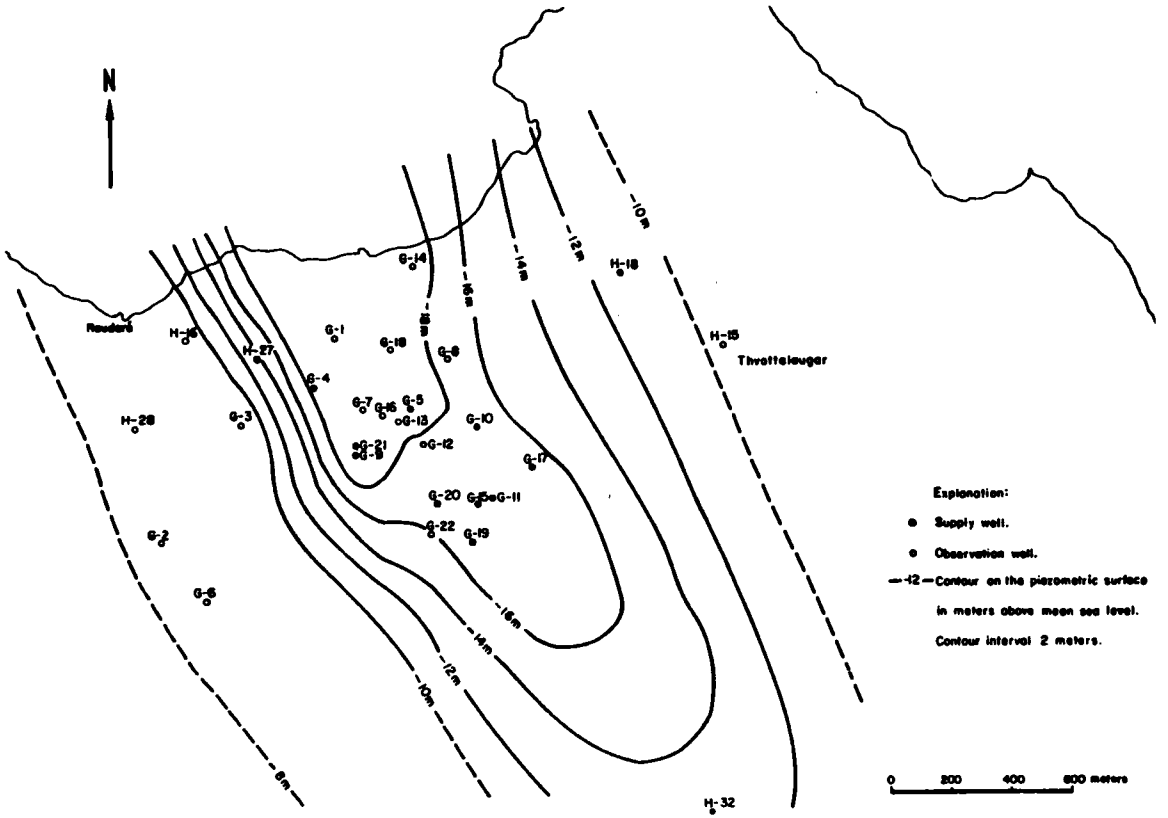

Figure 38. The water level in the Laugarnes area in November 1967. From Thorsteinsson and Eliasson (1970).

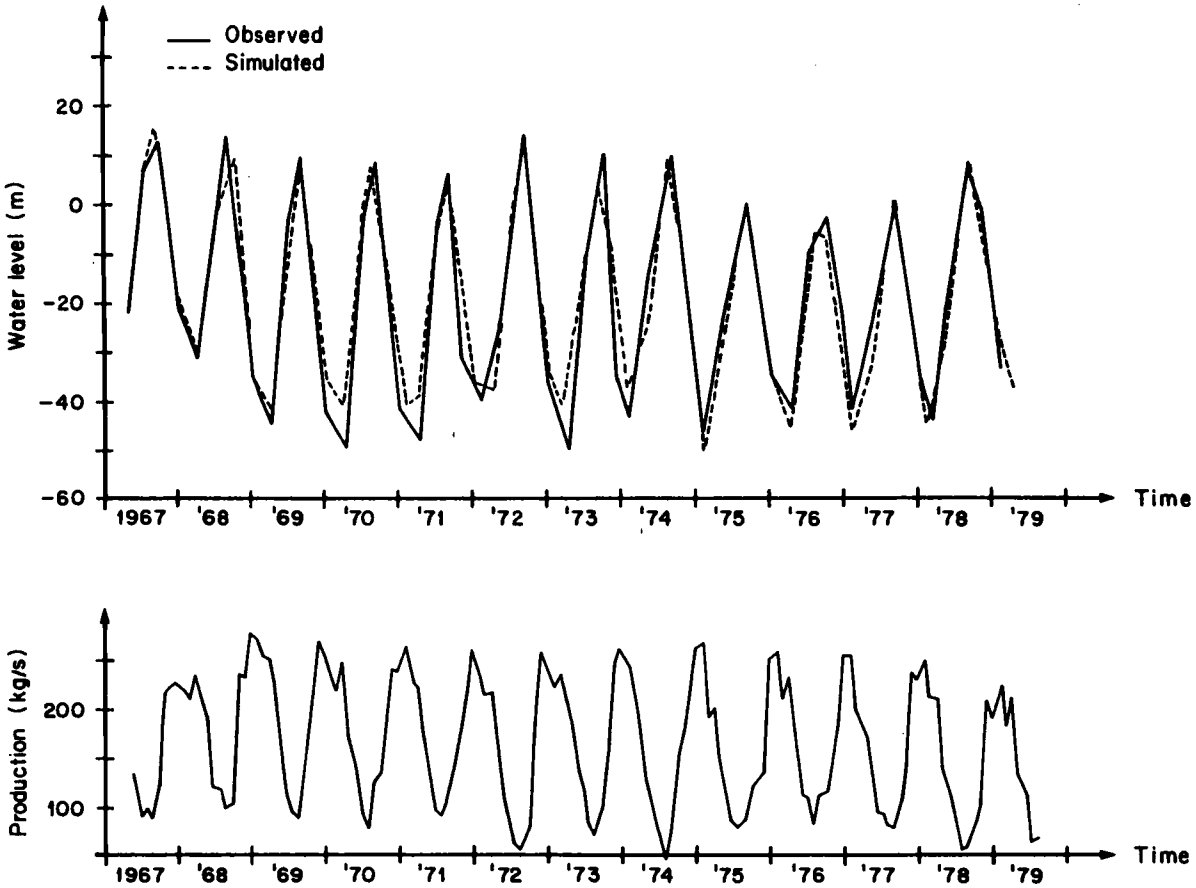

Figure 39. Observed and simulated response of the Laugarnes system (well G-7).

percent, we conclude that the Laugarnes-system must be open and the average recharge into the local system, over the 13 yr period before 1977, must be of the order of 100-150 kg/s.

We next turn to the free surface analysis in the hope of obtaining estimates of the global permeability (as well as porosity). Earlier estimates of permeability, obtained on the basis of short term interference tests, resulted in values of the order of 150 md (see section II.9 above). On the basis of 4 years of data prior to 1970 Bodvarsson and Zais (1978) obtain a rough estimate of 10 md. Finally Palmason et al. (1982) report an estimate of 15 md on basis of the buildup data presented in Figure 27 above. We will base our analysis on individual drawdown/buildup events in Figure 39 as well as on production/water-level amplitudes and phase relations for the annual cycle as estimated from the same data.

As an example of an individual event let us consider the period October 1972 through September 1973, presented in more detail in Figure 40. Considering the drawdown event only we can estimate an upper bound for the conductivity c based on a 3-D free surface model and equation (46), that is

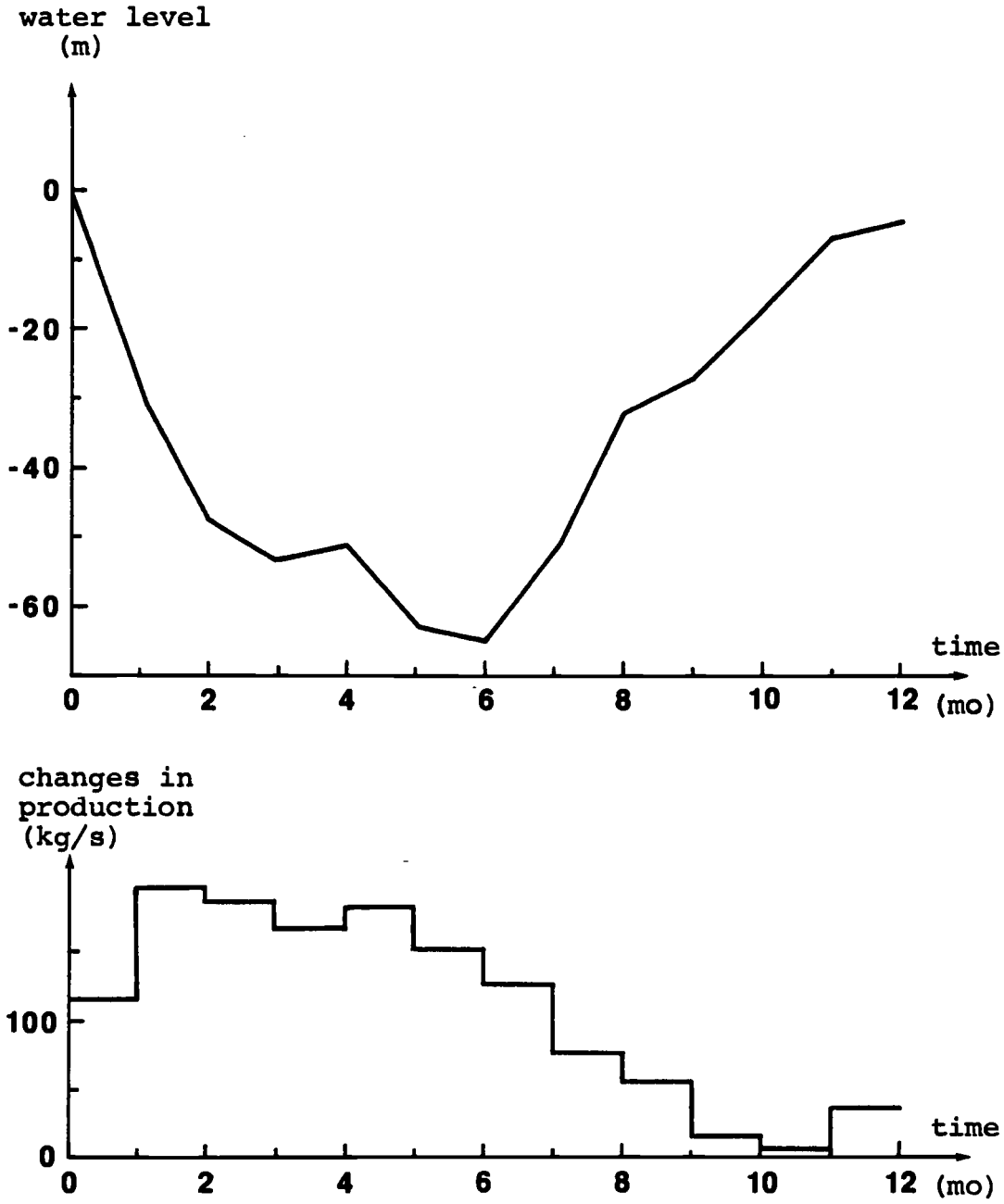

Figure 40. Response of the Laugarnes system October 1972 through September 1973.

$$(185) \qquad c < \frac{(\Delta f/\Delta h)}{2\pi\rho g d}$$

Estimating $\Delta h \simeq 65$ m, $\Delta f \simeq 180$ kg/s we obtain $c < 5.9\times10^{-8}$ s or $\beta < 18$ md. Now analyzing the drawdown event on the basis of the two simple 3-D and 2-D models used in section 19 above, assuming that the borehole data approximately represent the position of the true free liquid surface and using the nonlinear least-squares iterative technique, we obtain the results presented in Table XIV below. The results are very similar to the estimates obtained in section 19 above, on the basis of buildup data.

As the basis for the second part of our free surface analysis, based on amplitudes and phase relations for the annual cycle, we use the same simple 2-D model as above but assume that we can approximate the production rate by

$$(186) \qquad q(t) = q_o e^{i\omega t}$$

where q_o is the amplitude and ω the angular frequency. Using equations (49) and (59) we obtain the water level response of the free surface model

$$(187) \qquad h(S,t) = \frac{-wq_o e^{i\omega t}}{\pi\rho g c b} \int_o^t \frac{e^{-i\omega\tau}(w\tau+d)d\tau}{y^2+(w\tau+d)^2}$$

Table XIV Results of free surface analysis of Laugarnes data

	3-D drawdown (Fig.40)	2-D drawdown (Fig.40)	2-D annual cycle
cd(ms)	3.8×10^{-5}		
cb(ms)		3.4×10^{-4}	1.8×10^{-4}
w/d(s^{-1})	3.1×10^{-7}	2.7×10^{-6}	6.9×10^{-7}
d(m)	800	800	800
b(m)		1000	1000
c(s)	4.8×10^{-8}	3.4×10^{-7}	1.8×10^{-7}
β(md)[1]	14	100	53
ϕ	0.002	0.001	0.0025

1) $\nu = 3 \times 10^{-7} m^2/s$

Assuming, as before, the observation point to be directly above the source/sink point we can rewrite (187)

$$(188) \qquad h(0,t)\big|_{t=large} = \frac{-wq_o}{\pi\rho gcbd}\ (R + iI)e^{i\omega t}$$

where

$$R = \int_0^\infty \frac{\cos(\omega\tau)d\tau}{1+w\tau/d}$$

(189)

$$I = \int_0^\infty \frac{\sin(\omega\tau)d\tau}{1+w\tau/d}$$

Equation (188) can also be written

$$(190) \qquad -h(0,t) = \Delta h e^{i(\omega t+\alpha)}$$

with

$$(191) \qquad \Delta h = \frac{wq_o}{\pi\rho gbcd}\ (R^2+I^2)^{1/2}$$

the water level amplitude and

$$(192) \qquad \alpha = \tan^{-1}\ (\frac{I}{R})$$

the phase. Calculating the integrals (187) numerically we obtain the results in Figure 41.

Anayzing the data in Figure 39, for the approximate amplitudes and the apparent phase lag between production and water level, we obtain

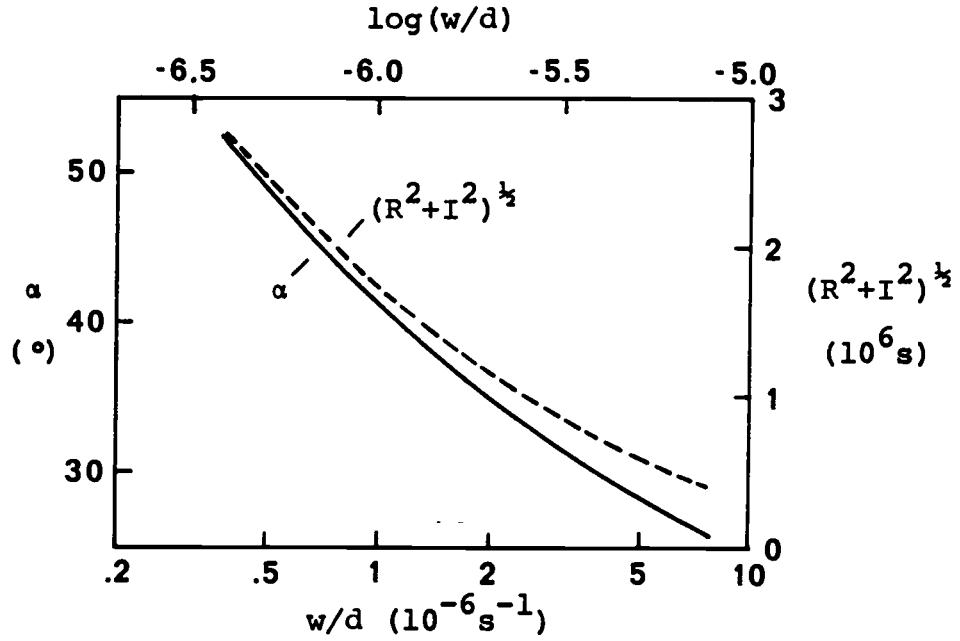

Figure 41. Theoretical amplitude and phase for periodic flow on the vertical slab 2-D model.

$$\Delta h/q_o = (0.28 \pm 0.04)\ \frac{ms}{kg}$$

$$\alpha = (1.5 \pm 0.4)mo = (45 \pm 12)^\circ$$

Comparing these estimates with the results in Figure 41 we finally obtain the estimates presented in the last column of Table XIV. The results of Bodvarsson and Zais (1978), β = 10 md and ϕ = 0.001, are obtained in a similar manner but based on the 3-D free surface model.

We note that the parameters estimated by the two different methods, individual event analysis and based on the periodicity, are in a rather good agreement for each model. We also note that the 2-D estimates are an order of magnitude greater than the 3-D estimates and comparable to short term test estimates (β = 150 md, Table IV above). This result may indicate that the 2-D vertical slab model may reflect the global hydrological characteristics of the Laugarnes system more accurately than a 3-D model (as well as for other hydrothermal systems in Iceland) and that a 2-D model may be approximately applicable to the long term evolution of the system. Results of short term well tests would not be affected by the boundaries of the system and result in comparable permeability estimates, yet based on 3-D models. This observation may thus explain the apparent

dependence of results on the time scale of the tests. Note that the drawdown surface (Figure 38) is obviously elongated in a NNW-SSE direction, supporting the observation above.

We should point out that our identification of the piezometric surface with the true free surface level is subject to some doubt. The borehole data may reflect the pressure level at some depth in the reservoir. Considering the extreme that this depth is of the order of the source/sink depth d, we conclude, on the basis of an elementary investigation of the results of section 6 above, that this would not affect our results seriously, probably by less than a factor of 2.

Finally we will attempt to develop a simulator for the Laugarnes-reservoir that fits all the data available (data in Figure 39). Since the data set is Figure 39 is really too long and detailed for a successful inversion in the manner of section 19, we will estimate a unit step response as follows:

- Based on individual drawdown/buildup events we estimate an initial short term unit step response.
- Using the known monthly production over the 12 year period (Figure 39) and the initial unit step response, we calculate a model response. Based on the difference, between the observed and calculated responses, we then correct the estimated unit step response, by a method of

trial and error, until we have obtained a satisfactory fit. The final result is thus a combined short term and long term unit step response for the Laugarnes-system.

We refrain from discussing details of the analysis, but present the initial short term response in Figure 42 and the final best fitting unit step response of the Laugarnes-system in Figure 43 and Table XV. The simulated 12 year response is presented in Figure 39 and the fit is apparently quite good, considering the fact that the production data is of limited accuracy. Note that the short term response appears to approach a constant value within 10 months. However, after 1 year the estimated long term unit step response still increases, yet very slowly. This very slow increase is important as it accounts for about 20m drawdown after 10 years at an average pumping rate of 150 kg/s.

We can now develop a capacitor/conductor-ladder in order to simulate the response of the Laugarnes-system. A closed three-capacitor ladder appears to be sufficient. Based on the unit step response in Figure 43 and the analytical results in Appendix C we arrive at the following results

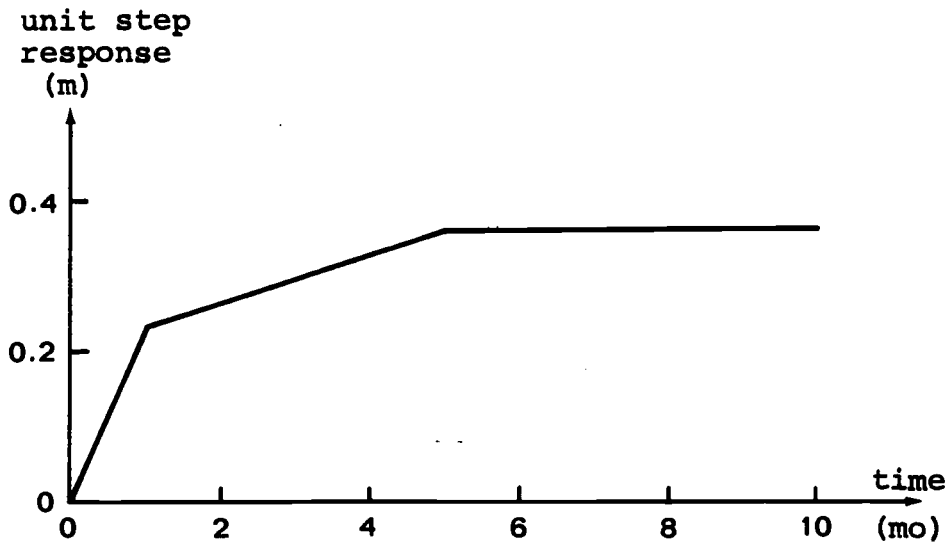

Figure 42. Initial short term unit step response of the Laugarnes system. Estimated from data in Figure 40.

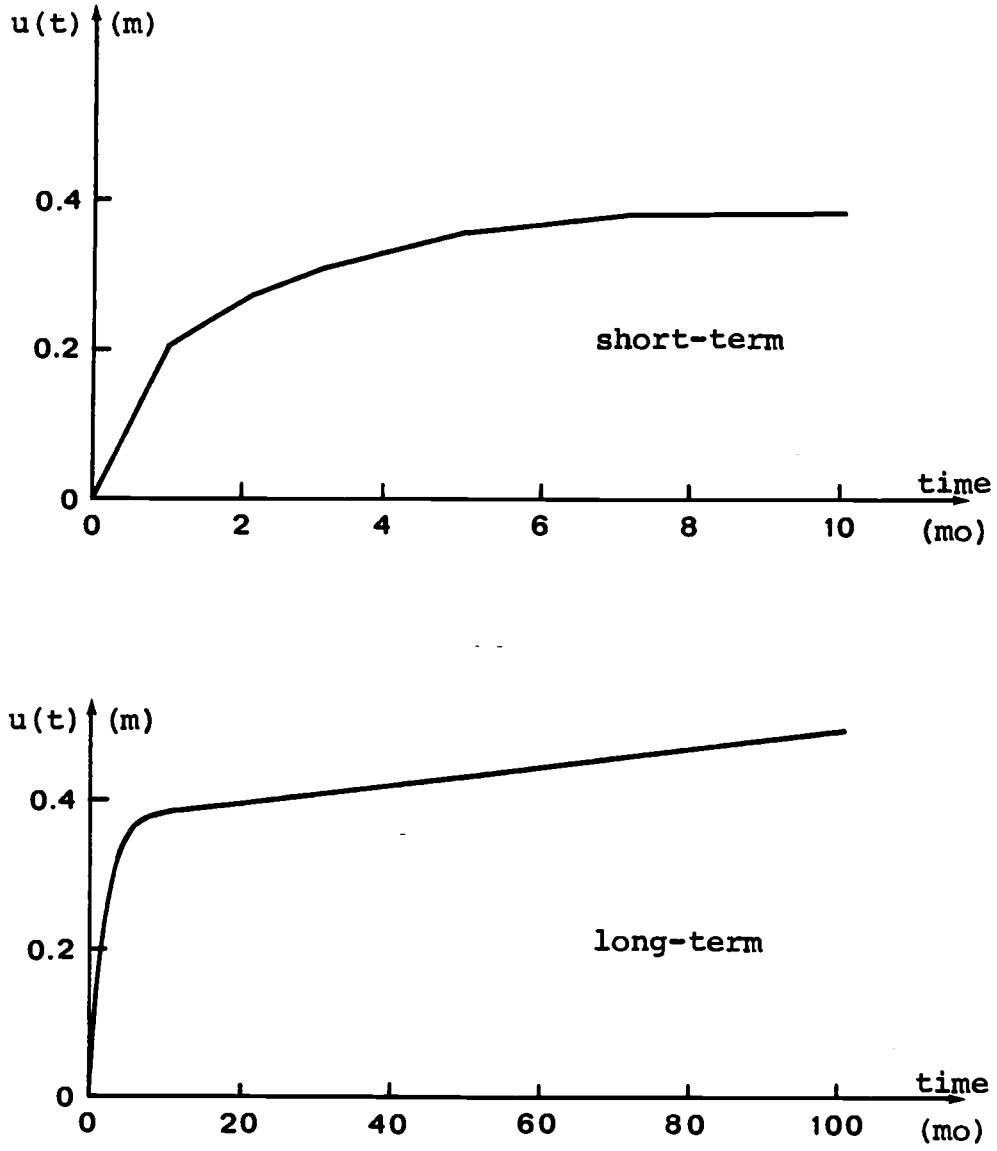

Figure 43. Unit step response of the Laugarnes system.

Table XV The estimated impulse response and unit step response of the Laugarnes-system.

t(mo)	Impulse response G(t) (m/kg)	Unit step response u(t) (ms/kg)
1	0.205	0.205
2	0.060	0.265
3	0.040	0.305
4	0.030	0.335
5	0.020	0.355
6	0.015	0.370
7	0.010	0.380
8	0.0012	0.381
9	-	0.382
10	-	0.384
20	-	0.396
30	-	0.408
40	-	0.420
50	-	0.432
60	-	0.444
70	-	0.456
80	-	0.468
90	-	0.480
100	0.0012	0.492
110	0.0	0.504
120	0.0	0.504

$$\tau_{11}^2 = 4.63 \times 10^{-10}\ m^{-1}s^{-2}$$
$$\tau_{12}^2 = 4.55 \times 10^{-4}\ m^{-1}s^{-2}$$
$$\lambda_2 = 1.79 \times 10^{-7}\ s^{-1}$$
$$\tau_{13}^2 = 1.84 \times 10^{-3}\ m^{-1}s^{-2}$$
$$\lambda_3 = 2.0 \times 10^{-6}\ s^{-1}$$

and obtain the corresponding simulation ladder parameters

$$a_1 = 4.3 \times 10^3 m^2$$
$$\sigma_1 = 7.1 \times 10^{-4} ms$$
$$a_2 = 2.2 \times 10^4 m^2$$
$$\sigma_2 = 4.8 \times 10^{-4} ms$$
$$a_3 = 2.24 \times 10^6 m^2$$

The first two capacitors probably correspond to the local Laugarnes-system, whereas we can envision the third capacitor as corresponding to a reservoir supplying the recharge for the system. The estimated capacitance, or area, of the first two capacitors ($a_1 + a_2$) is similar to the area estimated in section 19 above. Assuming ϕ = 0.01 we then estimate the area of the local system to be about 2 1/2 km^2 in a good agreement with the known surface area of 3-5km^2. Again assuming ϕ = 0.01, we estimate the surface area of the recharge reservoir to be about 200km^2, which is not unreasonable considering the fact that the recharge of the Laugarnes-system is believed to originate at about 50km distance inland, as mentioned earlier.

The conductance estimates are also similar to the estimates above. We can estimate the total conductance σ of the local Laugarnes system as follows:

$$(193) \qquad \frac{1}{\sigma} = \frac{1}{\sigma_1} + \frac{1}{\sigma_2} \quad , \quad \sigma = 2.9 \times 10^{-4} ms$$

and based on the model in Figure 36 and $A = 2km^2$, $L = 3km$ we obtain a rough estimate of the global conductivity $c = 4.4 \times 10^{-7} s$, and permeability $\beta = 130md$, of the system. This estimate is again in a good agreement with other estimates above.

IV. THERMOMECHANICS OF HYDROTHERMAL PHENOMENA

1. Introduction

The present chapter will be devoted to a quantitative study of some thermoelastic phenomena in hydrothermal systems, with particular emphasis on a possible dike/fault controlled source mechanism of LT-activity in Iceland.

Thermoelastic strain and stress result from nonuniform temperature fields. Since hydrothermal systems reflect perturbations of the equilibrium thermal state of the Earth's crust they are clearly associated with thermoelastic stresses. The magnitude of these effects is thus of interest but has received little attention in the geothermal literature.

Thermoelastic phenomena are certain to influence the evolution of hydrothermal systems, both in their natural state as well as under exploitation. Since temperature reduction results in thermoelastic contraction and enhanced flow conductivity, while heating results in the reverse effect, the distribution of permeability within hydrothermal systems is affected by thermoelastic stresses. Thermoelastic phenomena may also play a significant part in the source mechanism of HT as well as

LT activity, as has been briefly discussed earlier (chapter II) and will be considered to some length below.

Thermoelasticity has not received much attention in geothermal reservoir physics and engineering. Bodvarsson (1976, 1980) points out that the response of a geothermal reservoir to exploitation will result in a subtle thermoelastic response of the ground surface that may be observable as subsidence, strain and tilt or gravity field changes. Bodvarsson (1980) estimates that such thermoelastic effects tend to dominate other elastomechanical effects accompanying exploitation. Bodvarsson (1976) points out that temperature transients in a fluid flowing through a fracture result in fracture contraction or expansion thereby affecting the fracture fluid conductivity. He estimates that a relatively small temperature decrease or increase can lead to a greatly increased or decreased fluid conductivity, respectively. Hanson (1978) performs a more elaborate study of this phenomena. Bodvarsson (1976) also discusses qualitatively the large scale thermoelastic effects on flow permeability in an active geothermal system.

Thermoelastic phenomena are also important outside geothermal systems and on a more global scale. Thermoelastic stress is considered significant in young oceanic lithosphere (Turcotte and Oxburg, 1973; Turcotte, 1974). The distribution of earthquake source mechanisms

in the oceanic lithosphere appears to be consistent with the hypothesis that many of these earthquakes represent the response of the brittle portion of the lithosphere to accumulated thermal stress (Bergman and Solomon, 1985).

We will start the discussion of thermoelastic phenomena by a brief review of the theory of quasi-static linear thermoelasticity. Based on this theory, the magnitude of thermoelastic stress due to temperature profiles as measured in some hydrothermal systems in Iceland will be estimated. Then we will turn our attention to the CDM-process, a possible source mechanism for hydrothermal activity, discussed in chapter II above. We will briefly review previous discussions of this phenomena and then turn to a specific model of a downward migrating fracture, that is applicable to LT-activity in Iceland. We will estimate the possible downward rate of CDM by calculating the thermoelastic stresses near the fracture.

2. Quasi-static Linear Thermoelastic Theory

Thermoelastic theory describes the behavior of elastic solids under the influence of nonuniform temperature fields. The principal problem in thermoelasticity consists in deriving displacement and stress resulting from given temperature distributions.

But stress, strain and temperature fields are interrelated in a very complicated manner. Deformation of a solid causes secondary temperature changes in addition to the nonuniform temperature field causing deformation. Strain and temperature are therefore coupled in a non-linear manner and the general equations of thermoelasticity (Boley and Weiner, 1960) are in principle very difficult to solve.

Drastic simplifications are possible, however, in most cases of practical interest (Boley and Weiner, 1960):

- Temperature changes and deformations can be assumed to be so small that the basic equations can be linearized.
- The heat produced by thermoelastic deformations can be neglected, thus the basic equations decouple.
- Temperature changes are so slow that inertia can be neglected.

We can then derive the equations of the much simpler quasi-static linear thermoelastic theory (Parkus, 1976).

Consider a homogeneous and isotropic Hookean solid. In the absence of body forces the equations for translational equilibrium are

$$\sum_i \frac{\partial \sigma_{ij}}{\partial x_i} = o \qquad j = 1,2,3 \tag{194}$$

and the equations for rotational equilibrium

$$\sigma_{ij} = \sigma_{ji} \qquad i,j = 1,2,3 \tag{195}$$

where σ_{ij} are the components of the strain tensor and x_i the spatial coordinates. The temperature field is given by

$$T = T_o + \Delta T(x,y,z) \tag{196}$$

where T_o is uniform throughout the solid and ΔT is nonuniform. The components of strain due to the nonuniform temperature are given by

$$\begin{aligned} \epsilon_{xx}^{(1)} &= \epsilon_{yy}^{(1)} = \epsilon_{zz}^{(1)} = \alpha\Delta T \\ \epsilon_{xy}^{(1)} &= \epsilon_{yz}^{(1)} = \epsilon_{zx}^{(1)} = 0 \end{aligned} \tag{197}$$

where α is the coefficient of linear thermal expansion. Since the solid cannot expand freely stresses are generated which in turn result in additional strain $\epsilon_{ij}^{(2)}$. From Hooke's law

$$\epsilon_{ij}^{(2)} = \frac{1}{2\mu}\left(\sigma_{ij} - \frac{\lambda}{2\mu+3\lambda} s\delta_{ij}\right), \quad i,j = 1,2,3 \tag{198}$$

$$s = \sum_i \sigma_{ii}$$

where μ and λ are the Lame constants of the solid. The total strain is then given by

$$\epsilon_{ij} = \epsilon_{ij}^{(1)} + \epsilon_{ij}^{(2)} = \frac{1}{2}\left(\frac{\partial u_i}{\partial x_j} + \frac{\partial u_j}{\partial x_i}\right) \tag{199}$$

with u_i the components of the displacement vector $\bar{u}$. The components of the stress tensor are then obtained by a generalized thermoelastic Hooke's law:

$$\sigma_{ii} = 2\mu\varepsilon_{ii} + \lambda\nabla\cdot u - (3\lambda+2\mu)\alpha\Delta T$$

$$i,j = 1,2,3 \qquad (200)$$

$$\sigma_{ij} = 2\mu\varepsilon_{ij} \quad i \neq j$$

where the third term in the expression for σ_{ii} is an extra term resulting from the thermoelastic strain. Combining (194) and (200) the basic equations governing the quasi-static linear thermoelastic response of homogeneous and linear Hookean solids follow

$$\mu\nabla^2\bar{u} + (\lambda + \mu)\nabla\nabla\cdot\bar{u} = \alpha(3\lambda + 2\mu)\nabla(\Delta T) \qquad (201)$$

To obtain the thermoelastic stress we solve (201) with appropriate boundary conditions and then use equation (200). To such a solution we can then add stress due to body forces, such as gravity.

3. Whole Space Thermoelastic Solutions

In an infinite solid thermoelastic displacements are irrotational and thus we can set (Goodier, 1937)

$$\bar{u} = -\nabla\phi \qquad (202)$$

where ϕ is a so-called thermoelastic potential. Inserting this in equation (201) results in the basic equation for whole space

$$(203) \qquad -\nabla^2\phi = \alpha\Delta T \left(\frac{1-\nu}{1+\nu}\right),$$

where ν is Poisson's ratio. Now using the fact that $\nabla\cdot\bar{u} = -\nabla^2\phi$ and inserting in (200) we obtain the components of the stress tensor

$$(204) \qquad \sigma_{ij} = 2\mu\left(\varepsilon_{ij} - \left(\frac{1+\nu}{1-\nu}\right)\alpha\Delta T\delta_{ij}\right) \qquad i,j = 1,2,3$$

If the temperature is non-uniform in a domain V, the solution to equation (203) is given by

$$(205) \qquad \phi(P) = \frac{\alpha}{4\pi}\left(\frac{1+\nu}{1-\nu}\right)\int_V \frac{\Delta T(Q)dV_Q}{r_{PQ}}$$

where $P = (x,y,z)$ is the field point, $Q = (x',y',z')$, $dV_Q = dx'dy'dz'$ and

$$(206) \qquad r_{PQ} = ((x-x')^2 + (y-y')^2 + (z-z')^2)^{1/2}$$

In order to appraise the influence of domain geometry on whole space thermoelastic stresses we will estimate the thermoelastic stresses at the center of each of the three simple domains presented in Figure 44. The results can be used for order-of-magnitude estimates and are as follows:

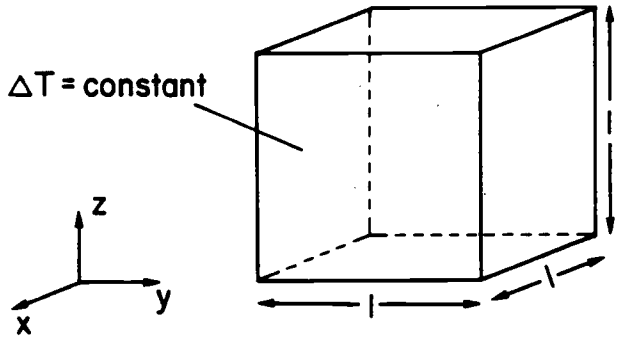

Figure 44a. Cube-domain of nonuniform temperature in an infinite solid.

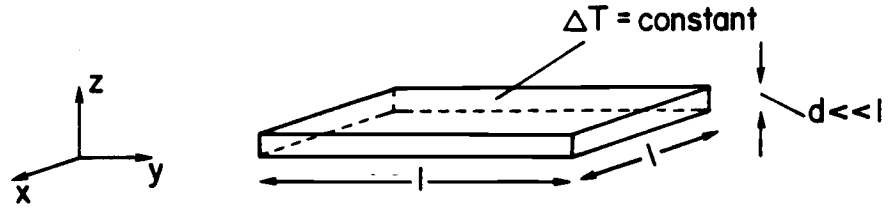

Figure 44b. Thin slab-domain of nonuniform temperature in an infinite solid.

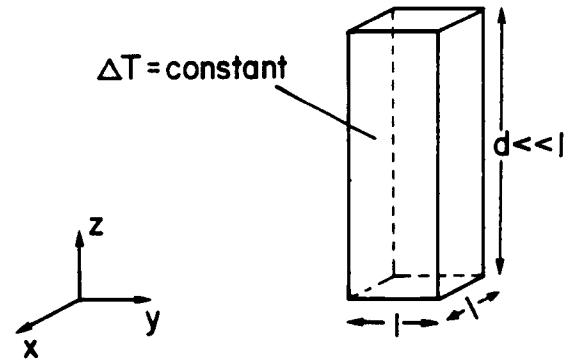

Figure 44c. Long box-domain of nonuniform temperature in an infinite solid.

- Cube-domain

Due to symmetry, the following holds at the center of the cube

$$\varepsilon_{xx} = \varepsilon_{yy} = \varepsilon_{zz}, \tag{207}$$

thus $\nabla \cdot \bar{u} = 3\ \varepsilon_{xx}$ and by (203)

$$\varepsilon_{xx} = \frac{1}{3}\ \alpha \Delta T\ \left(\frac{1+\nu}{1-\nu}\right) \tag{208}$$

Therefore at the center of the cube

$$\sigma_{xx} = \sigma_{yy} = \sigma_{zz} = -\ \frac{4}{3}\ \mu\ \left(\frac{1+\nu}{1-\nu}\right)\ \alpha \Delta T \tag{209}$$

- Thin slab-domain

Here we can assume that $\sigma_{zz} = 0$ (compared to σ_{xx} and σ_{yy}) and thus by (204)

$$\varepsilon_{zz} = \left(\frac{1+\nu}{1-\nu}\right)\ \alpha \Delta T \tag{210}$$

and since $\varepsilon_{xx} = \varepsilon_{yy}$, at the center of the slab

$$\varepsilon_{xx} = \varepsilon_{yy} = 0 \tag{211}$$

Therefore at the center of the slab

$$\sigma_{xx} = \sigma_{yy} = 2\mu\ \left(\frac{1+\nu}{1-\nu}\right)\ \alpha \Delta T\ ,\ \sigma_{zz} = o \tag{212}$$

- Long box-domain

At the center of the box

$$\varepsilon_{zz} = 0\ ,\ \varepsilon_{xx} = \varepsilon_{yy} \tag{213}$$

thus $\nabla \cdot \vec{u} = 2\varepsilon_{xx}$ and by (203)

$$\varepsilon_{xx} = \frac{1}{2}\left(\frac{1+\nu}{1-\nu}\right)\alpha\Delta T \tag{214}$$

Therefore

$$\begin{aligned} \sigma_{xx} &= \sigma_{yy} = -\mu\left(\frac{1+\nu}{1-\nu}\right)\alpha\Delta T \\ \sigma_{zz} &= -2\mu\left(\frac{1+\nu}{1-\nu}\right)\alpha\Delta T \end{aligned} \tag{215}$$

To take a specific numerical example, consider the case of common igneous rock with $\mu = 3 \times 10^{10}$ Pa, $\nu = 1/4$ and $\alpha = 5 \times 10^{-6}\ {}_{o}K^{-1}$. Then at the center of a cube-domain with $\Delta T = -50°K$, for example, $\sigma_{xx} = 170$bar. This is quite substantial or equal to the hydrostatic pressure at a water depth of 1700m.

As an example of a more complete solution let us solve the case of a spherical inclusion of radius a that has been heated by ΔT. Here we solve (203) directly and obtain

$$\phi = \begin{cases} \alpha\Delta T\left(\frac{1+\nu}{1-\nu}\right)\frac{(3a^2-r^2)}{6} & , r \leq a \\ \alpha\Delta T\left(\frac{1+\nu}{1-\nu}\right)\frac{a^3}{3r} & , r > a \end{cases} \tag{216}$$

In spherical coordinates

$$\varepsilon_{rr} = \frac{\partial u_r}{\partial r} \quad , \quad \varepsilon_{\theta\theta} = \varepsilon_{\phi\phi} = \frac{u_r}{r} \tag{217}$$

$$\varepsilon_{\theta\phi} = \varepsilon_{\phi r} = \varepsilon_{r\theta} = 0$$

where $u_r = -\partial\phi/\partial r$. Thus

$$\sigma_{rr} = \begin{cases} -\frac{4}{3}\mu\alpha\Delta T\left(\frac{1+\nu}{1-\nu}\right) & , \quad r < a \\ -\frac{4}{3}\mu\alpha\Delta T\left(\frac{1+\nu}{1-\nu}\right)\frac{a^3}{r^3} & , \quad r > a \end{cases} \tag{218}$$

$$\sigma_{\theta\theta} = \sigma_{\phi\phi} = \begin{cases} -\frac{4}{3}\mu\alpha\Delta T\left(\frac{1+\nu}{1-\nu}\right) & , \quad r < a \\ -\frac{2}{3}\mu\alpha\Delta T\left(\frac{1+\nu}{1-\nu}\right)\frac{a^3}{r^3} & , \quad r > a \end{cases} \tag{219}$$

$$\sigma_{\theta\phi} = \sigma_{\phi r} = \sigma_{r\theta} = 0 \tag{220}$$

Note that inside the spherical inclusion all stresses are compressive (if $\Delta T > 0$) but on the outside σ_{rr} is compressive whereas $\sigma_{\theta\theta}$ and $\sigma_{\phi\phi}$ are extensional. Note also that σ_{rr} is continuous at $r = a$ but $\sigma_{\theta\theta}$ and $\sigma_{\phi\phi}$ are discontinuous

$$\sigma_{\theta\theta}|_{a^+} - \sigma_{\theta\theta}|_{a^-} = 2\mu\alpha\Delta T\left(\frac{1+\nu}{1-\nu}\right) \tag{221}$$

(see Goodier, 1937).

Finally, equation (205) can also be employed to estimate whole space thermoelastic stresses. As an example consider the box-domain

$$(222)\quad V = \{(x,y,z)\,|\,-\ell/2 < x,y < \ell/2;\ -d/2 < z < d/2\}$$

then

$$(223)\quad \phi = \frac{\alpha}{4\pi}\left(\frac{1+\nu}{1-\nu}\right)\int_{-\ell/2}^{\ell/2}\int_{-\ell/2}^{\ell/2}\int_{-d/2}^{d/2}\frac{\Delta T(x',y',z')\,dz'dy'dx'}{((x-x')^2+(y-y')^2+(z-z')^2)^{1/2}}$$

The component of stress σ_{xx}, along the z-axis through the center of a domain with ΔT = constant, is obtained as follows,

$$\epsilon_{xx}\big|_{x=y=o} = -\frac{\partial^2\phi}{\partial x^2}\Big|_{x=y=o}$$

(224)

$$= \frac{\alpha\Delta T}{4\pi}\left(\frac{1+\nu}{1-\nu}\right)\int_{-\ell/2}^{\ell/2}\int_{-\ell/2}^{\ell/2}\int_{-d/2}^{d/2}\frac{(y'^2+(z-z')^2-2x'^2)\,dz'dy'dx'}{(x'^2+y'^2+(z-z')^2)^{5/2}}$$

and after some algebra

(225)

$$\epsilon_{xx} = \frac{\alpha\Delta T}{\pi}\left(\frac{1+\nu}{1-\nu}\right)\left(\frac{\ell}{2}\right)^2\int_{-d/2}^{d/2}\frac{dz'}{[(z-z')^2+(\ell^2/2)^2][(z-z')^2+\ell^2/2]^{1/2}}$$

The above integration is performed in Appendix G, resulting in

$$\epsilon_{xx} = \frac{\alpha \Delta T}{\pi}\left(\frac{1+\nu}{1-\nu}\right)\left[\tan^{-1}\left(\sin\left(\tan^{-1}\left(2^{1/2}\left(\frac{z+d/2}{\ell}\right)\right)\right)\right)\right.$$

(226)

$$\left. - \tan^{-1}\left(\sin\left(\tan^{-1}\left(2^{1/2}\left(\frac{z-d/2}{\ell}\right)\right)\right)\right)\right]$$

The numerical results are presented in Figure 45 below.

It should be mentioned that at surfaces of temperature discontinuities displacements and tractions are continuous (Goodier, 1937). Furthermore, we note that the thermoelastic stress at the center of a cube domain (equation (209)) is equal to the stress at the center of a spherical domain (equation (218)), that is, not affected by the sharp corners of the cube. Hence, modeling actual temperature perturbations by discontinuous box-like temperature distributions is valid.

4. Half Space Thermoelastic Solutions

The results of the above section are useful for order of magnitude estimates of the importance of thermoelastic stresses and reflect the more general aspects of thermoelastic stresses in and around inclusions of nonuniform temperature. These solutions are, however, for infinite solids and do not take into

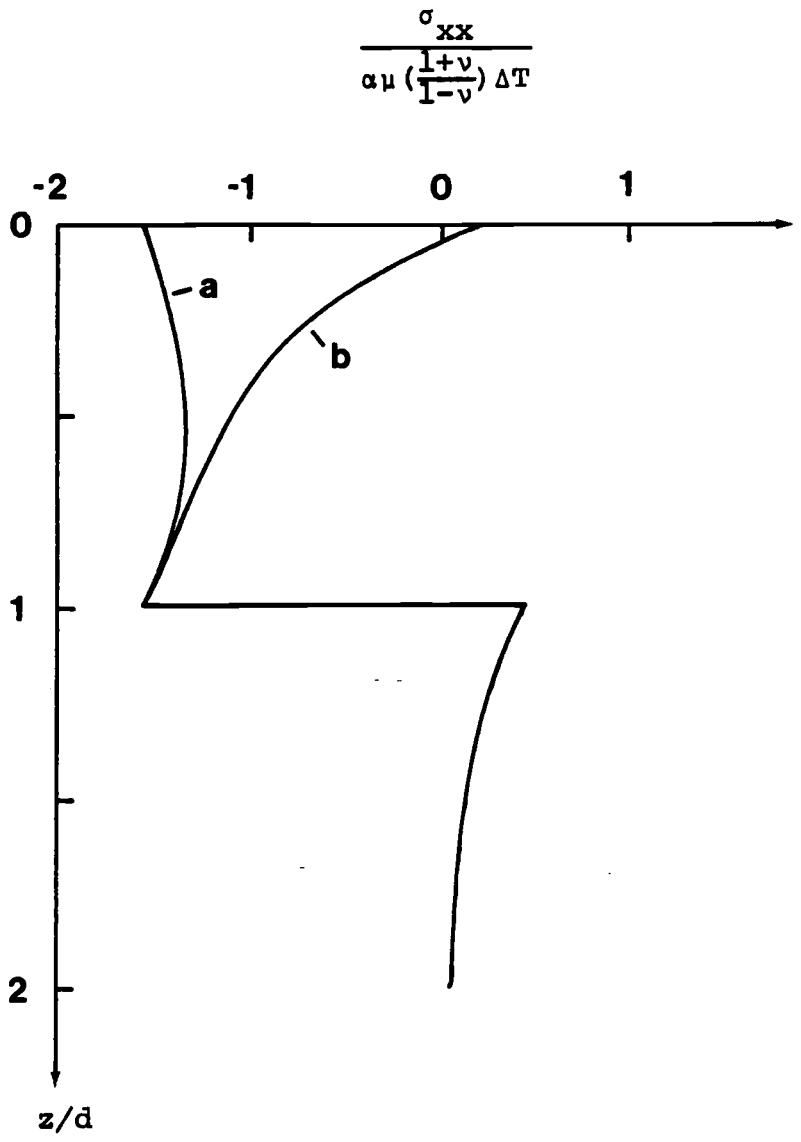

Figure 45. Horizontal thermoelastic stress through the center of a cube-domain of nonuniform temperature, in a) whole space and b) at a free surface (z=0).

account the effects of the Earth's stress free surface, which cannot be neglected in the case of geothermal systems. The appropriate model in such cases is the infinite half-space with a traction free surface.

The solution to this problem is based on the whole space solution, but to eliminate the stresses in the plane of the free surface we add an imaginary source volume V' in the second half space that is the reflection image of V in the free surface plane. This procedure eliminates the shear stress acting on the surface. To eliminate the normal stress on the free surface, due to the source-image pair, we add a negative virtual normal stress field of the same nagnitude in the free surface (Bodvarsson, 1976).

Mindlin and Cheng (1950) present this solution in operator form as follows. The thermoelastic displacement for the $z > 0$ half space is given by

(227) $$\bar{u} = - \nabla\phi - \nabla_2 \phi'$$

where

$$\phi = \frac{\alpha}{4\pi}\left(\frac{1+\nu}{1-\nu}\right) \int_V \frac{\Delta T(Q)\,dV_Q}{r_{PQ}}$$

(228)

$$\phi' = \frac{\alpha}{4\pi}\left(\frac{1+\nu}{1-\nu}\right) \int_{V'} \frac{\Delta T(Q)\,dV_Q}{r_{PQ}} = \frac{\alpha}{4\pi}\left(\frac{1+\nu}{1-\nu}\right) \int_V \frac{\Delta T(Q)\,dV_Q}{r_{PQ'}}$$

with

(229) $r_{PQ'} = ((x-x')^2 + (y-y')^2 + (z+z')^2)^{1/2}$

and the operator ∇_2 given by

(230) $\nabla_2 = (3-4\nu)\ \nabla + 2\nabla z\frac{\partial}{\partial z} - 4(1-\nu)\bar{k}\nabla^2 z$

where $\bar{k}$ is the unit vector in the z-direction. Since equation (204) is no longer applicable the stresses are calculated by equation (200).

Here

(231) $\nabla\cdot u = -\nabla^2\phi - (3-4\nu)\nabla^2\phi' - 2\nabla^2(z\frac{\partial\phi'}{\partial z})$

$$+ 4(1-\nu)\nabla\cdot(\bar{k}\nabla^2 z\,\phi'),$$

however $\nabla^2\phi' = 0$ for $z > 0$ and

(232) $\nabla^2(z\frac{\partial\phi'}{\partial z}) = 2\frac{\partial^2\phi'}{\partial z^2} + z\nabla^2\phi' = 2\frac{\partial^2\phi'}{\partial z}$

$$(233)\quad \nabla^2(z\phi') = 2\frac{\partial\phi'}{\partial z} + z\nabla^2\phi' = 2\frac{\partial\phi'}{\partial z}$$

or

$$(234)\quad \nabla\cdot(\bar{k}\nabla^2(z\phi')) = 2\frac{\partial^2\phi'}{\partial z^2}$$

Thus finally

$$(235)\quad \nabla\cdot\bar{u} = -\nabla^2\phi + 4(1-2\nu)\frac{\partial^2\phi'}{\partial z^2}$$

In Appendix H we verify that this solution does indeed satisfy the no stress boundary condition.

As an example of the effects of the free surface we can derive the horizontal component of stress σ_{xx} at the surface. From (227) and since

$$(236)\quad \left.\begin{aligned} \phi' &= \phi \\ \frac{\partial^n\phi'}{\partial x^n} &= \frac{\partial^n\phi}{\partial x^n}, \quad n = 1,2,\ldots \end{aligned}\right\} \text{at } z = o$$

we obtain

$$(237)\quad \epsilon_{xx}|_{z=o} = \frac{\partial u}{\partial x}|_{z=o} = -4(1-\nu)\frac{\partial^2\phi}{\partial x^2}$$

Based on (200) and (235), and the fact that $\nabla^2\phi|_{z=0} = 0$ if the free surface is outside V, then

$$(238) \qquad \sigma_{xx}|_{z=0} = -8(1-\nu)\mu \frac{\partial^2 \phi}{\partial x^2} + 4(1-2\nu)\lambda \frac{\partial^2 \phi}{\partial z^2}$$

Assuming symmetry in x and y and using $\nabla^2 \phi = 0$, then

$$(239) \qquad \frac{\partial^2 \phi}{\partial z^2} = -2 \frac{\partial^2 \phi}{\partial x^2}$$

Thus (using $\lambda = \frac{2\nu}{1-2\nu} \mu$)

$$(240) \qquad \sigma_{xx}|_{z=0} = -2\mu \frac{\partial^2 \phi}{\partial x^2} 4(1+\nu).$$

Hence, the horizontal stress near the free surface, due to a volume of nonuniform temperature, can become $4(1+\nu)$ times as great as the stress due to the same volume in an infinite medium. In common igneous rock this factor equals approximately five.

For later reference, it is now of interest to derive expressions for the component of horizontal stress σ_{xx} (or σ_{yy}), first in a general setting and later for more specific distributions of nonuniform temperature. By equation (200)

$$(241) \qquad \sigma_{xx} = 2\mu\varepsilon_{xx} + \lambda \nabla \cdot \bar{u} - (3\lambda + 2\mu)\alpha\Delta T$$

and thus by (235) (using again $\lambda = \frac{2\nu}{1-2\nu} \mu$)

$$(242)\quad \sigma_{xx} = 2\mu\left(\varepsilon_{xx} + 4\nu\,\frac{\partial^2\phi'}{\partial z^2} - \left(\frac{1+\nu}{1-\nu}\right)\alpha\Delta T\right)$$

where by (227)

$$(243)\quad \varepsilon_{xx} = -\frac{\partial^2\phi}{\partial x^2} - (3-4\nu)\,\frac{\partial^2\phi'}{\partial x^2} - 2z\frac{\partial^2}{\partial x^2}\left(\frac{\partial\phi'}{\partial z}\right)$$

The expressions for ϕ and ϕ' are given by equations (228). When dealing with a situation which is symmetric in x and y, we make use of the fact that (239) holds for ϕ' as well as ϕ and equations (242) and (243) simplify to

$$(244)\quad \sigma_{xx} = 2\mu\left(-\frac{\partial^2\phi}{\partial x^2} - (3+4\nu)\,\frac{\partial^2\phi'}{\partial x^2} - 2z\,\frac{\partial^2}{\partial x^2}\left(\frac{\partial\phi'}{\partial z}\right) - \left(\frac{1+\nu}{1-\nu}\right)\alpha\Delta T\right), \quad \text{if symmetric in x \& y}$$

Turning to a more specific example, consider the box domain V defined by

$$(245)\quad V = \{(x,y,z)\,|\,-\ell/2 < x,y < \ell/2,\ h < z < h + d\},$$

where $\Delta T = \Delta T(z)$, and derive analytical expressions for the stress component σ_{xx} along the z-axis through the center of the domain. Based on equations (228) and (244) we obtain after some tedious but elementary algebra

$$\frac{\sigma_{xx}(z)}{2\mu}\Big|_{x=y=o} =$$

$$\alpha\left(\frac{1+\nu}{1-\nu}\right)\left[\frac{(\ell/2)^2}{\pi}\int_h^{h+d}\Delta T(z')\left\{\frac{1}{((z-z')^2+(\frac{\ell}{2})^2)((z-z')^2+\ell^2/2)^{1/2}}\right.\right.$$

(246)

$$+\ \frac{3+4\nu}{((z+z')^2+(\frac{\ell}{2})^2)((z+z')^2+\ell^2/2)^{1/2}}$$

$$-\ \frac{2(z+z')z}{((z+z')^2+(\frac{\ell}{2})^2)((z+z')^2+\ell^2/2)^{3/2}}$$

$$\left.\left.-\ \frac{4(z+z')z}{((z+z')^2+(\frac{\ell}{2})^2)\ \ ((z+z')^2+\ell^2/2)^{1/2}}\right\}dz' - \Delta T(z)\right]$$

For given $\Delta T(z)$ this expression can be integrated numerically. Analytical expressions for $\sigma_{xx}(z)$, for the case ΔT = constant, are given in Appendix I. Numerical results are presented in Figure 45 above.

5. Estimates of Thermoelastic Stresses in Icelandic Hydrothermal Systems

We will now estimate the magnitude of stress of thermoelastic origin in two hydrothermal systems in Iceland, based on observed temperature profiles. The systems are considered to be domains of nonuniform temperature in a homogeneous, isotropic Hookean half space. The results of the last section are then applicable.

The analysis is based on the temperature profiles observed in the two LT systems of Laugarnes (or Reykjavik) and Laugaland (Figure 3). The main section of the temperature profiles, below the top 100-200m, are almost isothermal indicating predominantly advective vertical heat transport. Assuming the two systems evolved from a normal temperature environment, we can only conclude that in both systems the hydrothermal circulation has resulted in heating of the upper part of the formations and considerable cooling of the formations below 1 to 2km. This is certain to have strongly affected the distribution of flow permeability within the systems. To estimate the horizontal stress we use equation (246) with h = 0 and $\Delta T(z)$ given by

$$\Delta T(z) = T_{obs}(z) - \gamma z \tag{247}$$

where T_{obs} is the observed temperature and γ is the undisturbed regional temperature gradient of each area which we can estimate from the data of Palmason and Saemundsson (1979). It is important to point out that a linearly increasing temperature does not cause any thermoelastic stress (Boley and Weiner, 1960).

First we will estimate the thermoelastic stress in a hypothetical system where

$$(248) \qquad \Delta T = \begin{cases} 0 & \text{outside V} \\ T_o \sin(\frac{2\pi z}{d}) & \text{in V} \end{cases}$$

This functional form includes the general aspects of the nonuniform temperature observed in both systems and can be used as a good approximation for the ΔT observed in the Reykjavik system. The results for d = 2km and T_o = 50°C, applicable to the Laugarnes system, are presented in Figures 46, 47 and 48.

Also displayed is the horizontal stress due to the weight of the overburden in a Hookean half-space (Jaeger and Cook, 1976)

$$(249) \qquad \sigma_g = - \frac{\nu}{1-\nu} \rho g z$$

where ρ is the density of the subsurface material. It should be noted that the hydrostatic pressure of a water column extending from the surface would be approximately sufficient to balance the Hookean horizontal stress in

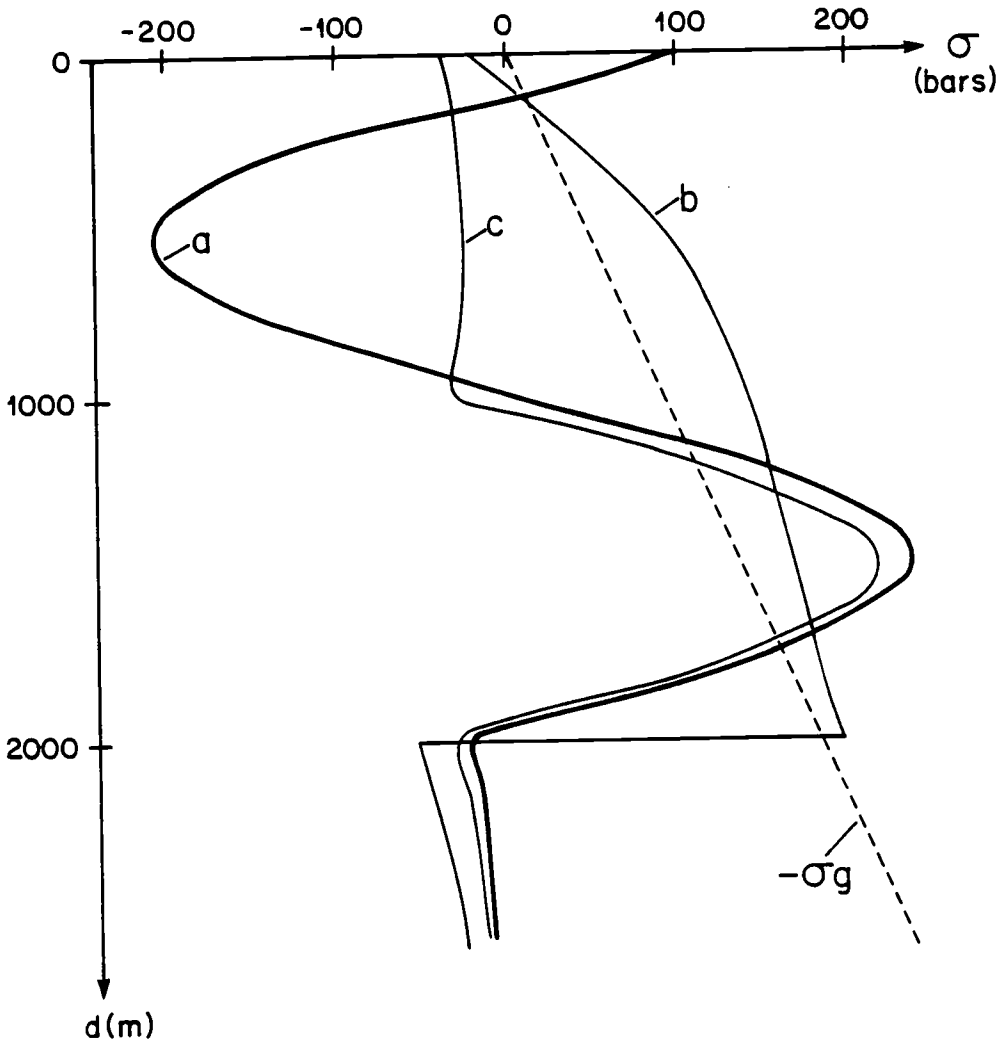

Figure 46. Horizontal thermoelastic stress through the center of a hypothetical geothermal system. The horizontal dimension l = 2km and a) $\Delta T = 50\sin(2\pi z/d)^\circ K$, $0 < z < 2km$, b) $\Delta T = -50^\circ K$, $0 < z < 2km$ and c) $\Delta T = 50\sin(2\pi z/d)^\circ K$, $1 < z < 2km$.

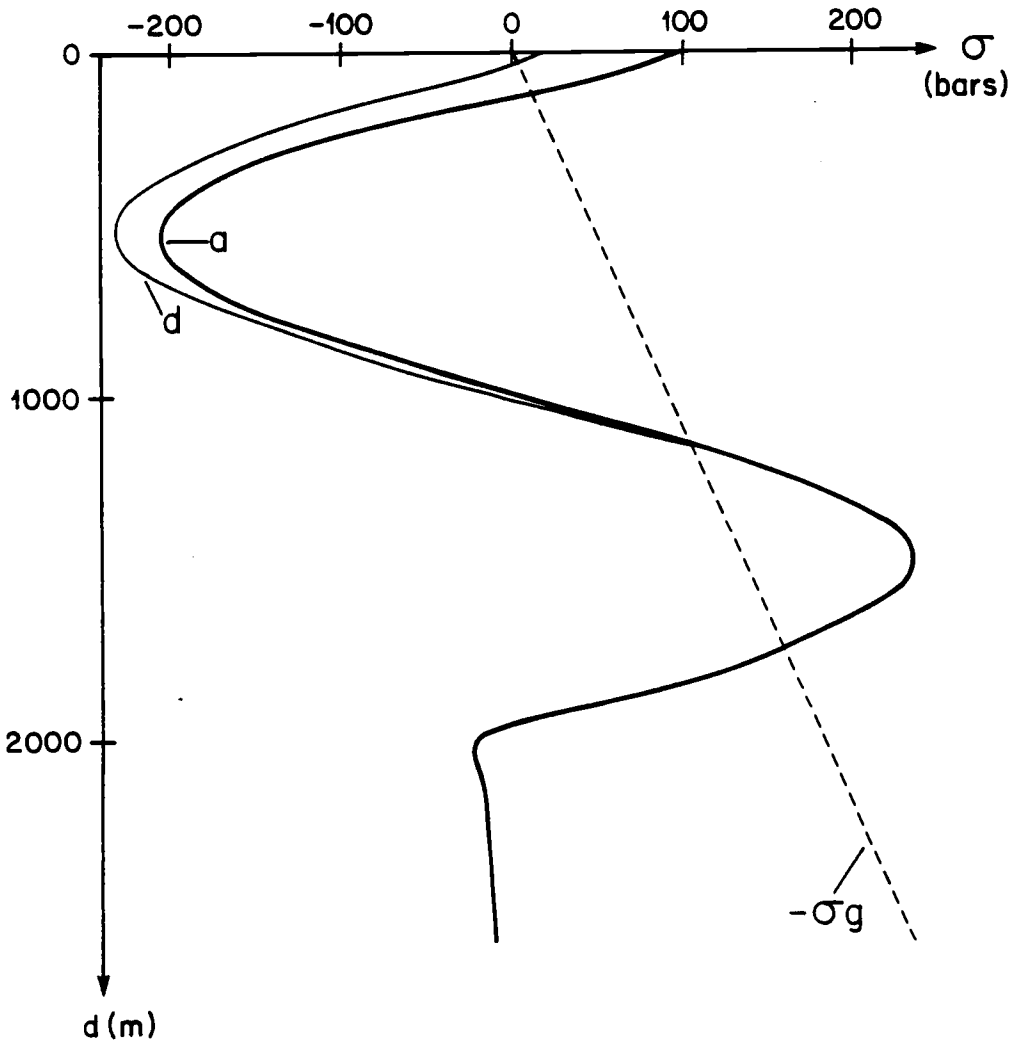

Figure 47. Horizontal thermoelastic stress through the center of a hypothetical geothermal system. The horizontal dimension l = 2km and a) $\Delta T = 50\sin(2\pi z/d)\,^{\circ}K$, $0 < z < 2km$ and d) whole space solution for comparison.

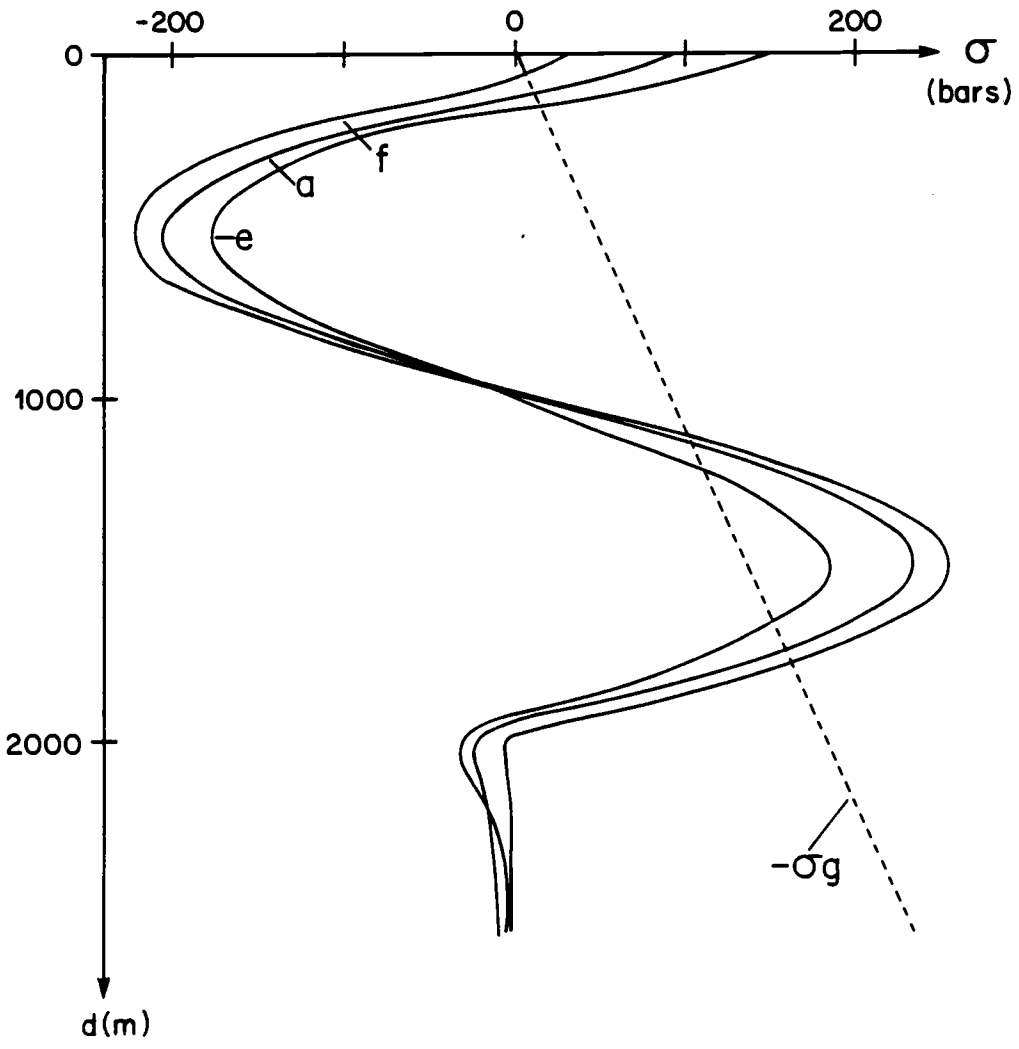

Figure 48. Horizontal thermoelastic stress through the center of a hypothetical geothermal system. $\Delta T = 50\sin(2\pi z/d)°K$, $0 < z < 2km$, and a) $l = 2km$, e) $l = 2/3km$ and f) $l = 4km$.

common igneous rock. However, all rocks have a non-vanishing rheidity and will therefore creep when acted on by forces of very long duration. The ideal Hookean situation is thus rarely found in nature. Due to rock creep, the horizontal stress in an initial Hookean state will gradually increase beyond the values given by equation (249) and will as time passes tend to a quasi-lithostatic stress, or

$$(250) \qquad \sigma_g = - \rho g z$$

which in common rock is approximately equal to 3-fold the Hookean stress.

The results in Figure 46 through 48 enable us to make the following observations

- The uppermost 100m experience considerable tensional stress, as a result of the expansion of the heated section below. This is likely to keep existing fractures open and cause additional fracturing. The next several hundred meters (down to 1000m) experience compressive stress, which in fact is considerably greater than hydrostatic pressure at the same water depth. This compressive stress will result in reduced fluid conductivity or even sealing of fractures. These effects have been discussed qualitatively by Bodvarsson (1976). The lower 1000m, on the other hand, experience considerable tensional stress which may enhance fluid

conductivity by keeping existing fractures open. The situation is of course affected by the regional horizontal stress that is superimposed on the thermoelastic stress.

- The tensional stress between 1200 and 1700m is somewhat greater than the compressive Hookean horizontal stress. Thus if the actual horizontal stress, due to the weight of the overburden and other forces, is less than about twice the Hookean stress, the thermoelastic stress and the hydrostatic pressure of water in fractures will suffice to keep fractures open. However, if the horizontal stress approaches the lithostatic limit, all fractures will close.
- Figure 46 indicates that the expansion of the top 1000m enhances the tensional thermoelastic stress at greater depth.
- The effect of the free surface is evident from the results of Figure 47.
- Finally, Figure 48 indicates the influence of the areal extent of the temperature anomaly. As we expect, on the basis of the results of section 3 above, the stress-magnitude increases with the areal extent, except in the top 100m where the reverse effect is seen. In the case of the Reykjavik field the areal extent of the anomaly is estimated at 3- 5km^2 (see section III.20 above) and the assumption d = ℓ thus seems reasonable.

- It should be mentioned that the above discussion is based on the assumption of a homogeneous, isotropic half space and the elastic effects of open fluid filled fractures, within the reservoir, are thus neglected.
- Hydrofracturing stress measurements at a depth of 400m in the Laugarnes field indicate horizontal compressive stress of the order 110-170 bars (Haimson and Rummel, 1982).

Turning now to the Laugaland-field, we model $\Delta T(z)$ as shown in Figure 49. Here $d \geq 3km$ and an unperturbed temperature gradient of 60°C/km is being assumed. We obtain the results presented in Figure 50. Being quite similar to the above results they require no additional comments.

The above estimates indicate that horizontal thermoelastic stress at depth in hydrothermal systems can be of the same order as the stress due to the weight of the overburden. Thermoelastic stress should thus be considered an important factor in the evolution of hydrothermal systems.

6. Penetration of Water into Hot Rock by Convective Downward Migration of Fractures

As discussed in section II.6 above the extremely high output of energy from some geothermal areas is difficult to explain unless water actually penetrates

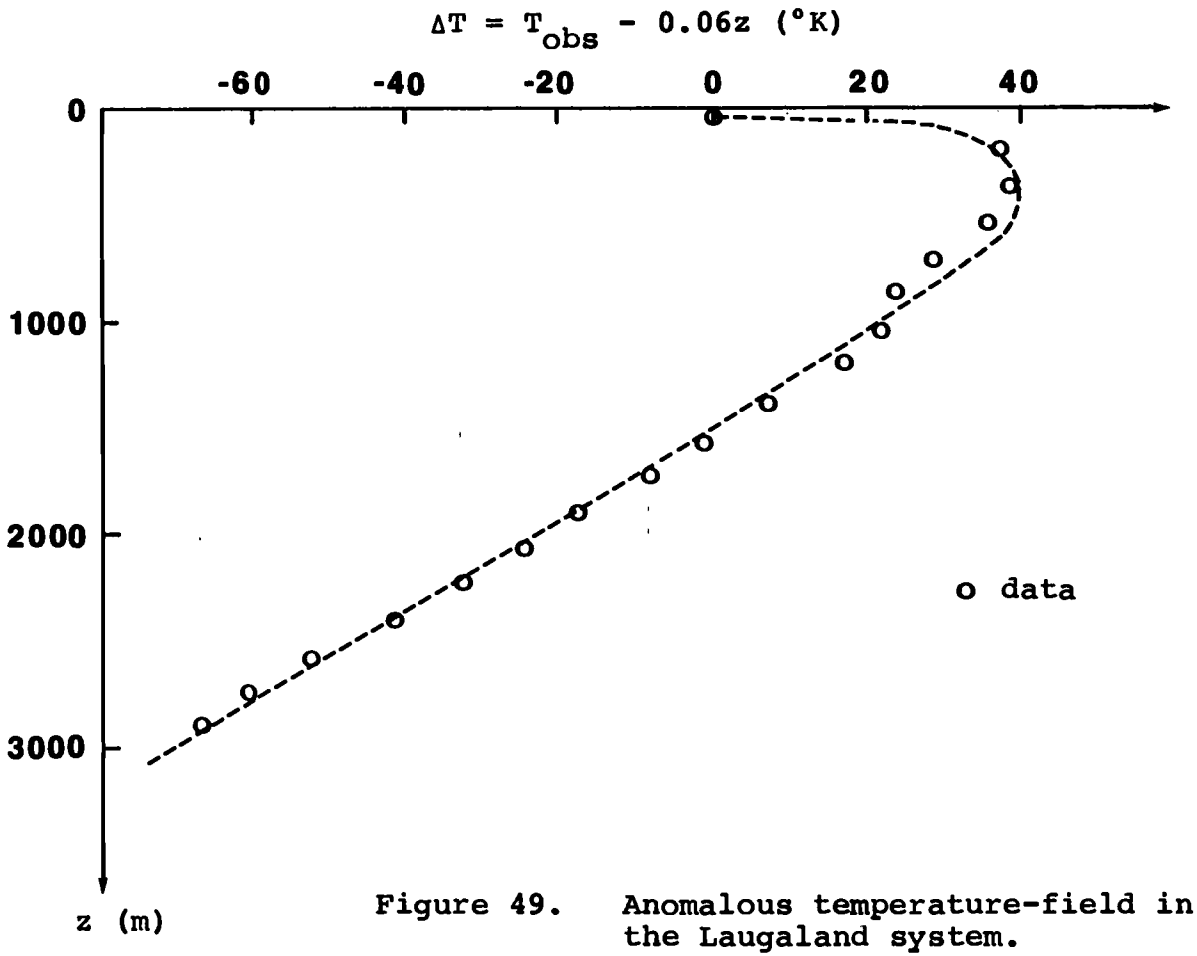

Figure 49. Anomalous temperature-field in the Laugaland system.

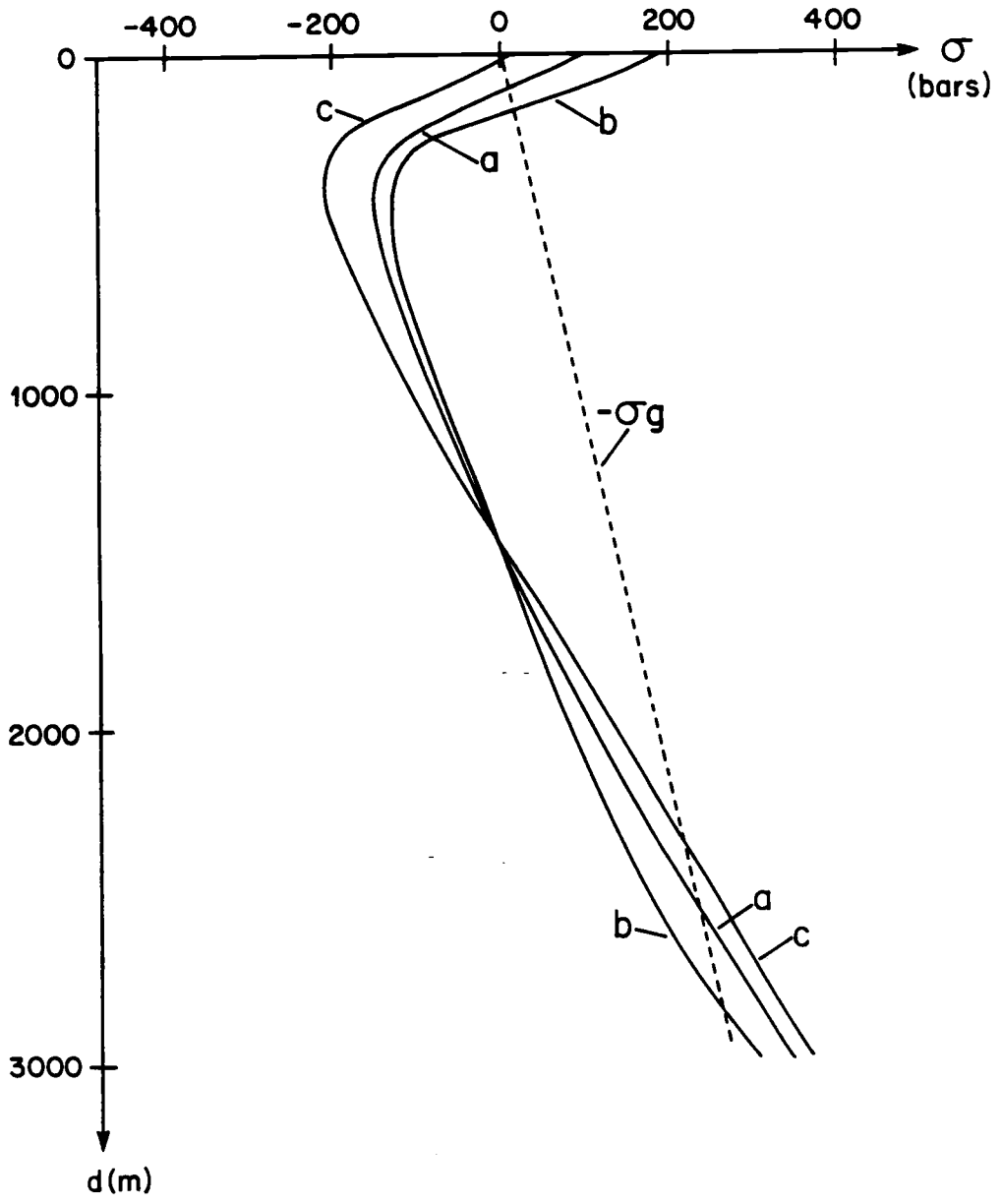

Figure 50. Estimates of the horizontal thermoelastic stress at depth in the Laugaland system. a) l = 3km, b) l = 1km and c) l = 9km.

into the hot rock, that is the heat source of the thermal activity, by a process such as the CDM-process. To reiterate, CDM operates on the principle that convective fluid motion in open vertical fractures is associated with the withdrawal of heat from the formation at the lower boundary resulting in thermoelastic contraction of the adjacent rock that tends to increase the local fracture aperture and cause further opening of additional fracture space at the bottom. Fractures harboring such convective fluid motion can therefore migrate downward by the process, greatly enhancing the rock/water heat transfer. We are here dealing with a highly complex problem of elastomechanical/hydrodynamical interaction that defies any exact mathematical description.

We are interested in the CDM-process as a possible source mechanism of the LT-activity in Iceland (see section II.7). The rate of migration, at various stress conditions, is the parameter of main interest, as well as estimates of the magnitude of the regional stress fields where CDM might be possible. Having obtained the rate of CDM, the heat transfer rate can be estimated.

Before presenting the results of our own analysis we will briefly review earlier estimates of Bodvarsson (1979; 1982b) and the related results of Lister (1974; 1976; 1982).

Based on the observation that the opening of new fracture flow space requires that the thermoelastic contraction extend to a sufficient distance from the fracture tip (see Figure 52) Bodvarsson (1982) roughly estimates the possible rate of CDM. The volume of temperature reduction, surrounding the fracture, decreases with increasing migration velocity. Hence the rate of penetration is determined by a proper balance between the required contraction volume and the volume of temperature reduction. On the basis of such considerations Bodvarsson (1982) obtains the order of magnitude estimate of the rate of migration $v = 0.3$ to 3 m/yr.

Lister (1974; 1982) carries out a lengthy and elaborate investigation of the possible penetration of seawater into hot ocean crust. He develops a theory for the mechanism of penetration of water into hot rock by considering the simplest possible 1-D model (Figure 51). The concept of a cracking front is used to separate the convective regime in cracked rock from the conductive boundary layer below it. The rock in the boundary layer cools, shrinks and builds up horizontal tensile stress as resistance to creep rises. Cracking occurs when the tensile stress slightly exceeds the tensile strength of the rock and on Lister's model results in the stable downward propagation of a polygonal pattern of vertical

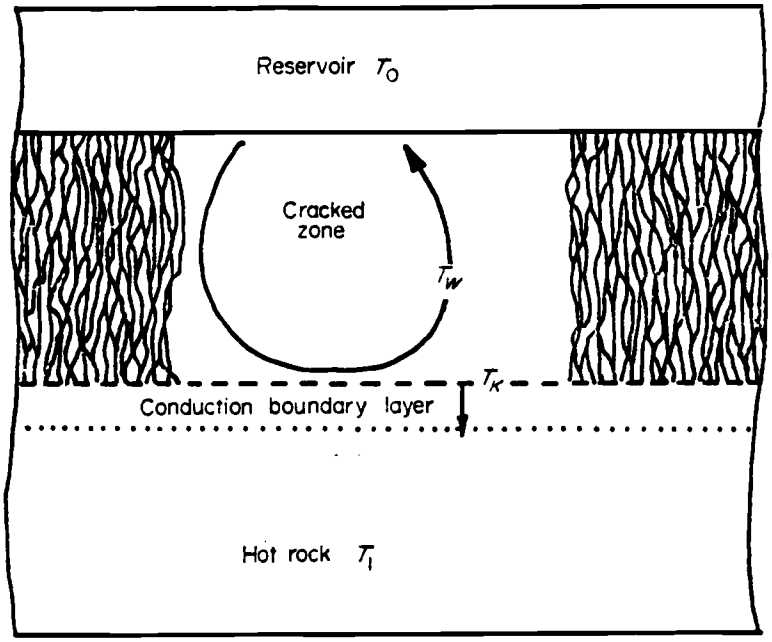

Figure 51. The one-dimensional cracking front model of Lister (1974).

cracks. Further cooling opens these cracks to the percolation of water. By combining various analytical and empirical results from rock mechanics, convection in porous media and heat conduction, he arrives at quasi-quantitative relationships for this physical process. Lister (1974) compares the estimated tensile stress of his model to a very crude estimate of the tensile stress in an experiment by Martin (1972) on the stable propagation of cracks in single-crystal quartz. Based on these data he obtains an estimate of the excess tensile stress needed to propagate the model crack system. This estimate, that is at the heart of his theory, appears quite uncertain. Based on this reasoning he arrives at a crack spacing which in turn enables him to estimate a mean permeability. Applying finally the experimental results of Elder (1965) on convection in porous media, which depend on the mean permeability, Lister (1974) obtains his estimate of the cracking front velocity. Assuming a cracking temperature, i.e. the temperature at which rock cracks due to the combination of incrasing tensile stress from the cooling and increased brittleness as its temperature drops, between 800 and 1000°K Lister (1974) obtains $v \approx 30\text{-}200$ m/yr. This estimate is very high and would result in a tremendous power output of 3 to 17 kW/m^2.

Lister (1976) extends his analysis to HT-hydrothermal systems and concludes, on the basis of qualitative consideration of 3-D effects, that penetration rates must be considerably slower. Later, Lister (1982) revises his 1974 theory and concludes that the rate of water penetration into cooling, shrinking and cracking rock is probably only of the order 10 m/yr.

Qualitatively, Lister's model is plausible and it seems likely that a similar process is the source mechanism of HT-activity (Bodvarsson, 1982b; Bjornsson et al., 1982). Moreover, it may possibly explain the penetration of water into the hot oceanic crust (Palmason, 1967; Bodvarsson and Lowell, 1972; Lister, 1972). However, Lister's quantitative results appear rather uncertain and the much simpler estimates of Bodvarsson (1982) may be as relevant. Bjornsson et al. (1982) estimate the rate of cooling front penetration in the Grimsvotn HT-area in Iceland (section II.6) at 5 m/yr on the basis of a simple heat balance argument. On the basis of these indications we surmise that the rate of CDM may be roughly of the order of magnitude of meters per year. Moreover, Lister's 1-D model appears too simple to do justice to the various complexities of the CDM-process.

7. Two-dimensional CDM Fracture Model

We now turn to a more specific, hypothetical model on which our analysis of CDM of fractures as a possible source mechanism of the LT-activity in Iceland will be based. This model is sketched in Figure 52 where CDM takes place in a single existing unwelded quasi-vertical fracture such as along the wall of a dike or within a fault zone. On this model the fracture is considered to be very long in the horizontal direction, such that a 2-D treatment of the problem is adequate. The open section of the fracture has migrated by the CDM-process down to some depth. Above this depth convective liquid motion transports heat vertically whereas below this depth the fracture is closed by the weight of the overburden and regional tectonic stresses. We will consider the cooling of the rock by the process to be linearly increasing with depth, which is consistent with the notion that LT-systems can evolve within a normal, constant temperature gradient environment. The associated volume of temperature reduction and thermoelastic contraction is, of course, dependent on the rate of migration, the parameter of main interest.

This rate is determined by a proper balance of the tensile thermoelastic stress and the impressed compressive stress at the tip of the fracture. On this

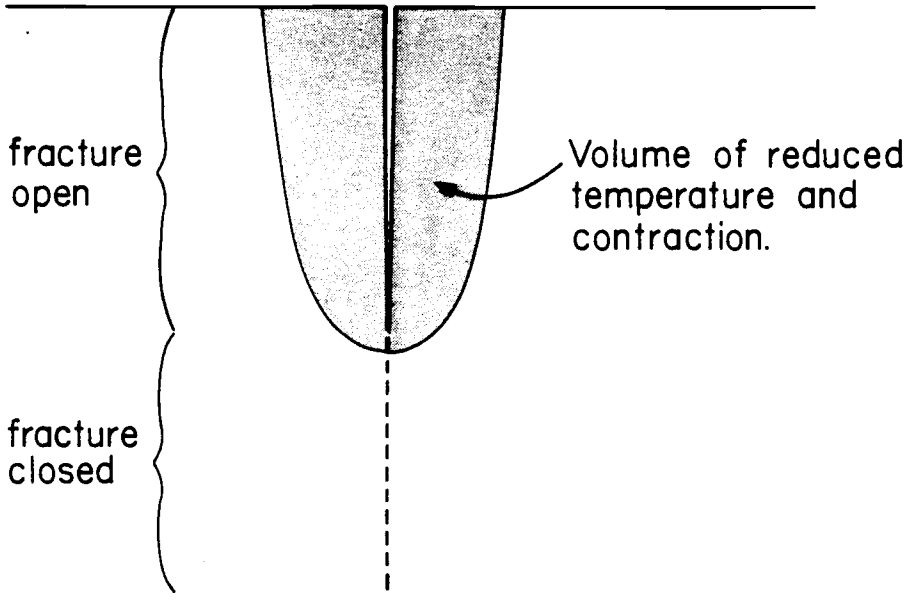

Figure 52. The two-dimensional single CDM fracture model.

model cold water is channeled down to the lower part of the open fracturee where the liquid is heated and rises, resulting in a convective flow system within the open fracture (see also Figure 5 above).

Before turning to calculations based on this model we compare it with the model proposed by Lister (1974) (Table XVI). Our results are based on a well defined mathematical problem, which should approximately reflect actual field situations.

The CDM-process involves a complex interaction of the following factors:

i) stress-field around the fracture,
ii) conduction of heat in the rock around the fracture and
iii) convection of water in the open fracture.

Although this problem defies an exact mathematical description, we are nevertheless able to present an approximate mathematical approach that enables us to obtain approximate CDM rate estimates. We proceed as follows:

- To simplify the calculation of the temperature-field around the migrating fracture, which results from the complex conductive/convective heat transport process, we assume the convection to be intense enough to maintain the walls of the open fracture at an approximately

Table XVI Model comparison

Lister (1974; 1982)	Present work
CDM in unfractured, virtually impermeable, hot crustal rock.	CDM in crust already in thermal equilibrium, after initial cooling of each dike, intrusion or flow, partially by CDM.
Water temperature > 200 °C.	LT-activity.
1-D model.	2-D model, one fracture.
CDM by fracturing of rock.	CDM in an already existent partially closed but unwelded vertical fracture.

constant temperature. This assumption is based on the observation that fractures as narrow as a few 10^{-4}m can maintain well developed convective flows (Bodvarsson, 1978). The implications of this assumption will later be estimated. This assumption is also supported by temperature-profiles observed in LT-areas in Iceland (Figure 3).

- Based on the above assumption we will calculate the temperature-field in the rock around the migrating fracture as a function of the rate of downward migration.
- Upon the temperature-field results we will estimate the thermoelastic stress at the tip of the open portion of the fracture, at various rates of migration.
- Upon estimating the stress at the tip of the fracture due to the weight of the overburden, other forces and the water pressure in the fracture, we balance the resulting stress with the thermoelastic stress to obtain the total stress at the tip of the fracture, that enables us to estimate the downward rate of migration.

These model-calculations are performed in the next three sections.

8. Temperature-field Around a Migrating Fracture

To estimate the temperature field around a fracture that contains a liquid of a given temperature and migrates at a velocity v into an isothermal, homogeneous and isotropic solid, we proceed as follows. In solving the heat conduction equation for this case, it is convenient to represent the fracture by a fixed source sheet in the -z portion of the xz-plane, of source density

$$(251) \qquad \begin{cases} \delta(y)\, S(z) & , \quad z < 0 \\ 0 & , \quad z > 0 \end{cases}$$

and let the solid move with velocity v in the -z direction (Figure 53). Assuming stationary conditions the equation for the temperature field T(y,z) is

$$(252) \qquad -\frac{v}{a}\,\partial_z T - (\partial_{yy} + \partial_{zz})T = \delta(y)S(z)/k$$

where a is the thermal diffusivity of the solid and k the thermal conductivity. To solve this equation set

$$(253) \qquad T(y,z) = e^{\alpha z}U(y,z),$$

with $\alpha = \frac{-v}{2a}$. Equation (252) then transforms to

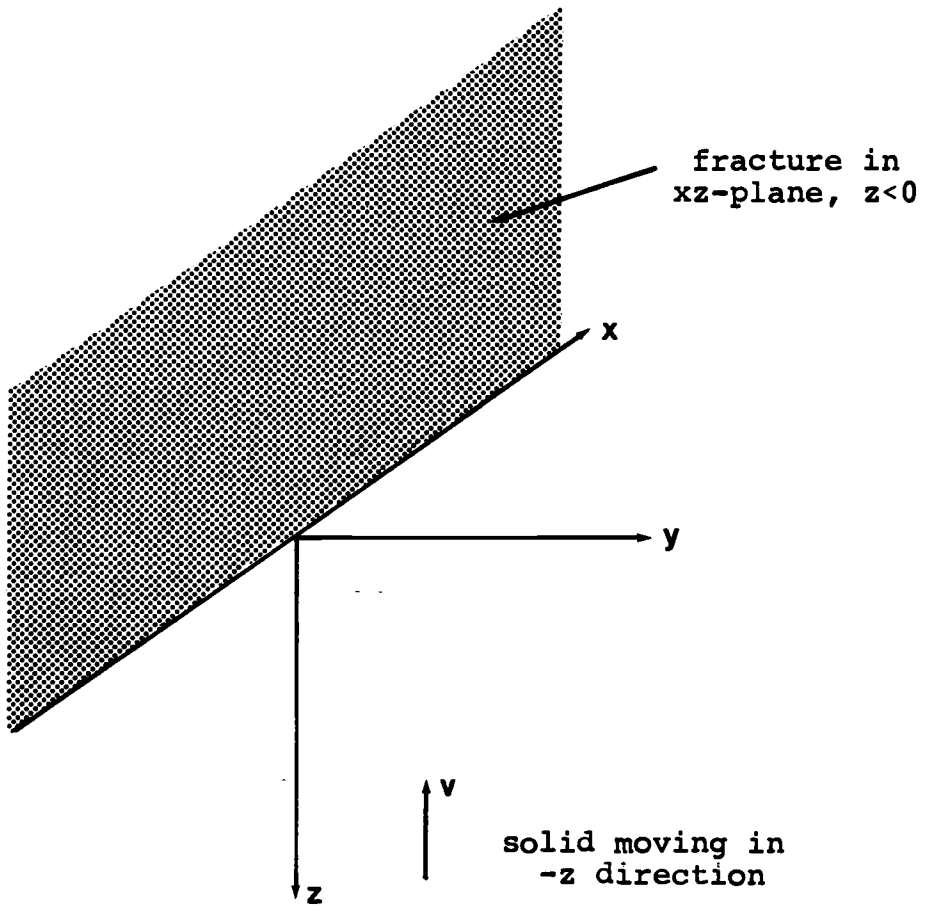

Figure 53. The fixed source sheet in a moving solid.

$$(254) \quad \left(\frac{v}{2a}\right)^2 U - (U_{zz} + U_{yy}) = \delta(y)S(z)\exp\left(\frac{vz}{2a}\right)/k$$

To solve (254), we first solve the simpler equation

$$(255) \quad \left(\frac{v}{2a}\right)^2 V - (V_{zz} + V_{yy}) = \delta(y)\delta(z)$$

and obtain U(y,z) by

$$(256) \quad U(y,z) = (1/k)\int_{-\infty}^{\infty} V(y,z-z')S(z')\exp\left(\frac{vz'}{2a}\right)dz'$$

Equation (255) can be rewritten

$$(257) \quad \left(\frac{v}{2a}\right)^2 V - \frac{1}{r}\frac{d}{dr}(rV_r) = \frac{\delta(r)}{2\pi r}$$

$$r^2 = y^2 + z^2$$

We Hankel transform (257) (Duff and Naylor, 1966)

$$(258) \quad \left(\frac{v}{2a}\right)^2 \hat{V} + s^2\hat{V} = \frac{1}{2\pi} ,$$

where $\hat{V}$ is the transform of V and s the transform variable. Hence

$$(259) \quad \hat{V} = \frac{1}{2\pi}\,\frac{1}{\left(\frac{v}{2a}\right)^2+s^2}$$

and inverting (259) (Duff and Naylor, 1966) leads to

$$(260) \qquad V(r) = \frac{1}{2\pi} K_o \left(\frac{vr}{2a}\right) ,$$

where K_o is the modified Bessel function of the second kind. The temperature around the migrating fracture is finally obtained by

$$(261) \quad T(y,z) = \frac{1}{2\pi k} \exp\left(-\frac{vz}{2a}\right) \int_{-\infty}^{o} \exp\left(\frac{vz'}{2a}\right) K_o\left(\frac{vr'}{2a}\right) S(z')dz'$$

$$\text{with } r' = (y^2+(z-z')^2)^{1/2}$$

with $S(z)$ the unknown source density.

We are here interested in estimating the temperature of the solid, $T(y,z)$, when the temperature of the fracture walls relative to the undisturbed temperature of the solid is known and equal to $T_o(z)$. To obtain the source density resulting in the given wall temperature we need to solve the following integral equation for $S(z)$

$$(262) \quad T_o(z) = \frac{1}{2\pi k} \exp\left(-\frac{vz}{2a}\right) \int_{-\infty}^{o} \exp\left(\frac{vz'}{2a}\right) K_o\left(\frac{v|z-z'|}{2a}\right) S(z')dz'$$

This equation can be approximately discretized and written in matrix form

$$(263) \qquad \bar{T} \simeq \frac{1}{2\pi k} G\bar{S}$$

where

$$T_j = T_o(z_j) \ , \ z_j = j(-\Delta z) \qquad j = 1,\ldots N$$

$$S_i = S([i-\tfrac{1}{2}][-\Delta z']) \qquad i = 1,\ldots N \tag{264}$$

$$G_{ij} = \int_{i(-\Delta z')}^{(i-1)(-\Delta z')} \exp\left(\frac{v(z'-z_j)}{2a}\right) K_o\left(\frac{v|z-z'|}{2a}\right) dz'$$

with Δz and $\Delta z'$ positive and appropriately chosen. The matrix G is a square matrix and the solution is thus given by

$$\bar{S} = 2\pi k G^{-1} \bar{T} \tag{265}$$

After numerically obtaining the inverse G^{-1}, we obtain for the case $T_o(z) = T_o$ the results presented in Figure 54. It is evident from the results that the source density can be fairly well approximated by

$$S(z) = 2kT_o \left(\frac{v}{\pi a}\right)^{1/2} |z|^{-1/2} \ , \ z < o \tag{266}$$

This result is not surprising considering that in the case of a half-space, with surface temperature T_o, that at time t = o is at zero temperature, the rate of heat transfer per unit surface area is (Carslaw and Jaeger, 1959)

$$q(t) = \frac{kT_o}{(\pi a t)^{1/2}} \ , \ t > o \tag{267}$$

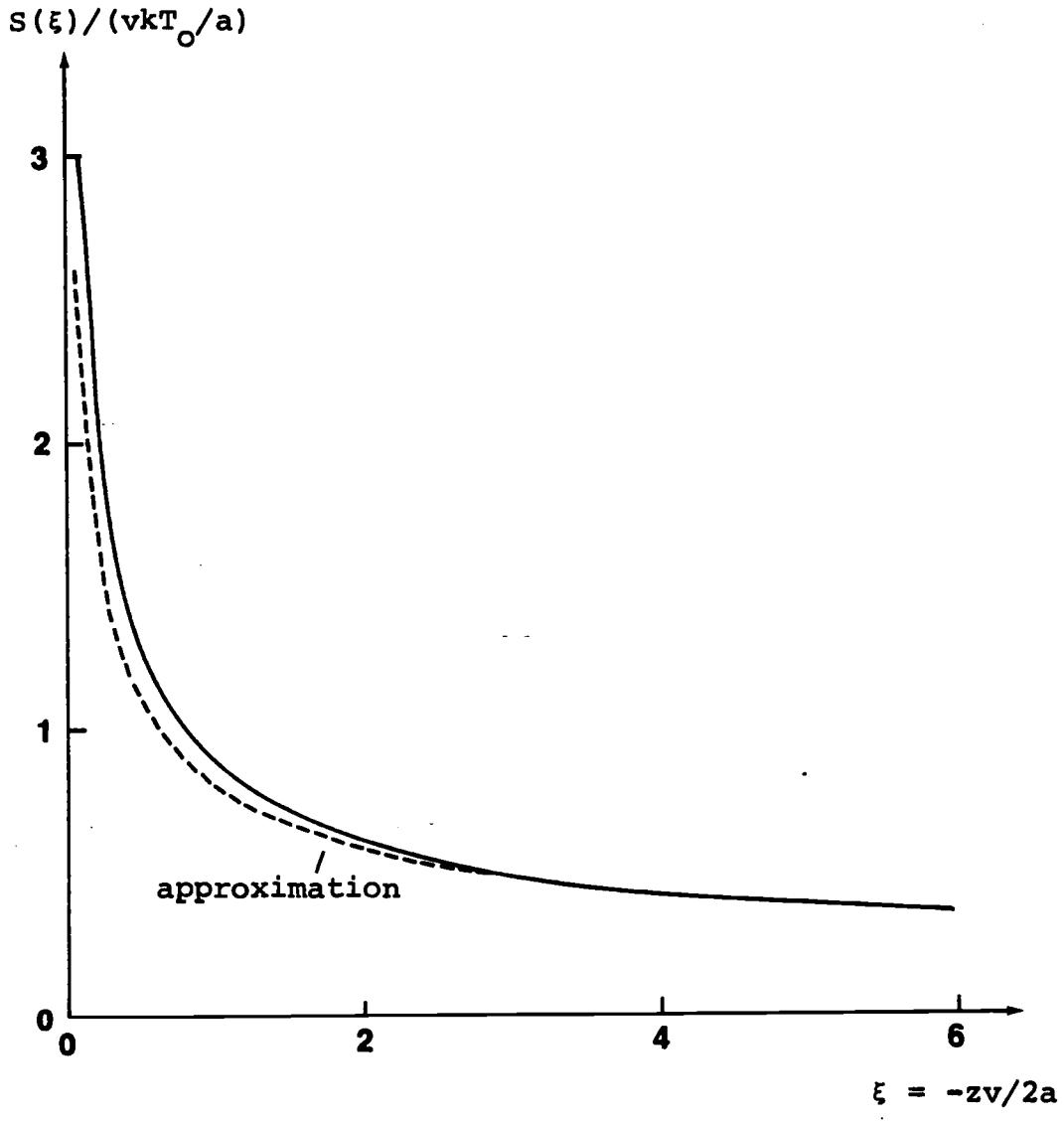

Figure 54. The source density S(z) for a migrating fracture with $T_o(z) = T_o$, along with the approximation $S(z) = 2kT_o(v/\pi a|z|)^{\frac{1}{2}}$.

In the case of a fracture migrating with a constant velocity v, the time since the fracture tip was at the depth z is given by $t = |z|/v$. Inserting this in equation (267) and multiplying by a factor of two, to account for both fracture walls, results in equation (266). This result indicates that the heat transfer is close to being one-dimensional, with negligible heat transfer in the z-direction, except right at the fracture tip.

To estimate the temperature field in the solid we use equation (261), with the source density given by equation (266), and numerically obtain the results presented in Figure 55.

A result of the apparent one-dimensional heat conduction is that the temperature of the solid can be approxiamted by (Carslaw and Jaeger, 1959)

$$(268) \qquad T(y,z) = T_o \operatorname{erfc}\left(\frac{y}{2(at)^{1/2}}\right)$$

where t is again the time since the fracture tip was at the depth z, thus t is a function of the depth, z, and the velocity, v. When the velocity is constant the temperature-field can be approximated by

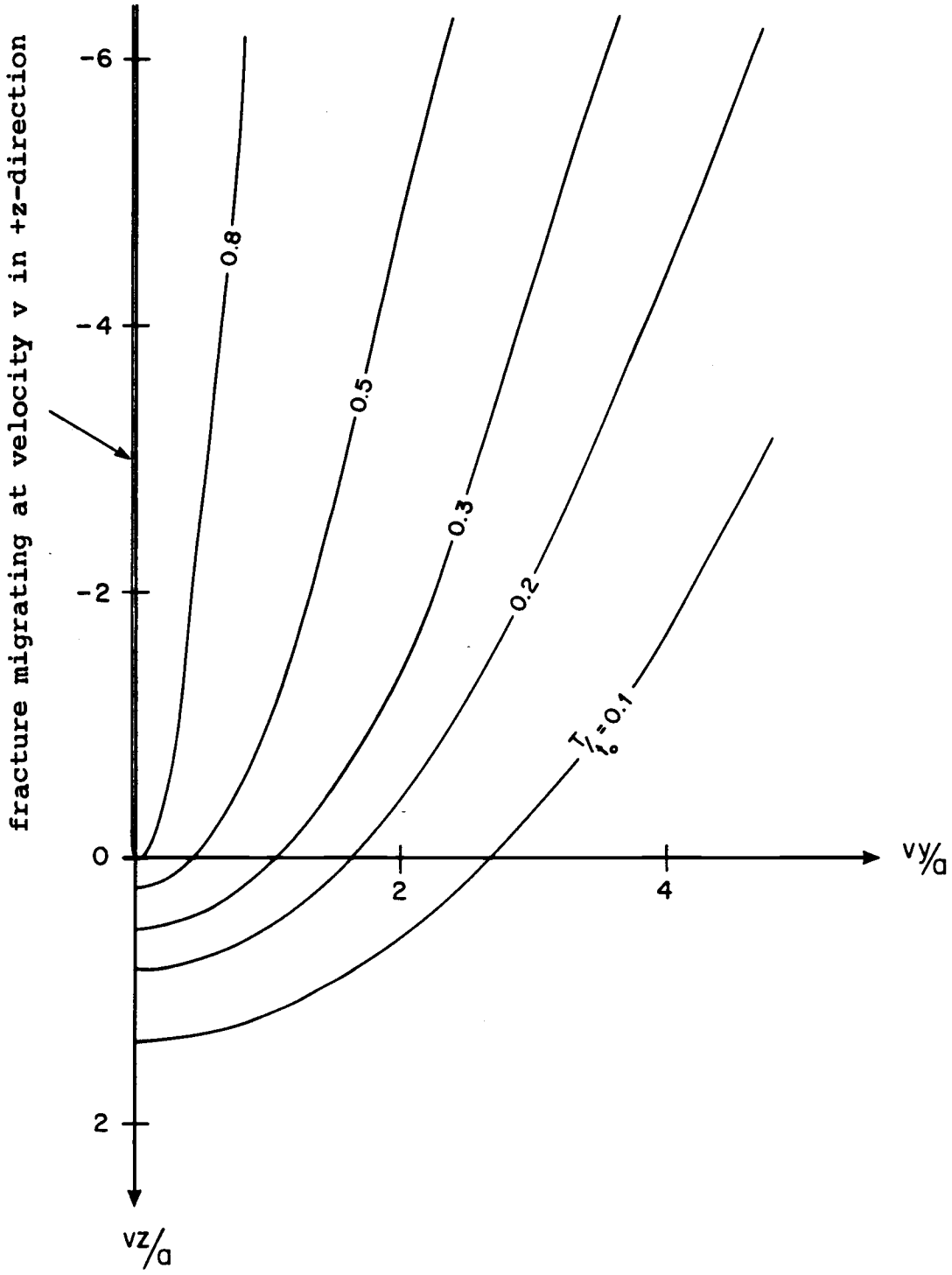

Figure 55. Temperature-field around a migrating fracture.

$$(269)\qquad T(y,z) = \begin{cases} T_o \operatorname{erfc}\left(\dfrac{vy/a}{2(v|z|/a)^{1/2}}\right) & , \quad z < o \\ o \end{cases}$$

By comparing (269) with the results in Figure 55, we find that this approximation is excellent for $r = (y^2 + z^2)^{1/2}$ greater than one to a few a/v.

9. Stress at Tip of CDM Fracture

To estimate the stress around the fracture of our model, in particular at the fracture tip, we need to solve the problem set up in equation (270) below (also see equation (201)) and in Figure 56. As mentioned above we will consider this a 2-D problem, thus

$$(270)\qquad \begin{aligned} &\mu\nabla^2\bar{u} + (\lambda + \mu)\nabla\nabla\cdot\bar{u} = 3\alpha k\nabla(\Delta T(y,z)) - \rho g\bar{k}, \text{ in } z > 0 \\ &\sigma_{xy} = \sigma_{zy} = 0 \quad , \quad y = 0 \\ &\sigma_{yy} = -p(z) \quad , \quad \begin{matrix} y = 0 \\ z < d \end{matrix} \\ &u_y = 0 \quad , \quad \begin{matrix} y = 0 \\ z > d \end{matrix} \\ &\sigma_{yy} = -P(z) \quad , \quad y >> d \end{aligned}$$

where $k = \dfrac{3\lambda+2\mu}{3}$, $\rho g\bar{k}$ is the force due to gravitation, p(z) the hydrostatic pressure of the water in the fracture, u_y the horizontal displacement of the fracture wall and P(z)

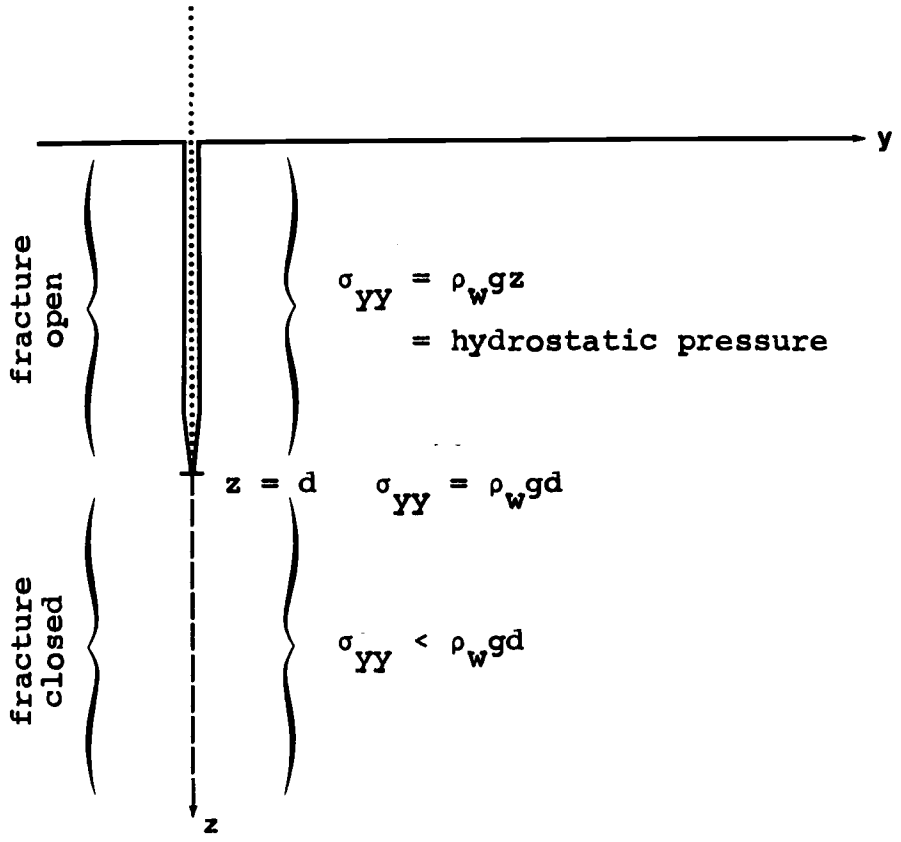

Figure 56. Stress conditions in the plane of an unwelded CDM-fracture.

accounts for all horizontal stress in addition to the stress due to the weight of the overburden, such as due to creep and tectonic forces. Other parameters are as defined in section 2 above. In addition the solution must satisfy a no-traction boundary condition on the surface z = 0.

By first solving

$$\mu\nabla^2\bar{u}_A + (\lambda + \mu)\nabla\nabla\cdot\bar{u}_A = 3\alpha k\nabla(\Delta T(y,z))$$

(271)
$$\sigma_{xy}^A = \sigma_{zy}^A = 0 \quad , \quad y = 0$$
$$u_y^A = 0 \quad , \quad y = 0$$

and then solving

$$\mu\nabla^2\bar{u}_B + (\lambda + \mu)\nabla\nabla\cdot\bar{u}_B = -\rho g\bar{k}$$

(272)
$$\sigma_{xy}^B = \sigma_{zy}^B = 0 \quad , \quad y = 0$$
$$\sigma_{yy}^B = -p(z) - \sigma_{yy}^A \quad , \quad \begin{matrix} y = 0 \\ z < d \end{matrix}$$
$$u_y^B = 0 \quad , \quad \begin{matrix} y = 0 \\ z > d \end{matrix}$$
$$\sigma_{yy}^B = -P(z) \quad , \quad y >> d$$

the solution to (270) is simply given by

(273) $$\bar{u} = \bar{u}_A + \bar{u}_B \ ,$$

as can be easily verified.

To solve (271) we observe that the boundary conditions are automatically satisfied since $\Delta T(y,z)$ is

symmetric in y. Furthermore, based on the results of section 4 above, we are justified in neglecting the free surface effects on z = 0. We are thus left with a simple thermoelastic problem that can be solved on the basis of section 3 above. Thus the horizontal component of stress σ_{yy}^{A} is given by equation (204) with

$$\frac{\partial u_y^A}{\partial x}\Big|_{x=y=o} = \tag{274}$$

$$\frac{\alpha}{4\pi}\left(\frac{1+\nu}{1-\nu}\right) \int_{-\infty}^{\infty}\int\int dz'dy'dx' \; \frac{[x'^2+(z-z')^2-2y'^2]}{r_{PQ}^5} \; \Delta T(y',z')$$

where r_{PQ} is defined as before. After considerable algebra (Appendix J) we are able to rewrite (274)

$$\frac{\partial u_y^A}{\partial y}\Big|_{x=y=o} = \frac{\alpha}{\pi}\left(\frac{1+\nu}{1-\nu}\right) \int_o^{\pi} d\theta \int_o^{\infty} dr \; \frac{\cos 2\theta}{r} \; \Delta T(r,\theta)$$

$$+ \frac{\alpha}{2}\left(\frac{1+\nu}{1-\nu}\right)\Delta T(y,z)\Big|_{y=o} \tag{275}$$

where $z' = z - r\cos\theta$
$y' = r\sin\theta$

thus

$$\sigma_{yy}^{A}\Big|_{y=o} = 2\mu\alpha\left(\frac{1+\nu}{1-\nu}\right)\left[I(z) - \frac{\Delta T(y,z)}{2}\Big|_{y=o}\right] \tag{276}$$

with

$$(277) \qquad I(z) = \frac{1}{\pi}\int_0^{\pi} d\theta \int_0^{\infty} dr \, \frac{\cos 2\theta}{r}\, \Delta T(r,\theta)$$

The function I(z) can be calculated numerically as follows

$$I(z) \approx \frac{1}{\pi}\int_0^{\pi} d\theta \int_0^{2d} dr \, \frac{\cos 2\theta}{r}\, \Delta T(r,\theta)$$

$$(278) \qquad \approx \frac{1}{\pi}\int_0^{\pi} d\theta \int_{\ln(2\varepsilon)}^{\ln(2d)} \cos(2\theta)\, \Delta T(e^s,\theta)\, ds$$

$$\text{with } s = \ln(r)$$
$$\varepsilon << d$$

or

$$I(z) \approx \frac{\Delta s \Delta\theta}{\pi} \sum_{i=1}^{N} \sum_{j=1}^{M} \cos(2\theta_j)\, \Delta T(r_i \sin\theta_j, z - r_i \cos\theta_j)$$

$$(279) \qquad \text{with } \Delta\theta = \pi/M$$
$$\theta_j = (j - 1/2)\Delta\theta$$
$$\Delta s = \ln(2d/\varepsilon)/N$$
$$r_i = \varepsilon^{1-\phi}(2d)^{\phi}$$
$$\text{and} \quad \phi = (i - 1/2)/N$$

with ΔT obtained as described in section 8 above.

Solving the second half of our problem, as presented by equation (272), is considerably more complex because of the mixed stress/displacement condition on the xz-

plane. Luckily, Sneddon and Lowengrub (1969) present an analytical solution to a quite similar problem, the problem of the Griffith crack. The Griffith crack is symmetric about the z = 0 plane and thus partially satisfies the no-traction condition on that surface (there are no shear stresses acting on the z = 0 surface). However, this solution results in some normal stress acting on the z = 0 surface. Considering other uncertainties involved in our model, and the fact that we are only interested in the stresses at the tip of the fracture, we are justified in neglecting this normal stress and basing our estimates on the solution of Sneddon and Lowengrub (1969).

We need to solve

$$\mu \nabla^2 \vec{u}_c + (\lambda + \mu) \nabla \nabla \cdot \vec{u}_c = 0$$

(280)
$$\sigma_{xy}^c = \sigma_{zy}^c = 0 \quad , \quad y = 0$$

$$\sigma_{yy}^c = - \zeta(z) \quad , \quad \begin{matrix} y = 0 \\ z < d \end{matrix}$$

$$u_y^c = 0 \quad , \quad \begin{matrix} y = 0 \\ z > d \end{matrix}$$

$$\sigma_{yy}^c = 0 \quad , \quad y >> d$$

with $\zeta(z) = p(z) + \sigma_{yy}^A + \sigma_g - P(z)$, where σ_g is the horizontal Hookean stress due to the weight of the overburden, given by equation (249) above. The solution to our problem is then given by

$$\sigma_{yy} = \sigma_{yy}^{c} + \sigma_{yy}^{A} + \sigma_g - P(z)$$

(281)

$$u_y|_{y=o} = u_y^c|_{y=o}$$

The solution of (280), in the plane of the fracture, is given by (Sneddon and Lowengrub, 1969):

$$\sigma_{yy}^{c}(o,z) = -\frac{2}{\pi}\frac{d}{dz}\int_o^d \frac{sq(s)ds}{(z^2-s^2)^{1/2}} \quad , z > d$$

(282)

$$\text{with} \quad q(s) = \int_o^s \frac{\zeta(r)dr}{(s^2-r^2)^{1/2}}$$

and

$$(283) \quad u_y(o,z) = \frac{2(1-\nu)}{\pi\mu}\int_z^d \frac{sq(s)ds}{(s^2-z^2)^{1/2}} \quad , z < d$$

The equation for the horizontal stress can be rewritten

$$\sigma_{yy}^{c}(o,z) = \frac{2z}{\pi}\int_o^d \frac{sq(s)ds}{(z^2-s^2)^{3/2}}$$

(284)

$$= \frac{2}{\pi}\left[\frac{z}{(z^2-d^2)^{1/2}}\,q(d) - z\int_o^d \frac{q'(s)ds}{(z^2-s^2)^{1/2}}\right]$$

Defining a stress intensity factor (Sneddon and Lowengrub, 1969) K as follows:

$$(285) \quad K = \frac{2d^{1/2}}{\pi} q(d) = \frac{2d^{1/2}}{\pi} \int_o^d \frac{\sum(r)dr}{(d^2-r^2)^{1/2}}$$

we can rewrite (284)

$$(286) \quad \sigma_{yy}^c(o,z) = \frac{zK}{(d(z^2-d^2))^{1/2}} - \frac{2z}{\pi} \int_o^d \frac{q'(s)ds}{(z^2-s^2)^{1/2}}$$

In Appendix K we show that

$$(287) \quad \lim_{z \to d+} \frac{2z}{\pi} \int_o^d \frac{q'(s)ds}{(z^2-s^2)^{1/2}} = \sum(d)$$

and thus

$$(288) \quad \lim_{z \to d+} (2(z-d))^{1/2} \sigma_{yy}(z,o) = K$$

We see that unless the stress intensity factor vanishes, the horizontal component of stress will be discontinuous at z = d and the stress would theoretically approach ∞. On the other hand if K = 0 the stress σ_{yy} is continuous at the fracture tip.

On our model we are dealing with an already existent unwelded fracture that is only closed by contact pressure below z = d. Thus on our model discontinuous stress is unacceptable. A stress intensity factor K > 0 would imply infinite tensile stress at the fracture tip, which

would result in the fracture being open to a greater depth, whereas $K < 0$ would imply that the fracture was only open to a depth less than d, the depth to the tip of our model-fracture. We thus come to the following very important conclusion

On our model the thermoelastic stress (σ_{yy}^{A}) and other stress (p, σ_g and P) must balance to give $K = 0$. That is, if we write $K = K_{\Delta T} + K_p$ where

$$(289) \qquad K_{\Delta T} = \frac{2d^{1/2}}{\pi} \int_0^d \frac{\sigma_{yy}^{A}(o,z)dz}{(d^2-z^2)^{1/2}} \quad , \quad K_{\Delta T} > o$$

and

$$(290) \qquad K_p = \frac{2d^{1/2}}{\pi} \int_0^d \frac{[p(z)+\sigma_g-P(z)]dz}{(d^2-z^2)^{1/2}} \quad , \quad K_p < o$$

then

$$(291) \qquad K_{\Delta T} = - K_p$$

and since $K_{\Delta T}$ depends on the velocity of CDM of our model fracture, as well as temperature conditions, we can estimate this velocity for different stress situations, i.e. different P(z). In the following section we will perform these estimates for specific models of the temperature reduction.

10. CDM Rate Estimates

To estimate rates of downward migration, in a specific stress situation, we note the following. Since at low-temperature conditions σ_g is about equal in magnitude to the hydrostatic pressure at the same depth (see section 5)

$$p(z) + \sigma_g \simeq 0. \tag{292}$$

We will then make the assumption that all additional stress, that is P(z), is proportional to σ_g, or

$$P(z) = -\chi\sigma_g = -\chi \frac{\nu}{1-\nu} \rho g z \tag{293}$$

$$\text{with } \chi = o \text{ to } \frac{1-2\nu}{\nu}$$

Then based on equation (290) the corresponding stress intensity factor can be easily estimated

$$K_p \simeq -\frac{2d^{1/2}}{\pi} \chi \frac{1-\nu}{\nu} \rho g d \tag{294}$$

and for normal igneous crustal rock

$$K_p \simeq -5800\chi d^{3/2} \tag{295}$$

Before turning to the specific model of section 7 above, we will present some estimates based on a simpler model of a constant temperature reduction

(296) $\Delta T(o,z) = -T_o \quad , \quad o < z < d$

Based on the results of section 8 above, on the temperature field around the migrating fracture, and using equations (276) and (279) we numerically estimate $\sigma_{yy}^{A}(o,z)$ for different rates of downward migration. We observe that $\sigma_{yy}^{A}(o,z)$ is approximately constant (denoted by $\sigma_{\Delta T}$) for $o < z < d$.

The results are presented in Figure 57. The corresponding stress intensity factor is then easily obtained by equation (289), giving

(297) $$K_{\Delta T} = \sigma_{\Delta T} \sqrt{d}$$

Balancing K_p and $K_{\Delta T}$ (equation (291)), resulting in $K = 0$ as discussed above, we obtain the migration velocity results presented in Figure 58. Note that the velocity of migration is strongly dependent on the depth to the fracture tip d, whereas the temperature results are obtained on the basis of a constant velocity. This, however, has only a minor effect on our results. In addition to velocity estimates, we can on the basis of equation (283) above estimate the width w of the migrating fracture. For this constant temperature reduction model we obtain

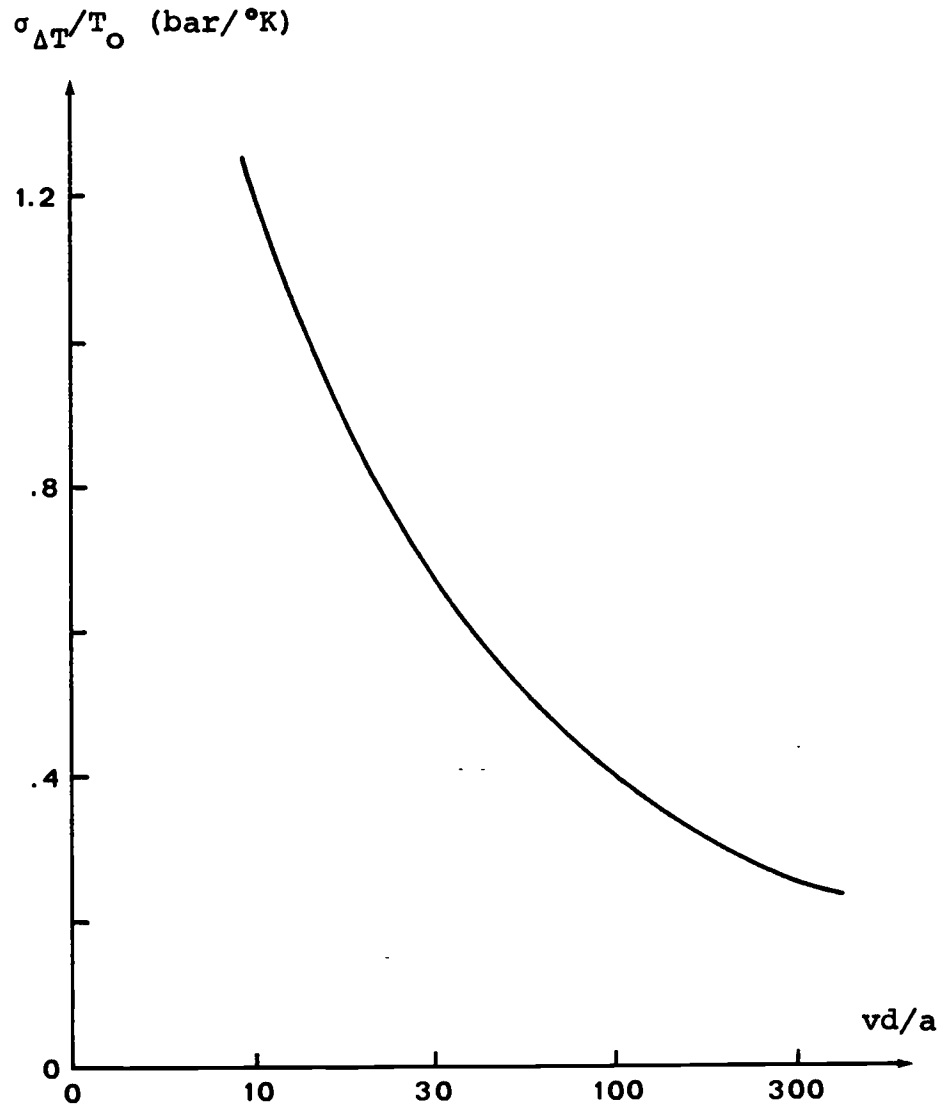

Figure 57. Thermoelastic stress in the plane of a CDM fracture for the constant temperature reduction case.

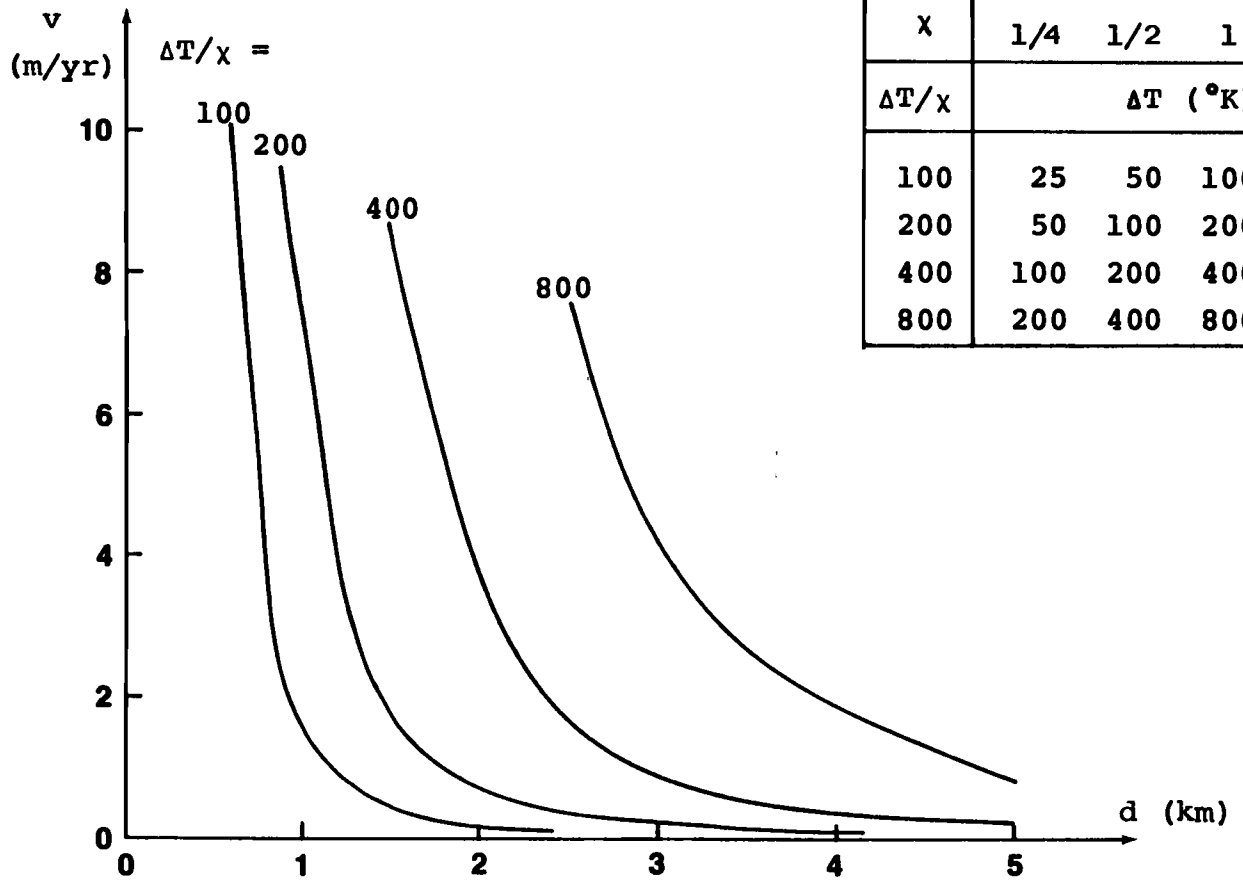

χ	1/4	1/2	1	1½
ΔT/χ	ΔT (°K)			
100	25	50	100	150
200	50	100	200	300
400	100	200	400	600
800	200	400	800	-

Figure 58. Velocity of CDM for the constant temperature reduction case.

$$w(z)/2 = u_y(o,z) = [\frac{1-\nu}{\mu}\ \sigma_{\Delta T} d(1-(\frac{z}{d})^2)^{1/2}$$

(298)

$$-\chi\ \frac{\nu\rho g}{\pi\mu} d^2[(1-(\frac{z}{d})^2)^{1/2}+(\frac{z}{d})^2 \ln\ \frac{1+(1-(z/d)^2/^{1/2}}{z/d}\ ]$$

For the lower half of the fracture, for example at z = 3d/4

(299) $\quad w(3d/4) = 3.3 \times 10^{-11}\ \sigma_{\Delta T} d - 1.6 \times 10^{-7}\ \chi d^2$

We should point out that the velocity results depend mostly on stress and temperature conditions near the tip of the fracture whereas the width depends on conditions over the entire length of the fracture. Width estimates are therefore unreliable and should only serve as indications of order of magnitude. Based on equation (299) we obtain estimates of one to several tens of mm corresponding to the results in Figure 58.

Turning now to the model of section 7 above, where

(300) $\quad \Delta T(o,z) = -\gamma z \quad , \quad o < z < d,$

we estimate the temperature field around the migrating fracture based on the methods and results of section 8. Then again using equations (276) and (279) we numerically estimate $\sigma_{yy}^{A}(o,z)$, for different rates of migration, and finally using (289) we estimate $K_{\Delta T}$. Balancing K_p and

$K_{\Delta T}$, as before, we observe that the velocity of migration is inversely proportional to the depth to the tip, i.e. $v(z) = dz/dt = c/z$. The temperature-field and thermoelastic stress results can be corrected for the non-uniform velocity by using

$$dt = \frac{z}{c}\, dz \qquad (301)$$

$$\& \quad t(z) = \frac{d^2}{2c} - \frac{z^2}{2c}$$

This modification results in only a minor correction. The results for $K_{\Delta T}$ are presented in Table XVII below, and the final migration velocity estimates are presented in Figure 59. These results are for temperature gradients, γ = 0.05 and 0.10 °C/m, which are characteristic for LT-systems in Iceland. The results of this section will be discussed in the section to follow.

11. Discussion

The rate estimates of Figure 59 above constitute the principal results of our analysis of the conjectured CDM-source mechanism for LT-activity in Iceland. It should be emphasized that these rate estimates are obtained on the basis of the assumption that the rate of CDM is predominantly determined by the stresses at the tip of the fracture rather than by the convective heat transfer

Table XVII Thermoelastic stress intensity factor on CDM-fracture model

vd/a	$K_{\Delta T}/\gamma d^{3/2}$ (Pa/°C)[1)]
10	7.89×10^4
20	6.30×10^4
60	4.27×10^4
160	2.99×10^4
300	1.84×10^4

1) assuming $\nu = 1/4$

$\alpha = 5 \times 10^{-6} °C^{-1}$

$\mu = 3 \times 10^{10} Pa$

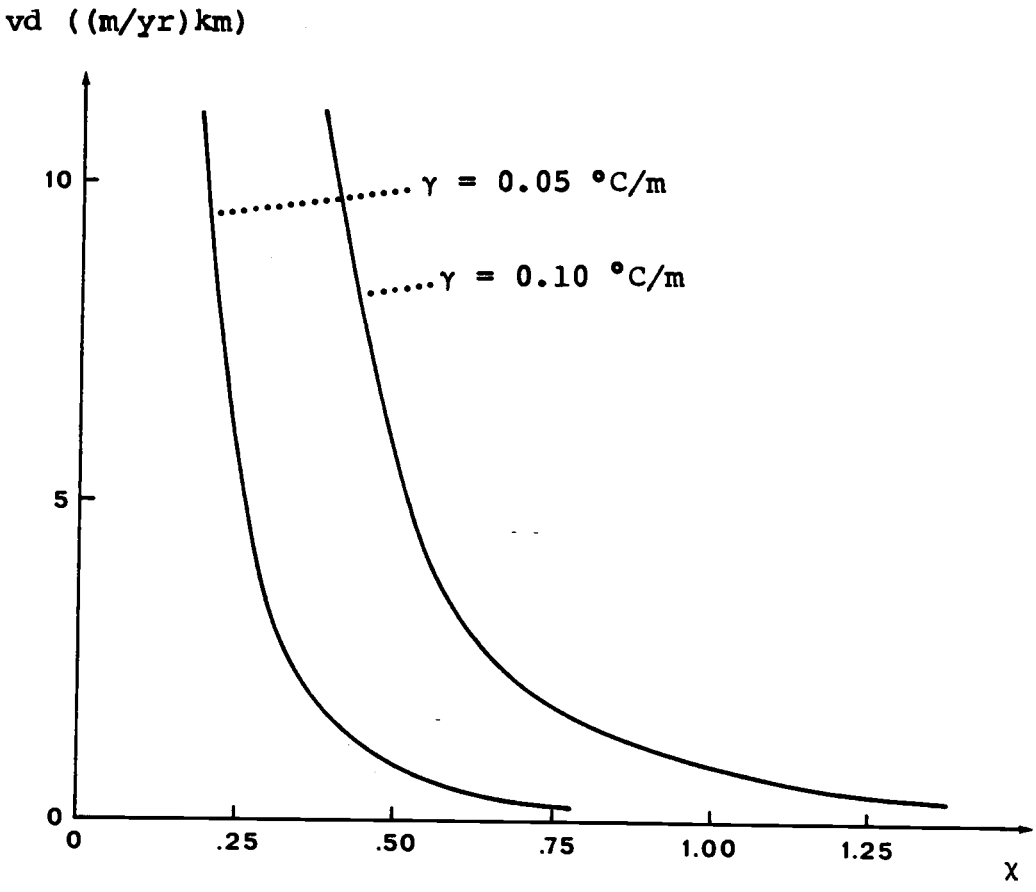

Figure 59. Velocity of CDM of a single unwelded fracture in a constant temperature-gradient environment.

in the fracture, provided the supply of water for the heat transfer is sufficient. We will present a further justification for this assumption, later in this section.

The results can be summarized as follows:

- The estimated rate is inversely proportional to the depth to the tip of the open section of the CDM fracture. This results from the fact that the thermoelastic stress at the tip of the fracture depends on the vertical extent of the temperature anomaly as well as the rate of migration. On this model both the temperature reduction and horizontal regional stress increase linearly with depth.
- As expected, the estimated rate is directly proportional to the unperturbed temperature gradient.
- The most important, while hardly surprising, result of our analysis is the very strong dependence of the rate estimates on the magnitude of the horizontal regional stress. Our results indicate that, at temperature conditions typical for the Icelandic crust, CDM will hardly be possible in locations where the minimum horizontal stress is greater than 50-70% of the weight of the overburden (= ρgz).

Thus crustal stress conditions may determine whether a LT-system can evolve at a given location. Bodvarsson (1983b) suggests that low horizontal stress may determine the locations where the CDM-process may take place. In

this respect stress conditions seem to be more important than temperature conditions. A corollary to this observation is that the CDM-process is likely to terminate when the fracture tip reaches a depth of enhanced horizontal stress.

While temperature conditions at shallow depth (to 2-3km) are fairly well known in the crust of Iceland stress conditions are very poorly known. Although much information on principal stress orientations in the Earth's crust has been obtained on the basis of geological observations and earthquake focal mechanisms (see the compilation on the US by Zoback and Zoback (1980)), the magnitude of crustal stress fields is poorly known. However, the hydraulic fracturing technique (Haimson and Fairhurst, 1970), which is currently the only reliable method of measuring stress at considerable depths, has enabled stress magnitude estimates in numerous boreholes in many subaerial regions of the Earth. The results indicate that horizontal stress is frequently of the same order and higher than the vertical stress. Near the surface observed horizontal stress is often very high and considerably higher than the vertical stress (Jaeger and Cook, 1976; Zoback,1983). Haimson (1976) has compiled the results of hydraulic fracturing observations from over 3000 boreholes in the US. Based on his results the average horizontal stress in the US is

about equal to the lithostatic stress. These results indicate that in the continental regions stress and temperature conditions are in general not favorable for LT-activity of the CDM-type.

Regions experiencing regional strain, such as the Basin and Range Province in the US, are clearly associated with lower horizontal stress. The minimum observed horizontal stress in the US reported by Haimson (1976) is about 50% of the lithostatic stress.

A very limited number of hydrofracturing measurements have been performed in Iceland to date. Tests performed in Reydarfjordur in East-Iceland are the deepest and most complete set of measurements undertaken so far in Iceland (Haimson and Rummel, 1982). Hydraulic fracturing was performed to a depth of 600m. The results from the Reydarfjordur drillhole indicate that both horizontal components of stress become smaller than the vertical stress at depths in excess of a few hundred meters. Their results, at three different depth levels, are presented in Table XVIII below. At a depth of 600m the minimum horizontal stress is as low as 50% of the lithostatic stress. The large stresses down to depths of few hundred meters could be of thermoelastic origin (see section 5 above). The top few hundred meters in this area have apparently been heated by a minor LT-system (Fridleifsson, 1982).

Table XVIII Results of hydraulic fracturing measurements in Reydarfjordur, East-Iceland.

depth (m)	compressive stress (bars) vertical $-\sigma_v$	horizontal $-\sigma_{max}$	horizontal $-\sigma_{min}$	Hookean $-\sigma_g$	x1)
200	50	70	50	17	1.9
400	105	250	150	35	(3.3)
600	160	100	80	53	0.5

1) based on σ_{min}

This very limited data does not enable us to infer anything on the stress conditions in LT-systems. Yet we can on the basis of the geology and tectonics of Iceland surmise that there must be regions where stress conditions are favorable for the CDM-process. In addition, there is some indirect field evidence that lends support to the notion that CDM is a major factor in the development and evolution of LT hydrothermal systems. This evidence, which includes structural control, temperature-depth relations and temperature-flow statistics, was reviewed in chapter II above and will not be repeated here.

Based on the migration rate estimates, it is now a simple matter to estimate the rate of heat transfer. We integrate the source density, given by equation (267) (with t(z) given by (301) and $T_o = \gamma z$), over the extent of the open fracture to obtain the average heat transfer rate per unit length of the model fracture

$$q = c_w T_w m = 2k\gamma \left(\frac{2c}{\pi a}\right)^{1/2} \int_o^d \frac{z\,dz}{(d^2-z^2)^{1/2}}$$

(302)

$$= 2\left(\frac{2}{\pi}\right)^{1/2} k(\gamma d) \left(\frac{v(d)d}{a}\right)^{1/2}$$

where m is the rate of mass flow per unit length of fracture, c_w the heat capacity and T_w the temperature of

the convecting fluid. Assuming k = 2w/m°C we obtain

$$(303) \qquad q = c_w T_w m = 3.19 \left(\frac{v(d)d}{a}\right)^{1/2} (\gamma d)$$

For comparison, in the simpler case of constant temperature reduction (ΔT) and velocity

$$(304) \qquad q = 4 \left(\frac{vd}{a}\right)^{1/2} \Delta T$$

Using equation (303) we obtain the results in Figure 60, corresponding to the rate estimates of Figure 59. Since our model relates to LT-activity with recharge at approximately 0°C we have assumed an average T_w = 100°C to estimate the mass transfer q. The estimated mass flow is in the range

$$(305) \qquad m \sim (0.002 - 0.05) \text{kg/ms}$$

Assuming predominantly laminar flow, the total mass flow M of a system can be related to the driving pressure differential Δp by

$$(306) \qquad M = C\Delta p \text{ or } MR = \Delta p$$

where $M = mB$ and $R = 1/C$

and C and R are the lumped flow conductance and resistance, respectively, of the fracture system, with B the length of the fracture. In the case of our model, we assume the flow is driven predominantly by

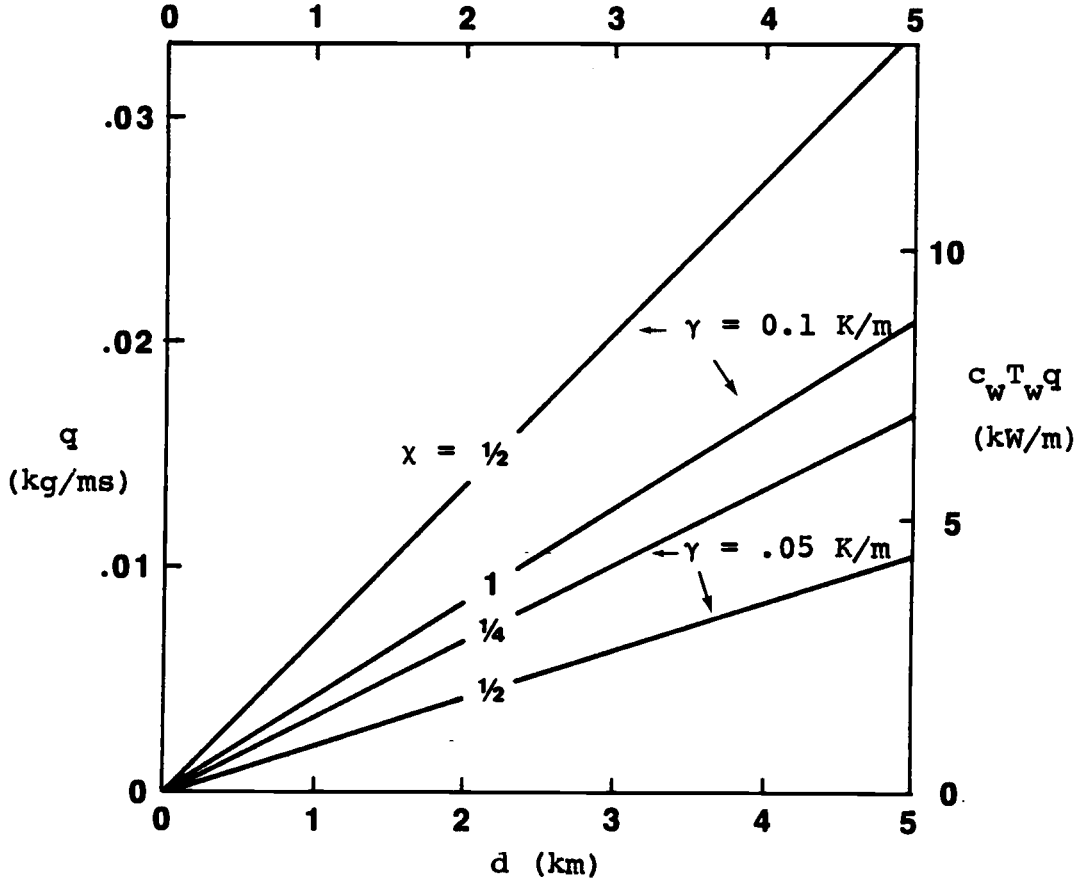

Figure 60. Rate of heat and mass transfer per unit length of a CDM-fracture.

thermobuoyancy. If the driving density differential is $\Delta\rho$, the driving pressure can be estimated by

(307) $$\Delta p = g\Delta\rho d$$

Since

(308) $$M = \frac{K}{\nu}\frac{dp}{dL} \quad \& \quad dp = M\,(\frac{\nu}{K})dL$$

the total flow resistance can be expressed (Bodvarsson, 1983b)

(309) $$R = \int(\nu/K)dL$$

where ν is the local kinematic viscosity, K the local permeance and dL the element of the flow path. The permeance is the area integral of the local permeability, which may vary greatly along the flow path. In the case of uniform-unidirectional flow through an open fracture of constant aperture h, this parameter follows from simple laminar flow theory (Lamb, 1932)

(310) $$K = h^3B/12$$

Defining an effective average flow permeance <K> and an effective average fracture aperture <h>,

(311) $$< K > = \frac{<h>^3 B}{12} = \frac{\nu L}{\int(\nu/K)dL},$$

then

$$(312) \qquad R = \frac{\nu L}{\langle K \rangle} \quad \text{and} \quad M = \frac{\langle K \rangle \Delta p}{\nu L}$$

and

$$(313) \qquad m = \frac{\langle h \rangle^3}{12} \frac{g \Delta \rho}{\nu} \frac{d}{L}$$

Assuming that the flow resistance is primarily encountered in the upflow section of our model, such that $L \approx d$, we can estimate the effective average fracture aperture $\langle h \rangle$ needed to sustain the mass flow on our model (equation (305)). We assume the recharge is at a temperature of 0°C and we have assumed an upflow temperature of 100°C, thus $\Delta \rho \approx 40$ kg/m^3. From (313)

$$(314) \qquad \langle h \rangle = (12 m \frac{\nu}{g \Delta \rho})^{1/3} = (2.1 m^{1/3}) \text{ mm}$$

if m in kg/ms

and we obtain

$$\langle h \rangle \approx (0.3 - 0.8) \text{mm}$$

This result is more than an order of magnitude smaller than the width estimates of last section, yet of the same order as estimated by Bodvarsson (1981; 1983b). Based on this result, we are justified in simplifying our treatment of the complex conductive/convective interaction, as described in section 7 above.

Based on our results, and the contention that CDM is important as a source mechanism for LT-activity in

Iceland, we can estimate dimensions of hypotehtical CDM-systems that would explain the estimated heat dissipation of LT-activity in Iceland. However, on our model the heat transfer is dependent on 4 variables, the undisturbed temperature gradient γ, the magnitude of the horizontal stress or χ, the current depth to the migrating front and the total length of the CDM-fracture system B. Of these 4 variables only one is fairly well known, that is the temperature graident. Some more data, in addition to the estimated heat dissipation, is therefore needed. As reviewed in chapter II above Bodvarsson (1982a) suggests that the onset of present LT-activity occurred after the end of the last period of glaciation, that is about 8000 to 10000 years ago. The time it takes the CDM-front to reach a depth d is given by

$$(315) \qquad t = \frac{d^2}{2c} = \frac{d}{2v_d} = \frac{d}{v_{av}}$$

where v_d is the velocity of migration at the depth d and $v_{av} = 2v_d$ the average velocity of migration up to the time t. Assuming t = 8000 yrs we obtain the estimates in Figure 61, for what we consider a likely depth interval. After obtaining these results, and based on the known temperature-gradient, we can estimate χ (based on results in Figure 59) as well as the total length of the CDM-fracture-system B needed to sustain a given heat

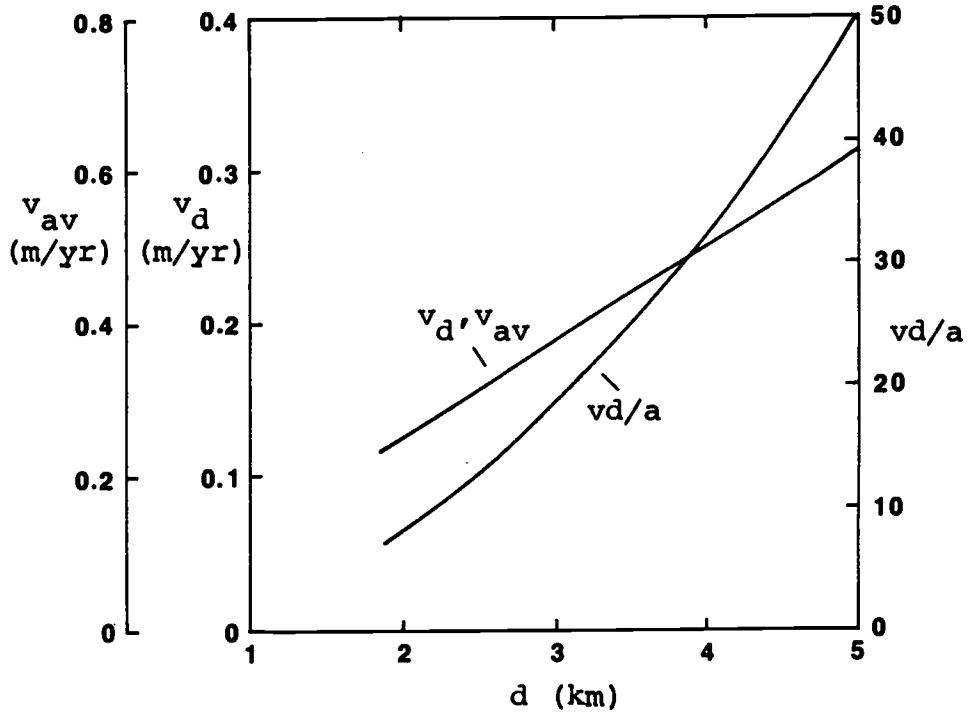

Figure 61. Average velocity of CDM, v_{av}, and the velocity at the depth d, v_d, when the CDM process has continued for 8000 years.

dissipation (B = Q/q, q given by equation (301)). We present the two following examples

- The total integrated rate of dissipation of heat by the LT-activity in Iceland is estimated at 600 MW (see chapter II above). Because of subsurface flow losses and locally elevated conductive heat flow, this is certainly an underestimate and we will assume Q = 1.2 GW. The average temperature-gradient in Iceland, outside the active zone of rifting and volcanism, is $\gamma \simeq 0.08°C/m$ (Palmason and Saemundsson, 1979).
- As a second example we take an individual LT-system, the Laugarnes system, which has been described in section III.20 above. Bodvarsson (1983) estimates the heat dissipated by this system, in its natural state, at 3.5 MW by advection and one W/m^2 by conduction. Estimating the area of the system to be about 2.5 km^2 we estimate the total heat dissipation to be Q = 6MW. The undisturbed regional temperature gradient equals $\gamma \simeq 0.1°C/m$.

The results for these two examples are presented in Figure 62 below.

Clearly, the above estimates are very uncertain, since none of the variables B, d or χ is actually known. We know, however, that d must be greater than 2-3km for many LT-systems (Figure 3). This allows us to estimate upper bounds for B and χ. We estimates B < 600 km and χ

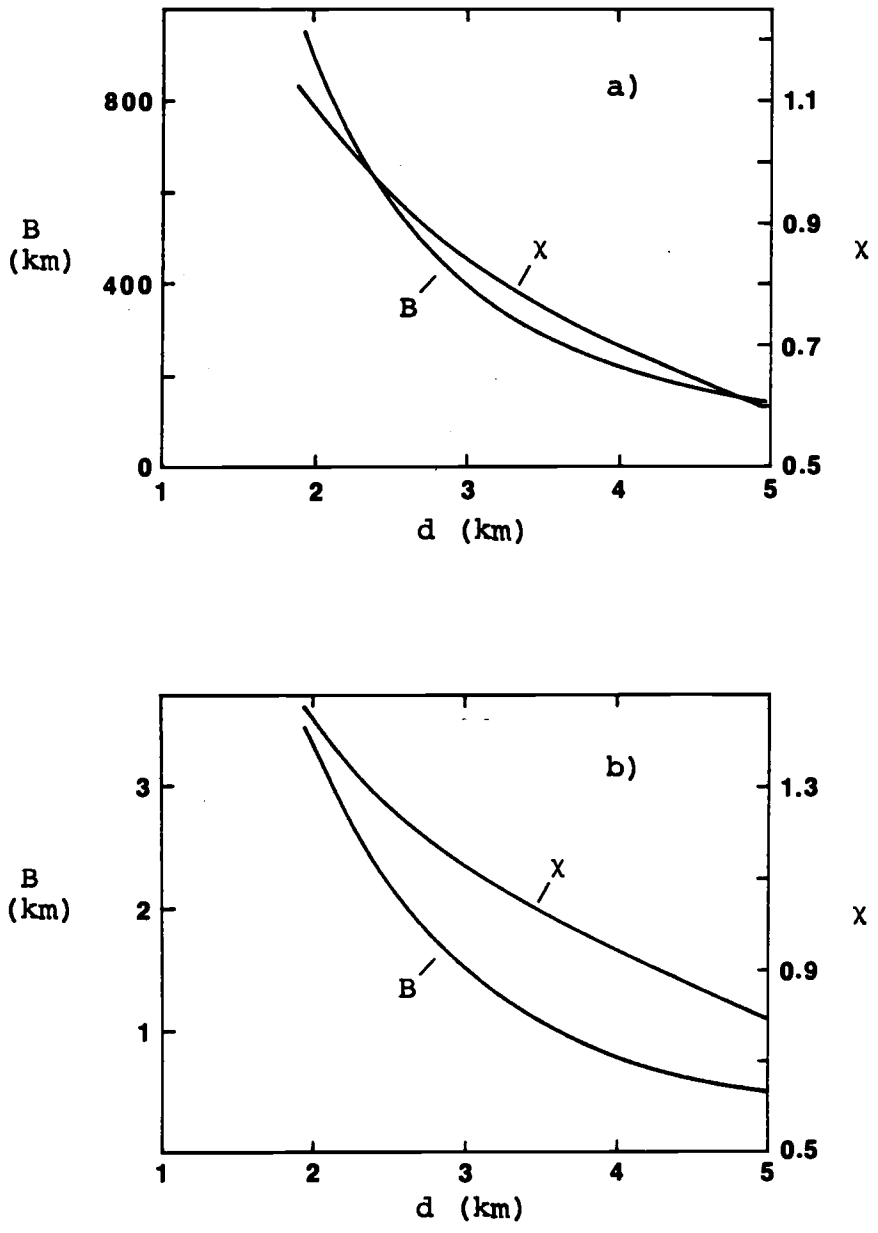

Figure 62. The total length of a CDM fracture system, B, and the associated horizontal stress, or χ, needed to sustain the heat dissipated by a) all LT-activity in Iceland and b) the Laugarnes system.

< 1.0 for all LT-activity in Iceland and $B < 2$ km, $\chi <$ 1.2 for the Laugarnes system. The length estimates are not unreasonable considering the fact that the length of the rift axis through Iceland is of the order of 300 km and the surface area of the Laugarnes system is of the order 3 km^2.

These results indicate that the dimensions of CDM-systems, needed to sustain the heat output of LT-systems, are quite small and we can easily envision such systems distributed throughout the crust of Iceland.

V. SUMMARY AND CONCLUDING REMARKS

The first objective of the present work has been to develop methods of production data analysis that are more readily applicable to the fracture/dike controlled hydrothermal systems in Iceland than conventional interpretation methods. Furthermore, the purpose was to investigate the role of the fracture/dike control in the heat uptake mechanism of low-temperature hydrothermal activity.

The analytical response functions of unconfined aquifer models have been presented, in particular, the long-term free-surface response when compressibility effects can be neglected. We have developed methods for production data analysis on the basis of such free-surface models and applied the methods to long-term data from several hydrothermal systems in Iceland. On the basis of homogeneous and isotropic reservoir models we have estimated an apparent global permeability of the order of 0.7 md for systems in Tertiary strata and of the order 5-20 md for systems in Quaternary strata. These estimates are much lower than permeability estimates obtained on the basis of shorter term well tests. However, a vertical slab two-dimensional flow model (section III.7) may more accurately reflect the global hydrological characteristics of many fracture-controlled

Icelandic hydrothermal systems. In particular permeability estimates for the Laugarnes-system in SW-Iceland of 50-100 md, that have been obtained on the basis of the two-dimensional flow model are in a better agreement with permeability estimates based on short-term well tests.

Our free-surface analysis has been based on very simple reservoir/source-distribution models. It is therefore of interest to consider more complex models. The non-linear least squares fitting method of section III.16 could, for example, be extended to analyze production data on the basis of the unconfined box-type reservoir model of section III.9 with unknowns w,c,R,D.

We have also developed methods of simulating long-term production data from complex liquid-dominated hydrothermal systems by much simpler lumped capacitor/conductor ladders. Such a simulation only requires production/drawdown data. We have shown that the response of both real as well as analytical reservoirs can be easily simulated by such lumped element systems. We are, for example, able to simulate/predict six years of the production history of the Svartsengi HT-system in SW-Iceland by an ultra-simple open one capacitor system.

It should be mentioned that the lumped capacitances of a simulation ladder can be interpreted as corresponding to the free-surface capacitance of an unconfined reservoir. Moreover the lumped conductances can be related to the conductance of the dike(s) and/or fractures that are the flow channels of the hydrothermal system in question.

Thermoelastic stress has not received much attention in the geothermal literature. Modeling hydrothermal systems as domains of nonuniform temperature in a Hookean half-space, we have estimated the magnitude of thermoelastic stress in two Icelandic LT-systems. Our results indicate that thermoelastic stress may be quite significant. In the uppermost 1000m we estimate compressive horizontal thermoelastic stress of up to 200 bars and at greater depth we estimate tensile thermoelastic stress of up to 200-400 bars. We conclude that thermoelastic stress must be an important factor in the evolution of hydrothermal systems.

In addition to providing the flow channels for thermal waters, dikes and fractures may play an important role in the source mechanism of hydrothermal activity. We have considered a possible dike/fault controlled source mechanism of LT-activity in Iceland where thermoelastic stress plays a major role. This mechanism, referred to as CDM, involves the downward migration of an

open section of a single, approximately two-dimensional, unwelded quasi-vertical fracture, such as along the wall of a dike. The migration involves conductive cooling and contraction in the rock adjacent to the fracture as well as vertical advective heat transport in the open section of the fracture. By balancing the tensile thermoelastic stress and compressive stress at the tip of the fracture we have estimated the rate of migration at temperature conditions typical for the Icelandic crust. At a depth of 3km and where the horizontal stress is about 50% of the weight of the overburden, we estimate the rate of CDM at about 1 m/yr.

One of the most important aspect of our results is the very strong dependence of the rate of migration on the magnitude of the horizontal regional stress. At temperature conditions typical for the Icelandic crust the CDM process does not appear to be possible, unless the minimum horizontal stress is lower than 50-70% of the weight of the overburden. We conclude that stress conditions may determine whether a LT-system can evolve at a given location as well as determine the intensity of the thermal activity.

Since very limited data is available on crustal stress conditions in Iceland this result cannot be tested by available observational data. Stress measurements at depth within as well as outside hydrothermal systems, by

f.ex. the hydraulic fracturing method, are therefore of interest.

Finally we should point out that the methods developed above and our results are applicable to hydrothermal activity in general. The CDM mechanism may be important as source mechanism of hydrothermal activity in other parts of the oceanic rift system. CDM may also be the source mechanism of the fault zone controlled thermal activity of the Basin and Range Province in Nevada and Oregon.

BIBLIOGRAPHY

Arnason, B., 1976, Groundwater systems in Iceland traced by deuterium, Soc. Sci. Islandica, 42, 236 pp.

Arnorsson, S., 1974, The composition of thermal fluids in Iceland. In Geodynamics of Iceland and the North Atlantic Area, L. Kristjansson (Editor), D. Reidel Publishing Co., 307-323.

Bath, M., 1960, Crustal structure of Iceland, J. Geophys. Res., 65, 1793-1807.

Beblo, M. and A. Bjornsson, 1980, A model of electrical resistivity beneath NE-Iceland: correlation with temperature, J. Geophys., 47, 184-190.

Bjornsson, A., 1980, Exploration and exploitation of low temperature geothermal fields near Akureyri in Northern Iceland (in Icelandic), Natturufraedingurinn, 50, 314-332.

Bjornsson, A., G. Johnsen, S. Sigurdsson, G. Thorbergsson and E. Tryggvason, 1979, Rifting of the plate boundary in North Iceland 1975-1978, J. Geophys. Res., 84, 3029-3038.

Bjornsson, H., S. Bjornsson and Th. Sigurgeirsson, 1982, Penetration of water into hot rock boundaries of magma at Grimsvotn, Nature, 580-581.

Bjornsson, S., 1980, Geothermal activity, ground water and heat (in Icelandic), Natturufraedingurinn, 50, 271-293.

Bjornsson, S., S. Arnorsson and J. Tomasson, 1972, Economic evaluation of Reykjanes thermal brine area, AAPG Bull., 56, 2380-2391.

Bodvarsson, G., 1950, Geophysical methods in the prospecting for hot water in Iceland (in Danish), J. Eng. Ass. Iceland, 35, 48-59.

Bodvarsson, G., 1951, Report on the Hengill thermal area (in Icelandic), J. Eng. Ass. Iceland, 36, 1-49.

Bodvarsson, G., 1954, Terrestrial heat balance in Iceland, J. Eng. Ass. Iceland, 39, 69-75.

Bodvarsson, G., 1964, Physical characteristics of natural heat sources in Iceland, Geothermal Energy, 1. Proc. UN Conf. on new sources of energy, Rome, 1961, 2, New York.

Bodvarsson, G., 1966, Direct interpretation methods in applied geophysics, Geoexploration, 4, 113-138.

Bodvarsson, G., 1976, Thermoelastic phenomena in geothermal systems, Second UN Symposium on the Development and Use of Geothermal Resources, San Francisco, 1975, 2, 903-907.

Bodvarsson, G., 1977, Unconfined aquifer flow with a linearized free surface condition, Jokull, 27, 84-87.

Bodvarsson, G., 1978, Convection and Thermoelastic Effects in Narrow Vertical Fracture Spaces with Emphasis on Analytical Techniques, Final report for U.S.G.S., 111 pp.

Bodvarsson, G., 1979, Elastomechanical phenomena and the fluid conductivity of deep geothermal reservoirs and source regions, 5th Workshop on Geothermal Reservoir Engineering, Dec. 1979, Stanford.

Bodvarsson, G., 1980, Reservoir exploration/testing by elastomechanical methods, 6th Workshop on Geothermal Reservoir Engineering, Dec. 1980, Stanford.

Bodvarsson, G., 1981, Interstitial fluid pressure signal propagation along fracture ladders, 7th Workshop on Geothermal Reservoir Engineering, Dec. 1981, Stanford.

Bodvarsson, G., 1982a, Glaciation and geothermal processes in Iceland, Jokull, 32, 21-28.

Bodvarsson, G., 1982b, Terrestrial energy currents and transfer in Iceland. In Continental and Oceanic Rifts, G. Palmason (Editor), Geodynamic Series, 8, Am. Geophys. Union, 271-282.

Bodvarsson, G., 1983a, Analogy between the uptake of heat and solutes by low-temperature thermal waters in Iceland, J. Volcanol. Geothermal Res., 19, 99-111.

Bodvarsson, G., 1983b, Temperature/flow statistics and thermomechanics of low-temperature geothermal systems in Iceland, J. Volcanol. Geothermal Res., 19, 255-280.

Bodvarsson, G., 1984, Linearization techniques and surface operatores in the theory of unconfined aquifers, Water Resour. Res., 20, 1271-1276.

Bodvarsson, G. and G. Axelsson, 1985, The analytical framework of the simulation of liquid reservoir response functions by lumped element models, unpublished manuscript, 44 pp.

Bodvarsson, G. and R.P. Lowell, 1972, Ocean floor heat flow and the circulation of interstitial waters, J. Geophys. Res., 77, 4472-4475.

Bodvarsson, G. and E. Zais, 1978, A field example of free surface testing, 4th Workshop on Geothermal Reservoir Engineering, Dec. 1978, Stanford.

Bodvarsson, G.B., S.M. Benson, O. Sigurdsson, V. Stefansson and E.T. Eliasson, 1984a, The Krafla geothermal field, Iceland. 1. Analysis of well test data, Water Resour. Res., 20, 1515-1530.

Bodvarsson, G.B., K. Pruess, V. Stefansson and E.T. Eliasson, 1984, The Krafla geothermal field, Iceland. 3. The generating capacity of the field, Water Resour. Res., 20, 1545-1559.

Boley, B.A. and J.H. Weiner, 1960, Theory of Thermal Stress, John Wiley and Sons, Inc., New York, 586 pp.

Bott, M.H.P., 1982, The Interior of the Earth: its structure, constitution and evolution, 2nd ed., Elsevier, New York, 403 pp.

Bratt, S.R., E.A. Bergman and S.C. Solomon, 1985, Thermoelastic stress: how important as a cause of earthquakes in young oceanic lithosphere, submitted to J. Geophys. Res.

Carslaw, H.W. and J.C. Jaeger, 1959, Conduction of Heat in Solids, 2nd ed., Claredon Press, Oxford, 496 pp.

Coats, K.H., L.A. Rapoport, J.R. McCord and W.P. Drews, 1964, Determination of aquifer influence functions from field data, J. Pet. Tech., 1417-1424.

Donaldson, I.G. and M.A. Grant, 1981, Heat extraction from geothermal reservoirs. In Geothermal Systems: Principles and Case Histories, L. Rybach and L.J.P. Muffler (Editors), John Wiley and Sons, Inc., 145-179.

Duff, G.F.D. and D. Naylor, 1966, Differential Equations of Applied Mathematics, John Wiley, New York, 423 pp.

Einarsson, T., 1942, Uber das Wesen der Heissen Quellen Islands, Soc. Sci. Islandica, 26, 91 pp.

Einarsson, T., 1966, The origin of geothermal activity (in Icelandic), J. Eng. Ass. Iceland, 51, 23-32.

Elder, J.W., 1965, Physical processes in geothermal areas, Am. Geophys. Un. Mono., 8, 211-239.

Ellis, A.J. and W.A.J. Mahon, 1964, Natural hydrothermal systems and experimental hot rock/water interactions, Geochim. Cosmochim. Acta, 28, 1323-1357.

Ellis, A.J. and W.A.J. Mahon, 1977, Chemistry and Geothermal Systems, Academic Press, New York, 392 pp.

Earlougher, Jr., R.C., 1977, Advances in well test analysis, Monogr. 5, Soc. of Pet. Eng., Dallas.

Flovens, O., 1980, Seismic structure of the Icelandic crust above layer 3 and the relation between body wave velocity and the alteration of the basaltic crust, J. Geophys., 47, 211-220.

Foulger, G. and R.E. Long, 1984, Anomalous focal mechanisms: tensile crack formation on an accreting plate boundary, Nature, 310, 43-45.

Fradkin, L.J., M.L. Sorey and A. McNabb, 1981, On identification and validation of some geothermal models, Water Resour. Res., 17, 929-936.

Fridleifsson, G.O., 1983, Mineralogical evolution of a hydrothermal system, Geothermal Resources Council, Transactions, 7, 147-152.

Fridleifsson, I.B., 1979, Geothermal activity in Iceland, Jokull, 29, 47-56.

Fridleifsson, I.B., 1982, The Iceland Research Drilling Project in relation to the geology of Iceland, J. Geophys. Res., 87, 6363-6370.

Georgsson, L., H. Johannesson, E. Gunnlaugsson and G.I. Haraldsson, 1984, Geothermal exploration of the Reykholt thermal system in Borgarfjordur, West Iceland, Jokull, 34, 105-116.

Goodier, J.N., 1937, Integration of thermoelastic equations, Phil. Mag., 23, 1017-1032.

Grant, M.A., I.G. Donaldson and P.F. Bixley, 1982, Geothermal Reservoir Engineering, Academic Press, New York, 369 pp.

Haimson, B.C., 1975, The state of stress in the Earth's crust, Rev. Geoph. Space Phys., 13, 350-352.

Haimson, B.C. and C. Fairhurst, 1970, In-situ stress determinations at great depth by means of hydraulic fracturing. In Rock Mechanics-Theory and Practice, 11th Symposium on Rock Mechanics, W.H. Somerton (Editor), Berkeley, 1969, 559-584.

Haimson, B.C. and F. Rummel, 1982, Hydrofracturing stress measurements in the Iceland Research Drilling Project drill hole at Reydarfjordur, Iceland, J. Geophys. Res., 87, 6631-6649.

Hanson, J., 1978, Heat Transfer Effects in Forced Geoheat Recovery Systems, Ph.D. Thesis, Oregon State University, 217 pp.

Jaeger, J.C. and N.G.W. Cook, 1976, Fundamentals of Rock Mechanics, Chapman and Hall, London.

Kerr, R.A., 1982, Extracting geothermal energy can be hard, Science, 218, 668-669.

Kjaran, S.P., G.K. Halldorsson, S. Thorhallsson and J. Eliasson, 1979, Reservoir engineering aspects of Svartsengi geothermal area, Geoth. Resources Council Trans., 3, 337-339.

Kristmannsdottir, H. and S.J. Johnsen, 1982, Chemistry and stable isotope composition of geothermal waters in the Eyjafjordur region, northern Iceland, Jokull, 32, 83-90.

Lamb, H., 1932, Hydrodynamics, 6th ed., Dover Publications, New York, 738 pp.

Lister, C.R.B., 1972, On the thermal balance of a mid-ocean ridge, Geophys. J. R. Astr. Soc., 26, 515-535.

Lister, C.R.B., 1974, On the penetration of water into hot rock, Geophys. J. R. Astr. Soc., 39, 465-509.

Lister, C.R.B., 1976, Qualitative theory on the deep end of geothermal systems, 2nd UN Symposium on the Development and Use of Geothermal Resources, San Francisco, 1975, 1, 459-463.

Lister, C.R.B., 1982, Active and passive hydrothermal systems in the oceanic crust; Predicted physical conditions. In The Dynamic Environment of the Ocean Floor, K.A. Fanning and F.T. Manheim (Editors), Lexington, Mass., 441-470.

Martin, R.J., 1972, Time-dependent crack growth in quartz and its application to the creep of rocks, J. Geophys. Res., 77, 1406-1419.

Menke, W., 1984, Geophysical Data Analysis: Discrete Inverse Theory, Academic Press, 260 pp.

Mindlin, R.D. and D.H. Cheng, 1950, Thermoelastic stress in the semiinfinite solid, J. App. Phys., 21, 931-933.

Palmason, G., 1967, On heat flow in Iceland in relation to the Mid-Atlantic Ridge. In Iceland and Mid-Ocean Ridges, S. Bjornsson (Editor), Soc. Sci. Islandica, 38, 111-127.

Palmason, G., 1971, Crustal Structure of Iceland from Explosion Seismology, Soc. Sci. Islandica, 40, 187 pp.

Palmason, G., 1974, Heat flow and hydrothermal activity in Iceland. In Geodynamics of Iceland and the North Atlantic Area, L. Kristjansson (Editor), D. Reidel Publishing Co., 297-307.

Palmason, G., 1980, A continuum model of crustal generation in Iceland; Kinematic aspects, J. Geophys., 47, 7-18.

Palmason, G., 1981, Crustal rifting, and related thermo-mechanical processes in the Lithosphere beneath Iceland, Geol. Rundschau, 70, 244-260.

Palmason, G., S. Arnorsson, I.B. Fridleifsson, H. Kristmannsdottir, K. Saemundsson, V. Stefansson, B. Steingrimsson, J. Tomasson and L. Kristjansson, 1979, The Iceland crust: Evidence from drillhole data on structure and processes. In Deep Drilling Results in the Atlantic Ocean: Ocean Crust, M. Talwani, C.G. Harrison and D.E. Hayes (Editors), Maurice Ewing Series, 2, Am. Geophys. Union, 43-65.

Palmason, G. and K. Saemundsson, 1974, Iceland in relation to the Mid-Atlantic Ridge, Ann. Rev. Earth Planet Sci., 2, 25-50.

Palmason, G. and K. Saemundsson, 1979, Summary of conductive heat flow in Iceland. In Terrestrial Heat Flow in Europe, V. Cermak and L. Rybach (Editors), Springer-Verlag, 218-220.

Palmason, G., V. Stefansson, S. Thorhallson and T. Thorsteinsson, 1983, Geothermal field development in Iceland, 9th Workshop on Geothermal Reservoir Engineering, Dec. 1983, Stanford.

Parkus, H., 1976, Thermoelasticity, Blaisdell Publishing Co., Waltham, Mass., 112 pp.

Ramey, Jr., H.J., 1982, Pressure transient testing, J. Pet. Tech. (July 1982), 1407-1413.

Saemundsson, K. and I.B. Fridleifsson, 1980, Application of geology in geothermal research in Iceland (in Icelandic), Natturufraedingurinn, 50, 157-188.

Sclater, J.G., C. Jaupart and D. Galson, 1980, The heat flow through oceanic and continental crust and the heat loss of the Earth, Rev. Geoph. Space Phys., 18, 269-311.

Sneddon, I.N. and M. Lowengrub, 1969, Crack Problems in the Classical Theory of Elasticity, John Wiley and Sons, Inc., New York, 221 pp.

Stefansson, V., 1984, Physical environment of hydrothermal systems in Iceland and on submerged oceanic ridges. In Hydrothermal Processes at Seafloor Spreading Centers, P.A. Rona, K. Bostrom, L. Laubier and K.L. Smith, Jr. (Editors), Plenum Publishing Corp., 321-360.

Stefansson, V. and S. Bjornsson, 1982, Physical aspects of hydrothermal systems. In Continental and Oceanic Rifts, G. Palmason (Editor), Geodynamic Series, 8, Am. Geophys. Union.

Thayer, R.E., A. Bjornsson, L. Alvares and J.F. Hermance, 1981, Magma genesis and crustal spreading in the northern Neovolcanic zone of Iceland: telluric-magnetotelluric constraints, Geophys. J. R. Astr. Soc., 65, 423-442.

Thoroddsen, Th., 1925, Die Geschichte der islandischen Vulkane, D. Kgl. Danske Vidensk. Selsk. Skrifter, 8 Raekke. Naturenvidenskap og Matematik Afd., IX, Copenhagen.

Thorsteinsson, T., 1976, Redevelopment of the Reykir hydrothermal system in Southwestern Iceland, Second UN Symposium on the Development and Use of Geothermal Resources, San Francisco, 1975, 2173-2180.

Thorsteinsson, T. and J. Eliasson, 1970, Geohydrology of the Laugarnes hydrothermal system in Reykjavik, Iceland, Geothermics, Spec. Iss. 2, 2, 1191-1204.

Turcotte, D.L., 1974, Are transform faults thermal contraction cracks?, J. Geophys. Res., 79, 2573-2577.

Turcotte, D.L. and E.R. Oxburg, 1973, Mid-plate tectonics, Nature, 244, 337-339.

Walker, G.P.L., 1960, Zeolite zones and dike distribution in relation to the structure of the basalts of Eastern Iceland, J. Geology, 68, 515-528.

Ward, P.L. and S. Bjornsson, 1971, Microearthquakes, swarms and the geothermal areas of Iceland, J. Geophys. Res., 76, 3953-3982.

White, D.E., 1968, Hydrology, activity and heat flow of the Steamboat Springs thermal system, Washoe County, Nevada, U.S. Geol. Surv. Prof. Pap. 458G, 109 pp.

Zais, E. and G. Bodvarsson, 1980, Analysis of Production Decline in Geothermal Reservoirs, Report for Lawrence Berkeley Laboratory, 34 pp.

Zoback, M.D., 1983, State of stress in the Lithosphere, Rev. Geophys. Space Phys., 21, 1503-1511.

Zoback, M.L. and M.D. Zoback, 1980, State of stress in the Conterminous United States, J. Geophys. Res., 85, 6113-6156.

APPENDICES

APPENDIX A

Formal solutions of inhomogeneous and anisotropic boundary value problems

To solve

$$\text{(A1)} \qquad \begin{aligned} -\nabla\cdot(c(P)\nabla u(P)) &= f(P) \quad \text{in } B : z > o \\ u &= g \quad \text{on } \Sigma : (x,y)\text{-plane} \end{aligned}$$

with

$$\text{(A2)} \qquad c(P) = \begin{bmatrix} c_x(P) & o & o \\ o & c(P) & o \\ o & o & c_z(P) \end{bmatrix}$$

we employ the Dirichlet type Green's function $G(P,Q)$, that is the solution to

$$\text{(A3)} \qquad \begin{aligned} -\nabla\cdot(c(P)\nabla G(P,Q)) &= \delta(P-Q) \quad \text{in } B \\ G &= o \quad \text{on } \Sigma. \end{aligned}$$

Using

$$\int_B \nabla_Q\cdot(uc\nabla_Q G)dV_Q - \int_B \nabla_Q\cdot(Gc\nabla_Q u)dV_Q$$

$$\text{(A4)} \quad = \int_B (\nabla_Q u)\cdot(c\nabla_Q G)dV_Q + \int_B u\nabla_Q\cdot(c\nabla_Q G)dV_Q$$

$$- \int_B (\nabla_Q G)\cdot(c\nabla_Q u)dV_Q - \int_B G\nabla_Q\cdot(c\nabla_Q u)dV_Q,$$

we obtain by (A1) and (A3)

$$u(P) = \int_B G(P,Q)f(Q)dV_Q + \int_B \nabla_Q\cdot(Gc\nabla_Q u)dV_Q - \int_B \nabla_Q\cdot(uc\nabla_Q G)dV_Q. \tag{A5}$$

By Gauss theorem

$$\int_B \nabla\cdot\bar{v}dV = \int_\Sigma \bar{v}\cdot\bar{n}dS\ , \tag{A6}$$

where for Σ the (x,y)-plane

$$\bar{n} = \begin{bmatrix} o \\ o \\ 1 \end{bmatrix}\ , \tag{A7}$$

thus

$$\int_B \nabla_Q\cdot(uc\nabla_Q G)dV_Q = \int_\Sigma uc_z \frac{\partial G}{\partial n_Q} dS_Q \tag{A8}$$

and

$$\int_B \nabla_Q\cdot(Gc\nabla_Q u)dV_Q = \int_\Sigma Gc_z \frac{\partial u}{\partial n_Q} dS_Q. \tag{A9}$$

The formal solution of (A1) then follows from (A5)

$$u(P) = \int_B G(P,Q)f(Q)dV_Q - \int_\Sigma c_z(Q)\frac{\partial G(P,Q)}{\partial n_Q}g(Q)dS_Q. \tag{A10}$$

To solve

$$\begin{aligned} -\nabla\cdot(c(P)\nabla u(P)) &= f(P) \quad \text{in } B : z > o \\ \frac{\partial u}{\partial n} &= h \qquad \text{on } \Sigma : (x,y)\text{-plane} \end{aligned} \tag{A11}$$

we employ the Neumann type Green's function $N(P,Q)$, that is the solution to

$$\text{(A12)} \qquad \begin{aligned} -\nabla\cdot(c(P)\nabla N(P,Q)) &= \delta(P-Q) \text{ in } B \\ \frac{\partial N}{\partial n} &= 0 \qquad \text{on } \Sigma. \end{aligned}$$

By equation (A8)

$$\text{(A13)} \qquad \int_B \nabla_Q\cdot(uc\nabla_Q N)dV_Q = 0$$

and by (A9)

$$\text{(A14)} \qquad \int_B \nabla_Q\cdot(Nc\nabla_Q u)dV_Q = \int_\Sigma Nc_z \frac{\partial u}{\partial n_Q} dS_Q$$

Thus the formal solution of (A11) follows from (A5)

$$\text{(A15)} \qquad u(P) = \int_B N(P,Q)f(Q)dV_Q + \int_\Sigma c_z(Q)N(P,Q)h(Q)dS_Q.$$

APPENDIX B

Two integral identities

We want to evaluate the integral (equation (42))

$$p_2(P) = \frac{1}{2\pi c}\frac{z}{2\pi}\int_{\Sigma}\frac{1}{r_{PR}^3}\frac{1}{r_{RQ}}\,dS_R \tag{B1}$$

with

$$\begin{aligned} P &= (x,y,z)\\ Q &= (o,o,d)\\ R &= (x",y",o)\\ dS_R &= dx"dy" \end{aligned} \tag{B2}$$

and Σ the z = o plane. Thus

$$p_2(P) = \frac{1}{2\pi c}\frac{z}{2\pi}\int_{-\infty}^{\infty}\frac{dx"dy"}{((x-x")^2+(y-y")^2+z^2)^{3/2}(x"^2+y"^2+d^2)^{1/2}} \tag{B3}$$

which is a 2-dimensional convolution

$$p_2(P) = \frac{1}{2\pi c}\frac{z}{2\pi}\int_{-\infty}^{\infty} dx"dy" f(x-x",y-y")g(x",y") \tag{B4}$$

Taking a 2-dimensional Fourier transform of (B4) we obtain

$$\hat{p}_2(k) = \frac{1}{2\pi c}\, z\, \hat{f}(k)\hat{g}(k) \tag{B5}$$

where $\hat{}$ indicates the transformed function, $k = k_x^2+k_y^2$, and (Duff and Naylor, 1966)

$$\text{(B6)} \qquad \begin{aligned} \hat{f}(k) &= \frac{1}{z}\, e^{-kz} \\ \hat{g}(k) &= \frac{1}{k}\, e^{-kd}. \end{aligned}$$

Hence

$$\text{(B7)} \qquad \hat{p}_2(k) = \frac{1}{2\pi ck}\, e^{-k(z+d)}$$

or

$$\text{(B8)} \qquad p_2(P) = \frac{1}{2\pi c r_{PQ'}} \quad ; \quad Q' = (o,o,-d)$$

We also want to evaluate (equation (53))

$$\text{(B9)} \qquad p_2(P) = \frac{1}{\pi c}\,\frac{z}{2\pi}\int_{-\infty}^{\infty} \frac{\ln(r_{RQ}^2)}{r_{PR}^2}\, dy_R$$

with

$$\text{(B10)} \qquad \begin{aligned} P &= (y,z) \\ Q &= (o,d) \\ R &= (y'',o) \\ dy_R &= dy'' \end{aligned}$$

Thus

$$\text{(B11)} \qquad p_2(P) = \frac{1}{\pi c}\,\frac{z}{2\pi}\int_{-\infty}^{\infty} dy''\, \frac{\ln(y''^2+d^2)}{((y-y'')^2+z^2)}$$

which is a 1-dimensional convolution

$$(B12) \qquad p_2(P) = \frac{1}{\pi c} \frac{z}{2\pi} \int_{-\infty}^{\infty} dy'' g(y'') f(y-y'')$$

Taking a Fourier transform of (B12)

$$(B13) \qquad \hat{p}_2(k) = \frac{1}{\pi c} \frac{z}{(2\pi)^{1/2}} \hat{g}(k) \hat{f}(k)$$

with k the transform variable and (Duff and Naylor, 1966)

$$(B14) \qquad \begin{aligned} g(k) &= -(2\pi)^{1/2} \frac{e^{-kd}}{k} \\ \hat{f}(k) &= \frac{1}{z} \left(\frac{\pi}{2}\right)^{1/2} e^{-kz} \end{aligned}$$

Hence

$$(B15) \qquad \hat{p}_2(k) = \frac{-1}{\pi c} \left(\frac{\pi}{2}\right)^{1/2} \frac{e^{-k(z+d)}}{k}$$

or

$$(B16) \qquad p_2(P) = \frac{1}{\pi c} \ln(r_{PQ'}) \; ; \; Q' = (o,-d)$$

APPENDIX C

Response of a closed three capacitor ladder

In this specific case

$$(C1) \qquad A = \begin{bmatrix} \sigma_1 & -\sigma_1 & 0 \\ -\sigma_1 & (\sigma_1+\sigma_2) & -\sigma_2 \\ 0 & -\sigma_2 & \sigma_2 \end{bmatrix}, \quad K = \begin{bmatrix} \kappa_1 & 0 & 0 \\ 0 & \kappa_2 & 0 \\ 0 & 0 & \kappa_3 \end{bmatrix}$$

and we consider

$$(C2) \qquad \bar{f}(t) = \begin{bmatrix} -q_1 \\ 0 \\ 0 \end{bmatrix} \quad 0 < t \leq T \; ; \; \bar{f}(t) = 0 \quad t > T$$

The response is then as follows

$0 < t \leq T$, drawdown

$$(C3) \qquad p_1(t) = -\frac{q_1}{A} t - \frac{q_1 \tau_{12}^2}{\lambda_2}(1-e^{-\lambda_2 t}) - \frac{q_1 \tau_{13}^2}{\lambda_3}(1-e^{-\lambda_3 t})$$

$t > T$, buildup

$$(C4) \qquad p_1(t) - p_1(T) = \frac{q_1 \tau_{12}^2}{\lambda_2}(1-e^{-\lambda_2 T})(1-e^{-\lambda_2 \Delta t}) + \frac{q_1 \tau_{13}^2}{\lambda_3}(1-e^{-\lambda_3 T})(1-e^{-\lambda_3 \Delta t})$$

where $\Delta t = t - T$ and

$$\lambda_2 = \frac{B-(B^2-4CA\sigma_1\sigma_2)^{1/2}}{2C}$$

$$\lambda_3 = \frac{B+(B^2-4CA\sigma_1\sigma_2)^{1/2}}{2C}$$

(C5)

$$\tau_{12}{}^2 = \frac{(c\lambda_2-b+a/\lambda_2)}{C(\lambda_2-\lambda_3)}$$

$$\tau_{13}{}^2 = \frac{(b-c\lambda_3-a/\lambda_3)}{C(\lambda_2-\lambda_3)}$$

with

$$A = \kappa_1+\kappa_2+\kappa_3$$

$$B = \kappa_1\sigma_2(\kappa_2+\kappa_3)+\kappa_3\sigma_1(\kappa_1+\kappa_2)$$

(C6)

$$C = \kappa_1\kappa_2\kappa_3$$

$$a = \sigma_1\sigma_2$$

$$b = \kappa_2\sigma_2+\kappa_3\sigma_2+\kappa_3\sigma_1$$

$$c = \kappa_2\kappa_3$$

APPENDIX D

The even-determined linear programming problem with constraints

To set (161) up as a linear programming problem we add 3N unknowns, α_i, x_i and x_i' for i = 1,2...N, and (Menke, 1984)

$$\text{(D1)} \qquad \text{minimize} \quad \sum_{i=1}^{N} \alpha_i$$

with constraints

$$\text{(D2)} \qquad \begin{aligned} (G\bar{m})_i + \alpha_i - x_i &= d_i \\ (G\bar{m})_i - \alpha_i + x_i' &= d_i \quad , \quad i = 1,2,\ldots N \\ m_{i-1} - m_i &\geq o \quad , \quad i = 2,\ldots N \end{aligned}$$

$$\text{and} \quad m_i \geq o \ , \ \alpha_i \geq o \ , \ x_i \geq o, \ x_i' \geq o$$

A linear programming problem consists of solving

$$\bar{c}^T \cdot \bar{y} = \text{minimum}$$

$$\text{(D3)} \qquad \text{subject to} \quad A\bar{y} \begin{Bmatrix} \leq \\ = \\ \geq \end{Bmatrix} \bar{b}$$

Making the following definitions

$$\bar{y}^T = [m_1, m_2, \ldots m_N, \alpha_1, \ldots \alpha_N, x_1, \ldots x_N, x_1', \ldots x_N']$$

$$\bar{c}^T = [o, o, \ldots o, 1, \ldots 1, o, \ldots o, o, \ldots o]$$

(D4)

$$A = \begin{bmatrix} \begin{bmatrix} G \end{bmatrix} \begin{bmatrix} I \end{bmatrix} \begin{bmatrix} -I \end{bmatrix} \begin{bmatrix} O \end{bmatrix} \\ \begin{bmatrix} G \end{bmatrix} \begin{bmatrix} -I \end{bmatrix} \begin{bmatrix} O \end{bmatrix} \begin{bmatrix} I \end{bmatrix} \\ \begin{bmatrix} 1\text{-}1o \ \ldots \\ o\ 1\text{-}1 \ldots \\ \\ o \ldots\ 1\text{-}1 \end{bmatrix} \begin{bmatrix} O \end{bmatrix} \begin{bmatrix} O \end{bmatrix} \begin{bmatrix} O \end{bmatrix} \end{bmatrix}$$

$$\bar{b}^T = [d_1, \ldots d_N, d_1, \ldots d_N, o, \ldots\ o]$$

with the inequality/equality vector

(D5) $\qquad [= , \ldots\ =, =, \ldots\ =, \geq, \ldots \geq]$

we have set problem (161) up as a linear programming problem.

APPENDIX E

The data kernel for non-linear free surface analysis

The elevation of the free surface, directly above a point sink of variable strength, in the case of the unconfined half space model (section III.6) is given by

$$h(t) = A \int_0^t \frac{q(\tau)d\tau}{(1+\alpha(t-\tau))^2} \tag{E1}$$

$$\text{with} \quad A = \frac{-w}{2\pi\rho g c d^2}, \quad \alpha = \frac{w}{d}$$

By equation (169), with $g_i(\bar{m}) = h(t)$,

$$(G_n)_{il} = \int_0^{t_i} \frac{q(\tau)d\tau}{(1+\alpha(t_i-\tau))^2}$$

(E2)

$$= \sum_{\ell=1}^{i} \frac{q_\ell}{\alpha} \left[\frac{1}{1+\alpha(i-\ell)\Delta t} - \frac{1}{1+\alpha(i-\ell+1)\Delta t}\right]$$

and

$$(G_n)_{i2} = -2A \int_0^{t_i} \frac{(t_i-\tau)q(\tau)d\tau}{(1+\alpha(t_i-\tau))^3}$$

$$(E3) \quad = -2A \sum_{\ell=1}^{i} \frac{q_\ell}{\alpha^2} \left[\frac{1}{1+\alpha(i-\ell)\Delta t} - \frac{1}{1+\alpha(i-\ell+1)\Delta t}\right.$$

$$\left. + \frac{1}{2}\left(\frac{1}{(1+\alpha(i-\ell+1)\Delta t)^2} - \frac{1}{(1+\alpha(i-\ell)\Delta t)^2}\right)\right]$$

$$\text{with} \quad A = (m_n^{est})_1$$

$$\alpha = (m_n^{est})_2$$

The elevation of the free surface, directly above a line sink of variable strength, in the case of the unconfined vertical slab model (section III.7) is given by

$$(E4) \qquad h(t) = A \int_0^t \frac{q(\tau)d\tau}{(1+\alpha(t-\tau))}$$

$$\text{with} \quad A = \frac{-w}{\pi\rho g c b d}, \quad \alpha = \frac{w}{d}$$

Then

$$(G_n)_{i1} = \int_0^{t_i} \frac{q(\tau)d\tau}{1+\alpha(t_i-\tau)}$$

(E5)

$$= \sum_{\ell=1}^{i} \frac{q_\ell}{\alpha} \ln\left(\frac{1+\alpha(i-\ell+1)\Delta t}{1+\alpha(i-\ell)\Delta t}\right)$$

and

$$(G_n)_{i2} = -A \int_0^{t_i} \frac{(t_i-\tau)q(\tau)d\tau}{(1+\alpha(t_i-\tau))^2}$$

(E6)

$$= -A \sum_{\ell=1}^{i} \frac{q_\ell}{\alpha^2} \left[\ln\left(\frac{1+\alpha(i-\ell+1)\Delta t}{1+\alpha(i-\ell)\Delta t}\right) + \frac{1}{1+\alpha(i-\ell+1)\Delta t} - \frac{1}{1+\alpha(i-\ell)\Delta t}\right]$$

APPENDIX F

The data kernel for non-linear lumping

For the case of an open two capacitor ladder

(F1) $$h(t) = m_1 e^{-m_3 t} + m_2 e^{-m_4 t}$$

Approximating the flow rate by $q(t) = q_i$, for $(i-1)\Delta t \leq t < i\Delta t$, equations (182) and (183) result in

$$(G_n)_{ij} = \frac{(e^{\Delta t m_{j+2}} - 1)}{m_{j+2}} \sum_{\ell=1}^{i} q_{(i-\ell+1)} e^{-\ell \Delta t m_{j+2}} \qquad j = 1,2$$

(F2)

$$(G_n)_{ij} = \frac{m_{j-2}}{m_j} \sum_{\ell=1}^{i} q_{(i-\ell+1)} e^{-\ell \Delta t m_j} \cdot [(\ell \Delta t + 1/m_j)(1-e^{m_j \Delta t}) + \Delta t e^{m_j \Delta t}] \qquad j = 3,4$$

where $\bar{m} = \bar{m}_n^{est}$.

For the case of a closed two capacitor ladder (or an open one capacitor ladder)

(F3) $$h(t) = m_1 e^{-m_3 t} + m_2$$

then

$$(G_n)_{i1} = \frac{(e^{\Delta t m_3} - 1)}{m_3} \sum_{\ell=1}^{i} q_{(i-\ell+1)} e^{-\ell \Delta t m_3}$$

$$(G_n)_{i2} = \sum_{\ell=1}^{i} q_{(i-\ell+1)\Delta t}$$

(F4)

$$(G_n)_{i3} = \frac{m_1}{m_3} \sum_{\ell=1}^{i} q_{(i-\ell+1)} e^{-\ell m_3 \Delta t}$$

$$\cdot[(\ell \Delta t + 1/m_3)(1-e^{m_3 \Delta t}) + \Delta t e^{m_3 \Delta t}]$$

APPENDIX G

Whole space thermoelastic strain in box-domain with ΔT = constant

The component of strain ϵ_{xx} along the z-axis through the center of the domain V (equation (222)) is given by equation (225). Change variables and

$$\text{(G1)} \qquad \epsilon_{xx} = \frac{\alpha \Delta T}{\pi} \left(\frac{1+\nu}{1-\nu}\right) \int_{\frac{2z-d}{\ell}}^{\frac{2z+d}{\ell}} \frac{ds}{(s^2+1)(s^2+2)^{1/2}}$$

Changing variables again, with

$$s = 2^{1/2} \tan u$$

$$\text{(G2)} \qquad ds = 2^{1/2} \frac{1}{\cos^2 u} du$$

$$s^2+2 = \frac{2}{\cos^2 u} ,$$

then

$$\epsilon_{xx} = \frac{\alpha\Delta T}{\pi}\left(\frac{1+\nu}{1-\nu}\right)\int_{u_1}^{u_2}\frac{\text{cosudu}}{2-\cos^2 u}$$

(G3)

$$\text{with}\quad u_1 = \tan^{-1}\left(\frac{2z-d}{2^{1/2}\ell}\right)$$

$$u_2 = \tan^{-1}\left(\frac{2z+d}{2^{1/2}\ell}\right)$$

Finally using

(G4)

$$\text{sinu} = x$$
$$\text{cosudu} = dx$$

we obtain

$$\epsilon_{xx} = \frac{\alpha\Delta T}{\pi}\left(\frac{1+\nu}{1-\nu}\right)\int_{\text{sinu}_1}^{\text{sinu}_2}\frac{dx}{1+x^2}\,dx$$

(G5)

$$= \frac{\alpha\Delta T}{\pi}\left(\frac{1+\nu}{1-\nu}\right)[\tan^{-1}(\sin(u_2))-\tan^{-1}(\sin(u_1))]$$

APPENDIX H

Thermoelastic stress at a free surface

Below we will show that the Mindlin and Cheng (1950) solution does result in zero normal stress, σ_{zz}, on the free surface z = o. From equation (200)

$$\text{(H1)} \qquad \sigma_{zz} = (\lambda+2\mu)\epsilon_{zz} + \lambda(\epsilon_{xx}+\epsilon_{yy})$$

and based on (227) the z-component of displacement equals

$$\text{(H2)} \qquad w = -\frac{\partial\phi}{\partial z} - (3-4\nu)\frac{\partial\phi'}{\partial z} - 2\frac{\partial\phi'}{\partial z} - 2z\frac{\partial^2\phi'}{\partial z^2} + 4(1-\nu)\nabla^2(z\phi')$$

The last term on the right of this equation can be written

$$\text{(H3)} \qquad \nabla^2(z\phi') = \nabla\cdot\bar{k}\phi' + \nabla\cdot(z\nabla\phi') = \frac{\partial\phi'}{\partial z} + \frac{\partial\phi'}{\partial z} + z\nabla^2\phi'$$

where $\nabla^2\phi' = o$ for $z \geq o$. Thus

$$\text{(H4)} \qquad w = -\frac{\partial\phi}{\partial z} + (3-4\nu)\frac{\partial\phi'}{\partial z} - 2z\frac{\partial^2\phi'}{\partial z^2}$$

and

$$(H5) \qquad \varepsilon_{zz}|_{z=o} = \frac{\partial w}{\partial z}|_{z=o} = -\frac{\partial^2 \phi}{\partial z^2} + (1-4-\nu)\frac{\partial^2 \phi'}{\partial z^2}$$

Since $\partial^2\phi'/\partial z^2 = \partial^2\phi/\partial z^2$ at $z = o$

$$(H6) \qquad \varepsilon_{zz}|_{z=o} = -4\nu \frac{\partial^2 \phi}{\partial z^2}$$

The x-component of displacement equals

$$(H7) \qquad u = -\frac{\partial \phi}{\partial x} - (3-4\nu)\frac{\partial \phi'}{\partial x} + 2z\frac{\partial^2 \phi'}{\partial x \partial z},$$

thus

$$(H8) \qquad \varepsilon_{xx}|_{z=o} = \frac{\partial u}{\partial x}|_{z=o} = -\frac{\partial^2 \phi}{\partial x^2} - (3-4\nu)\frac{\partial^2 \phi'}{\partial x^2}$$

and based on equation (236)

$$(H9) \qquad \varepsilon_{xx}|_{z=o} = -4(1-\nu)\frac{\partial^2 \phi}{\partial x^2}$$

We can also show that

$$(H10) \qquad \varepsilon_{yy}|_{z=o} = -4(1-\nu)\frac{\partial^2 \phi}{\partial y^2}$$

Combining (H1), (H6), (H9) and (H10) and using

$$(H11) \qquad \nu = \frac{\lambda}{2(\lambda+\mu)}$$

results in

(H12) $$\sigma_{zz}\big|_{z=o} = -4\lambda \frac{\lambda+2\mu}{2(\lambda+\mu)} \nabla^2\phi$$

Since the plane z=o is outside the domain of nonuniform temperature $\nabla^2\phi=o$ and we have shown that

(H13) $$\sigma_{zz}\big|_{z=o} = o$$

APPENDIX I

Thermoelastic stress in a box-domain with ΔT = constant, near a free surface

The component of stress σ_{xx}, along the z-axis through the center of a box-domain V located at a depth h below a free surface (equation (243)), is given by equation (244). In the case of ΔT = constant we obtain by changing variables

$$\frac{\sigma_{xx}(z)}{2\mu}\Big|_{x=y=o} = \frac{\alpha}{\pi}\left(\frac{1+\nu}{1-\nu}\right)\Delta T \left\{\int_{\xi_1}^{\xi_2} \frac{ds}{(s^2+1)(s^2+2)^{1/2}}\right.$$

$$(I1) \quad + (3+4\nu) \int_{\eta_1}^{\eta_2} \frac{ds}{(s^2+1)(s^2+2)^{1/2}} - 4\frac{z}{\ell} \int_{\eta_1}^{\eta_2} \frac{sds}{(s^2+1)(s^2+2)^{3/2}}$$

$$\left. - 8\frac{z}{\ell} \int_{\eta_1}^{\eta_2} \frac{sds}{(s^2+1)(s^2+2)^{1/2}} - \mathrm{II}\Delta T(z)\right\}$$

$$\text{with} \quad \xi_1 = \frac{2(z-(h+d))}{\ell}, \quad \xi_2 = \frac{2(z-h)}{\ell}$$

$$\eta_1 = \frac{2(z+h)}{\ell}, \quad \eta_2 = \frac{2(z+h+d)}{\ell}$$

In Appendix G above we have shown that

$$\int_{x_1}^{x_2} \frac{ds}{(s^2+1)(s^2+2)^{1/2}} =$$

(I2)

$$[\tan^{-1}(\sin(\tan^{-1}(x_2/2^{1/2})))-\tan^{-1}(\sin(\tan^{-1}(x_1/2^{1/2})))]$$

Using the change of variables (G2) we can rewrite

$$\text{(I3)} \qquad \int_o^x \frac{sds}{(s^2+1)(s^2+2)^{3/2}} = \frac{1}{2^{1/2}} \int_o^u \frac{\sin u \cos^2 u}{2-\cos^2 u}\, du$$

$$\text{with} \quad u = \tan^{-1}(x/2^{1/2})$$

and using

$$\text{(I4)} \qquad \begin{aligned} \cos u &= x \\ -\sin u du &= dx \end{aligned}$$

$$\text{(I5)} \qquad \int_o^x \frac{sds}{(s^2+1)(s^2+2)^{3/2}} = -\frac{1}{2^{1/2}} \int_1^{\cos u} \frac{x^2}{2-x^2}\, dx$$

Similarily

$$\text{(I6)} \qquad \int_o^x \frac{sds}{(s^2+1)(s^2+2)^{1/2}} = -2^{1/2} \int_1^{\cos u} \frac{x^2}{(2-x^2)^2}\, dx$$

Finally

$$\int \frac{x^2}{2-x^2}\,dx = -x + 2^{-1/2}\ln\left(\frac{2^{1/2}+x}{2^{1/2}-x}\right)$$

(I7)

$$\int \frac{x^2}{(2-x^2)^2}\,dx = \frac{x}{2(2-x^2)} - \frac{1}{2^{5/2}}\ln\left(\frac{2^{1/2}+x}{2^{1/2}-x}\right)$$

and equation (I1) can be rewritten

$$\frac{\sigma_{xx}(z)}{2\mu}\Big|_{x=y=o} = \frac{\alpha}{\pi}\left(\frac{1+\nu}{1-\nu}\right)\Delta T \left\{\tan^{-1}(r_2)-\tan^{-1}(r_1)\right.$$

(I8) $$+ (3+4\nu)[\tan^{-1}(s_2)-\tan^{-1}(s_1)]$$

$$\left. + 4\,\frac{z}{\ell}\left[2^{-1/2}(t_1-t_2)+2^{1/2}\left(\frac{t_2}{2-t_2^2}-\frac{t_1}{2-t_1^2}\right)\right] - b\right\}$$

$$\text{where} \quad b = \begin{cases} \pi & \text{in } V \\ o & \text{outside } V \end{cases}$$

and $r_1 = \sin(\tan^{-1}(\xi_1/2^{1/2}))$, $r_2 = \sin(\tan^{-1}(\xi_2/2^{1/2}))$

$t_1 = \cos(\tan^{-1}(\eta_1/2^{1/2}))$, $t_2 = \cos(\tan^{-1}(\eta_2/2^{1/2}))$

$s_1 = \sin(\tan^{-1}(\eta_1/2^{1/2}))$, $s_2 = \sin(\tan^{-1}(\eta_2/2^{1/2}))$

APPENDIX J

Horizontal thermoelastic strain in the plane of a 2-D CDM fracture

We evaluate the integral given by equation (275) as follows. First change variables

$$z' = z - r\cos\theta$$

$$y' = r\sin\theta \tag{J1}$$

$$dz'dy' = rdr$$

resulting in

$$\frac{\partial u_y^A}{\partial y}\Big|_{x=y=o} =$$

$$\frac{\alpha}{\pi}\left(\frac{1+\nu}{1-\nu}\right)\int_o^{\pi} d\theta \int_o^{\infty} rdr\,\Delta T(r,\theta) \int_o^{\infty} dx' \frac{x'^2+r^2(1-3\sin^2\theta)}{(x'^2+r^2)^{5/2}} \tag{J2}$$

$$= \frac{\alpha}{\pi}\left(\frac{1+\nu}{1-\nu}\right)\int_o^{\pi} d\theta \int_o^{\infty} rdr\,\Delta T(r,\theta)$$

$$\cdot \left[\int_o^{\infty} \frac{dx'}{(x'^2+r^2)^{3/2}} - 3r^2\sin^2\theta \int_o^{\infty} \frac{dx'}{(x'^2+r^2)^{5/2}}\right]$$

Now use

$$\int_0^\infty \frac{dx'}{(x'^2+r^2)^{5/2}} = \lim_{\delta\to 0} \int_\delta^\infty \frac{dx'}{(x'^2+r^2)^{5/2}}$$

(J3)

$$= \lim_{\delta\to 0} \left[\frac{\delta}{3r^2(\delta^2+r^2)^{3/2}}\right] + \frac{2}{3}\frac{1}{r^2}\int_0^\infty \frac{dx'}{(x'^2+r^2)^{3/2}}$$

Thus

$$\frac{\partial u_y^A}{\partial y}\Big|_{x=y=0} = \frac{\alpha}{\pi}\left(\frac{1+\nu}{1-\nu}\right)\int_0^\pi d\theta \int_0^\infty r dr\, \Delta T(r,\theta)$$

(J4)

$$\cdot\left[(1-2\sin^2\theta)\int_0^\infty \frac{dx'}{(x'^2+r^2)^{3/2}} - \sin^2\theta \lim_{\delta\to 0}\left(\frac{\delta}{(\delta^2+r^2)^{3/2}}\right)\right]$$

Then use

$$\lim_{\delta\to 0}\frac{1}{\pi}\int_0^\pi \sin^2\theta \int_0^\infty \frac{\delta\,\Delta T(r,\theta)}{(\delta^2+r^2)^{3/2}}\, r dr d\theta$$

(J5)

$$= \frac{\Delta T|_{r=0}}{2} \lim_{\delta\to 0}\int_0^R \frac{r dr}{(\delta^2+r^2)^{3/2}} = \frac{\Delta T|_{r=0}}{2}$$

where R is such that

(J6) $\Delta T(r,\theta) \simeq \Delta T|_{r=0}$ for $r < R$

Also

$$\int_0^\infty \frac{dx'}{(x'^2+r^2)^{3/2}} = \frac{1}{r^2} \tag{J7}$$

and since $1-2\sin^2\theta = \cos 2\theta$ we finally obtain

$$\frac{\partial u_y^A}{\partial y}\Big|_{x=y=o} = \frac{\alpha}{\pi}\left(\frac{1+\nu}{1-\nu}\right)\int_0^\pi d\theta \int_0^\infty dr \frac{\cos 2\theta}{r}\,\Delta T(r,\theta)$$

(J8)

$$+ \frac{\alpha}{2}\left(\frac{1+\nu}{1-\nu}\right)\Delta T(y,z)\Big|_{y=o}$$

APPENDIX K

Stress at the tip of a Griffith crack

In the plane of the crack

$$(K1)\quad \sigma_{yy}(o,z) = \frac{2}{\pi}\left[\frac{z}{(z^2-d^2)^{1/2}}\, q(d) - z\int_o^d \frac{q'(s)ds}{(z^2-s^2)^{1/2}}\right],\quad z>d$$

Integrating by parts we obtain

$$(K2)\quad q'(s) = \frac{1}{s}\int_o^s \frac{r\zeta'(r)dr}{(s^2-r^2)^{1/2}} + \zeta(o)\lim_{r\to o}\ \frac{r}{s}\,\frac{1}{(s^2-r^2)^{1/2}}$$

Thus

$$\frac{2z}{\pi}\int_o^d \frac{q'(s)ds}{(z^2-s^2)^{1/2}} = \frac{2z}{\pi}\left[\int_o^d \frac{ds}{s(z^2-s^2)^{1/2}}\int_o^s \frac{r\zeta'(r)dr}{(s^2-r^2)^{1/2}}\right.$$

(K3)

$$\left. + \zeta(o)\lim_{r\to o} r\int_o^d \frac{ds}{s(z^2-s^2)^{1/2}(s^2-r^2)^{1/2}}\right]$$

By changing the order of integration and taking the limit $z \to d^+$

$$\frac{2d}{\pi}\int_o^d \frac{q'(s)ds}{(d^2-s^2)^{1/2}} = \frac{2d}{\pi}\left[\int_o^d r\sum'(r)dr \int_r^d \frac{ds}{s(d^2-s^2)^{1/2}(s^2-r^2)^{1/2}}\right.$$

(K4)

$$\left. + \sum(o)\lim_{r\to o} r \int_r^d \frac{ds}{s(d^2-s^2)^{1/2}(s^2-r^2)^{1/2}}\right]$$

We can show that

(K5) $$\int_r^d \frac{ds}{s(d^2-s^2)^{1/2}(s^2-r^2)^{1/2}} = \frac{\pi}{2rd} \quad ,$$

thus

(K6) $$\frac{2d}{\pi}\int_o^d \frac{q'(s)ds}{(d^2-s^2)^{1/2}} = \int_o^d \sum'(r)dr + \sum(o)$$

or

(K7) $$\frac{2d}{\pi}\int_o^d \frac{q'(s)ds}{(d^2-s^2)^{1/2}} = \Sigma(d)$$